



**UNIVERSITY OF  
TECHNOLOGY SYDNEY**

**Determination of Embedded Length and General  
Condition of Utility Poles Using Non-Destructive  
Testing Methods**

By  
**Amir Zad**

A thesis submitted in fulfilment  
of the requirements for the degree of  
**Doctor of Philosophy**

Faculty of Engineering and Information Technology  
University of Technology Sydney

October 2013

## CERTIFICATE OF AUTHORSHIP/ORIGINALITY

I certify that the work in this thesis has not previously been submitted for a degree nor has it been submitted as part of requirements for a degree except as fully acknowledged within the text.

I also certify that the thesis has been written by me. Any help that I have received in my research work and the preparation of the thesis itself has been acknowledged. In addition, I certify that all information sources and literature used are indicated in the thesis.

Signature of candidate

Amir Zad

October 2013

## **Abstract**

Timber utility poles play a key role for electricity distribution systems in Australia and in many other countries. There are over 5 million timber utility poles currently used in Australian energy networks which are more than 80% of total utility poles in the network. Lack of knowledge about the current condition of existing poles such as embedded length, the degree of deterioration and damage below the ground level or on top of the pole, leads to uncertainty for replacement or maintenance works. Hence, it is essential to develop a cost effective and reliable non-destructive method to ensure safety and to reduce maintenance costs.

Different Non-destructive Testing (NDT) methods such as Sonic Echo, Bending Waves and Ultraseismic methods have been used in field applications over the past decades as simple and cost-effective tools for identifying the condition and underground depth of embedded structures, such as timber poles or piles in service. Despite the wide spread use of these methods by consultants around the world, reports describing field applications have shown that the results lack both consistency and reliability. Difficulties faced in field applications are often associated with complicated and imperfect/deteriorated materials, environmental effects, interaction of soil and structure and unknown boundary conditions, which lead to a great deal of uncertainties. In order to address this problem and develop reliable methods for embedment length determination and identification of damage below ground level, an R&D program commenced in 2008 at the University of Technology Sydney in collaboration with the Electricity Network Association of Australia. The aim of this study is to investigate and future develop the current non-destructive test methods with acceptable accuracy and repeatability, whilst being cost efficient for condition assessment of timber poles and piles as a part of the main program.

To tackle the problems and evaluate effects of various factors associated with timber materials, on these NDT methods, thorough numerical investigations using Finite Element (FE) was necessary. In this study on isotropic model was used for timber material as the main object of the numerical study was to get a better understanding of wave travel in materials without any other uncertainties. The numerical evaluation will start with a free timber pole without embedment to understand the behaviour of the

timber poles under surface NDT Methods. The results will be used for benchmarking in further investigations involving structure and soil interaction and boundary conditions. The model is verified with static analysis. Then, the FE beam model is enhanced with more advanced features requiring more steps to simulate other boundary conditions. According to the results, stress wave velocity will decrease with increase in embedded length. Therefore, two different velocities, one for stress wave travelling above the soil level and one travelling inside the soil with around 20% decrease in velocity was calculated. The error of length estimation averaged between 5% and 9% depending on the boundary conditions and the reference sensor for calculations.

In order to address this problem and develop a reliable method for embedment length and identification of damage below ground level, also the bending wave method is fully investigated and verified for the potentials and limitations. The success of determining these parameters (embedded length and location of damage) mainly depends on the accuracy of measuring the bending wave velocity. However, bending wave is highly dispersive in nature and, hence, it is important to find its frequency dependent velocity. Short Kernel Method (SKM) has been used as a signal processing tool to calculate the frequency dependent velocity and also the embedded length. As there are no guidelines to select those kernel frequencies, different kernel frequencies were selected based on the results of FFT and then applying the SKM method. As a result of the bending wave velocity investigation, the appropriate kernel frequency is identified to be between 600 to 800 Hz. The results are verified using Bernoulli-Euler Beam theory and Timoshenko beam theory. Based on the length estimation, the kernel frequency of between 650 Hz to 800 Hz will result in less than 8% error in embedded length estimation.

Furthermore, the Ultraseismic method is also applied on the results of timber modelling. Based on the results of velocities below and above the soil, the stress wave velocity is decreased by 22% overall below the soil in comparison with stress wave velocity above the soil. Based on the Ultraseismic method, the length of the timber pole is estimated by cross correlating the first arrival and reflection waves. Ultraseismic test applying impact at the middle was also investigated for a 12m timber pole. It was found that, impact at middle of the specimen generated two compressional waves (travelling down and reflecting at the butt) and tensile waves (travelling up and reflecting at the top). This wave interference makes the analysis complicated. In addition, impact from the middle

with 45 degree angle generates the combination of horizontal and vertical forces which result in contribution of bending waves to longitudinal waves. As a result, the signal will include multiple wave modes which are required to be separated before calculation of velocity and length determination. It should be mentioned that, Timber pole is modelled as an isotropic material here and if the anisotropy of the material is included the analysis will be more complicated.

This study also presents the results of Sonic Echo, Impulse Response, Bending Wave and Ultraseismic methods, investigated for determining the stress wave velocity and embedded length of poles with different testing conditions in the structural laboratories at UTS and in the field at Mason Park (NSW) and Horsham (Victoria).

According to the laboratory results, the coefficient of variation of velocity estimation of timber pole is relatively higher than steel beam and timber beam due to uncertainties in timber material such as anisotropy of timber material, stress direction in regards to grain angle of timber, location of a sensor relative to other sensors in regards to the annual growth ring orientation and existence of knots or any imperfections in timber. Choosing the reflection peak for length determination is one of the main parts of these methods and this could be affected by geotechnical conditions. Based on the results, the stress wave velocity will decrease inside the soil and a reduction factor is required to be applied to stress wave velocity above the soil to obtain the stress wave velocity below the soil. This reduction factor varies depending on the different testing/boundary conditions as well as the soil depth. In SE method, the scatter of the average error for the pole specimen, associated with different tests, ranged between 1% and 20% for all cases except layer 6 with 26% using sensor 1 for calculations. By using sensor 2 for estimation of the length, the average error becomes less than 9% for all cases except for layer 7 with 32%. However, more uncertainties are involved in terms of length calculation using sensors 3 and 4 located 1.5m and 2m from the impact location in comparison with using sensors 1 and 2 for calculations.

The phase velocity is calculated for each kernel frequency under different pull out testing conditions. Also based on the results of bending wave method, the kernel frequency between of 400-800 Hz was identified for use in SKM method for phase velocity calculations. Using the SKM to estimate the length of the pole with Bending Wave method for a 5m timber pole under different pull out conditions shows the

percentage of error for all boundary conditions to be between -10.5% and 0%. If the kernel frequency above 600Hz is selected, the average error for length estimation becomes less than 5% for most boundary conditions.

Also Ultraseismic method was considered for stress wave velocity estimation of timber poles impacted at the top. According to the results, using sensors close to impact location (up to 2-3m) will result in good estimation of the velocity calculations. However, these will not necessarily lead to accurate estimations. According to the results, the average error in length determination for timber poles under different pull out conditions which is more relevant to timber poles in-service is less than 18%. According to the results for Ultraseismic method using impact at the top in Horsham, the stress wave velocities were calculated with relatively good accuracy.

By considering relatively good and damaged poles in Horsham, it was found that the severe termite damage can be identified by the irregular patterns of FFT from impacted timber pole. This can be used to classify which timber poles are required to be replaced in the field.

## Acknowledgements

This PhD project could not have been possible without the support provided by numerous people. In particular, the author would like to express his appreciation and gratitude to his principal supervisor, Associate Professor Jianchun Li for his outstanding guidance, encouragement, wisdom and caring support provided throughout this project. Utmost gratitude is also forwarded to Prof. Bijan Samali who had given the author invaluable advice, encouragement and assistance through the course of his study and in preparation of his thesis. Special thanks for prof. Keith Crews for providing the opportunity for collaboration of industrial partner (Energy Australia) for this study. I wish to sincerely thank Dr. Fook Choon Choi for his encouragement, help and support and especially for his exceptional personality and source of inspiration as a role model for my professional and personal development. The author also gratefully acknowledges the financial assistance provided by the University of Technology Sydney and Centre for Built Infrastructure Research (CBIR) of the Faculty of Engineering, UTS and Energy Australia an industrial partner.

Furthermore, the author would like to thank the Structures Laboratory staff for their help in the experimental and field work. Special thanks must also go to Rami Haddad, David Hooper, David Dicker, Peter Brown and Richard Turnell. I wish to sincerely thank for the members of timber pole project; Dr. Ulrike Dackermann, Saad, Bahram and Ning. To friends and/or colleagues at UTS, the author wishes to express his gratitude. Special thanks must go to Behnam, Ali, Nassim, Mohsen, Muhammad and others who shared their time and friendship with the author

The administrative and the support staff at UTS Faculty of Engineering and IT, Phyllis Agius, Craig Shuard, Van Lee and the IT support team for performing an excellent job in keeping the show running.

To My **Mum** and **Dad**



# List of Publications Based on This Research

## Journal Articles

1. Zad, A., Li, J., Samali, B. (2013), 'Limitation of surface non-destructive tests on timber utility poles', *In preparation*
2. Zad, A., Li, J., Samali, B. (2013), 'Comprehensive investigation of dispersive wave on timber utility poles', *In preparation*

## Book Chapters

3. Zad, A., Li, J., Samali, B., & Crews, K. (2011), 'Finite element evaluation of non-destructive testing methods for embedded timber poles in service', *Incorporating Sustainable Practice in Mechanics and Structures of Materials*, Taylor & Francis Group, London, pages 909-914

## Conference Papers

4. Zad, A., Li, J., Crews, K. & Samali, B. (2010), 'Determination of embedment depth of timber poles and piles using non-destructive evaluation (NDE) techniques', *Proceedings of the 13th International Conference on Structural Faults + Repair*, 15-17 June 2010, Edinburgh, Scotland, Paper #TB CREWS - SFR, (published on CD).

## Guidelines

5. Li, J., Dackermann, U., Zad, A., Subhani, S., Samali, B. & Crews, K., 'Recommended Best Practice for Assessment of Timber Structures using Surface Stress Wave Methods', RILEM, *In press*.

## Table of Contents

|   |          |
|---|----------|
| <b>CHAPTER 1 .....</b>  | <b>1</b> |
| <b>1 INTRODUCTION.....</b>  | <b>1</b> |
| 1.1 Background .....  | 1        |
| 1.2 Research Scope.....   | 3        |
| 1.3 Research Objectives .....   | 4        |
| 1.4 Summary of Contributions .....  | 5        |
| 1.5 Outline of the Thesis .....   | 7        |
| <b>CHAPTER 2 .....</b>  | <b>9</b> |
| <b>2 LITERATURE REVIEW.....</b>   | <b>9</b> |
| 2.1 Timber poles in Australia .....   | 9        |
| 2.2 Types of degradation and location of timber piles and utility poles ..... | 11       |
| 2.3 Conventional methods for assessment of timber structures .....            | 12       |
| 2.3.1 Visual inspection method.....   | 12       |
| 2.3.2 Probing.....  | 13       |
| 2.3.3 Sounding .....  | 13       |
| 2.3.4 Drilling and coring .....   | 13       |
| 2.4 Non-destructive evaluation methods for timber structures .....            | 14       |
| 2.5 Stress wave testing based methods.....                                    | 15       |
| 2.5.1 Sonic Echo (SE) method.....   | 15       |
| 2.5.2 Impulse response method.....  | 16       |
| 2.5.3 Bending Wave method.....  | 19       |
| 2.5.4 Ultraseismic Method .....   | 22       |
| 2.5.5 Parallel Seismic (PS).....  | 23       |
| 2.5.6 Borehole radar .....  | 26       |
| 2.6 Review of stress wave propagation in solids.....                          | 28       |
| 2.6.1 Wave propagation in an elastic half-space.....                          | 28       |

|  |   |           |
|--|---|-----------|
| 2.6.2  | Longitudinal wave propagation in thin rods .....                            | 31        |
| 2.6.3  | Flexural wave propagation in thin rod .....                                 | 33        |
| 2.7  | Signal processing for stress wave methods .....                             | 36        |
| 2.7.1  | The discrete and fast Fourier transform .....                               | 36        |
| 2.7.2  | Short-Kernel Method (SKM) .....   | 39        |
| 2.7.3  | Wavelet transform .....   | 41        |
| 2.8  | Finite element modelling of wave propagation in cylindrical pile/pole ..... | 42        |
| 2.9  | Research gaps identified .....  | 44        |
| 2.10   | Summary .....   | 46        |
| <b>CHAPTER 3 .....</b>   |   | <b>49</b> |
| <b>3 FINITE ELEMENT MODELLING OF TIMBER POLE WITH/WITHOUT SOIL EMBEDMENT .....</b> |   | <b>49</b> |
| 3.1  | Introduction .....  | 49        |
| 3.2  | Numerical Modelling of timber poles .....                                   | 50        |
| 3.2.1  | Finite Element Modelling of Intact Beam .....                               | 50        |
| 3.2.2  | Consideration of various boundary conditions .....                          | 51        |
| 3.2.3  | Material properties and geometry .....                                      | 53        |
| 3.3  | Simulation of wave propagation in timber pole .....                         | 54        |
| 3.3.1  | Simulation of impact loading .....  | 56        |
| 3.3.2  | Stress wave propagation through the pole under impact load .....            | 56        |
| 3.4  | Behaviour of wave propagation in timber pole .....                          | 57        |
| 3.5  | Effect of types of impact and their location on timber pole .....           | 59        |
| 3.6  | Application of Sonic Echo/Impulse Response test on timber pole .....        | 62        |
| 3.6.1  | Velocity calculation .....  | 62        |
| 3.6.2  | Embedded length determination .....   | 65        |
| 3.7  | Application of Bending Wave Test on timber pole .....                       | 66        |
| 3.7.1  | Velocity calculation .....  | 67        |

|                        |   |           |
|------------------------|---|-----------|
| 3.7.2                  | Embedded length determination .....                                     | 72        |
| 3.7.3                  | Velocity calculation and length determination of filtered results ..... | 74        |
| 3.8                    | Application of Ultraseismic test impact on timber pole.....             | 77        |
| 3.8.1                  | Velocity calculation .....  | 77        |
| 3.8.2                  | Embedded length determination .....                                     | 81        |
| 3.8.3                  | Alternative impact location.....  | 82        |
| 3.9                    | Preliminary damage identification of timber pole.....                   | 84        |
| 3.10                   | Summary.....  | 87        |
| <b>CHAPTER 4 .....</b> |   | <b>90</b> |
| <b>4</b>               | <b>EXPERIMENTAL INVESTIGATION OF TIMBER UTILITY POLES.....</b>          | <b>90</b> |
| 4.1                    | Introduction .....  | 90        |
| 4.2                    | Test Equipment.....   | 90        |
| 4.2.1                  | Impact hammer.....  | 90        |
| 4.2.2                  | Accelerometers.....   | 91        |
| 4.2.3                  | Signal Conditioning and computer .....                                  | 93        |
| 4.2.4                  | Laboratory testing frame .....  | 94        |
| 4.3                    | Testing Scenarios .....   | 96        |
| 4.3.1                  | Testing Procedure.....  | 96        |
| 4.3.2                  | Test specimens .....  | 99        |
| 4.3.3                  | Different types of testing.....   | 100       |
| 4.3.4                  | Damage scenario induced for timber pole .....                           | 103       |
| 4.4                    | Test set-up for Sonic Echo and Impulse Response Method.....             | 104       |
| 4.5                    | Test Set-Up for Bending Wave Method.....                                | 108       |
| 4.6                    | Controlled field tests .....  | 110       |
| 4.7                    | Field tests on decommissioned utility poles.....                        | 112       |
| 4.8                    | Classification of damage of field utility timber poles .....            | 113       |
| 4.9                    | Soil samples.....   | 116       |

|                        |  |            |
|------------------------|--|------------|
| 4.10                   | Summary.....   | 119        |
| <b>CHAPTER 5 .....</b> |  | <b>121</b> |
| <b>5</b>               | <b>ANALYSIS AND DISCUSSION OF LABORATORY AND FIELD TESTS</b>   | <b>121</b> |
| 5.1                    | Introduction .....   | 121        |
| 5.2                    | Sonic Echo (SE) test.....                                      | 122        |
| 5.2.1                  | Velocity calculation .....                                     | 123        |
| 5.2.2                  | Length Estimation .....  | 134        |
| 5.3                    | Impulse Response (IR) test.....                                | 144        |
| 5.3.1                  | Impact at the top.....   | 144        |
| 5.3.2                  | Impact at the middle.....                                      | 148        |
| 5.4                    | Bending Wave test.....   | 149        |
| 5.4.1                  | Application of SKM for the calculation of phase velocity ..... | 151        |
| 5.4.2                  | Velocity calculation .....                                     | 153        |
| 5.4.3                  | Length Estimation .....  | 157        |
| 5.5                    | Ultraseismic test .....  | 159        |
| 5.5.1                  | Velocity calculation .....                                     | 159        |
| 5.5.2                  | Length Estimation .....  | 172        |
| 5.6                    | Effects of damage scenarios on timber pole in laboratory ..... | 173        |
| 5.7                    | Controlled field tests .....                                   | 175        |
| 5.7.1                  | Sonic Echo/Impulse response test at the middle .....           | 175        |
| 5.7.2                  | Ultraseismic test at the middle .....                          | 180        |
| 5.8                    | Field tests of decommissioned utility poles.....               | 184        |
| 5.8.1                  | Sonic Echo (SE) test impact at top.....                        | 185        |
| 5.8.2                  | Sonic Echo/Impulse Response test impact at the middle.....     | 187        |
| 5.8.3                  | Ultraseismic test impact at the top .....                      | 189        |
| 5.9                    | Summary .....  | 192        |

|  |            |
|--|------------|
| <b>CHAPTER 6 .....</b>                             | <b>196</b> |
| <b>6 CONCLUSION AND RECOMMENDATION .....</b>       | <b>196</b> |
| 6.1 Summary .....                                  | 196        |
| 6.2 Concluding remarks .....                       | 198        |
| 6.3 Recommendation of future study .....           | 202        |
| <b>REFERENCES.....</b>                             | <b>203</b> |
| <b>APPENDIX A.....</b>                             | <b>208</b> |
| <b>TIMBER POLE AUTOPSY .....</b>                   | <b>208</b> |
| <b>APPENDIX B .....</b>                            | <b>225</b> |
| <b>RESULTS OF IMPULSE RESPONSE (IR) TEST .....</b> | <b>225</b> |
| <b>APPENDIX C .....</b>                            | <b>228</b> |
| <b>RESULTS OF ULTRASEISMIC TEST.....</b>           | <b>228</b> |

## List of Figures

|   |    |
|---|----|
| Figure 2.1 Three principal axes of wood with respect to grain direction and growth rings (Green, Winandy et al. 1999).....                                  | 11 |
| Figure 2.2 Possible decay patterns in underground sections of utility poles (Nguyen, Foliente et al. 2004).....   | 12 |
| Figure 2.3 Schematic principle of SE testing.....   | 16 |
| Figure 2.4 Schematic principle of IR testing .....  | 17 |
| Figure 2.5 Schematic principle of Bending Wave testing .....  | 21 |
| Figure 2.6 Schematic principle of Ultraseismic testing .....  | 23 |
| Figure 2.7 Parallel Seismic setup .....   | 24 |
| Figure 2.8 Parallel Seismic data and velocity lines.....  | 25 |
| Figure 2.9 Borehole Radar system.....   | 27 |
| Figure 2.10 A thin prismatic rod with coordinate $x$ and displacement $u$ of a section.....   | 31 |
| Figure 2.11 A differential element of a thin rod undergoing transverse motion due to a vertical impact.....   | 33 |
| Figure 2.12 Dispersion relation for different theories (After Graff, 1975).....   | 36 |
| Figure 2.13 Kernel shifted along signal .....   | 40 |
| Figure 2.14 Consideration of damage identification for determination of the underground length of a timber pole.....  | 45 |
| Figure 3.1 The geometric properties of SOLID45 (ANSYS Inc 2011).....  | 50 |
| Figure 3.2 A typical set-up for the embedded timber pole .....  | 52 |
| Figure 3.3 A typical FE model of embedded timber pole.....  | 52 |
| Figure 3.4 The geometric properties of CONTACT178 (ANSYS Inc 2011).....   | 53 |
| Figure 3.5 An example of applied impact loading in the transient dynamic analysis. ...  | 56 |
| Figure 3.6 Geometry of the model and location of the sensors placed on the timber pole .....  | 57 |
| Figure 3.7 Velocity results in $y$ direction under free-free condition.....   | 58 |
| Figure 3.8 Velocity results in $y$ direction for patch sensors with same distance under free-free condition.....  | 58 |
| Figure 3.9 Cross section of FE modelling.....   | 59 |
| Figure 3.10 Stress wave velocity in $y$ direction under free end condition and different loading condition by impact from the top for accelerometer 1 ..... | 60 |

|  |    |
|--|----|
| Figure 3.11 Stress wave velocity in y direction under free end condition and different loading condition by impact from the top for accelerometer 4 .....  | 60 |
| Figure 3.12 Stress wave velocity in x direction under free end condition by impact from the top for accelerometers 4 and 13 .....  | 61 |
| Figure 3.13 Stress wave velocity in x direction under free end condition by impact at the edge for accelerometers 4 and 13 .....   | 61 |
| Figure 3.14 Geometry of the model and location of the sensors placed on the timber pole for Sonic Echo test .....  | 63 |
| Figure 3.15 Acceleration results in y direction for patch sensors under 5 pull out conditions .....  | 63 |
| Figure 3.16 Effect of different embedded lengths for velocity calculation .....  | 64 |
| Figure 3.17 Acceleration result of 5m timber pole under 2 <sup>nd</sup> pull out condition.....  | 64 |
| Figure 3.18 Acceleration result of 5m timber pole under 4 <sup>th</sup> pull out condition.....  | 65 |
| Figure 3.19 Geometry of the model and location of the sensors placed on the timber pole for Bending Wave test.....   | 67 |
| Figure 3.20 SKM coefficient plot at 410 Hz of 5 m timber pole under 1 <sup>st</sup> pull out for sensors 1,2 and 4. ....   | 69 |
| Figure 3.21 SKM coefficient plot at 410 Hz of 5 m timber pole under 1 <sup>st</sup> pull out for sensor 1 .....  | 69 |
| Figure 3.22 Bending wave velocity for different kernel frequencies of 5 m timber pole under different boundary conditions using sensor 1 as a reference a) using sensor 2 as a reflection wave, b) using sensor 3 as a reflection wave, c) using sensor 4 as a reflection wave ..... | 71 |
| Figure 3.23 Bending wave velocity for different kernel frequencies of 5 m timber pole under different boundary conditions using sensor 2 as a reference, a) using sensor 3 as a reflection wave, b) using sensor 4 as a reflection wave.....   | 72 |
| Figure 3.24 Embedded length determination for different kernel frequencies of 5 m timber pole under 1 <sup>st</sup> pull out condition. ....   | 73 |
| Figure 3.25 Embedded length determination for different kernel frequencies of 5 m timber pole under 3 <sup>rd</sup> pull out condition.....  | 73 |
| Figure 3.26 Embedded length determination for different kernel frequencies of 5 m timber pole under 8 layer soil condition. ....   | 74 |



|  |    |
|--|----|
| Figure 3.27 Bending wave velocity for different kernel frequencies of 5 m timber pole under 3 <sup>rd</sup> pull out condition using filtered results. ....                          | 75 |
| Figure 3.28 Embedded length determination for different kernel frequencies of 5 m timber pole under 3 <sup>rd</sup> pull out condition after filtering. ....                         | 75 |
| Figure 3.29 Embedded length error for different frequencies of 12 m timber pole under 2m embedment condition using continues wave length and short kernel method.....                | 76 |
| Figure 3.30 Acceleration results for selected sensors in y direction under 3 <sup>rd</sup> pull out condition using Ultraseismic method a) arrival wave and b) reflection wave ..... | 79 |
| Figure 3.31 Acceleration results in y direction under 3 <sup>rd</sup> pull out condition using Ultraseismic method.....  | 79 |
| Figure 3.32 Acceleration results for selected sensors in y direction under 5 <sup>th</sup> pull out condition using ultraseismic method a) arrival wave and b) reflection wave.....  | 80 |
| Figure 3.33 Acceleration results in y direction under 5 <sup>th</sup> pull out condition using Ultraseismic method.....  | 81 |
| Figure 3.34 Effect of soil in stress wave velocity .....   | 81 |
| Figure 3.35 Length estimation using sensors above the soil level under 3 <sup>rd</sup> pull out condition using Ultraseismic method in 2D graph.....                                 | 82 |
| Figure 3.36 Geometry of the model and location of the sensors placed on the timber pole for Ultraseismic test impacted at the middle .....   | 83 |
| Figure 3.37 Acceleration-time history of 12m timber pole under 5 <sup>th</sup> pull out condition using Ultraseismic method with impact at the middle .....                          | 83 |
| Figure 3.38 Velocity results for decay type 1 under three different damage scenarios; 1S, 1M and 1L.....   | 84 |
| Figure 3.39 Comparison of the free end test with external decay and without decay ....   | 85 |
| Figure 3.40 Side view of a damage inflicted in timber pole identical to the laboratory case.....   | 86 |
| Figure 3.41 Acceleration-time history results for intact and damaged pole of 5m timber pole for sensor 3 .....   | 86 |
| Figure 3.42 Acceleration-time history results for intact and damaged pole of 5m timber pole for sensor 6 .....   | 87 |
| Figure 4.1 Impact hammer (a) stiff tip, (b) soft tip .....   | 91 |
| Figure 4.2 Typical response of hammer impact.....  | 91 |

|  |     |
|--|-----|
| Figure 4.3 Testing accelerometers (a) piezoelectric accelerometer - model PCB 356A08, (b) piezoelectric accelerometer - model PCB 337A26, (c) piezoresistive accelerometer chip ADXL320 (d) piezoresistive accelerometer with housing..... | 92  |
| Figure 4.4 Accelerometers mounted to the a) steel beam and b) timber beam by screws .....  | 92  |
| Figure 4.5 Calibration of the accelerometers using a shake table.....  | 93  |
| Figure 4.6 (a) Multi-channel signal conditioner - model PCB 483B03 and (b) DC power supply.....  | 93  |
| Figure 4.7 A personal computer for laboratory and field testing.....   | 94  |
| Figure 4.8 Steel frame used as a container.....  | 95  |
| Figure 4.9 Using scaffold and scissor lift to build and access the top of the frame.....   | 95  |
| Figure 4.10 Testing procedure: (a) setting up of equipment, (b) mounting of accelerometer, (c) attached bracket and accelerometers and (d) execution of the test. ..   | 98  |
| Figure 4.11 Laboratory free-free test for steel beam.....  | 99  |
| Figure 4.12 Laboratory free-free test set-up for timber beam.....  | 100 |
| Figure 4.13 a) location of the accelerometers on steel and timber beam specimens, b) laboratory set-up for NDT method under free-end conditions with timber pole specimen .....  | 100 |
| Figure 4.14 Test set-up of bedrock condition in laboratory.....  | 101 |
| Figure 4.15 Filing the sand a) into the buckets and b) into the frame.....   | 102 |
| Figure 4.16 The laboratory set-up for NDT methods under embedded conditions for a timber pole .....  | 103 |
| Figure 4.17 The laboratory set-up for NDT methods using pull out to simulate various embedment depths (timber beam specimen).....  | 103 |
| Figure 4.18 Side view of a typical damage inflicted in timber pole in laboratory.....  | 104 |
| Figure 4.19 Impact bracket mounted to the side of a timber pole to provide a surface for longitudinal impact excitation.....   | 104 |
| Figure 4.20 Impact bracket mounted to the side of a a) steel pole b) timber beam to provide a surface for longitudinal impact excitation.....  | 105 |
| Figure 4.21 Test set-up for free-free testing of (a) and (b) laboratory testing and (c) to (e) field testing. ....   | 106 |
| Figure 4.22 Test set-up of embedded testing in laboratory.....   | 107 |
| Figure 4.23 Test set-up of embedded testing in the field.....  | 107 |

|  |     |
|--|-----|
| Figure 4.24 Schematic test set-up of free-free BW tests for (a) laboratory testing and (b) field testing.....  | 108 |
| Figure 4.25 Schematic and photo of test set-up of embedded BW tests for laboratory testing.....  | 109 |
| Figure 4.26 Schematic and photo of test set-up of embedded BW tests for field testing.....   | 109 |
| Figure 4.27 Location of the Mason Park (courtesy of Google Maps) .....   | 110 |
| Figure 4.28 Location of timber poles at Mason Park.....  | 110 |
| Figure 4.29 Timber poles before installation in Mason Park.....  | 111 |
| Figure 4.30 Timber poles after installation in Mason Park.....   | 111 |
| Figure 4.31 Cross sections of pole No 288 .....  | 115 |
| Figure 4.32 Compaction test equipment .....  | 117 |
| Figure 4.33 Filling the compaction mould with soil .....   | 118 |
| Figure 4.34 Compacted soil with mould after compaction completed .....   | 118 |
| Figure 4.35 Compaction curve of soil sample in Mason Park .....  | 118 |
| Figure 5.1 Test set-up for (a) free-free testing and (b) embedded testing condition ....   | 123 |
| Figure 5.2 Velocity calculation of steel beam (free end condition).....  | 124 |
| Figure 5.3 Velocity calculation of timber beam (free end condition).....   | 124 |
| Figure 5.4 Velocity calculation of timber pole (free end condition).....   | 125 |
| Figure 5.5 Minimum, maximum and average longitudinal wave velocity for steel beam .....  | 125 |
| Figure 5.6 Minimum, maximum and average longitudinal wave velocity for timber beam .....   | 126 |
| Figure 5.7 Minimum, maximum and average longitudinal wave velocity for timber pole .....   | 126 |
| Figure 5.8 The three principal axes of wood with respect to grain direction and growth rings (Kretschmann 2010).....   | 133 |
| Figure 5.9 Direction of load in relation to direction of annual growth rings: 90° or perpendicular (R), 45°, 0° or parallel (T) (Kretschmann 2010).....  | 133 |
| Figure 5.10 Relationship of fibre orientation (O–O) to different axes, as shown by the schematic of wood specimens containing straight grain and cross grain. Specimens A through D have radial and tangential surfaces; E through H do not. Specimens A and E |     |

|   |     |
|---|-----|
| contain no cross grain; B, D, F, and H have spiral grain; C, D, G, and H have diagonal grain (Kretschmann 2010).....                                      | 133 |
| Figure 5.11 Schematic of fibre orientation and sensor location .....  | 134 |
| Figure 5.12 Stress wave velocity in timber material with knots .....  | 134 |
| Figure 5.13 Acceleration-time history result of a 5m timber pole under free-free and bedrock conditions .....   | 136 |
| Figure 5.14 Percentage errors for different tests estimating the length of the steel beam for sensor 1 (located on top of the specimen).....              | 137 |
| Figure 5.15 Percentage errors for different tests estimating the length of the steel beam for sensor 2 (located 1m below the top of the specimen) .....   | 138 |
| Figure 5.16 Percentage errors for different tests estimating the length of the steel beam for sensor 3 (located 1.5m below the top of the specimen) ..... | 138 |
| Figure 5.17 Percentage errors for different tests estimating the length of the steel beam for sensor 4 (located 2m below the top of the specimen) .....   | 139 |
| Figure 5.18 Percentage errors for different tests on the timber beam for Sensor 1(located on top of the specimen) .....                                   | 140 |
| Figure 5.19 Percentage errors for different tests on the timber beam for Sensor 2 (located 1m below the top of the specimen) .....                        | 140 |
| Figure 5.20 Percentage errors for different tests on the timber beam for Sensor 3(located 1.5m below the top of the specimen) .....                       | 141 |
| Figure 5.21 Percentage errors for different tests on the timber beam for Sensor 4(located 2m below the top of the specimen) .....                         | 141 |
| Figure 5.22 Percentage errors for different tests on the timber pole for Sensor 1(located on top of the specimen) .....                                   | 142 |
| Figure 5.23 Percentage errors for different tests on the timber pole for Sensor 2 (located 1m below the top of the specimen) .....                        | 143 |
| Figure 5.24 Percentage errors for different tests on the timber pole for Sensor 3(located 1.5m below the top of the specimen) .....                       | 143 |
| Figure 5.25 Percentage errors for different tests on the timber pole for Sensor 4(located 2m below the top of the specimen) .....                         | 144 |
| Figure 5.26 FRFs of different sensors of (a) free-free and (b) embedded laboratory IE testing of a timber beam with impact from top. ....                 | 146 |
| Figure 5.27 Percentage errors for different tests on steel beam.....  | 147 |

|  |     |
|--|-----|
| Figure 5.28 Percentage errors for different tests on timber beam.....  | 147 |
| Figure 5.29 Percentage errors for different tests on timber pole.....  | 148 |
| Figure 5.30 FRFs of different sensors of (a) free-free and (b) embedded laboratory IR testing of a timber beam with impact from the side.....  | 150 |
| Figure 5.31 Schematic test set-up of embedded BW tests for laboratory testing.....   | 151 |
| Figure 5.32 An example of Raw signals vs SKM plots at specific kernel frequency...   | 152 |
| Figure 5.33 An example of the frequency response function (FRF) from a timber pole under 3rd pull out condition.....   | 152 |
| Figure 5.34 SKM plot at frequency of 725 Hz: Timber pole under 3rd pull out condition.....   | 153 |
| Figure 5.35 Bending wave velocity for different kernel frequencies of 5 m timber pole under different boundary conditions using sensors 1 and 2.....   | 155 |
| Figure 5.36 Bending wave velocity for different kernel frequencies of 5 m timber pole under different boundary conditions using sensors 1 and 3.....   | 155 |
| Figure 5.37 Bending wave velocity for different kernel frequencies of 5 m timber pole under different boundary conditions using sensors 1 and 4.....   | 156 |
| Figure 5.38 Bending wave velocity for different kernel frequencies of 5 m timber pole under different boundary conditions using sensors 2 and 3.....   | 156 |
| Figure 5.39 Bending wave velocity for different kernel frequencies of 5 m timber pole under different boundary conditions using sensors 2 and 4.....   | 157 |
| Figure 5.40 Percentage errors for different kernel frequencies of the timber pole under 1 <sup>st</sup> pull out condition.....  | 158 |
| Figure 5.41 Percentage errors for different kernel frequencies of the timber pole under 3 <sup>rd</sup> pull out condition.....  | 158 |
| Figure 5.42 Percentage errors for different kernel frequencies of the timber pole under 5 <sup>th</sup> pull out condition.....  | 159 |
| Figure 5.43 Acceleration results for all sensors in y direction under free-free condition for 5 m steel beam using Ultraseismic method.....  | 161 |
| Figure 5.44 Acceleration results for selected sensors in y direction under free-free condition for 5 m steel beam using Ultraseismic method (sensors at 0, 1, 1.5 and 2 m from the top)..... | 162 |
| Figure 5.45 Acceleration results for all sensors in y direction under free-free condition for the 5 m timber beam using Ultraseismic method.....   | 163 |

|   |     |
|---|-----|
| Figure 5.46 Acceleration results for selected sensors in y direction under free-free condition for the 5 m timber beam using Ultraseismic method (sensors at 0, 1, 1.5 and 2 m from the top).....       | 164 |
| Figure 5.47 Acceleration results for all sensors in y direction under free-free condition for the 5 m timber pole using Ultraseismic method.....  | 166 |
| Figure 5.48 Acceleration results for selected sensors in y direction under free-free condition for the 5 m timber pole using Ultraseismic method (sensors at 0, 1.5 , 3 and 5m from the top).....       | 167 |
| Figure 5.49 Acceleration results for selected sensors in y direction under 1 layer soil condition for the 5 m timber pole using Ultraseismic method (sensors at 0, 1, 1.5 , 2 and 3m from the top)..... | 170 |
| Figure 5.50 Acceleration results for selected sensors in y direction under 1 layer soil condition for the 5 m timber pole using Ultraseismic method (sensors at 0, 1.5 and 3m from the top).....        | 171 |
| Figure 5.51 Embedded length determination of 5 m timber pole under different boundary conditions using sensors at 0, 1.5 and 3m from the top.....   | 173 |
| Figure 5.52 Schematic set up for intact and damaged timber pole in laboratory.....  | 174 |
| Figure 5.53 Acceleration results for an intact and damaged timber pole under free-free condition for sensor 3.....  | 174 |
| Figure 5.54 Acceleration results for an intact and damaged timber pole under free-free condition for sensor 4.....  | 174 |
| Figure 5.55 Test set-up of embedded testing in Mason Park.....  | 175 |
| Figure 5.56 FFT result of the timber pole with 1 m of embedment.....  | 176 |
| Figure 5.57 FFT result of the timber pole with 1.5 m of embedment.....  | 176 |
| Figure 5.58 FFT result of the timber pole with 2 m of embedment.....  | 176 |
| Figure 5.59 Velocity calculation of pole 8 with 1m embedded length .....  | 177 |
| Figure 5.60 Velocity calculation of pole 14 with 1.5m embedded length .....   | 177 |
| Figure 5.61 Velocity calculation of pole 1 with 2m embedded length .....  | 177 |
| Figure 5.62 Percentage errors for different sensors estimating the length of the timber pole for 1 m embedment .....  | 178 |
| Figure 5.63 Percentage errors for different sensors estimating the length of the timber pole for 1.5 m embedment .....  | 179 |

|  |     |
|--|-----|
| Figure 5.64 Percentage errors for different sensors estimating the length of the timber pole for 2 m embedment .....                         | 179 |
| Figure 5.65 Acceleration results for all sensors in y direction under 1m embedment using Ultraseismic method (Pole 8) .....                  | 181 |
| Figure 5.66 Acceleration results for all sensors in y direction under1.5m embedment using Ultraseismic method (Pole 14) .....                | 182 |
| Figure 5.67 Acceleration results for all sensors in y direction under1.5m embedment using Ultraseismic method (Pole 1) .....                 | 183 |
| Figure 5.68 Percentage errors for different embedment conditions estimating the length of the timber pole using ultraseismic method .....    | 184 |
| Figure 5.69 Test set-up for free-free testing of field testing in Horsham, (a) impact from the side, (b) impact from the end .....           | 185 |
| Figure 5.70 FFT result of the timber pole under free-free condition (Pole3-293) impact from location 3(at the top).....                      | 186 |
| Figure 5.71 FFT result of the damaged timber poles under free-free condition (Pole288, 183 and 299) impact from location 3(at the top).....  | 187 |
| Figure 5.72 Acceleration-time history of timber pole under free-free condition (Pole293) impact from location 3(at the top).....             | 188 |
| Figure 5.73 Acceleration-time history of timber pole under free-free condition (Pole288) impact from location 3(at the top).....             | 188 |
| Figure 5.74 FFT result of the timber pole under free-free condition (Pole293) impact from location 1(at the middle).....                     | 189 |
| Figure 5.75 FFT result of the timber pole under free-free condition (Pole 288) impact from location 1(at the middle).....                    | 189 |
| Figure 5.76 Results of the timber pole under free-free condition using Ultraseismic method (Pole293) impact from location 3(at the top)..... | 190 |
| Figure 5.77 Results of the timber pole under free-free condition using Ultraseismic method (Pole288) impact from location 3(at the top)..... | 191 |
| Figure 6.1 a) Stable case b) Unstable case.....  | 198 |

## List of Tables

|   |     |
|---|-----|
| Table 2.1 Estimated quantities of poles in-service throughout Australia in 2004 (Kent 2006) .....   | 9   |
| Table 3.1 Material properties used in the FE model .....  | 54  |
| Table 3.2 Length determination of a 5m timber pole under different embedded lengths using the first four sensors with Sonic Echo test ..... | 66  |
| Table 3.3 Material properties used in guided wave solution (Subhani 2013).....  | 78  |
| Table 3.4 Decay pattern type 1 modelling using FE .....   | 84  |
| Table 4.1 Field test details .....  | 112 |
| Table 4.2 Timber pole classifications based on the existing defects at Horsham.....   | 113 |
| Table 4.3 Defect description of different timber poles at Horsham.....  | 116 |
| Table 5.1 The coefficient of variation of the velocity calculation for repeated tests of steel beam under different conditions. ....        | 130 |
| Table 5.2 The coefficient of variation of the velocity calculation for repeated tests of timber beam under different conditions. ....       | 131 |
| Table 5.3 The coefficient of variation of the velocity calculation for repeated tests of timber pole under different conditions.....        | 132 |
| Table 5.4 Calculation of Characteristic Impedance for different materials .....   | 135 |
| Table 5.5 Timber pole classifications based on the existing defects at Horsham.....   | 186 |



# CHAPTER 1

## 1 INTRODUCTION

### 1.1 BACKGROUND

Round timber poles are used extensively for utility poles by electrical distribution and telecommunications industries in Australia as well as in many other countries. There are more than 5 million utility timber poles used in the Australia's energy network for distribution of power and communications. Anecdotal evidence suggest that more than 70% of timber poles are installed after the end of World War II and these poles are likely to require replacement or remedial maintenance in the future. While the other countries are facing same challenges to ensure the optimum management of extensive pole replacement, Australian timber pole inquiries are also facing critical pole supply shortages.

When life cycle cost is considered, timber poles are considerably less expensive than other alternative materials such as steel, concrete or fibreglass-reinforced plastic composite materials. In addition, non-timber poles have different conductive and strength properties and often require different fittings. While alternative materials may be practical to be used for manufactured poles, the cost to completely replace timber poles is most likely to be prohibitive. In addition, timber poles have considerable environmental advantages compared to the other materials. Less energy is required to produce timber poles and significantly less greenhouse gasses are produced.

Lack of reliable information concerning their in-service condition, including the degree of deterioration or damage below ground level makes it extremely difficult for the asset managers to make decisions on the replacement/maintenance process with due consideration to economy, operational efficiency, risk/liability and public safety. While there are a number of techniques used to prevent deterioration and decay (from a combination of insects and fungi) of timber piles/poles, a widespread practice is to simply replace all the piles at regular time intervals. This practice for replacement is

currently based on traditional methods of determining a timber poles condition by visual inspection and sounding. Unfortunately, this method is not accurate and in many cases relies on interpretation of information and measurable parameters which leads to unnecessary replacement of the piles/poles. For example, each year around 30,000 electricity poles are replaced in the eastern states of Australia, despite the fact that up to 80% of these poles are still in a very good serviceable condition. In addition, accurately determining the timber properties is challenging due to existence of anisotropy and inhomogeneity of natural timber with decay and deterioration adding to complications of determining the embedded length and condition of timber poles.

Visual inspection, sounding and coring are the current methods of timber pole condition used all around the world as well as in Australia. These methods do not give an adequate indication of pole condition. A need has been developed for a method that produces more quantitative results. A non-destructive testing procedure for the determination of timber pole condition has become necessary.

Different types of Non Destructive Testing (NDT) methods were developed in the past and used to evaluate the embedment depth and the quality of materials of embedded structures such as concrete piles. Some of these tests have also been utilised on timber piles or poles. Despite development of various types of NDT methods for evaluating the embedment depth and below ground quality of piles, especially for timber structures and foundations, analysis of results is not straightforward and there is a pressing need to develop reliable methods that adequately consider the inherent variability of the materials, complexities of unknown geological conditions and interactions between the structure/foundation and the soil (Davis 1994). When it comes to field applications, these developed/to be developed surface NDTs face a significant challenge due to presence of uncertainties such as complicated material properties (e.g. timber), environmental conditions, interaction of soil and structure, defects and deteriorations as well as coupled nature of unknown length and condition. Moreover, due to the dispersive nature of the stress wave propagation which is related to the types of the wave (especially shear wave & surface wave) and wave modes, many frequency components exist in the measured signals and each frequency component corresponds to an individual phase velocity.

NDTs utilising stress wave for determination of the unknown depth of foundations and defects of piles/poles can be divided into two groups: Surface NDT, if access is required only at the surface of the testing structures, or Borehole NDT, if a borehole is drilled close to the foundation structure and extends along its length. Considering the cost/benefit, complexity and applicability in the field, the NDT to be considered in this research will be limited to the surface methods. Therefore, the current available NDTs relevant to this research are Sonic Echo (SE) method, Impulse Response (IR) method (based on longitudinal waves), Bending Wave (BW) method (based on flexural waves) and, Ultraseismic (US) method (based on longitudinal and flexural waves).

This Research involves full scale investigations for use of selected NDT methods for identification of condition and in-ground length of embedded timber poles through finite element (FE) modelling, laboratory experiments and field testing. The project provides comprehensive evaluation of the selected NDT methods in terms of reliability, accuracy and quantifying limitations for timber poles. In addition, the research will provide guidelines for implementation of these NDT methods including any necessary improvements of the methods and their analysis and application on timber materials.

## **1.2 RESEARCH SCOPE**

This research is concerned with the development and use of robust and cost effective surface NDTs for length determination and condition evaluation in timber pole/pile structures. The scope of this study is limited to the following areas:

1. The investigation and application of existing non-destructive methods used for timber pole/pile applications.
2. The development and understanding of the complexities of the stress wave generation in different Non-Destructive Testing methods
3. The investigation of surrounding environment, including soil embedment, that influences the performance of current and proposed methods, especially those associated with field applications.
4. The investigation of analysis techniques such as Short Kernel method for improvement of reliability and accuracy of length determination and damage detection.

5. The numerical verification of selected NDTs to gain understanding of stress wave propagation in timber poles without any uncertainties related to experimental testing.
6. The experimental and field validation of selected NDTs with laboratory and in field structures.

### **1.3 RESEARCH OBJECTIVES**

The literature study suggests that there are very limited research conducted in surface wave based NDT on pole applications while applications on piles are rather field practice- driven from practicing engineers and consultants which are based on the methods developed few decades ago.

The aim of this research is to apply selected NDT methods to evaluate condition and underground-embedded length of the piles/poles considering the interaction between soil and piles/poles as well as deterioration and defects of the piles/poles. The capabilities and limitations of employing advanced signal processing methods are investigated using numerical and experimental and field studies. The specific objectives of this research work are:

1. To conduct laboratory investigations to evaluate and assess the current NDT techniques in terms of reliability, accuracy and limitations, with the following objectives:
  - To develop an understanding of the complication on timber material including its damage/defect and needs for developing appropriate models to adequately reflect such complexity
  - To develop an understanding of the stress wave propagation of a longitudinal and dispersive bending wave using multiple sensors
  - To investigate the applicability of the practical proposed procedures on laboratory to induce stress waves by impacting a pole aside at a reachable height above ground level
  - To investigate the impact of the environment including soil embedment and needs for incorporating such factors in modelling and signal processing
  - To study selected advanced signal processing methods for pole condition and embedded length determination

- To improve the surface NDT methods in current practice for determining the embedded length and condition of the timber poles
2. To develop finite element models to investigate different NDT testing methods for stress wave velocity calculation and length determination.
    - To simulate stress wave propagation in in timber utility pole to obtain data and to gain understanding of wave behaviour. To apply the proposed methods to develop understanding of the complications on generated waves modes
    - To investigate the effects of various boundary conditions i.e. traction-free and embedded condition independently in FE modelling
    - To investigate and modify signal processing approaches to deal with the complication of wave generation such as SKM method
  3. To conduct field investigations to validate, experimentally, the modified methods:
    - To investigate the applicability of the practical proposed procedures in laboratory to induce stress waves by impacting a pole on its side at a reachable height above ground level by an angled wave guided hammer.
    - To investigate the impact of in-situ environmental conditions and related uncertainties including soil embedment and needs for incorporating such factors in modelling and signal processing

## **1.4 SUMMARY OF CONTRIBUTIONS**

The principal contribution of this study is the development of appropriate Non-destructive testing methods to determine the embedded length and to evaluate the condition of timber poles and identify the limitation and some improvements to increase the accuracy of outcomes. The original contributions of this research work will, therefore, include:

From literature review, it is clear that there are only few works reported on using surface non-destructive techniques to determine the embedded length and evaluate damage in timber structures. Therefore, in this study, existing non-destructive methods are examined for length determination and condition assessment of a timber pole and to gain an understanding of the generated waves/wave modes by impacting a pole on its

side at a reachable height above the ground level by an angled wave guided hammer. In addition, changes in geotechnical and boundary conditions and interference of other media on determination of length and evaluation of condition of timber poles are considered.

1. From numerical analysis, it is found that stress wave velocity will decrease with increase in embedded length. Therefore, two different velocities, one for stress wave travelling above the soil level and one travelling inside of the soil is calculated. By increasing the soil depth, the error of the length estimation is increased. Indeed, considering timber pole as an isotropic material, leads to a maximum error of 8% for length determination under embedded conditions using multi sensors for velocity calculation.
2. Investigating the effects of three different specimens including a hollow section steel beam, a rectangular timber pole and an actual timber pole on the results of NDT methods by conducting experimental tests. The results show that the standard derivation of the velocity estimation in a timber pole is relatively higher than steel beam and more uncertainties are involved in stress wave propagation in timber material.
3. Considering a parametric study, including both experimental and field investigations to evaluate the selected NDTs in terms of reliability, accuracy and limitations, for determination of embedded length of poles below the ground level. For the Sonic Echo test, the scatter of the averaged error for length determination of pole specimens associated with different test conditions ranged between 1% and 20% for most testing conditions.
4. Investigating the SKM method to purpose a guidelines to select the appropriate kernel frequency to calculate the phase velocity and determine the embedded length of timber pole.
5. Based on the experimental results, the kernel frequency between 400-800 Hz was identified to use in SKM method for phase velocity calculation. Using the SKM to estimate the length of the pole using Bending Wave method on a 5m timber pole under different pull out conditions show the percentage of error for all boundary conditions to be between -10.5% and 0%.

6. Providing guidelines for implementation of suggested NDT methods for utility timber poles including recommendations for any necessary improvements of the methods.
7. Ultraseismic method is considered for stress wave velocity estimation of timber pole impact at the top. According to the results, using sensors close to impact location (up to 2-3m) will result in good estimation of the velocity.
8. By considering the relatively good and damaged pole in the field, it is found that severe termite damage can be identified by the irregular pattern of FFT from impact timber pole signals. This can be used to classify which timber poles are required to be replaced in the field.

## **1.5 OUTLINE OF THE THESIS**

This thesis consists of six main chapters, organised as follows:

Chapter 1 presents an introduction to the work, the objectives of the study, the scope of the work and the contribution to knowledge.

Chapter 2 outlines a literature review and a brief history of timber pile/poles in Australia and application of different non-destructive test techniques used for determining length and condition of timber piles/poles. In addition, this chapter provides the theoretical background for stress wave propagation used to evaluate properties of stress wave propagation. It also covers classification of different wave types including relevant characteristics of those wave types.

Chapter 3 deals with developing finite element models that can represent the real structures well including, intact and damaged timber poles and piles, respectively. It covers the details of tests and influence of different types of damage on the results.

Chapter 4 describes the test procedures and test equipment used in the experimental and field testing. The overview of the test specimens, experimental set up and damage scenarios are presented in this chapter. Different types of tests are discussed and the proposed signal processing methods are used to identify the length and evaluate the condition.

In the longitudinal and flexural impact method, a stress wave is generated with an impact from a modal hammer. In both cases, the responses are measured with accelerometers. For both methods, the input and response are recorded with a program coded in the LabVIEW programming language. The measured results are filtered to remove portions of the signal for which the frequency content lies outside the frequency range of the input. The time-varying frequency content of the flexural method is analysed by the Short Kernel Method (SKM). The process of damage pattern recognition is discussed later.

Chapter 5 presents the results of longitudinal and lateral impact tests performed on the experimental and field testing under traction-free conditions and embedded conditions to verify the applicability of the longitudinal and flexural wave theory presented in Chapter 2. A longitudinal wave has been induced by a hammer impact to the top of the pole and a flexural wave is induced by a hammer impact to the side of the pole, and the response is measured by means of triaxial accelerometer. The accelerometer was mounted to the side of the pole. The results are analysed to determine the stress wave and embedded length of three different specimens; a steel beam, a timber beam and a timber pole.

Chapter 6 summarises the work presented in this thesis and presents conclusions regarding the applicability of non-destructive testing methods on timber utility poles and draws conclusions and gives recommendations for future work.



# CHAPTER 2

## 2 LITERATURE REVIEW

### 2.1 TIMBER POLES IN AUSTRALIA

Timber utility poles play a significant role in Australia's infrastructure, which have been taken for granted (Crews & Horrigan 2000). Those timber poles are used extensively as utility poles by electricity distribution and telecommunications industries. According to (Kent 2006) there are more than 5 million utility timber poles currently in-service throughout Australia's energy networks (Table 2.1).

*Table 2.1 Estimated quantities of poles in-service throughout Australia in 2004 (Kent 2006)*

| <b>State / Territory</b>           | <b>Timber</b> | <b>Concrete</b> | <b>Metal</b> | <b>Other</b> | <b>State Total</b> |
|------------------------------------|---------------|-----------------|--------------|--------------|--------------------|
| New South Wales (NSW)              | 2,055,651     | 93,398          | 40,229       | 400          | 2,189,678          |
| Queensland (Qld.)                  | 1,260,042     | 35,951          | 27,764       | 0            | 1,323,757          |
| Victoria (Vic.)                    | 823,934       | 265,282         | 21,949       | 5,370        | 1,116,535          |
| South Australia (SA)               | 0             | 78              | 211          | 655,763      | 656,052            |
| Tasmania (Tas.)                    | 194,451       | 46              | 7,108        | 6,868        | 208,473            |
| Western Australia (WA)             | 681,536       | 12,334          | 20,808       | 0            | 714,678            |
| Northern Territory (NT)            | 0             | 95              | 38,125       | 0            | 38,220             |
| Australian Capital Territory (ACT) | 50,098        | 7,031           | 2,758        | 375          | 60,262             |
| Total                              | 5,065,712     | 414,215         | 158,952      | 668,776      | 6,307,655          |

Based on the review of Australian Timber Pole Resources for energy networks conducted by (Francis & Norton 2006), many of the currently installed timber poles are likely to require replacement or remedial maintenance over the next decade. Based on the cost assumption of \$500 for a new timber pole, 1.75 billion dollars would need to be invested to achieve 3.5 million replacement timber poles that may soon be required. Additionally, poles are required for new lines, costing 13.5 million dollars per annum with the assumption of constant demand at half of the total demand by utilities in 2005

in future years. Furthermore, Australian timber pole stakeholders are facing a critical pole supply shortage.

Although using alternative materials may be practical in some locations, the cost to completely replace timber poles is likely to be prohibitive. Considering the whole life cycle costs, timber poles are considerably less expensive than most manufactured alternative poles made of steel, concrete or fibreglass-reinforced composite materials. Moreover, non-timber poles have different conductive and dynamic strength properties and require different fittings.

Timber poles produced from sustainably-managed forests are a renewable resource, and in addition to economic benefits, life cycle analyses show that timber poles have considerable environmental advantages compared with poles constructed from more energy intensive manufactured materials. Analyses, accounting for raw material production, treatment, installation, inspection, maintenance and disposal, have highlighted that considerably less energy is required to produce timber poles and significantly less greenhouse gasses are therefore, produced.

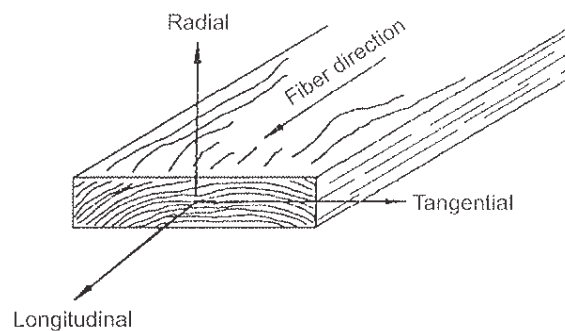
The major disadvantages of using timber poles are the current supply shortage, their shorter service-life, the necessity for more regular maintenance and the need for recycling industries to continue to be established and preservative recovery technologies to be fully optimised.

Because the timber is a natural material, their properties could not be controlled by manufacturing or such and these properties exhibit inherent variability. The presence of natural defects such as knots, splits, and checks, and the wide diversity of species available for various end uses, add to this variability.

Wood may be described as an orthotropic material. It has unique and independent mechanical properties in the directions of three mutually perpendicular axes: longitudinal, radial, and tangential. The longitudinal axis is parallel to the fibre; the radial axis is normal to the growth rings (perpendicular to the grain in the radial direction); and the tangential axis is perpendicular to the grain but tangent to the growth rings. These axes are shown in Figure 2.1. In wood, the speed of sound varies with grain direction because the transverse modulus of elasticity is much less than the longitudinal value. The speed of sound across the grain is about one-fifth to one-third of the

longitudinal value (Green, Winandy & Kretschmann 1999). The speed of sound decreases with increasing temperature or moisture content in proportion to the influence of these variables on the modulus of elasticity.

The structural properties of a wood member depend not only on its orientation when cut from a log, but also on its distribution, size and shape of the strength-reducing characteristics within the piece. The environmental conditions in which wood is used are very important because moisture content of the wood dramatically affects its mechanical properties and its susceptibility to degradation by decay (Falk, Patton-Mallory & McDonald 1990).



*Figure 2.1 Three principal axes of wood with respect to grain direction and growth rings (Green, Winandy & Kretschmann 1999)*

## **2.2 TYPES OF DEGRADATION AND LOCATION OF TIMBER PILES AND UTILITY POLES**

Timber poles acts as simple cantilever beams and/or slender columns. According to Rural Utilities Service construction standards, these poles may have a maximum line angle of 5 degrees (Stockton 2003). Because tangent poles are not to be located at a sharp angle turn in the line, they typically resist only the forces due to wind, ice, gravity, and the forces from unbalanced tension in the conductors or other utility wires. For some poles, In addition to horizontal forces and their resulting moments caused by wind and vertical forces from permanent actions, poles must resist loads in both horizontal and vertical directions due to guywires. Therefore, they should have sufficient embedded length to resist against those forces. Some of the utility poles

installed in the past, lack any available information regarding the depth of the utility poles. On the other hand, timber materials are subjected to environmental attacks including weather, age and even moisture. But the main damage occurring around the ground line are associated with where conditions suitable for the growth of fungi. (Nguyen, Foliente & Wang 2004) suggested four typical decay patterns of a timber pole's cross section below the ground line as illustrated in Figure 2.2.

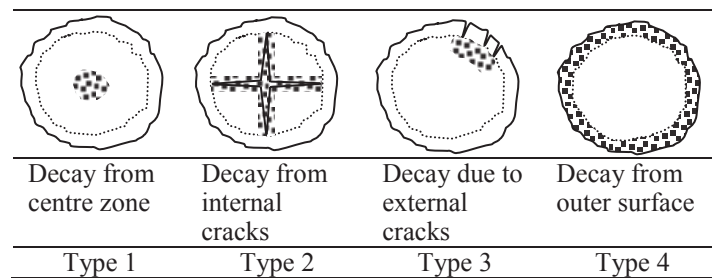


Figure 2.2 Possible decay patterns in underground sections of utility poles (Nguyen, Foliente & Wang 2004)

## 2.3 CONVENTIONAL METHODS FOR ASSESSMENT OF TIMBER STRUCTURES

Currently used inspection methods for timber poles involve visual inspection, which cannot determine the extent of deterioration in timber structures accurately. There are factors affecting the cross sectional area of a timber pole or pile which are the duration of exposure to weathering and fungi.

### 2.3.1 Visual inspection method

The simplest method and the first step towards locating deterioration is visual inspection. The inspector observes the structure for signs of actual or potential deterioration, noting areas for further investigation. Visual inspection requires strong light and is useful for detecting intermediate or advanced surface decay. Visual inspection cannot detect decay in the early stages, when remedial treatment is most effective, and should never be the sole method used (Ross et al. 1999).

### **2.3.2 Probing**

Probing with a moderately pointed tool, such as an awl or knife, locates decay near the wood surface as indicated by excessive softness or a lack of resistance to probe penetration and the breakage pattern of the splinters. A brash break indicates decayed wood, whereas a splintered break reveals sound wood. Although probing is a simple inspection method, experience is required to interpret the results. Care must be taken to differentiate between decay and water-softened wood that may be sound but somewhat softer than dry wood. It is also sometimes difficult to assess damage in soft-textured woods such as western red cedar (Ross et al. 1999).

### **2.3.3 Sounding**

Sounding the wood surface by striking it with a hammer or other objects is one of the oldest and most commonly used inspection methods to detect interior deterioration. Based on the tonal quality of the ensuing sounds, a trained inspector can interpret dull or hollow sounds that may indicate the presence of large interior voids or decay. Although sounding is widely used, it is often difficult to interpret the results because conditions other than decay can also contribute to variations in sound quality. In addition, sounding provides only a partial picture of the extent of decay present and will not detect wood in the early or intermediate stages of decay. Nevertheless, sounding still has its place in the inspection process and can quickly identify seriously decayed structures. When suspected decay is encountered, it must be verified by other methods such as boring or coring. Practical experience has shown that sounding only works with members less than 89 mm (3.5 in.) thick (Ross et al. 1999).

### **2.3.4 Drilling and coring**

Drilling and coring are the most common methods used to detect internal deterioration in wood members. Both techniques are used to detect the presence of voids and determine the thickness of the residual shell when voids are present. Drilling and coring are similar in many respects and are discussed together. Drilling is usually done with an electrical power drill or hand-crank drill equipped with a 9.5- to 19-mm- (3/8- to 3/4-in.-) diameter bit. Power drilling is faster, but hand drilling allows the inspector to monitor drilling resistance and may be more beneficial in detecting pockets of deterioration. In general, the inspector drills into the member in question, noting zones

where the drilling becomes easier, and observes the drill shavings for evidence of decay. The presence of common wood defects, such as knots, resin pockets, and abnormal grain, should be anticipated while drilling and should not be confused with decay

## **2.4 NON-DESTRUCTIVE EVALUATION METHODS FOR TIMBER STRUCTURES**

By definition, non-destructive materials evaluation is the science of identifying physical and mechanical properties of a piece of material without altering its end-use capabilities. Such evaluations rely upon non-destructive testing (NDT) techniques to provide information about properties, performance, or condition of the material in question (Ross & Pellerin 1994).

Traditionally, NDT methods have been developed for sorting and grading of wood products in wood industry. Then, it was used in the evaluation of wood in structures due to increase in the amount of resources being devoted to repair and rehabilitation of existing structures.

In these methods, the waves traveling in a structure (Wang, Chang & Finno 2011) and the wave velocity is a function of frequency, and displacement that may be different along the structural element. Many researchers have studied these waves to establish new formulas and concepts regarding their properties and use (Finno, Chao & Lynch 2001; Lynch 2007b; Wang, Chang & Finno 2011). In a study, laboratory and field timber piles have been tested for non-destructive dispersive wave propagation (Chen & Kim 1996). The results of this study show that this test is to examine the extend of deterioration and border damage in timber piles. There are conditions for this evaluation, which are the comparison of the phase velocity between the first and return pass; and wave speed versus test location.

NDTs which use surface reflections have been used to work out the length and defects in poles and piles. The most widely used techniques are: Sonic echo and impulse response methods, which are both, based on longitudinal wave propagation.

## **2.5 STRESS WAVE TESTING BASED METHODS**

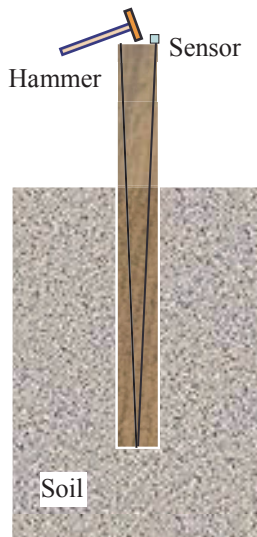
Stress waves are generated from striking the specimen with an impact on the surface of the material under investigation. The stress waves propagate through the material and reflect from external surfaces, internal flaws, and boundaries between adjacent materials. Reflections are identified as increase in response of acceleration-time history or velocity-time history or as peaks in the acceleration spectrum or velocity spectrum. The most common method of utilizing stress waves is the time it takes for a stress wave to travel a specified distance. If the material dimensions are known, stress wave timing can be used to locate decay in timber members. Since stress waves travel slower through decayed wood than sound wood, the localized condition of a member can be determined by measuring stress wave time at incremental locations along the member ((Kasal, Lear & Tannert 2011), (Emerson et al. 1998)). Depending on the strike direction of the specimen and the method for analysis of the results, the stress wave testing is categorised under Sonic Echo and Impulse Response method. These two methods have been used for over 30 years for deep foundation and specially for concrete materials (Davis & Robertson 1975) (Finno & Gassman 1998; Gassman & Finno 2000).

### **2.5.1 Sonic Echo (SE) method**

Sonic Echo (SE) test is performed to evaluate the integrity of the pole / pile material and determine the length of deep foundations. It requires measurement of the travel time of seismic waves in the time domain. The reflection of longitudinal compression waves from the bottom of the tested structural element or from a discontinuity such as a crack or a termite void is measured for identification of embedment length or detection of damage.

In traditional SE testing, a small impulse (usually generated by an impact hammer) is delivered at the head centre of the test structure (e.g. foundation or pole). This impact generates longitudinal compression waves, which travel down the structure until a change in acoustic impedance (a function of velocity, density and changes in diameter) is encountered. At this point, the wave reflects back and is recorded by a receiver placed next to the impact point as shown in Figure 2.3. The amplitude and time of the hammer impact will be recorded along with measurements of the time travel of the longitudinal waves by sensors located in the proximity to the impact point. According to (Sansalone

& Carino 1986), the hammer produce a maximum frequency equal to the inverse of the duration of the impact.



|  |
|--|
| <p>Impact:</p> <ul style="list-style-type: none"> <li>- Longitudinal impact from centre top of structure (impact from side possible with rigidly attached bracket)</li> </ul> <p>Measurements:</p> <ul style="list-style-type: none"> <li>- Time of impact</li> <li>- Longitudinal response of the structure</li> </ul> <p>Data analysis:</p> <ul style="list-style-type: none"> <li>- Time domain analysis of longitudinal signals</li> </ul> |
|--|

Figure 2.3 Schematic principle of SE testing

The recorded measurements are used to determine the length of the structure based on the time separation between the first arrival and the first reflection (echo) event or between any two consecutive reflection events ( $\Delta t_{WEcho\_SE}$ ) according to:

$$OL_{SE} = TL_{SE} + V_{SE} * \frac{\Delta t_{WEchoSE}}{2} \quad (2.1)$$

where  $OL_{SE}$  is the overall length of the structure,  $TL_{SE}$  the measured distance between the specimen's top and the sensor location and  $V_{SE}$  the velocity of longitudinal waves. Defects or any other types of damage can be recognised by multiple/early wave echoes (wave reflections from damage) that appear in the measured time-history data. Hence, when the length of the structure is known, an early arrival of the reflected wave means that it has encountered a reflector (change in stiffness or density) other than the bottom of the structure.

### 2.5.2 Impulse response method

The Impulse Response (IR) method (termed also as Sonic Transient Response, Mobility, Transient Dynamic Response and Sonic method) was developed as an



extension to a technique originally proposed by (Davis & Dunn 1974). Similar to the SE method, the IR method is based on the time travel of longitudinal waves generated by an impact force executed from the top centre of a structure. With the IR method, embedment length of foundations/poles can be determined and damage detected. Whereas the SE method processes measured data in the time domain, the IR method operates in the frequency domain.

The test set-up, equipment and testing procedure of the IR method are identical to the SE method with the only difference being that the impact force of the modal hammer must be recorded during testing. The schematic principle of IR testing is illustrated in Figure 2.4.

(Gassman & Finno 2000) identified limits of the IR method, such as the cutoff frequencies caused by the presence of intervening structures on the drilled shafts at the National Geotechnical Experimental Site (NGES) at Northwestern University were evaluated non-destructively before and after construction of the caps and resolution as a function of length to diameter ratio ( $L/D$ ) and soil type ((Finno & Gassman 1998)). (Gassman & Finno 1999) provided some improvements to the IR method such as using the multiple geophone approach applied to the drilled shafts.

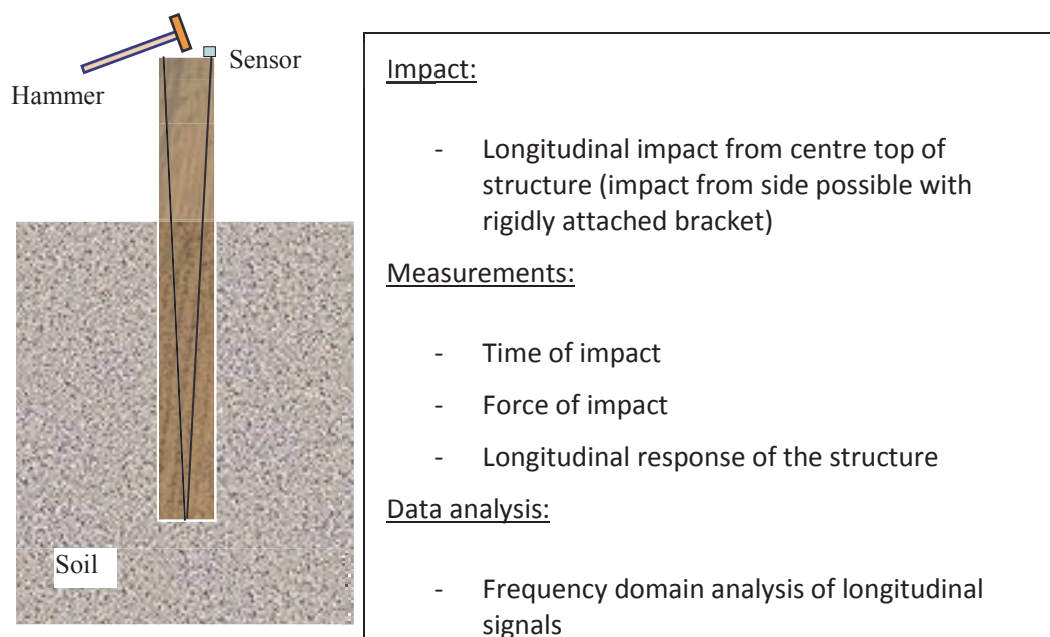


Figure 2.4 Schematic principle of IR testing

To estimate the length and soundness of the test structure, the measured signals are converted into the frequency domain and the corresponding Frequency Response Functions (FRFs) are determined. By analysing the FRFs, the length can be calculated according to the following equation:

$$OL_{IR} = TL_{IR} + \frac{V_{IR}}{2*\Delta f_{IR}} \quad (2.2)$$

where  $OL_{IR}$  is the overall length of the structure,  $TL_{IR}$  the measured distance between the specimen's top and the sensor location,  $V_{IR}$  the velocity of longitudinal waves and  $\Delta f_{IR}$  the distance between two peaks in the FRF. When the length of the test structure is known, a shorter apparent length measurement will indicate the presence of anomaly/damage.

In IR testing, the recorded impact force of the hammer (measured in force time-history) and the response of the structure (measured in acceleration time-history) are transformed into the frequency spectra using Fast Fourier Transform (FFT). By dividing the frequency spectra signals of the response data by the frequency spectra of the excitation data, FRFs are obtained. To estimate the length and soundness of the test structure, the FRFs are analysed and distances between two adjacent frequency peaks ( $\Delta f_{IR}$ ) are determined. Further, it is necessary to calculate the wave velocity. Following equation 2.2, the length of the test specimen can be calculated.

When the stress wave velocity and pile length are both unknown, the interpretation of results can become especially difficult. It can be difficult to locate defects that are located near the toe as these defects produce reflections that could easily be interpreted as the toe itself. The hammer impact causes Rayleigh waves to propagate along the shaft surface and makes it difficult to detect defects close to the shaft head (Hanifah 1999).

To detect a small defect, high frequency compression waves are required. However, according to (Hearne, Reese & Stokoe 1981), the wavelength should not be less than the shaft diameter or the assumption of one dimensional stress will not hold and reflection will occur from the shaft boundaries.

### 2.5.3 Bending Wave method

As the top of deep foundation or pole not always accessible, the Bending Wave (BW) method is introduced to evaluate the foundation non-destructively if the side of the structure/foundation could be accessible. The Bending Wave (BW) method uses flexural (bending) waves, rather than the longitudinal waves used in the SE and IR method, to determine integrity and unknown depth of deep foundations. This method is based on the propagation of flexural waves that are highly dispersive in nature. The flexural wave velocity decreases with increasing wavelength, with most of the velocity decrease occurring at wavelengths that are longer than the pole diameter. To determine the length of a structure (e.g. timber pile or pole) by means of flexural wave propagation, dispersive analysis is required in which wave data is extracted from a selected group of frequencies. These frequencies are analysed for the individual time required to travel to one end of the structure and back.

The traditional BW method involves striking the test structure on its side and recording the structural response by sensors placed on the same side of the structure as the impact location (see Figure 2.5). Thereby, the method is potentially useful in case where the top of the structure is obscured.

The problem of bending wave propagation in cylinders was first investigated in terms of elastic equations by (Chree 1889). Various details of the derivation can be found by (Love 2013), (Kolsky 1963) and (Wasley 1973). The solution describes the motion of a wave of infinite duration traveling along a cylinder of constant diameter. The cylinder is composed of a homogeneous, isotropic, linearly elastic material. The solution yields expressions for both phase and group velocities of flexural waves. (Kolsky 1963), (Hudson 1943) produced graphs showing the relationship between the ratio of the cylinder's radius to the wave length of the wave for a given value of Poisson's ratio for the material. Since the frequency equation consists of Bessel functions, there are infinite number of solutions to the problem as discussed by (Abramson 1956). This means there are an infinite number of branches present in a cylinder's dispersion field. This infinite number of branches indicates that any single frequency can possess more than one velocity. The general elastic equation have not been solved for transient bending wave motion in a tapered cylinder of finite length. Neither have they been solved for a tapered cylinder composed of an orthotropic material (Holt 1996a).

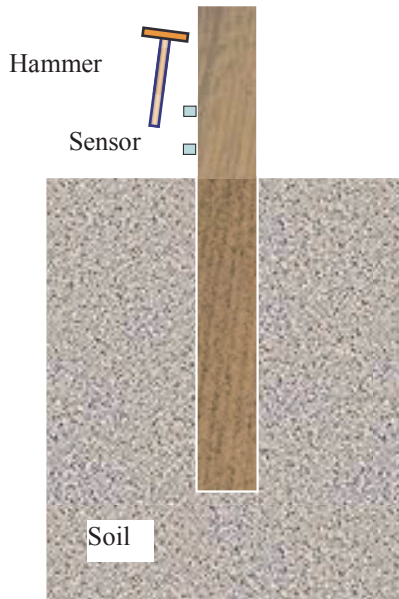
To calculate the length of a structure, the BW method requires special signal processing techniques, such as Short-Kernel Method (SKM) analysis (Holt 1996b) (Holt, Shunyi & Douglas 1994) (Hughes, Rix & Jacobs 1998) or flexural wave identification (FWI) method (Finno, Chao & Lynch 2001). In Short kernel method, as proposed by (Holt 1996b), the so-called phase velocity of wave travel is determined, which is the velocity associated with a particular frequency. From SKM plots, one can identify the initial wave arrivals and subsequent reflections (echoes), and calculate the depths and locations of the reflection events. In the SKM analysis, one or more cycles are used as “Kernel Seed” in order to cross-correlate with a number of seed frequencies between 500-4000 Hz.

In the BW method, the response is measured with two accelerometers mounted along the side of the pile. The group velocity is computed from the spacing between the accelerometers and time lag between the first arrivals at the two accelerometers. Reflections are identified from the first pass and return to both accelerometers.

In the bending wave method proposed by (Holt, Shunyi & Douglas 1994) (Holt 1996b), the response is measured with two accelerometers and the results are interpreted by isolating one phase of the wave, i.e., one frequency, and identifying the return of the reflected phase. The details of this method are provided later in this section.

In the bending wave method proposed by (Hughes, Rix & Jacobs 1998), evaluation of a deep foundation consisted of multiple tests in which the response was measured with one accelerometer, but the accelerometer was placed in a different position for each test.

(Chao 2002) installed a set of full size intact and damaged drilled shafts at the National Geotechnical Experimental Site (NGES) at Northwestern University and evaluated the shafts non-destructively to determine the dynamic properties and deep foundation by using flexural wave evaluation.



Impact:

- Transverse impact from side of the structure

Measurements:

- Time of impact
- Force of impact
- Transverse response measured by at least two sensors mounted to the same side of the structure as the impact

Data analysis:

- Short-Kernel Method applied to transverse signals

*Figure 2.5 Schematic principle of Bending Wave testing*

In BW testing, the acquired time-history signals of the impact hammer and the sensors are first transformed into the frequency domain to calculate corresponding Frequency Response Functions (FRFs). From FRF analysis, the central frequencies of the signals are determined and the SKM kernel for a frequency equal to, or greater than, a central frequency is formed for each sensor signal. From SKM plots of two sensors, characteristic features (positive or negative amplitude peaks) that are visible in both SKM plots are located and the amount by which this feature has shifted in time between the two sensors is determined. This time shift is then used to compute the frequency's phase velocity according to:

$$V_{BW} = \frac{\Delta L_{BW}}{N_{pts} * \Delta t_{WTravel-BW}} \quad (2.3)$$

where  $V_{BW}$  is the phase velocity of the frequency from which the kernel is formed,  $\Delta L_{BW}$  the distance between the two sensors,  $N_{pts}$  the number of data points by which the feature (peak) has shifted between the two sensors and  $\Delta t_{WTravel-BW}$  the time step in which the time records are stored. The length of a test structure is determined by identifying significant positive or negative amplitude peaks (features) of the first arrival and the returning signals (reflections/echoes from an end of the specimen) in the SKM plot of a single sensor signal. By determining the time difference between the peak of

the first signal and its corresponding peak in the return wave, the overall length of the structure can be calculated following:

$$OL_{BW} = TL_{BW} + V_{BW} * \frac{N_{pts} * \Delta t_{WEcho-BW}}{2} \quad (2.4)$$

where  $OL_{BW}$  is the overall length of the structure,  $TL_{BW}$  the measured distance between the specimen's top and the sensor location,  $V_{BW}$  the computed wave velocity of the frequency used to create the kernel,  $N_{pts}$  the number of data points by which the feature (peak) has shifted between the two sensors and  $\Delta t_{WEcho-BW}$  the time step in which the time records are stored.

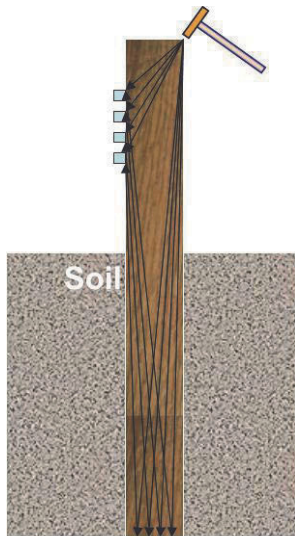
#### 2.5.4 Ultraseismic Method

The condition and also length of both shallow and deep foundations can be determined using Ultraseismic (US) method. This test can be performed on different structural materials such as concrete, masonry stone, steel and wood. In steel foundations, the damping energy is much greater than concrete and wood. This behaviour is due to the larger surface of the wood and concrete comparing to steel.

This method has been developed to overcome the problems in interpreting Sonic Echo response and bending wave methods. This method is more useful and accurate especially in complex structures such as bridges due to numerous reflecting boundaries. Utilization of multi-channel seismic reflection together in bounded engineering structures has resulted in this innovative method.

This method is invented using multi-channel , three component data processed in a computer adopting seismic exploration method. Usually impulse hammer and accelerometers mounted on the surface or side of the accessible bridge substructure at every 300mm or less help record the seismograph data. There are four wave modes recorded using this method: longitudinal (compressional), torsional (shear) body waves, flexural (bending) and Rayleigh surface waves.

Data quality can be improved using seismic processing by identifying and analysing data gathered from the foundation bottom and eliminating the unwanted wave reflections gathered from the top and attached beams.



Impact:

- Longitudinal or Transverse impact from top/side of structure

Measurements:

- Time of impact
- Force of impact
- Longitudinal/Transverse response measured by at least two sensors mounted to the same side of the structure as the impact

Data analysis:

- Seismic analysis

*Figure 2.6 Schematic principle of Ultraseismic testing*

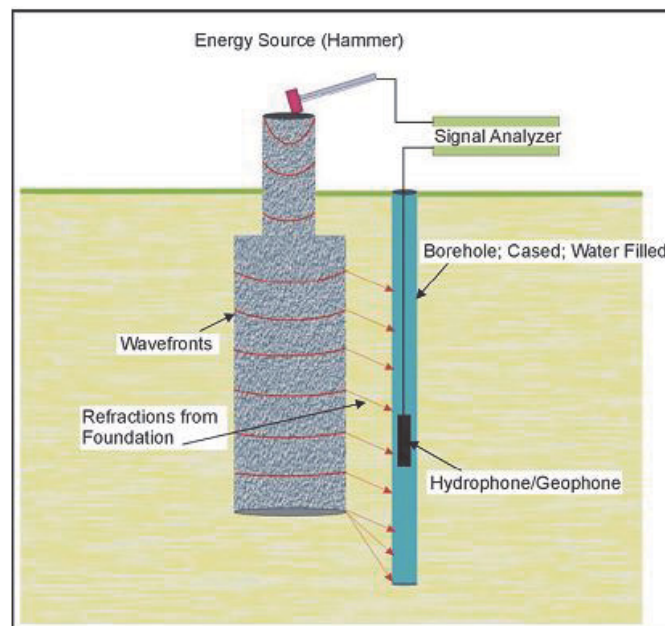
To gather two dimensional reflection waves from structure such as bridges or dams, which are rather complex, this method can be widely used. The known developed techniques in this method can be utilized in seismic exploration methods. This technique, uses multiple channel recording for separating the bottom echo from other waves gathered which makes it a more reliable method than that of a single channel. US test can be used as a versatile test on drilled shafts and auger cast piles, testing abutments and wall piers of bridges. It can measure the depth of a foundation with an accuracy of up to 95% and requires about 1500 to 1800 mm of exposed structural member. It should be noted that if a very deep foundation exists, accurate bottom echoes may not be possible to gather as the energy is absorbed and damped by the surrounding soil. Therefore, buried piles (poles) length can not be accurately determined using this method. Figure 2.6 depicts the principles of Ultraseismic testing.

### **2.5.5 Parallel Seismic (PS)**

The Parallel Seismic (PS) method is a borehole test method for determining depths of foundations. The method can also detect major anomalies within a foundation as well as provide the surrounding soil velocity profile. The method requires the installation of cased borehole close to the foundation being tested. The method can be used when the foundation tops are not accessible or when the piles are too long and slender (such as H piles or driven piles) to be testable by sonic echo techniques.

In a PS test, a hammer strikes the structure, and the response of the foundation is monitored by a hydrophone or a geophone receiver placed in the borehole. A signal analyser records the hammer input and the receiver output. The receiver is first lowered to the bottom of the hole, and a measurement is taken. Then, the receiver is moved up 30 cm or 60 cm and the second measurement is made. This process is continued until the receiver has reached the top of the boring. A hydrophone or a three-component geophone located in a nearby borehole records the compressional and/or shear waves travelling down the foundation. Therefore, the PS test requires drilling a 5- to 10-cm-diameter hole as close as possible to the foundation being tested (preferably within 1.5 m). The borehole should extend at least 3 to 5 m below the expected bottom of the foundation. The field setup for Parallel Seismic tests is shown in Figure 2.7.

PS tests can be performed on concrete, wood, masonry, and steel foundations. Some portion of the structure that is connected to the foundation must be exposed for the hammer impacts.



*Figure 2.7 Parallel Seismic setup*

Analysis of the PS data is performed in the time domain. The PS tests are performed at 300 to 600 mm vertical receiver intervals in the borehole. The first arrival times are plotted as a function of depth and the depth where a change of slope occurs is observed to find the foundation depth. Also, the foundation depth can be obtained by observing the depth where the signal amplitude of the first arrival energy is significantly reduced. In



addition, geophysical processing techniques can be used to help optimize the Parallel Seismic data. These techniques include Automatic Gain Control (AGC) and filtering to enhance weak events.

For hydrophone data, the time arrival of compressional waves is picked from the data for all receiver locations. A plot of the arrival time -versus-depth is prepared, an example of which is illustrated in Figure 2.8. In Figure 2.8, the velocity of the concrete in the shaft is 5,155 m/s. A break in the graph occurs at a depth of 8.5 m indicating the depth of the shaft.

For uniform soil conditions, two lines are identified in the plot as shown in Figure 2.8. The slope of the upper line is indicative of the velocity of the tested foundation, and the second line is indicative of the velocity of the soil below the bottom of the foundation. The intersection of the two lines gives the depth of the foundation. For non-uniform soil conditions, the interpretation of data from hydrophone use can be difficult due to the nonlinearity of the first time arrival. For geophone data in uniform soil conditions, the data can be interpreted in a way similar to the hydrophone data. When variable soil velocity conditions exist, an alternative to the first arrival time in data interpretation is used. All the traces are stacked, and a V-shape is searched for in the data because the bottom of the foundation acts as a strong source of energy, which produces upward and downward travelling waves.

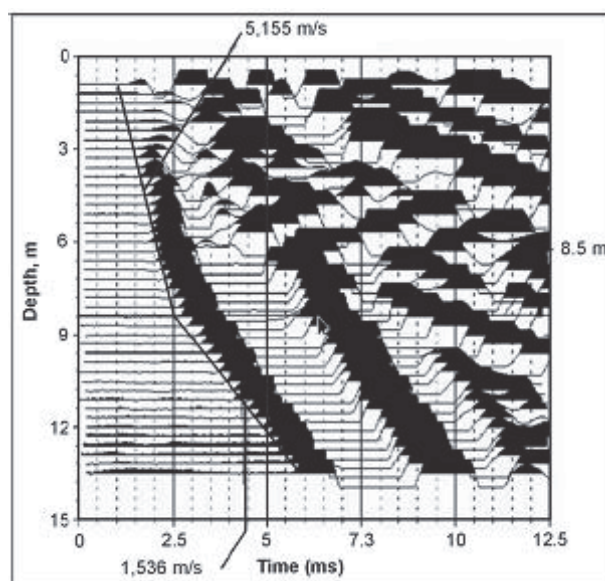


Figure 2.8 Parallel Seismic data and velocity lines

The Parallel Seismic method is more accurate and more versatile than other non-destructive surface techniques for determining unknown foundation depths. The accuracy of the method depends on the variability of the velocity of the surrounding soil and the spacing between the borehole and the foundation element.

A borehole is needed for Parallel Seismic tests, which adds to the cost of the investigation (unless borings are also required for other geotechnical purposes). The borehole should be within 1.5 m of the foundation, which sometimes cannot be achieved. Note that for very uniform soil (such as saturated sands), a successful test can be performed with up to 4.5 to 6 m spacing between the source and the borehole. As the borehole moves away from the foundation, interpretation of the PS data becomes more difficult and the uncertainty in the tip depth determination becomes greater.

### **2.5.6 Borehole radar**

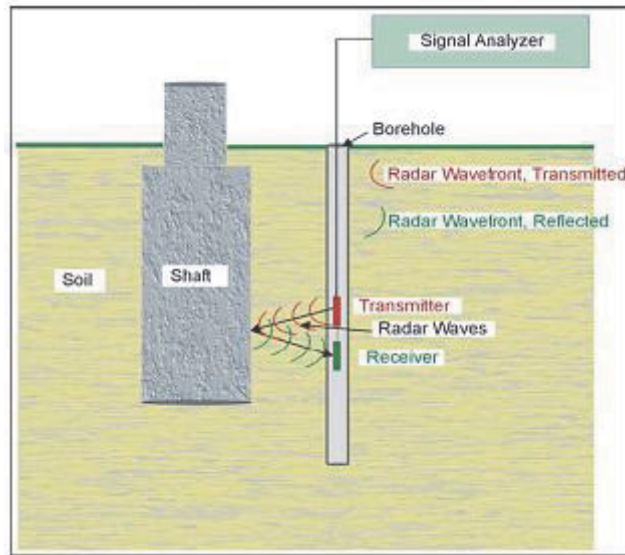
Borehole Radar uses borehole ground penetrating radar (GPR) antenna to obtain reflection echoes from a foundation for the determination of unknown depth and geometry of foundation.

In borehole radar, an antenna transmits radar energy into the surrounding rock and soil, and a receiver then records reflections that occur as the radar signals encounter and reflect from interfaces with different dielectric properties. The method is very similar to the borehole sonic method, where seismic waves are used rather than electromagnetic waves.

Borehole radar can be used in reflection mode or in cross-hole tomography mode. The radar measurements are either directional or omnidirectional, depending on the type of equipment and antennas. Only the reflection mode will be discussed in this document.

Radar uses radio waves with frequencies varying generally between 10 and 2,000 MHz. These waves are influenced primarily by the dielectric properties of the medium through which they are travelling and the electrical conductivity of the medium. Highly conductive materials attenuate the radar signals and limit its depth of penetration. Although the lower frequencies penetrate more than higher frequencies, they have less resolution.

For radar frequencies of 100 MHz, penetration varies from 10 to 40 m in resistive rocks. In conductive, clay-rich rocks, penetration will be less than 5 m. Figure 2.9 shows the borehole radar system.



*Figure 2.9 Borehole Radar system.*

In the unknown depth of foundation applications, the borehole radar signal will be reflected from the foundation until the bottom of the foundation is reached. There will be no reflections beneath the foundation, except for those emanating from geological conditions. The observed change in the reflected signal is used to locate the bottom of the foundation.

Borehole radar requires a PVC-cased borehole; the method will not work if the hole is steel-cased. The depth of penetration is significantly influenced by the electrical conductivity of the rocks and soil surrounding the borehole, which may not be known before the radar survey is completed. Penetrations up to about 10 m may be achieved in resistive conditions. In conductive materials, since the penetration of the GPR signal will be limited, getting the borehole as close to the pile as possible will be advantageous.

## 2.6 REVIEW OF STRESS WAVE PROPAGATION IN SOLIDS

### 2.6.1 Wave propagation in an elastic half-space

For any point  $p$  in a three-dimensional body, six independent components of stress can be identified relative to planes passing through point  $p$  which are parallel to the coordinate planes of a Cartesian coordinate system  $x, y, z$ . The components  $\sigma_x, \sigma_y, \sigma_z, \tau_{yz}, \tau_{xy}, \tau_{xz}$  determine the state of stress at point  $p$  and can be represented through the stress-strain relations (constitutive equations) for the material. For a linearly elastic isotropic solid, two elastic constants,  $\lambda$  and  $\mu$  are required to relate stress to strain. For convenience, normally modulus  $k$ , and the rigidity modulus, which is identical to Lamé's constant  $\mu$  are considered.  $E$  is then defined as the ratio between the applied stress and the fractional extension that results when a cylindrical or prismatic specimen is subjected to a uniform stress over its plane ends and its lateral surface and free from constraint (Kolsky 1963). The six components of stress acting on an infinitesimal rectangular parallelepiped can be expressed in the form of Hook's Law as follows:

$$\begin{aligned}
 \tau_{xy} &= \mu\gamma_{xy}, \\
 \tau_{zx} &= \mu\gamma_{zx}, \\
 \sigma_x &= \lambda\Delta + 2\mu\varepsilon_x, \\
 \tau_{yz} &= \mu\gamma_{yz}, \\
 \sigma_y &= \lambda\Delta + 2\mu\varepsilon_y, \\
 \sigma_z &= \lambda\Delta + 2\mu\varepsilon_z
 \end{aligned} \tag{2.5}$$

where,

$$\lambda, \mu = \text{Lame's constants}$$

$$\Delta = \varepsilon_x + \varepsilon_y + \varepsilon_z$$

If the x-axis is taken parallel to the axis of the cylinder,  $\sigma_x$  equals the applied stress and the other five components are zero. Thus, the first three equations can be simplified and expressed as:

$$\sigma_x = (\lambda + 2\mu)\varepsilon_x + \lambda(\varepsilon_y + \varepsilon_z)$$

$$\sigma_y = (\lambda + 2\mu)\varepsilon_y + \lambda(\varepsilon_x + \varepsilon_z)$$

$$\sigma_z = (\lambda + 2\mu)\varepsilon_z + \lambda(\varepsilon_x + \varepsilon_y) \quad (2.6)$$

By solving equation 2.6 for  $\varepsilon_x, \varepsilon_y, \varepsilon_z$

$$\varepsilon_y = \varepsilon_z = -\frac{\lambda}{2\mu(3\lambda + 2\mu)}\sigma_x \text{ and } \varepsilon_x = -\frac{\lambda + \mu}{\mu(3\lambda + 2\mu)}\sigma_x \quad (2.7)$$

The expression for Young's modulus  $E$ , can be written in the following form:

$$E = \frac{\mu(3\lambda + 2\mu)}{\lambda + \mu} \quad (2.8)$$

Poisson's ratio  $\nu$  is the ratio between the lateral contraction and longitudinal extension of the specimen (Kolsky 1963), the lateral surface being free, i.e.,  $\nu = -\frac{\varepsilon_y}{\varepsilon_x}$ . From equation 2.27 Poisson's ratio can be expressed in terms of Lamé's constants in the form:

$$\nu = \frac{\lambda}{2(\lambda + \mu)} \quad (2.9)$$

The shear modulus or rigidity,  $\mu$ , corresponds to the ratio between the shear stress and the shear strain. The shear modulus is given by the following equation:

$$\mu = G = \frac{\lambda(1 - 2\nu)}{2\nu} \quad (2.10)$$

The dynamic equilibrium equations in a Cartesian coordinate system for an infinitesimal element are expressed as:

$$\begin{aligned} \frac{\partial \sigma_x}{\partial x} + \frac{\partial \tau_{xy}}{\partial y} + \frac{\partial \tau_{xz}}{\partial z} &= \rho \frac{\partial^2 u}{\partial t^2} \\ \frac{\partial \tau_{zx}}{\partial x} + \frac{\partial \tau_{yz}}{\partial y} + \frac{\partial \sigma_z}{\partial z} &= \rho \frac{\partial^2 w}{\partial t^2} \\ \frac{\partial \tau_{xy}}{\partial x} + \frac{\partial \sigma_y}{\partial y} + \frac{\partial \tau_{yz}}{\partial z} &= \rho \frac{\partial^2 v}{\partial t^2} \end{aligned} \quad (2.11)$$

Where  $\sigma$  and  $\tau$  represent the normal and shear stresses on the surface identified by the corresponding suffixes: the first of which represents the plane on which the stress is

acting while the latter represents the direction. The components of the displacement in the  $x, y$  and  $z$  directions are denoted by  $u, v$  and  $w$  while  $\rho$  represents the mass density of the material. Next, by substituting the stress components from equation 2.5 into 2.11, one obtains:

$$\begin{aligned}\frac{\partial}{\partial x}(\mu\lambda_{xx}) + \frac{\partial}{\partial y}(\mu\gamma_{yz}) + \frac{\partial}{\partial z}(\lambda\Delta + 2\mu\varepsilon_z) &= \rho \frac{\partial^2 w}{\partial t^2} \\ \frac{\partial}{\partial x}(\mu\gamma_{xy}) + \frac{\partial}{\partial y}(\lambda\Delta + 2\varepsilon_y) + \frac{\partial}{\partial z}(\mu\gamma_{yz}) &= \rho \frac{\partial^2 v}{\partial t^2} \\ \frac{\partial}{\partial x}(\lambda\Delta + 2\mu\varepsilon_x) + \frac{\partial}{\partial y}(\mu\gamma_{xy}) + \frac{\partial}{\partial z}(\mu\gamma_{yz}) &= \rho \frac{\partial^2 u}{\partial t^2}\end{aligned}\quad (2.12)$$

By definition,

$$\gamma_{xy} = \frac{\partial u}{\partial y} + \frac{\partial v}{\partial x}, \gamma_{xz} = \frac{\partial u}{\partial z} + \frac{\partial w}{\partial x}, \varepsilon_x = \frac{\partial u}{\partial x}\quad (2.13)$$

Replacing  $\varepsilon_x, \gamma_{xz}$  and  $\gamma_{xy}$  in equation 2.12 with the above definitions yields:

$$\begin{aligned}(\lambda + \mu)\frac{\partial\Delta}{\partial x} + \mu\nabla^2 u &= \rho \frac{\partial^2 u}{\partial t^2} \\ (\lambda + \mu)\frac{\partial\Delta}{\partial z} + \mu\nabla^2 w &= \rho \frac{\partial^2 w}{\partial t^2} \\ (\lambda + \mu)\frac{\partial\Delta}{\partial y} + \mu\nabla^2 v &= \rho \frac{\partial^2 v}{\partial t^2}\end{aligned}\quad (2.14)$$

Where the Laplacian Operator is given by:

$$\nabla^2 = \frac{\partial^2}{\partial x^2} + \frac{\partial^2}{\partial y^2} + \frac{\partial^2}{\partial z^2}\quad (2.15)$$

These are the equations of motion of an isotropic elastic solid in which body forces are absent (Kolsky 1963). Differentiating the dynamic equations of equilibrium with respect to the dilatation ( $\Delta$ ) and rotation  $\Omega$ , yields the wave equations for longitudinal and shear waves respectively:

$$V_c = \sqrt{\frac{(\lambda + 2\mu)}{\rho}} \quad (2.16)$$

$$V_c = \sqrt{\frac{\mu}{\rho}} \quad (2.17)$$

where,

$V_c$  = Compression wave velocity

$\lambda, \mu$  = Lamé's constants

$\rho$  = Mass density

### 2.6.2 Longitudinal wave propagation in thin rods

The wave equation which governs the motion of compression waves in an elastic-half space, also governs the longitudinal rod motion. Let us consider a straight, prismatic rod shown in Figure 2.10 and the corresponding differential element.

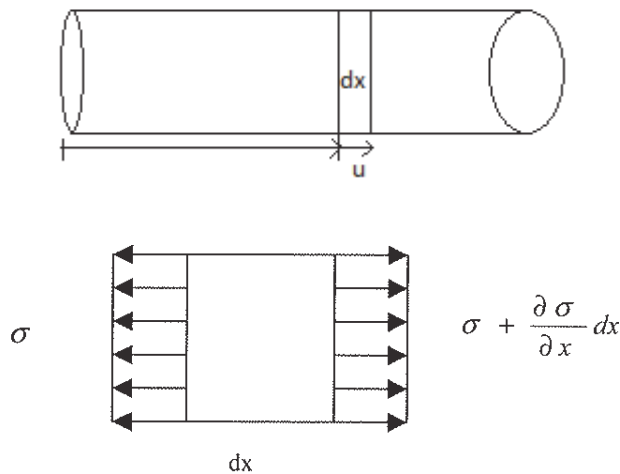


Figure 2.10 A thin prismatic rod with coordinate  $x$  and displacement  $u$  of a section

Referring to Figure 2.10, the coordinate  $x$  refers to a cross-section of the rod, while the longitudinal displacement of that section is given by  $u(x, t)$ . According to (Graff 1975), if we assume the rod to be under a dynamically-varying stress field  $\sigma(x, t)$  such that adjacent sections are subjected to varying stress, the equation of motion in the  $x$  direction by considering the differential element shown in Figure 2.10 become

$$-\sigma A + \left(\sigma + \frac{\partial \sigma}{\partial x} dx\right)A + qAdx = \rho Adx \frac{\partial^2 u}{\partial t^2} \quad (2.18)$$

where  $A$  represents the cross-sectional area of the rod. If we assume the tensile stress to be positive, equation 2.18 reduces to:

$$\frac{\partial \sigma}{\partial x} + q = \rho \frac{\partial^2 u}{\partial t^2} \quad (2.19)$$

Assuming the material behaves elastically, Hook's law can be applied,

$$\sigma = E\varepsilon \quad (2.20)$$

Where  $\varepsilon = \frac{\partial u}{\partial x}$

It is assumed that all parallel cross-sections remain plane and that a uniform distribution of stress exists. Assuming the rod is homogeneous, that is the mass density and Young's modulus does not vary with  $x$ , the equation of motion reduces to:

$$E \frac{\partial^2 u}{\partial x^2} + q = \rho \frac{\partial^2 u}{\partial t^2} \quad (2.21)$$

It is also important to note that there are lateral expansions and contractions arising for the axial stress. At this point, the lateral inertia effects associated with these contraction-expansions have been neglected (Graff 1975). In the absence of body forces ( $q$ ), equation 2.21 reduces to:

$$E \frac{\partial^2 u}{\partial x^2} = \rho \frac{\partial^2 u}{\partial t^2}$$

or,

$$\frac{\partial^2 u}{\partial x^2} = \frac{1}{c_0^2} \frac{\partial^2 u}{\partial t^2} \quad (2.22)$$

Hence, the longitudinal wave propagation speed is given by:

$$c_0 = V_c = \sqrt{\frac{E}{\rho}} \quad (2.23)$$



According to equation 2.23, the longitudinal wave velocity is a function of the material properties and it is independent of the wave frequency.

A research on non-destructive evaluation of timber poles and piles (Anthony & Philips 1989), based on longitudinal stress wave propagation have provided information and contributions to evaluate the length of the pile and pole embedment.

### 2.6.3 Flexural wave propagation in thin rod

The theory which governs the transverse motion in thin rods is based on the Bernoulli-Euler theory of beams. The first assumption made is that plane cross-sections initially perpendicular to the axis of the beam remain plane and perpendicular to the neutral axis during bending. This assumption implies that the longitudinal strains vary linearly across the depth of the beam and that, for elastic behaviour, the neutral axis of the beam passes through the centroid of the cross-section (Graff 1975). Consider a differential element of a thin rod undergoing transverse motion, as shown in Figure 2.11.

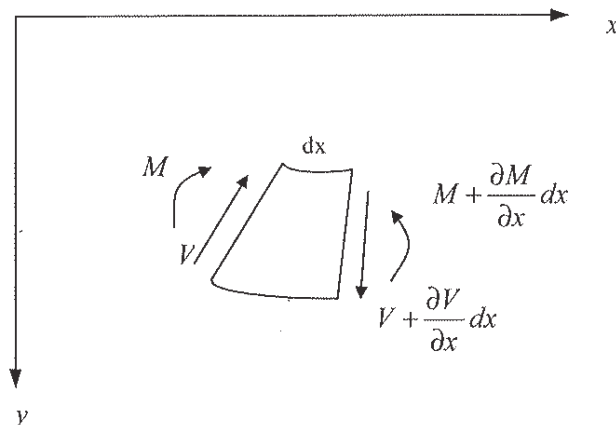


Figure 2.11 A differential element of a thin rod undergoing transverse motion due to a vertical impact

As the beam begins to bend, a variation of bending moments  $M$  and shear forces  $V$  are acting on the element. The relationship between curvature and the bending moment is given by:

$$\frac{\partial^2 y}{\partial x^2} = -\frac{M}{EI} \quad (2.24)$$

Where  $x$  is the direction along the axis of the bar and  $y$  is the coordinate of the natural surface of the beam. Knowing that the theory holds for small deflection of beams and

neglecting any loading on the element, the equation in the vertical direction can be written as:

$$-V + (V + \frac{\partial V}{\partial x} dx) = \rho A dx \frac{\partial^2 y}{\partial t^2} \quad (2.25)$$

where,

$A$  = Cross-sectional area of the beam

$\rho$  = Mass density per unit volume

Next, upon summation of moments while neglecting the rotational-inertia effects of the element (Graff 1975), and knowing that the shear and moment are related in the following manner:

$$V = \frac{\partial M}{\partial x} \quad (2.26)$$

one can show that:

$$\frac{\partial^2 M}{\partial x^2} = \rho A \frac{\partial^2 y}{\partial t^2} \quad (2.27)$$

Substituting equation 2.24 into equation 2.27 will yield the following governing equation for the transverse motion of a thin rod or beam:

$$\frac{\partial^2}{\partial x^2} (EI \frac{\partial^2 y}{\partial x^2}) + \rho A \frac{\partial^2 y}{\partial t^2} = 0 \quad (2.28)$$

Furthermore, if the material is homogeneous and the cross-section is constant so that  $I$  is constant, the equation for transverse motion reduces to:

$$\frac{\partial^4 y}{\partial x^4} = \frac{1}{\alpha^2} \frac{\partial^2 y}{\partial t^2} \quad (2.29)$$

yielding a velocity such that:

$$\alpha^2 = \frac{EI}{\rho A} \quad (2.30)$$

where,  $I$  = moment of inertia;  $A$  = Cross sectional area.

It should be noted that  $\alpha$  does not have the dimensions of velocity and that the restrictions for the development of this relationship were accounted for; that is, material homogeneity and constant-cross section.

If a harmonic wave is propagating, then the flexural wave velocity,  $c_f$  can be found by,

$$c_f = \sqrt{\alpha w} \quad (2.31)$$

where,  $w$  = angular frequency

From Equation 2.31, it can be seen that the flexural wave velocity will increase with the increase of wave frequency without converting to a certain value due to neglecting the rotary inertia and shear effects. Rayleigh theory considered only the rotary inertia effect and Timoshenko considered both rotary inertia and shear effect in addition to bending effect in the beam theory. The comparison of these three theories is shown in Figure 2.12. The axes of the figure are non-dimensional wavenumber  $\bar{\gamma}$  and non-dimensional velocity  $\bar{c}$  which can be defined as:

$$\bar{c} = \frac{c}{c_0} \quad (2.32)$$

$$\bar{\gamma} = \frac{r\gamma}{2\pi} \quad (2.33)$$

$$c_0 = \sqrt{E/\rho} \quad (2.34)$$

$$\gamma = \frac{w}{c} \quad (2.35)$$

$$w = 2\pi f \quad (2.36)$$

where,  $c_0$  is bar velocity;  $\gamma$  = wavenumber;  $f$  = cyclic frequency;  $r$  = radius of the cylinder.

As shown in Figure 2.12, using all three theories will lead to almost similar results for low wavenumber and low frequency as was the case for experimental tests in this study.

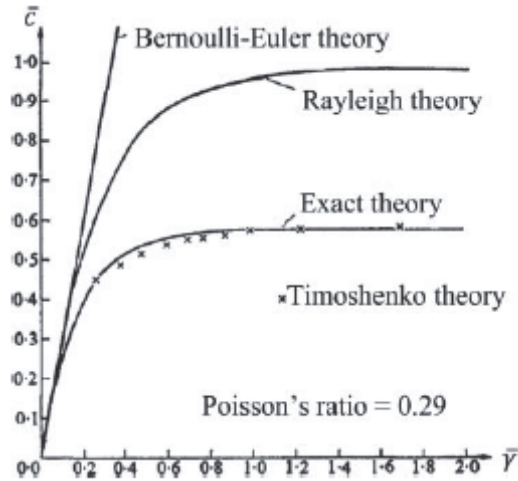


Figure 2.12 Dispersion relation for different theories (After Graff, 1975).

## 2.7 SIGNAL PROCESSING FOR STRESS WAVE METHODS

### 2.7.1 The discrete and fast Fourier transform

In 1807 Jean Baptiste Joseph Fourier introduced Fourier series, which was the first systematic application of a trigonometric series to a problem solution. Fourier series and the Fourier integral allow transformation of physically realizable time-domain waveforms to the frequency domain and vice versa (Ramirez 1985).

A typical signal obtained from the NDT methods is non-periodic by nature. To transform these waveforms, which are obtained as a function of time, to a function of frequency, the Fourier transform can be utilized. The continuous Fourier transform of  $x(t)$  is defined as;

$$X(f) = \int_{-\infty}^{\infty} x(t)e^{-j2\pi(f)t}dt \quad (2.37)$$

This formulation is used to define a waveform in the frequency domain for a continuous time interval. As signals obtained in practice are in digitized form, a variation of the Fourier transform was developed for use in digital signal processing (Ramirez 1985). The discrete Fourier transform (DFT) of  $x(n\Delta t)$  is defined as:

$$X(k\Delta f) = \Delta t \sum_{n=0}^{N-1} x(n\Delta t)e^{-j2\pi(k\Delta f)(n\Delta t)} \quad (2.38)$$

where,

$x(n\Delta t)$  = The discrete set of time samples that defines the waveform to be transformed.

$X(k\Delta f)$  = The set of Fourier coefficients obtained by the DFT of  $x(n\Delta t)$

$\Delta t$  = Time increment between data points, sec.

$\Delta f$  = Frequency interval in the frequency domain  $\left(\frac{1}{N\Delta t}\right)$ , Hz.

$k$  = The index for the computed set of discrete frequency components,  $k = 0, 1, 2, \dots, N - 1$ .

$n$  = The time sample index,  $n=0, 1, 2, \dots, N-1$ .

$N$  = Total number of data points being considered from the digitized signal

$X(f)$  is a complex number with a real component  $X_{Re}(f)$  and an imaginary component  $X_{Im}(f)$ , and, therefore, can be represented as a vector in a complex coordinate system (Katzke 1997). Using Euler's identity,  $e^{\pm j\theta} = \cos \theta \pm j \sin \theta$ , yields:

$$X(k\Delta f) = X_{Re}(k\Delta f) - jX_{Im}(k\Delta f) \quad (2.39)$$

while,

$$X_{Im}(k\Delta f) = \Delta t \sum_{n=0}^{N-1} x(n\Delta t) \sin[2\pi(k\Delta f)(n\Delta t)] \quad (2.40)$$

and,

$$X_{Re}(k\Delta f) = \Delta t \sum_{n=0}^{N-1} x(n\Delta t) \cos[2\pi(k\Delta f)(n\Delta t)] \quad (2.41)$$

where,

$x(n\Delta t)$  = The discrete set of time samples that defines the waveform to be transformed

$X(k\Delta f)$  = The set of Fourier coefficients obtained by the DFT of  $x(n\Delta t)$ .

$\Delta t$  = Time increment between data points, sec.

$\Delta f$  = Frequency interval in the frequency domain  $\left(\frac{1}{N\Delta t}\right)$ , Hz.

$k$  = The index for the computed set of discrete frequency components,  $k = 0, 1, 2, \dots, N - 1$ .

$n$  = The time sample index,  $n=0, 1, 2, \dots, N-1$ .

$N$  = Total number of data points being considered from the digitized signal

$X_{Re}(k\Delta f)$  = The real part of the frequency domain

$X_{Im}(k\Delta f)$  = The imaginary part of the frequency domain.

By letting  $f = k(\Delta f) = k/N\Delta t$ , the magnitude of the discrete Fourier transform is defined as:

$$A(f) = |X(f)| = \sqrt{(X_{Re}(f))^2 + (X_{Im}(f))^2} \quad (2.42)$$

While the phase angle of the Discrete Fourier transform is defined as:

$$\phi(f) = \tan^{-1} \left( \frac{X_{Im}(f)}{X_{Re}(f)} \right) \quad (2.43)$$

Generally, the idea of the FFT is to transform a digitized signal in the time domain to the frequency domain by placing sine and cosine curves next to the digitized waveform so the data points in the curves line up with the sample points in the signal. Points which are adjacent between the sine and cosine curves and the points representing the digitized waveform are then multiplied (equation 2.40, 2.41). The resulting cross-products, one corresponding to the cosine curve and one corresponding to the sine curve are summed. This summation  $X(k\Delta f)$ , is the form of the complex vector representing the set of Fourier transform coefficients.

Using this set of frequencies obtained from the Fourier transform of the digitized waveform, a plot of amplitude versus frequency can be made, which will identify the most prominent frequency contained within the waveform, known more commonly as a dispersive curve. Due to the lengthy calculations performed during discrete Fourier transform, a fast Fourier transform (FFT) algorithm is commonly used.

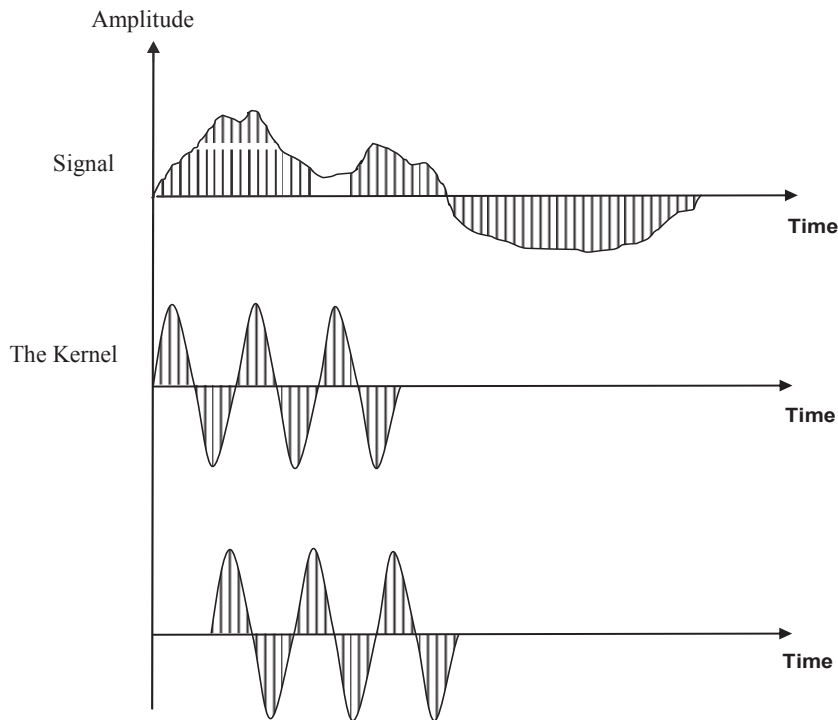
### 2.7.2 Short-Kernel Method (SKM)

SKM is a mathematical technique based on the cross-correlation procedure described by (Bendat & Piersol 1980). It was developed for digital signal processing and determines the location and velocity of selected frequencies inside dispersive time records. In SKM, a single value of a specific frequency is stated as follows:

$$SKM(j, k) = \sum_{i=1}^{N-1} g(\tau_i + j\Delta t) f[\tau_i, k] \Delta t \quad \text{with } j = 1 \text{ to } N2 - N1 \quad (2.44)$$

where SKM (j,k) is the  $j^{\text{th}}$  term of the cross-correlation currently being performed at the  $k^{\text{th}}$  frequency, g the time record from one sensor, f the kernel of  $k^{\text{th}}$  frequency used to perform the cross-correlation, N1 the number of data points in f, N2 the number of data points in g, and  $\Delta t$  the time step at which the time record g is stored. Thereby, Eq. 2.44 calculates each single SKM value as the cross-correlation of a given frequency with a digitized signal.

The SKM technique is better summarised in a more descriptive form through the following discussion. Given is a user-determined frequency for comparison with a digitized record, referred to as the kernel seed. The method places the kernel, whose length is to be determined by the user, next to the time record so its individual data points coincide with the data points in the signal. The process begins by cross multiplying the amplitude of the kernel at each time step by its corresponding signal amplitude. Products from all multiplications are then summed with all algebraic signs to obtain a single SKM value. This SKM value indicates how well the kernel fits with its frequency counterpart inside the data string. The value is graphed on an SKM plot at the point where the beginning of the kernel was placed. The kernel is then shifted along the data string by a predetermined number of points and the cross products are formed again (see Figure 2.13). Another SKM value result is to be plotted at the point where the kernel is now placed. This procedure is continued for some specified number of kernel shifts. The data points in the SKM plot corresponding to a significant maximum peak represents the location of good alignment between the kernel and its frequency counterpart in the signal. A positive global maximum represents the location where the kernel fits best and is in phase with its frequency counterpart, and a negative global maximum is a location where the kernel is also well-aligned, but out-of-phase by one hundred eighty degrees with its frequency counterpart.



*Figure 2.13 Kernel shifted along signal*

### **2.7.2.1 Other Applications of SKM**

Other than determining the embedment length, SKM method can also be used for other purposes as well. Working out below characteristics can also help with improving the accuracy and reliability of length determination test.

- Moisture content determination in a specimen
- Deterioration determination of a specimen
- Defect Localization and Damage evaluation

In the BW method, the reflections of flexural waves, generated by transversal impact, are analysed using SKM analysis as advanced signal processing technique. Due to the dispersive nature of flexural waves, each phase velocity of a wave is related to its own frequency. Using SKM, sensor signals are scanned with a kernel frequency to filter or reduce irrelevant frequency components in the signal and phase velocities of central frequencies are calculated. Through the identification of initial wave arrivals and subsequent reflections, the depths and locations of reflection events can be calculated, and thereby, the length and soundness of a structure be determined.



### 2.7.3 Wavelet transform

In the traditional Sonic Echo (SE) method, a short-duration mechanical impact is executed on a structure to generate a stress pulse that propagates through the specimen in all directions generating longitudinal, transverse and Rayleigh waves. Wave reflections from internal flaws and external surfaces are recorded and by processing signals in the time or frequency domain, damage/defects and geometric features of the structure are identified. Because of the generation of multiple types of waves, the determination of length and soundness of the test structure with data analysis in the time or frequency domain can be error-prone due to transient effects. To overcome this issue, data can be processed by time-frequency analysis using Wavelet Transform (WT). Time-frequency analysis provides information on how the spectral content of a signal evolves in time. Thereby, transient effects of frequency components can better be differentiated and improved length and integrity identification be achieved.

The continuous wavelet transform (CWT), which is a type of WT, can be used as advanced signal processing technique for SE testing. In CWT, the Fourier transform is applied to individual sections/windows of a time-history signal and thereby both, the frequency content and time information, are preserved. Whereas in Short Time Fourier Transform the width of the time window is fixed, in CWT it changes according to the chosen frequency. Higher frequencies have better time resolution and lower frequencies have better frequency resolution. Thereby, the CWT allows the low-frequency components, which usually give a signal its main characteristics, to be distinguished from one another in terms of frequency content, while providing an excellent temporal resolution for the high frequency components, which add nuances to the signal's behaviour (Robertson & Basu 2008). The CWT is obtained by convolving the signal  $f(t)$  with a set of basis functions created from the translations ( $u$ ) and dilations ( $s$ ) of a mother wavelet  $\Psi$  following:

$$WT(U, S) = \frac{1}{\sqrt{s}} \int_{-\infty}^{+\infty} f(t) \Psi^* \left( \frac{t-u}{s} \right) dt \quad (2.45)$$

where  $u$  is the time shift,  $s$  the scale and  $*$  denotes the complex conjugate. The basis functions are defined as:

$$\Psi_{(u,s)}(t) = \frac{1}{\sqrt{s}} \Psi\left(\frac{t-u}{s}\right) \quad (2.46)$$

There exist a number of different mother wavelet functions  $\Psi$  (e.g. Paul, Gaussian, Morlet, b-spline and Shannon mother wavelets). Depending on the characteristics of a data set, the most appropriate mother wavelet function is to be chosen. For the signals recorded from IE testing of timber poles, Morlet and Gaussian wavelets were found to deliver the best results.

In the SE method using wavelet analysis, the impact response of a structure is recorded by either geophone velocity transducers (in velocity time-history) or accelerometers (in acceleration time-history). If accelerometers are used in the testing, acceleration signals must first be integrated to time-velocity data in order to facilitate data processing using WT and to enable length and soundness determination of the tested structures. During the integration process, high pass filtering and damping compensation must be applied. Next, the time-velocity signals are converted into the time-frequency domain using CWT. According to (Chiang, Cheng & Liu 2004) the effect of CWT is similar to a multi-channel bandpass filter; however, with CWT, not only frequency components are separated but also the transient behaviour of the signals is preserved. After data processing with CWT, a three-dimensional coefficient plot can be generated where the x-axis displays the time, the y-axis corresponds to the scale (which is inversely related to the frequency), and the z-axis gives the absolute value and phase angle of resulting wavelet coefficients. For selected frequencies/scales, two-dimensional wavelet coefficient plots give information on wave propagation in the test structure, and depth and integrity of test specimen can be determined.

## **2.8 FINITE ELEMENT MODELLING OF WAVE PROPAGATION IN CYLINDRICAL PILE/POLE**

For cylindrical geometries, Pochhammer was the first person to derive the three dimensional equation of motion in 1876 by transferring the equation into cylindrical coordinates and solve it for compressional, flexural and torsional waves in an infinite rod. The frequency equation was generated for traction free surfaces. This equation describes the modes of both steady vibration and transient wave propagation (Miklowitz 1966). The frequency equation is valid for an infinite cylinder with traction free surfaces

and the equation also shows the dispersive nature of the waves for all propagating modes in the three-dimensional cylinder.

(Puckett 2000) indicated that despite the completeness of the wave equation few analytical results have been developed because of the complexity of the relationships. He indicated that research on wave propagation in cylinders is concerned with three areas: understanding the Pochhammer frequency equation and exploring the equation numerically and developing approximate solution for wave propagation in semi-finite bars and exploration of a one-dimensional approximation of the Pochhammer frequency equation.

(Field 1931) was first to investigate the one dimensional wave equation for low frequency and compared it with field data for fluid cylinders. The results show that the phase velocity approaches the wave speed in an infinite medium; So Field concluded the same must be true for the phase velocity in a solid cylinder.

(Bancroft 1941) followed Field's research and investigated the effect of Poisson's ratio on the first mode dispersion curve. Bancroft's results were in good agreement when compared to experimental data published by (Shear & Focke 1940). Bancroft concluded that in the case of infinite medium, the wave involves no motion in the plane of the wave front and the displacement is uniform. In the case of long bar, motion in the plane of the wave front is inevitable and the displacement is far from uniform.

In the previous works, only the first mode was explored. (Davies 1948) investigated the phase velocity of the first three modes of the Pochhammer frequency equation and the group velocities of the first two modes. Davies' analytical results were in good agreement with Bancroft. Davis introduced a way to measure the axial and radial displacements separately on a circular bar and produced experimental results using Hopkinson bar. The results were in good agreement with Pochhammer theory and he confirmed the phenomenon of dispersion experimentally (Al-Mousawi 1986).

(Onoe, McNiven & Mindlin 1962) mapped the relation between the frequency and propagation constant for axially symmetric wave in an infinitely long isotropic cylinder. Real and imaginary and complex propagation constants were calculated for a large frequency spectrum. The influence of Poisson's ratio was also further studied. (Zemanek Jr 1972) confirmed theoretical results with experimental results. (Peterson

1999) investigated the multi-mode waveguide signals using Pochhammer solution that are comparable to those measured in experimental configuration.

Low strain pile integrity testing has been used widely to assess the construction quality of piles due to its relatively low cost and expediency. The integrity test results, in the form of velocity curves as a function of time, are interpreted using one dimensional stress wave theory. According to one dimensional wave theory, the displayed positive and negative characteristics of the signal in the time domain, as well as the amplitude of this cycled signal, will be a function of the relative reduction of pile impedance. More information associated with numerical simulation of the piles in low strain integrity testing could be found in (Kim & Kim 2003), (Liao & Roesset 1997a), (Liao & Roesset 1997b), (Said, De Gennaro & Frank 2009), (Ni et al. 2006), (Randolph 2003), (Chow et al. 2003), (Paikowsky & Chernauskas 2003).

## **2.9 RESEARCH GAPS IDENTIFIED**

It is important to acknowledge the difficulties in assessing the condition and dimensions embedded structures, especially for timber structures and foundation materials, due to nature of the timber materials, complexities of unknown geotechnical conditions and interaction between structure and the soil (Hertlein & Davis). It is not surprising that many existing methods, based on idealised models and first principles of structural mechanics, have failed to produce reliable and consistent results, especially in term of damage identification. It is, therefore, necessary and critical to evaluate, in a systematic fashion, the currently available NDT methods for assessing either poles or piles through theoretical and experimental/field testing to fully understand the issues and form workable guidelines for implementation of the methods.

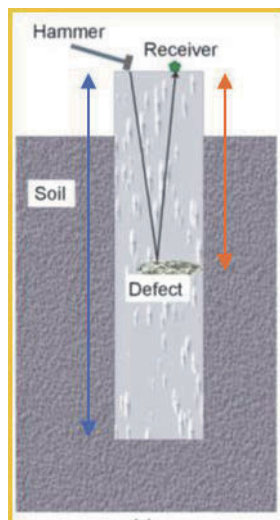
Shortcomings of the surface NDT methods could be addressed as:

- Despite the wide-spread use of these methods by consultants around the world, reports describing field applications have shown that the results lack consistency and reliability.
- Difficulties faced in field applications are often associated with complicated/imperfect material properties and environmental effects which need to be considered in test results. In particular, there is not much research done to

address the application of NDT for timber pile/pole due to many uncertainties in the nature of the timber material.

- Beside development of computer and multi-channel high-speed acquisition systems in recent decades, which has led to significant advances in the fields of advanced signal processing and structural damage detection, not many of those new developments have been utilised in NDT such as for condition and underground depth determination of timber poles in service.
- Interpretation of results is necessary to deal with such issues as different geotechnical conditions and the interaction of the foundation and the soil in terms of experimental work as well as the numerical simulation.

In addition, determining the underground length of timber poles could not be accurate by not considering the damage identification as shown in Figure 2.14.



*Figure 2.14 Consideration of damage identification for determination of the underground length of a timber pole*

Different methods have been introduced to measure the embedded length of timber pole or piles. In a research (Davis March 1994), use of sonic echo methods for estimating pile length has been studied. The author indicates that using sonic echo method when structures are placed on the pile is difficult. This is due to damping of stress wave and multiple wave reflections and difficulty in attaching accelerometers to the pile and finally applying a direct impact to the pile.

There are many challenges facing the proposed research including:

- Dispersive equations for longitudinal and flexural waves exist for infinite media
- There are equations for bounded media too, but they are mainly for rod like/cylindrical structures, not for columnar structure.
- There are no analytical equations considering the effect of soil.
- Impact at top of the pole creates mainly longitudinal wave which is easy to analyse, but practically the impact is made at some mid length. Indeed alternative impact location is required to be investigated.
- It is not possible to attach sensors on the timber pole below ground level. So, the result has to rely on the reflection from bottom. As a result, if there is defect present in the timber, the contour of this defect may match with the contour from reflection.
- As timber is a natural product, their exact inner structure has many uncertainties. So, it is difficult to create a perfect benchmark, because it is tough to know whether the damage free timber is really defect free or not.

## **2.10 SUMMARY**

This chapter presented a review of important literature published in the area of Non-destructive testing methods over the last years. From the review, it was found that researchers have used broad types of NDTs over last few decades to evaluate the quality of concrete materials. A variety of non-destructive testing devices have been proposed or tried for the inspection of timber bridges in Australia in addition to the timber poles in service poles.

Stress wave NDT techniques have been investigated under laboratory conditions and used by inspection professionals on limited basis. However, many questions remain unanswered regarding the effectiveness of stress wave NDT techniques to evaluate members in complicated structures. There are not many published works documenting how wave behaviour is affected by the varied boundary conditions found in wood structures. In addition, little information has been published on the relationship between

excitation, system characteristics, and wave behaviour. Research efforts in these two areas would advance state-of-the-art inspection techniques considerably (Ross & Pellerin 1994).

Traditionally, the most popular method for damage detection in timber pole is inspection of the pole by an experienced person to use a hammer to evaluate the condition of the pole above the ground and long drill for the bottom part. However, this method only relies on the expertise of the person and also drilling will make its own damage over the regular inspections. As most damages occur between the ground level and through the embedded length, using drilling will make the timber more exposed to the environmental conditions and decrease the strength of the timber.

According to the literature and to the present day, none of these has come into routine and general use in the industry despite some serious attempts to achieve this end (Crews & Horrigan 2000). Although a large number of publications for other applications of these methods exist, the area of non-destructive testing methods for timber materials is still an active field of research and several problems still need to be resolved before applicable methods become readily available. Some major challenges include the following:

- Uncertainties from field testing conditions such as measurement noise, measurement errors and environmental fluctuations affecting timber properties.
- Real testing limitations such as limited number of sensors and incomplete data sets.
- Complex behaviour of wave propagation for embedded conditions.
- Identification of existence, location and severity of different damage scenarios, i.e. various types of damage at different locations and with varying severities.
- Complexity of wave propagation between structure and soil.

Even though researchers have addressed parts of these problems, the algorithms previously proposed are still far from resolving them. The research presented in this thesis aims to improve currently available non-destructive testing methods under consideration to address some of the unsolved challenges listed above. The key issues that were identified from the literature review and considered in this thesis are: robustness of non-destructive testing methods to measurement errors, problems related to limited number of measurement sensors and incomplete data sets, accuracy and

reliability in identification of damage location and severity, detection of different damage types, identification of small size damage, and complexity of different types of wave propagation in timber materials as an orthotropic material.

Based on the literature review, the following steps will be taken to develop improved non-destructive testing methods. Firstly, thorough investigations will be undertaken on a free-free structure to provide an in-depth understanding on the effects of wave propagation on material characteristics. Secondly, currently available non-destructive methods (identified from the literature review) will be applied to the timber pole and their performance will be evaluated in regards to key issues identified above. Thirdly, the studied methods will be improved and refined while employing modified advanced signal processing techniques to overcome identified problems. Fourthly, the improved methods will be applied to a timber pole in the field to verify the methods and to study their performance under more complex boundary conditions.

From the literature review, three methods are identified to be applicable in the field of non-destructive testing of timber poles. All methods fulfil three set criteria: first, they are cost effective methods; second, they have some current shortcomings; and third, they have a great potential for improvement. These methods have been successfully applied by several researchers in various fields and applications. Despite reported successful applications of these techniques, these methods have several issues for timber structures. For example, if damage is present in the structure, this adds more uncertainty in terms of length determination. Also false positive damage identifications are often produced especially when only limited measurements are available. The reliability and accuracy of these methods are greatly jeopardised when exposed to field testing conditions such as measurement noise interferences, limited number of sensors, experimental modal analysis uncertainties and environmental influences. Although a number of researchers developed modified versions of these methods, this technique is still in need of improvement to overcome the issues highlighted above.



# CHAPTER 3

## 3 FINITE ELEMENT MODELLING OF TIMBER POLE WITH/WITHOUT SOIL EMBEDMENT

### 3.1 INTRODUCTION

This chapter presents the Finite Element (FE) modelling of the timber pole in order to generate stress waves for thorough investigation of the Sonic Echo/Impulse Response, Bending Wave and Ultraseismic methods without uncertainties associated with experimental imperfections (i.e. manufacturing faults, laboratory testing inaccuracies and signal processing disturbances). A numerical model allows the study of a stress wave generation of embedded timber poles without being significantly more labour intensive (compared to laboratory testing). Further, by simulating different damage scenarios, thorough preliminary investigations on the influence of damage type on the results can be undertaken.

In this chapter, the finite element modelling of the timber pole using ANSYS Classic is first presented. Secondly, finite element model of a vertical/horizontal impact loading test on a timber pole is discussed. Then, The FE model is progressively developed to incorporate more advanced features, such as simulating different types of boundary conditions in the laboratory (i.e. free-free and bedrock) and real environments (timber poles embedded in different geotechnical conditions). In order to obtain the dynamic data, numerically, transient dynamic analysis is employed using a finite element analysis software package to obtain the time series data. The data will then be used in the relevant non-destructive testing (NDT) methods to calculate the stress wave velocity and predict the length of timber pole. Finally, different damage scenarios are modelled and the results are explained.

## 3.2 NUMERICAL MODELLING OF TIMBER POLE

### 3.2.1 Finite Element Modelling of Intact Beam

To create a numerical model of the tested laboratory timber pole, the commercial finite element analysis package ANSYS Classic (ANSYS Inc 2011) was used. An FE model was firstly generated under free-free condition using isotropic material properties aiming to gain an understanding on stress wave behaviour of a timber pole without any uncertainty of material properties and also boundary conditions. This model was verified with static analysis for model verification. Then, FE beam model was enhanced with more advanced features requiring more steps to simulate other boundary conditions (i.e. embedded condition). The element type used is SOLID45, which is an orthotropic three-dimensional structural solid defined by eight nodes having three degrees of freedoms (DOFs) at each node, namely, translations in the nodal  $x$ ,  $y$  and  $z$  directions. This element is chosen as it is recommended by ANSYS Classic documentation (ANSYS Inc 2011) for three-dimensional modelling of solid structures and because saw-cut damage can easily be modelled for this element. The geometric properties of element type SOLID45 are illustrated in Figure 3.1. The link element was used as a free-free condition for the timber pole.

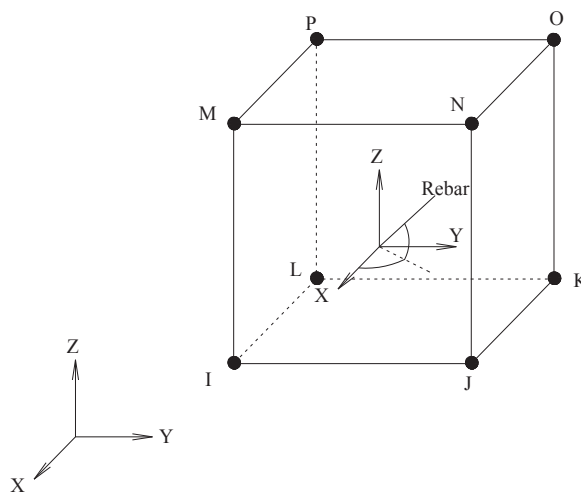


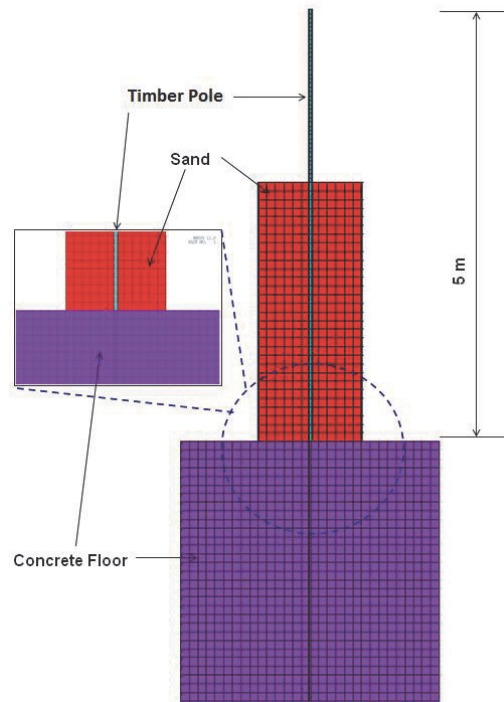
Figure 3.1 The geometric properties of SOLID45 (ANSYS Inc 2011)

### 3.2.2 Consideration of various boundary conditions

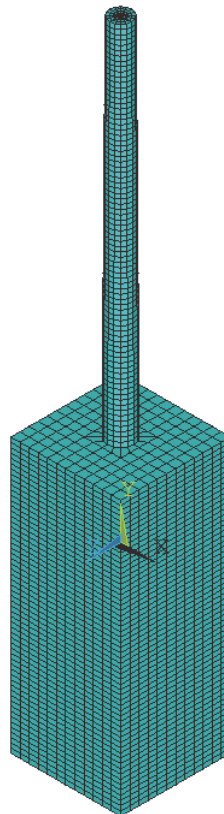
In the next step, the soil and geotechnical conditions were considered for modelling an embedded timber pole, firstly, bedrock as shown in Figure 3.2 and then, embedded condition as shown in Figure 3.3. The FE timber model as shown in Figure 3.3 adopted the standard timber material properties and the actual geometrical dimensions of the model.

In the laboratory, a strong concrete floor is used to simulate the bedrock where some utility poles may have been embedded. The concrete floor element is represented by the 8-node solid element. The floor is modelled as 3m (wide) by 3m (long) and 3m (high) concrete mass, which deemed sufficient to represent a strong concrete floor. The concrete floor FE model is illustrated in Figure 3.2. CONTACT178 element was used for the connection of timber pole and the floor. CONTACT178 represents contact and sliding between any two nodes of any element type. The element has two nodes with three degrees of freedom at each node with translations in the X, Y, and Z directions. It can also be used in 2-D and axisymmetric models by constraining the UZ degree of freedom. The geometric properties of element type CONTACT178 are illustrated in Figure 3.4. The element is capable of supporting compression in the contact normal direction and Coulomb friction in the tangential direction. User-defined friction with the USERFRIC subroutine is also allowed. The element may be initially preloaded in the normal direction or it may be given a gap specification. A longitudinal damper option can also be included. The value of keypot (3) is chosen as 4 to model open contact or free sliding plane to model the laboratory bedrock condition.

The soil element, i.e. the sand, was represented by an 8-node element. The sand is modelled by a 1.2m (wide) by 1.2m (long) and 3m (high) soil mass as depicted in Figure 3.2. The FE model for the embedded condition is also established accordingly as shown in Figure 3.2. The contact between timber pole and soil are considered as coupled degrees of freedom at the interface for embedded condition.



*Figure 3.2 A typical set-up for the embedded timber pole*



*Figure 3.3 A typical FE model of embedded timber pole*

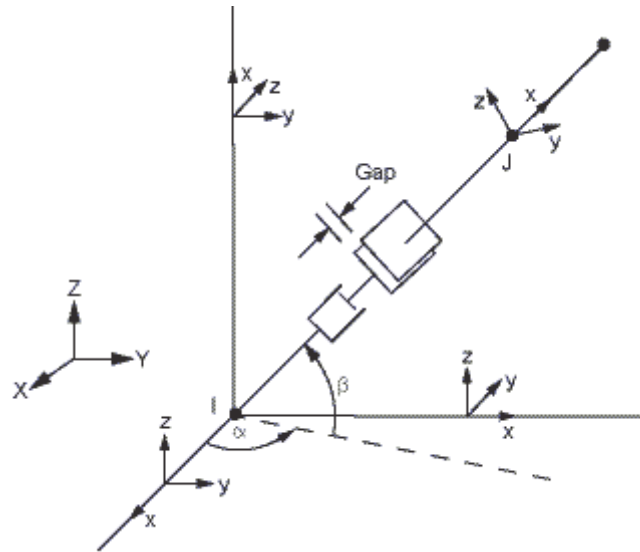


Figure 3.4 The geometric properties of CONTACT178 (ANSYS Inc 2011)

### 3.2.3 Material properties and geometry

The Finite Element Analysis (FEA) software program, ANSYS (2011), is used to create a preliminary three-dimensional (3-D) model to capture the dynamic behaviour of the model beam. The solid elements (SOLID45) is utilised to model the timber beam/pole and soil. The material parameters such as modulus of elasticity of timber and soil are obtained from the relevant standards and literature such as AS1720.1-1997 for timber, as presented in Table 3.1. In this study the isotropic model has been used for timber material as the main object of the numerical study was to get better understanding of wave travel in material without any other uncertainties.

After the elements were selected, typical timber poles were modelled similar to the laboratory and field tested poles, respectively. The dimensions of the FE beam/pole were identical to the laboratory pole (5,000 mm in length and 300 mm in diameter at one end and tapered to 270mm at the other end). The beam/pole was divided into 100 elements along the length, 4 elements along the depth and 4 elements along the width. The fixed boundary conditions were set at the bottom and all four external sides of the soil. Also the dimensions of the FE beam/pole identical to the field pole were 12,000 mm in length and 350 mm in diameter at one end and tapered to 170mm at the other end. The beam/pole is divided into 240 elements along the length, 4 elements along the depth and 4 elements along the width.

Table 3.1 Material properties used in the FE model

| Material Parameters          | Timber | Concrete | Soil  |
|------------------------------|--------|----------|-------|
| Modulus of Elasticity (MPa)  | 23,000 | 32,000   | 100   |
| Poisson's Ratio              | 0.3    | 0.5      | 0.3   |
| Density (kg/m <sup>3</sup> ) | 950    | 2,400    | 1,520 |

### 3.3 SIMULATION OF WAVE PROPAGATION IN TIMBER POLE

Transient dynamic analysis (sometimes called time-history analysis) is employed to numerically acquire the displacement response time history of the timber poles after being impacted either vertically or horizontally. This is an important tool to obtain the stress waves of timber beam under impulse loading as it is usually expensive to perform experimental work for parametric studies. Transient analysis can be used to determine time-varying displacements, strains, stresses and forces in a structure as it responds to any combination of static and transient loads.

As described above, in order to generate numerical data, transient analysis is performed to obtain response time histories for the beam models. In general, transient analysis is a numerical technique to determine the dynamic response of a structure under the action of any general time-dependent load. A simple formulation of the technique is given below (ANSYS Inc 2011).

The basic equation of motion solved by transient dynamic analysis is:

$$M \ddot{y}(t) + C \dot{y}(t) + K y(t) = f(t) \quad (4.1)$$

where  $M$  is the mass matrix,  $C$  the damping matrix,  $K$  the stiffness matrix,  $y$  the nodal displacement vector,  $\dot{y}$  the nodal velocity vector,  $\ddot{y}$  the nodal acceleration vector and  $f(t)$  the load vector. At any given time,  $t$ , equation 4.1 can be thought of as a 'static' equilibrium equation that also takes into account inertia forces  $M \ddot{y}(t)$  and damping forces  $C \dot{y}(t)$ . In this study, the Newmark time integration method is used to solve equation 4.1 at discrete time points. The Newmark method uses finite difference expansions in the time interval  $\Delta t$ , in which it is assumed that:

$$\dot{y}(t+1) = \dot{y}(t) + [(1-\delta) \ddot{y}(t) + \delta \ddot{y}(t+1)] \Delta t \quad (4.2)$$

$$y(t+1) = y(t) + \dot{y}(t) \Delta t + \left[ \left( \frac{1}{2} - \alpha \right) \ddot{y}(t) + \alpha \ddot{y}(t+1) \right] \Delta t^2 \quad (4.3)$$

where  $\alpha$  and  $\delta$  are Newmark integration parameters. Since the primary aim is the computation of displacement  $y(t+1)$ , the governing equation 4.1 is evaluated at time  $t+1$  as:

$$M \ddot{y}(t+1) + C \dot{y}(t+1) + K y(t+1) = f(t) \quad (4.4)$$

The solution for the displacement at time  $t+1$  is obtained by first rearranging equations 4.2 and 4.3 such that:

$$\ddot{y}(t+1) = a_0 [y(t+1) - y(t)] - a_2 \dot{y}(t) - a_3 \ddot{y}(t) \quad (4.5)$$

$$\dot{y}(t+1) = \dot{y}(t) + a_6 \ddot{y}(t) - a_7 \ddot{y}(t+1) \quad (4.6)$$

with  $a_0 = \frac{1}{\alpha \Delta t^2}$ ,  $a_2 = \frac{1}{\alpha \Delta t}$ ,  $a_3 = \frac{1}{2\alpha} - 1$ ,  $a_6 = \Delta t(1-\delta)$  and  $a_7 = \delta \Delta t$ . Noting that

$\ddot{y}(t+1)$  in equation 4.5 can be substituted into equation 4.6 and equations for  $\ddot{y}(t+1)$

and  $\dot{y}(t+1)$  can be expressed in terms of only one unknown,  $y(t+1)$ . The equations

for  $\ddot{y}(t+1)$  and  $\dot{y}(t+1)$  are then combined with equation 4.4 to form:

$$(a_0 M + a_1 C + K) y(t+1) = f(t) + M [a_0 y(t) + a_2 \dot{y}(t) + a_3 \ddot{y}(t)] + C [a_1 y(t) + a_4 \dot{y}(t) + a_5 \ddot{y}(t)] \quad (4.7)$$

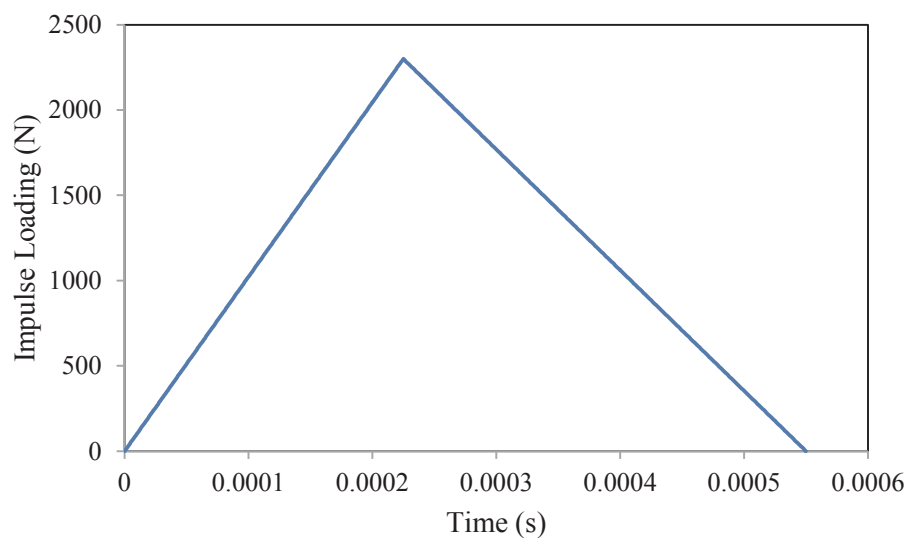
with  $a_1 = \frac{\delta}{\alpha \Delta t}$ ,  $a_4 = \frac{\delta}{\alpha} - 1$ ,  $a_5 = \frac{\Delta t}{2} \left( \frac{\delta}{\alpha} - 2 \right)$

Once a solution is obtained for  $y(t+1)$ , velocities and accelerations are updated as described in equations 4.5 and 4.6.

In the following subsection, step-by-step procedures to obtain response time history are explained:

### 3.3.1 Simulation of impact loading

Using the FE model, a transient dynamic analysis is performed. The “full method” (details given in ANSYS (2010)), which uses the full system matrices to calculate the transient response, has been adopted for the transient dynamic analysis. In the transient dynamic analysis, an impact loading, for example the loading shown in Figure 3.5, was imparted on the beam, at a designated location. The location of the impact loading is chosen to be the same as the one in the laboratory or field tests as wave propagation modes are dependent on the location of impact.



*Figure 3.5 An example of applied impact loading in the transient dynamic analysis.*

### 3.3.2 Stress wave propagation through the pole under impact load

From the transient dynamic analysis, the displacements of nodal points corresponding to the measurement points in the laboratory or field tests were obtained. In addition, displacements at other locations of interest were also obtained to study the behaviour of stress wave propagation in timber pole. The measurement locations may change with different test set ups. Using numerical differentiation technique, the velocities and accelerations were calculated from the displacements obtained. With the velocity and acceleration results, further analyses using various NDT methods can be performed to estimate the timber pole conditions and embedded length.



### 3.4 BEHAVIOUR OF WAVE PROPAGATION IN TIMBER POLE

As mentioned earlier, Finite Element model was firstly generated under free-free condition to study the stress wave generation in timber pole.

Figure 3.6 shows the location of the sensor patch arrangement (including 11 sensors on one side and 5 other sensors on the other side), used to obtain stress wave data of the timber poles.

Figure 3.7 presents the results of velocity patterns for sensors from different locations along the timber pole on one side. As shown in the figure, under free-end condition, the propagation of compressional wave could be traced and identified by following the sensor patch. Also signal arrival time can be identified from this figure; the arrival time for sensor 11 (placed at the end of pole) is located in the middle between starting and reflected signals of sensor 1 (placed on top of the pole). Reflected signal for the sensors located closer to the end of the pole such as sensor 10 often merges with arriving signal to form a single peak. Similar results are seen in Figure 3.8 for the sensors located in the middle of timber. These sensors have the same time delay due to the same distance between them.

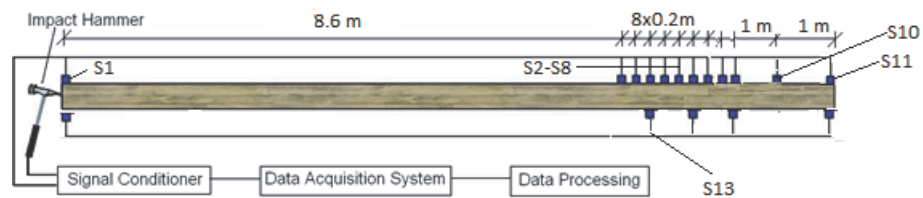


Figure 3.6 geometry of the model and location of the sensors placed on the timber pole

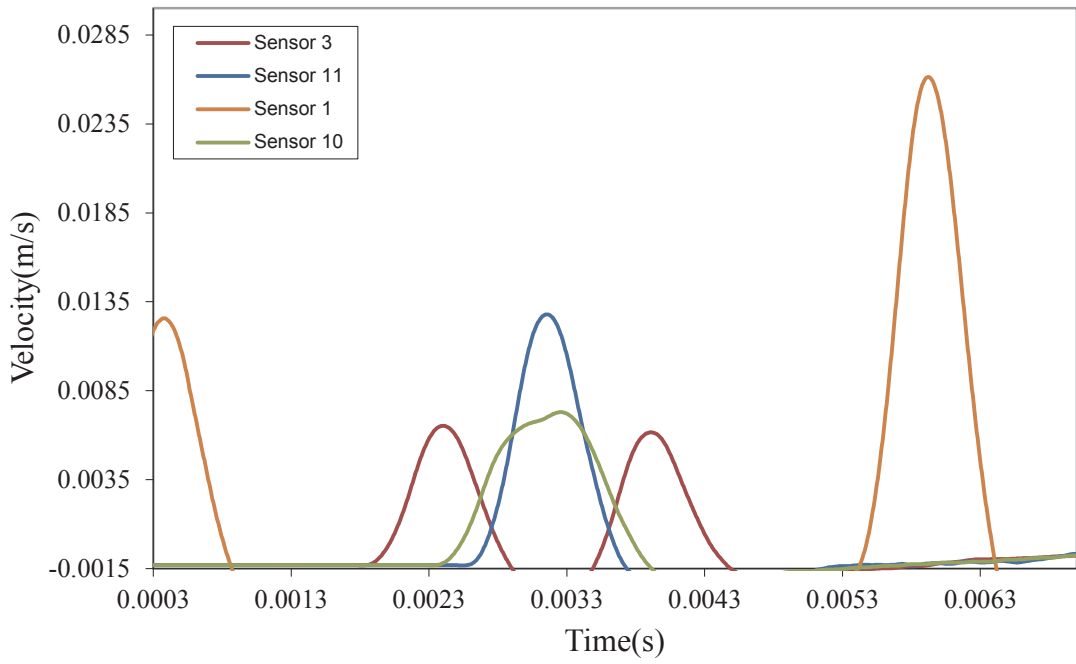


Figure 3.7 Velocity results in y direction under free-free condition

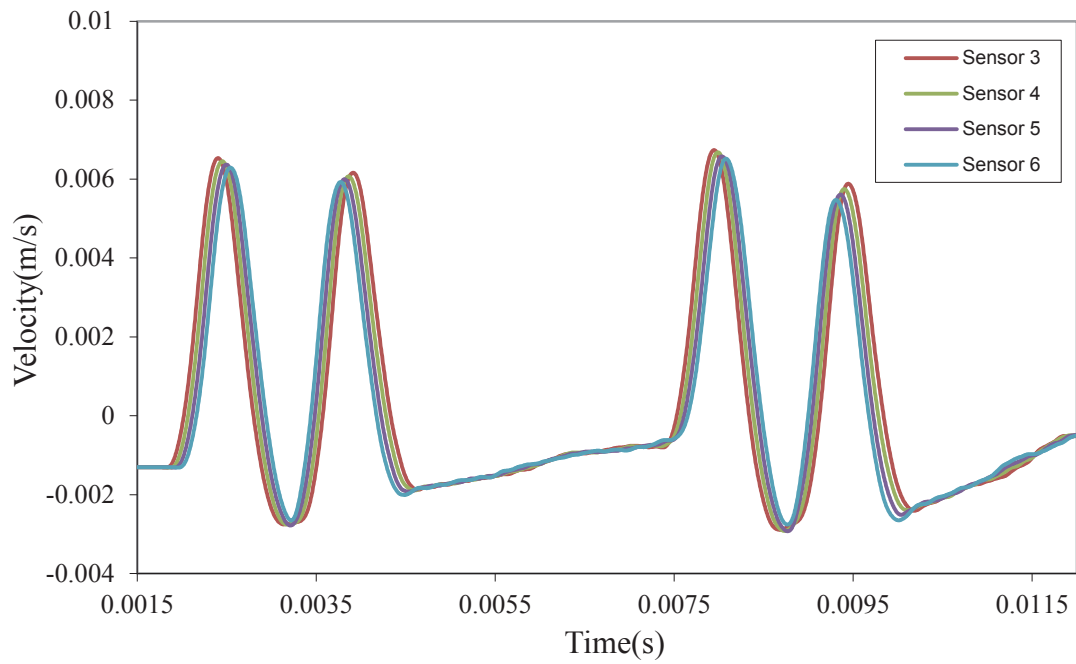
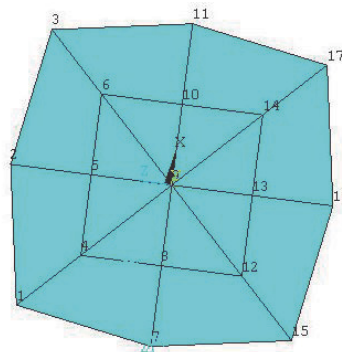


Figure 3.8 Velocity results in y direction for patch sensors with same distance under free-free condition

### 3.5 EFFECT OF TYPES OF IMPACT AND THEIR LOCATION ON TIMBER POLE

Three different types of impact loading from the top of the timber beam, namely concentrated load at centre (Node 9 as shown in Figure 3.9), concentrated load offset at edge (Node 11) and uniform distributed load (Nodes 1 to 17 as shown in Figure 3.9) were considered. Figure 3.10 and Figure 3.11 show the stress wave velocity in y direction for two different sensors located at the top and 9m from the top, respectively. As it can be observed, the wave patterns due to concentrated load at the centre of the cross section and uniformly distributed load are fairly similar to each other. However, concentrated load offset at edge has a slightly different pattern compared to the previous cases due to interference of wave modes (i.e. compressional, Raleigh wave and shear wave).

The wave modes (i.e. compressional (Symmetric) wave or Shear (Asymmetric) wave) due to impact locations on the timber pole were investigated. As seen in Figure 3.12 and Figure 3.13, when two sensors were placed on opposite sides of the specimen along the length, the wave patterns can be observed through wave velocity results in x direction. For concentrated loads imparted at the centre of the cross section only symmetrical wave is generated while loading imparted offset at the edge produced both symmetrical and asymmetrical waves. This can be used for damage identification using two sensors on the opposite sides of the pole to determine the location of damage.



*Figure 3.9 Cross section of FE modelling.*

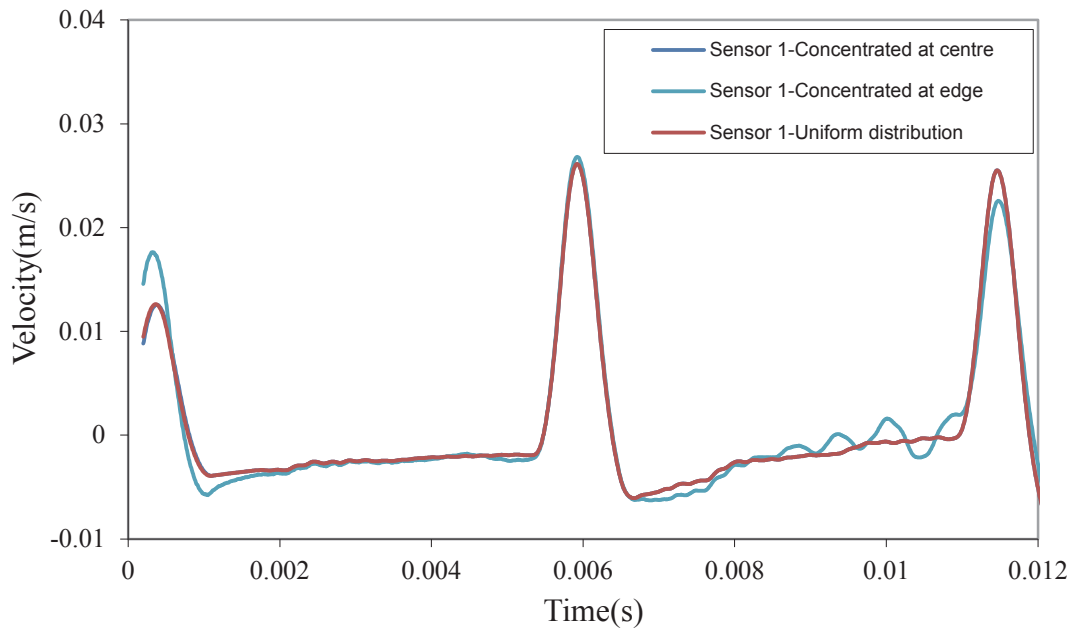


Figure 3.10 Stress wave velocity in y direction under free end condition and different loading condition by impact from the top for accelerometer 1

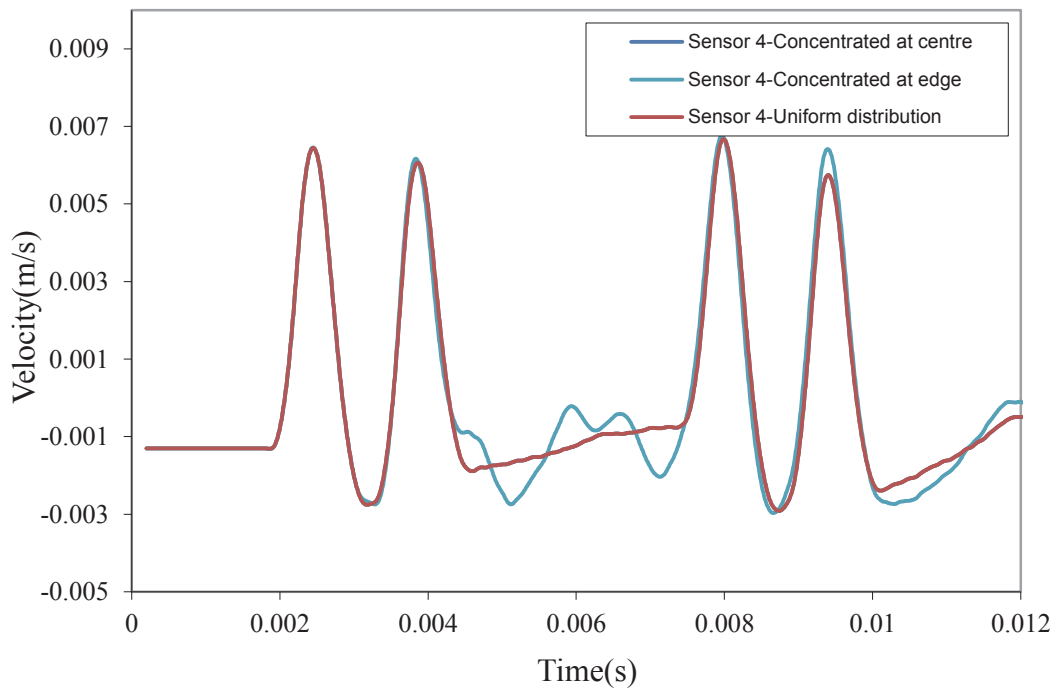


Figure 3.11 Stress wave velocity in y direction under free end condition and different loading condition by impact from the top for accelerometer 4

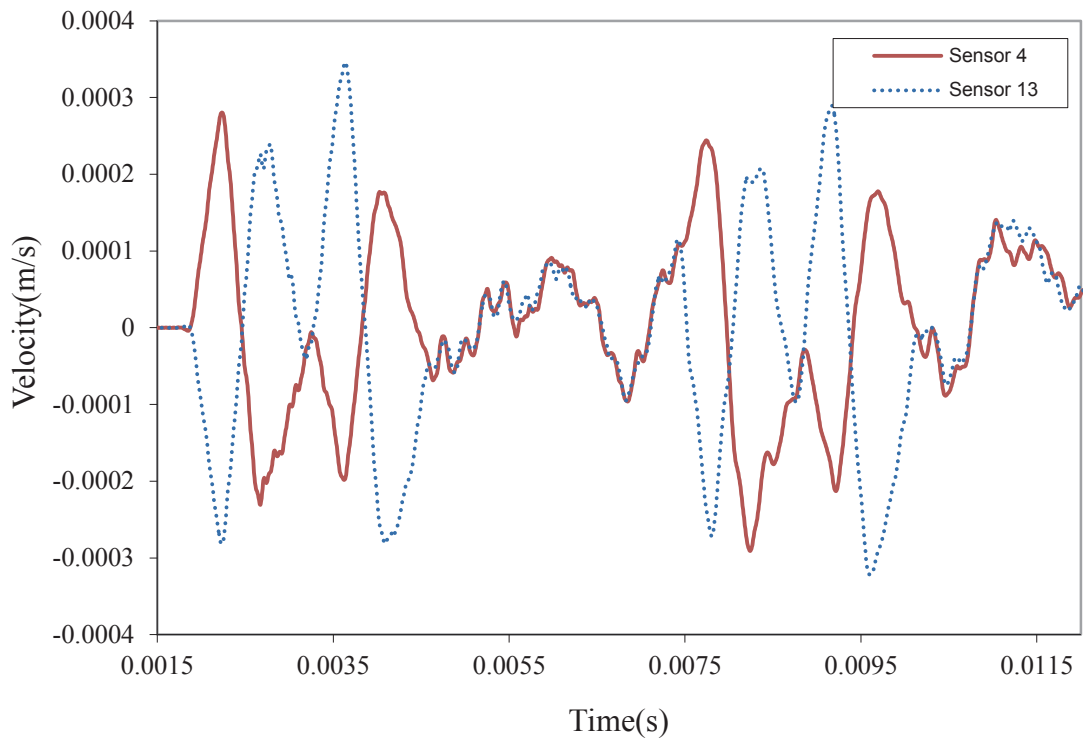


Figure 3.12 Stress wave velocity in  $x$  direction under free end condition by impact from the top for accelerometers 4 and 13

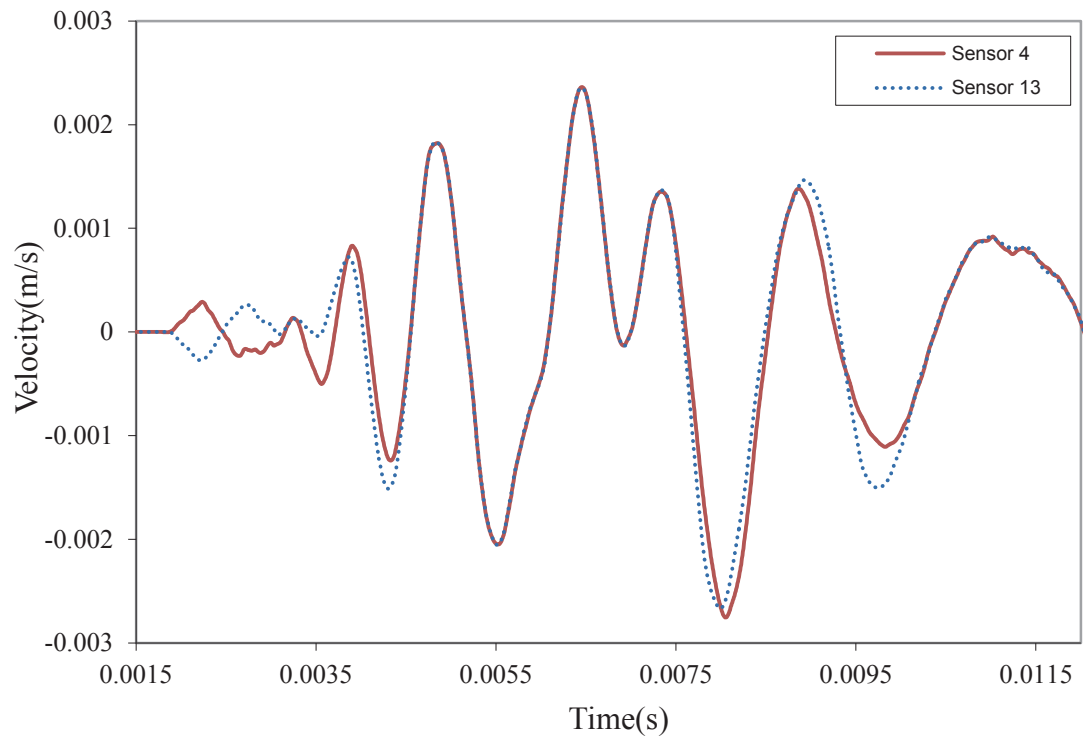


Figure 3.13 Stress wave velocity in  $x$  direction under free end condition by impact at the edge for accelerometers 4 and 13

## 3.6 APPLICATION OF SONIC ECHO/IMPULSE RESPONSE TEST ON TIMBER POLE

To investigate the effect of geotechnical conditions, a timber pole under pull out conditions identical to the laboratory tested pole is used for numerical modelling. The dimensions of the pole are described earlier in this chapter. Figure 3.14 shows the location of the sensors used to obtain stress wave data of the timber poles identical to 5 pull out conditions in laboratory for Sonic Echo testing method (see Chapter 4).

### 3.6.1 Velocity calculation

Figure 3.15 displays the normalised acceleration-time history in y direction vs. sensors location of all sensors located above the soil level. The slope of this graph has been used for velocity calculation. To increase the accuracy of stress wave velocity calculation, a trend line is used for calculation considering multi sensors above the soil. Figure 3.15 displays the arrival and reflection stress wave. As can be seen in this figure, the first arrival peak and the first reflection peak could be easily identified.

To investigate the effect of surrounding soil on stress velocity determination, different pull out conditions identical to the experimental test are modelled. The pull out tests corresponds to cases where the pole was pulled out at 0.3 m intervals. For example, “5<sup>th</sup> pull out” corresponds to the case where the beam or pole is pulled out by 1.5m (5 pull-out x 0.3 m) leaving 1.5m of sand below the bottom of the beam or pole with 1.5m of embedment length in the sand. The idea behind these pull out tests is to simulate different embedded lengths and varying soil mass under the pole. The results of the first arrival peak vs. sensor location are displayed in Figure 3.16 for all pull out conditions. Figure 3.17 and Figure 3.18 show the results for 2<sup>nd</sup> and 4<sup>th</sup> pull outs, respectively. As shown in these figures velocity will decrease with increase in embedded length. Therefore, two different velocities, one for stress wave travel above the soil level and one when travelling inside the soil were calculated. As can be seen in Figure 3.17, the stress wave velocity will decrease from 5277 m/s above the soil to 3968 m/s (around 20% decrease) below the soil. The same trend is observed for a timber pull under 4<sup>th</sup> pull out condition as shown in Figure 3.18. As a result, when soil is present, two different velocities need to be calculated and if there is no sensor used below the soil, the velocity decrease should be considered for waves travelling inside of the soil. The

velocities can be calculated from the slopes of sensor locations vs. time graphs in Figure 3.17 and Figure 3.18.

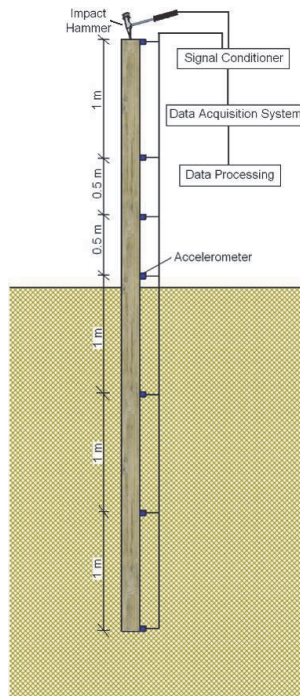


Figure 3.14 geometry of the model and location of the sensors placed on the timber pole for Sonic Echo test

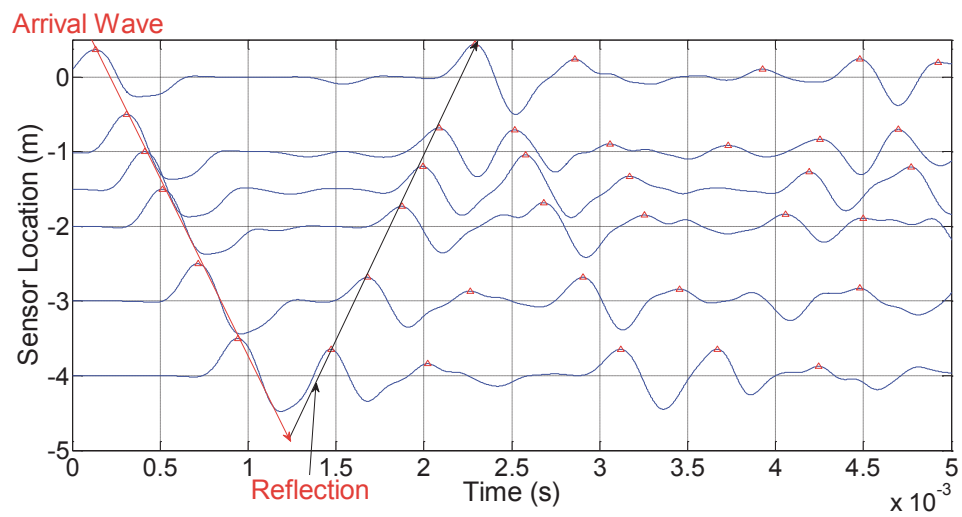


Figure 3.15 Acceleration results in y direction for patch sensors under 5 pull out conditions

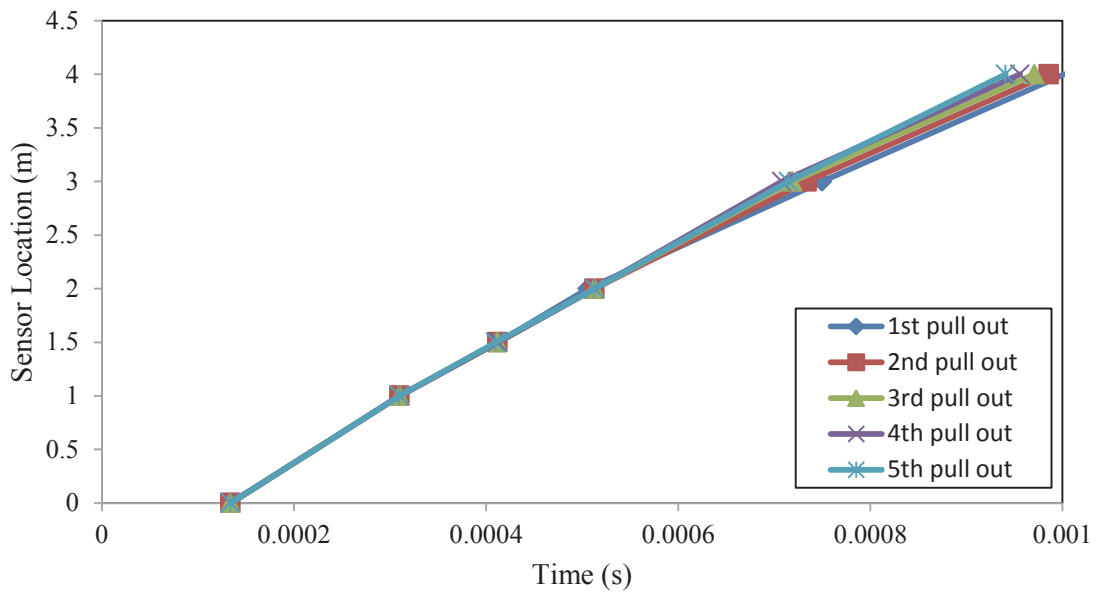


Figure 3.16 effect of different embedded lengths for velocity calculation

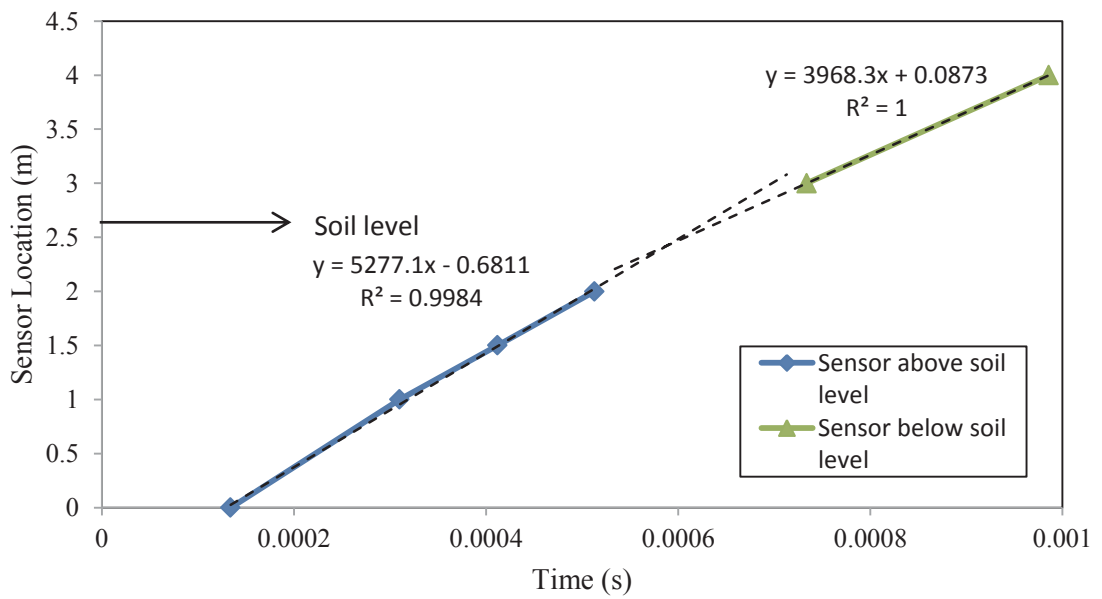


Figure 3.17 Acceleration result of 5m timber pole under 2<sup>nd</sup> pull out condition



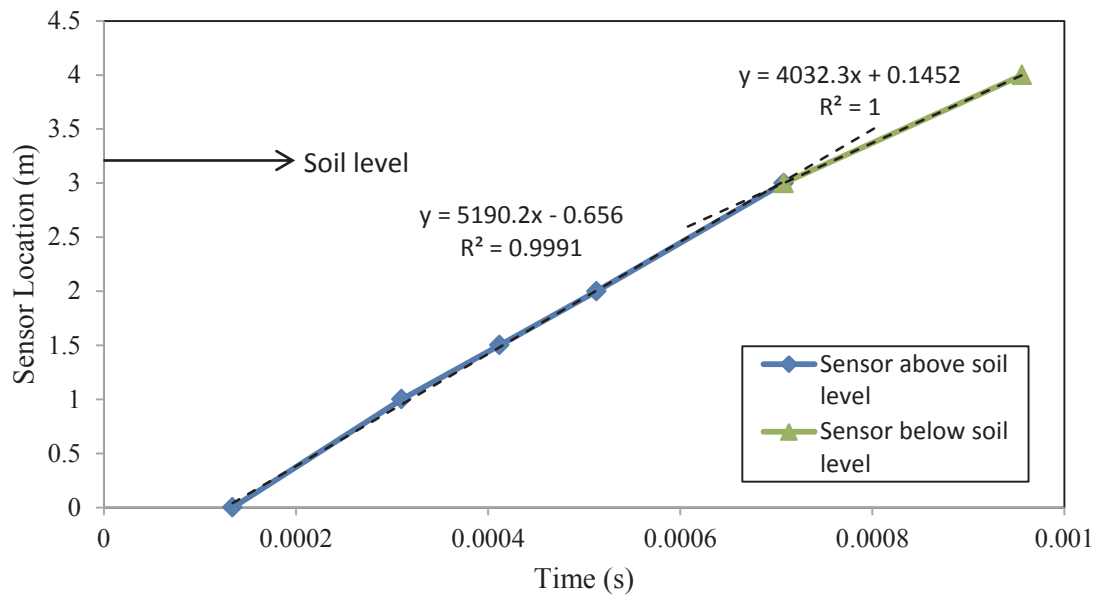


Figure 3.18 Acceleration result of 5m timber pole under 4<sup>th</sup> pull out condition

### 3.6.2 Embedded length determination

Based on the velocity calculations from the last step, the length of the pole is determined. The results of length determination for first four top sensors are presented in Table 3.2 under different pull out conditions. As mentioned before, in this calculation two different stress wave velocities above and below the soil have been used. As shown in Table 3.2, the error of length estimation averaged between 5% and 9% depending on the boundary conditions and the reference sensor for calculation. By increasing the soil depth the error of the length estimation is increased from 5.5% for 1.5m embedment to 7.1% for 2.7m embedment using sensor 1. Indeed, considering timber pole as an isotropic material, leads to the maximum error of 8% for length determination under embedded condition using multi sensor for velocity calculation. It should be mentioned that the velocity decrease below the soil was considered for velocity and length determination.

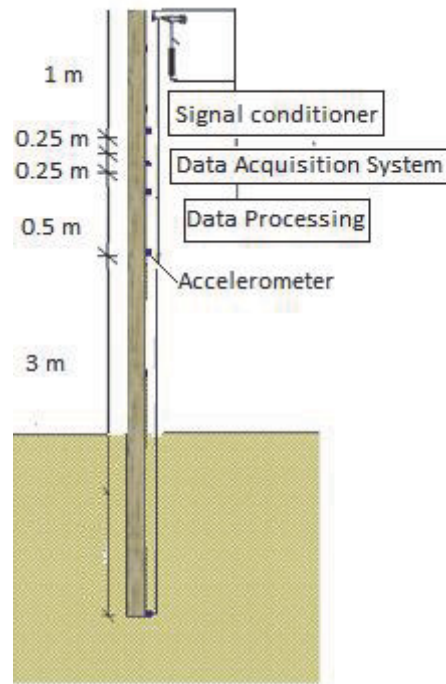
*Table 3.2 Length determination of a 5m timber pole under different embedded lengths using the first four sensors with Sonic Echo test*

| Embedded length (m) | Sensor No. | Sensor location (m) | 2*Predicted length (m) | 2*Actual length (m) | Error (%) |
|---------------------|------------|---------------------|------------------------|---------------------|-----------|
| 1.5                 | 1          | 0                   | 10.55                  | 10                  | 5.5       |
|                     | 2          | 1                   | 8.57                   | 8                   | 7.7       |
|                     | 3          | 1.5                 | 7.55                   | 7                   | 7.9       |
|                     | 4          | 2                   | 6.39                   | 6                   | 6.5       |
|                     | 5          | 3                   | 4.29                   | 4                   | 7.3       |
| 1.8                 | 1          | 0                   | 10.56                  | 10                  | 5.6       |
|                     | 2          | 1                   | 8.56                   | 8                   | 7         |
|                     | 3          | 1.5                 | 7.5                    | 7                   | 7.1       |
|                     | 4          | 2                   | 6.48                   | 6                   | 8         |
|                     | 5          | 3                   | 4.3                    | 4                   | 7.5       |
| 2.1                 | 1          | 0                   | 10.7                   | 10                  | 7         |
|                     | 2          | 1                   | 8.69                   | 8                   | 8.5       |
|                     | 3          | 1.5                 | 7.55                   | 7                   | 7.9       |
|                     | 4          | 2                   | 6.46                   | 6                   | 7.7       |
|                     | 5          | 3                   | 4.25                   | 4                   | 6.3       |
| 2.4                 | 1          | 0                   | 10.7                   | 10                  | 7         |
|                     | 2          | 1                   | 8.65                   | 8                   | 8.1       |
|                     | 3          | 1.5                 | 7.58                   | 7                   | 8.3       |
|                     | 4          | 2                   | 6.44                   | 6                   | 7.3       |
|                     | 5          | 3                   | 4.22                   | 4                   | 5.5       |
| 2.7                 | 1          | 0                   | 10.71                  | 10                  | 7.1       |
|                     | 2          | 1                   | 8.66                   | 8                   | 8.3       |
|                     | 3          | 1.5                 | 7.57                   | 7                   | 8.1       |
|                     | 4          | 2                   | 6.49                   | 6                   | 8.2       |
|                     | 5          | 3                   | 4.3                    | 4                   | 7.5       |

### **3.7 APPLICATION OF BENDING WAVE TEST ON TIMBER POLE**

In the next stage, a horizontal force is applied on timber specimen to simulate the bending wave test for 1<sup>st</sup> and 3<sup>rd</sup> pull out conditions in addition to 8 layer soil as boundary conditions, identical to the experimental test for a 5m timber pole. It should

be noted that in a 8 layer soil condition, timber pole is located on concrete floor simulating bedrock condition. However, under pull out conditions, the specimen stands on soil layers. Figure 3.19 shows the location of the sensors used to obtain stress wave data of the timber poles under the 5<sup>th</sup> pull out condition using bending wave method.



*Figure 3.19 geometry of the model and location of the sensors placed on the timber pole for Bending Wave test*

### 3.7.1 Velocity calculation

Fast Fourier Transform (FFT) is applied on the sensor data first to find the dominant frequency. As the impact generates broadband frequencies, the FFT would have different frequencies. Indeed choosing the appropriate kernel frequency is one of the challenges of this method as there are no guidelines to select those kernel frequencies from FFT results. However, based on the results of FFT, different kernel frequencies were selected and then, by applying the SKM method, the acceleration-time history graph was generated for each of them. Figure 3.20 shows an example of SKM plot at 410 Hz kernel frequency of a 5m timber pole under 1<sup>st</sup> pull out for sensors 1, 2 and 4 which are located on the pole with the same distance (0.5 m). The same phase is considered from all three sensors to determine the phase velocity. Solid arrows show the first arrival for all three sensors.

(Lynch 2007a) suggested that the reflected peak can be determined from the fact that, due to pulse distortion, the amplitude of the consecutive peaks will reduce until there will be an increase in amplitude of a certain peak. This higher amplitude peak, corresponding to the previous peak, is considered as reflection or the beginning of the reflected wave. The reflection was chosen by the same method suggested by (Lynch 2007a), but also considers the fact that the arrival will reach sensor 1 first in the first path and then sensor 2 and 4, but after reflection it will reach sensor 4 first (Kim & Ranjithan 2000).

Figure 3.21 shows the first arrival and reflection of sensor 1. It can be seen that, it satisfies the aforementioned method of choosing reflection peak. After calculating the time difference, velocity is determined for different kernel frequency and different sensors of 5m timber pole under 1<sup>st</sup>, 3<sup>rd</sup> pull out and 8 layer soil as testing conditions and the results are shown in Figure 3.22 and Figure 3.23.

To verify the appropriate range of kernel frequencies, the results of bending wave velocity calculation were compared with Bernoulli-Euler Beam theory and Timoshenko beam theory. It should be mentioned that in using Bernoulli-Euler Beam theory and Timoshenko beam theory, the timber material is considered as an isotropic material. The material properties for timber in Bernoulli-Euler Beam and Timoshenko beam are the same as those described before in Table 3.1. As can be seen in Figure 3.22, the bending wave velocity between sensor 1~2, 1~3 and 1~4 are in a good agreement with the Bernoulli-Euler Beam and Timoshenko beam for frequencies between 600-800 Hz. As a result, the appropriate kernel frequency should be chosen between 600-800 Hz to be in line with the theoretical equation in order to better estimate the embedded length.

It should also be mentioned that the same impact as those used in the experiments were used which generated relatively low frequencies. Using a low frequency, will generate high wavelength which was not captured separately by sensors 1 and 2 mounted on the pole with 0.25m distance between them. Also as it can be seen from Figure 3.23, that bending wave velocities between sensors 1~4 and between sensors 2~4 have better agreement with Bernoulli-Euler Beam and Timoshenko beam as the distance between the sensors are 0.5m or more.

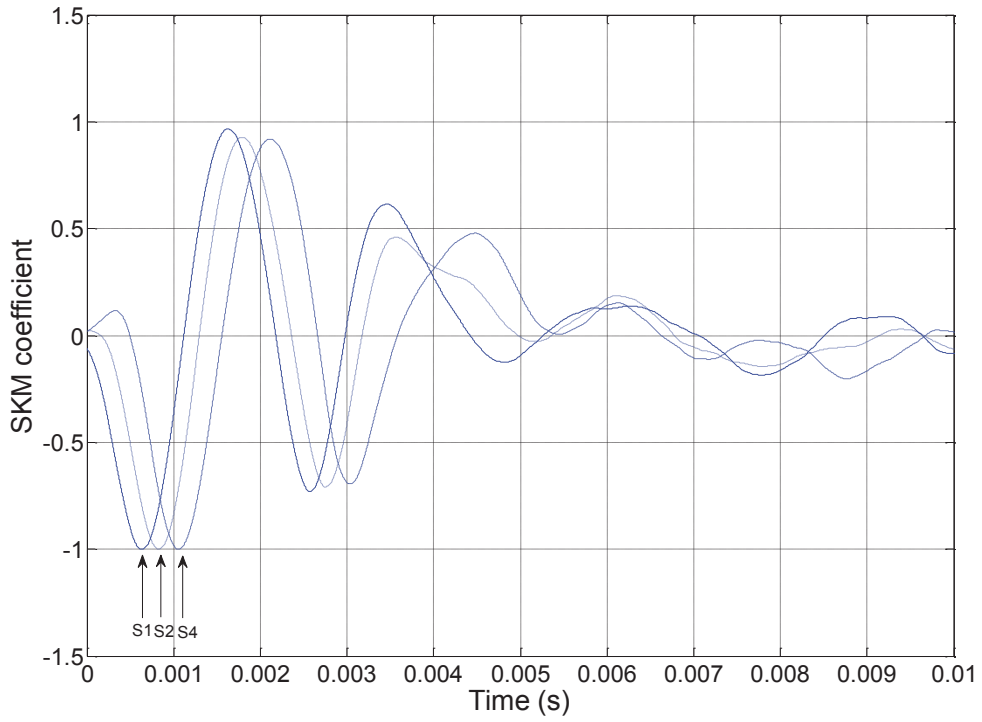


Figure 3.20 SKM coefficient plot at 410 Hz of 5 m timber pole under 1<sup>st</sup> pull out for sensors 1,2 and 4.

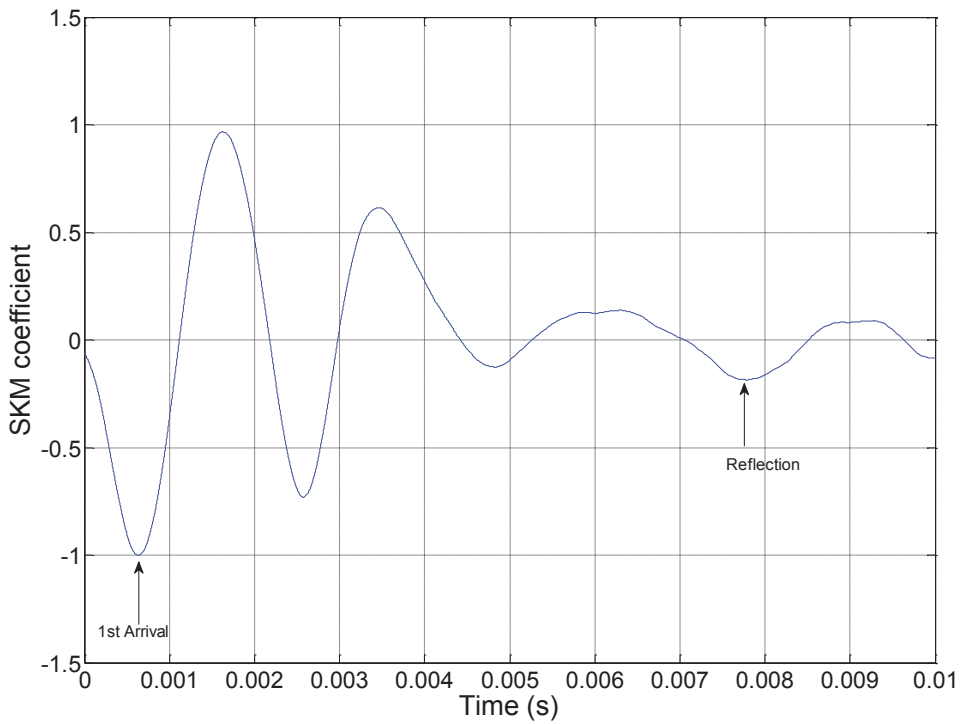
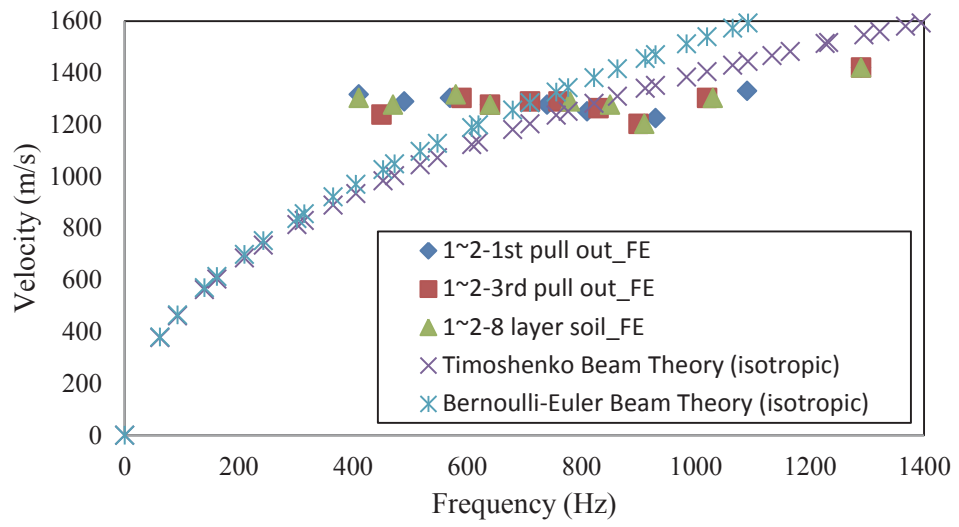
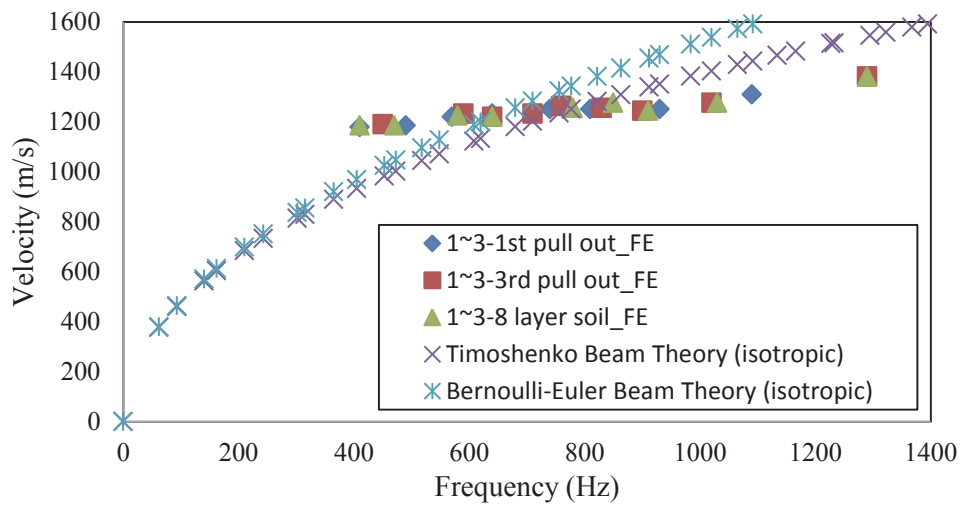


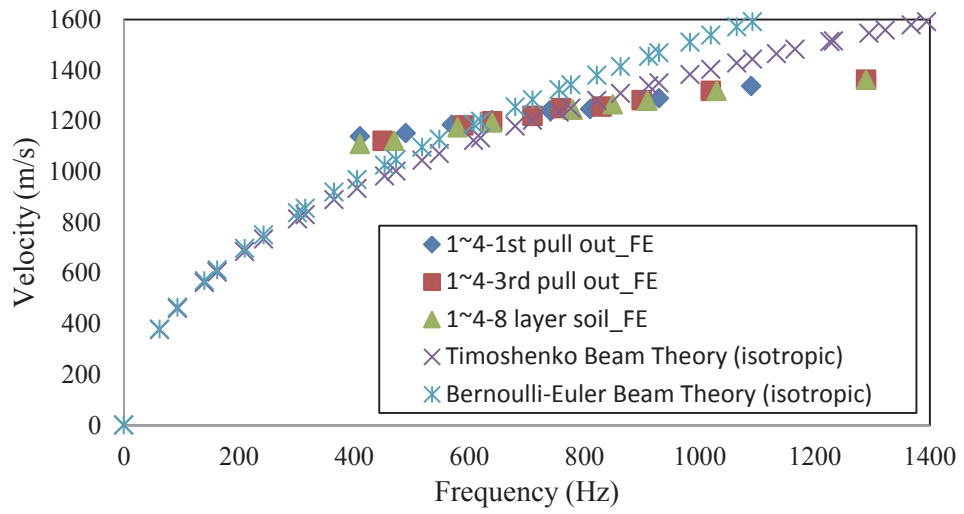
Figure 3.21 SKM coefficient plot at 410 Hz of 5 m timber pole under 1<sup>st</sup> pull out for sensor 1



a)

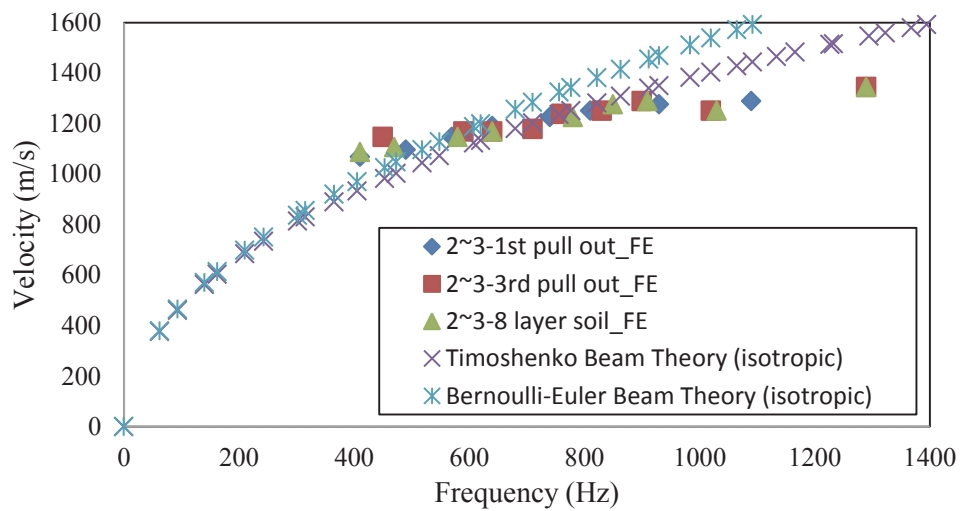


b)

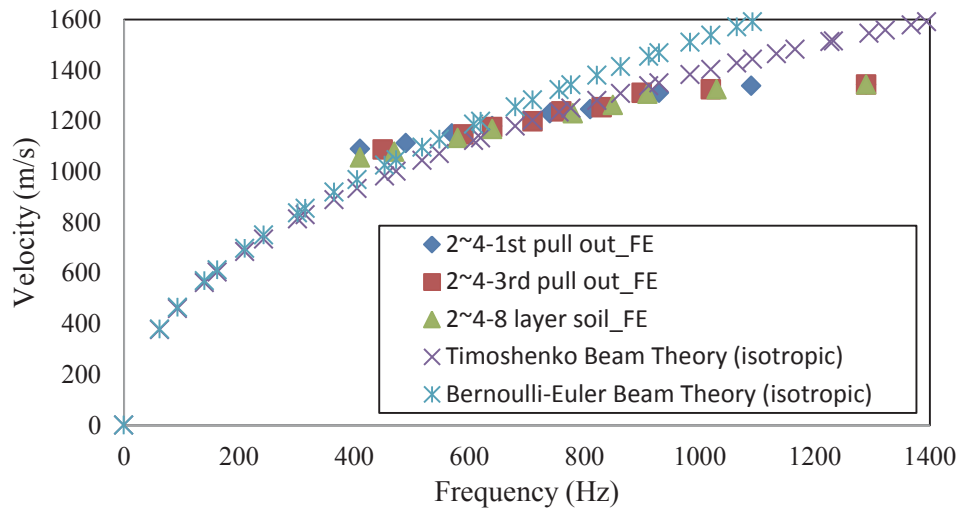


c)

Figure 3.22 Bending wave velocity for different kernel frequencies of 5 m timber pole under different boundary conditions using sensor 1 as a reference a) using sensor 2 as a reflection wave, b) using sensor 3 as a reflection wave, c) using sensor 4 as a reflection wave



a)



b)

Figure 3.23 Bending wave velocity for different kernel frequencies of 5 m timber pole under different boundary conditions using sensor 2 as a reference, a) using sensor 3 as a reflection wave, b) using sensor 4 as a reflection wave

### 3.7.2 Embedded length determination

After investigation of the kernel frequency range for bending wave calculation of 5 m timber pole under different boundary conditions, the embedded length is estimated. Based on the results of the velocity calculation from last step, the calculation of embedded length between sensors 1 and 2 is eliminated from the results as the wavelength will not pass through them due to the small distance between the two sensors. Figure 3.24, Figure 3.25 and Figure 3.26 show the error in embedded length determination with different kernel frequencies using sensor 1 as reference and sensors 3 and 4 for reflection wave. As can be seen in these figures the kernel frequency between 650 Hz to 800 Hz will result in less than 8% error in embedded length determination. Indeed, these ranges between 650 to 800 Hz are recommended to be used as kernel frequencies. It is believed that the frequencies less than 600 Hz should not be used as the wavelength will not catch all sensors.



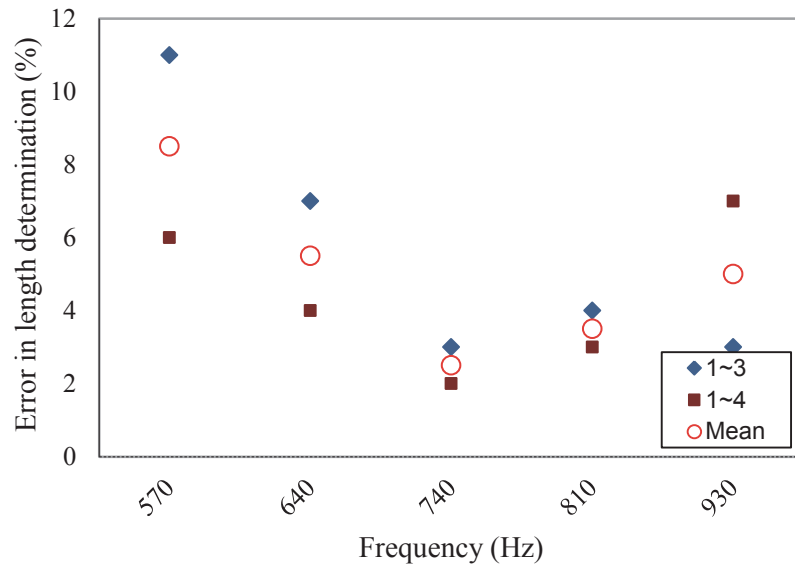


Figure 3.24 Embedded length determination for different kernel frequencies of 5 m timber pole under 1<sup>st</sup> pull out condition.

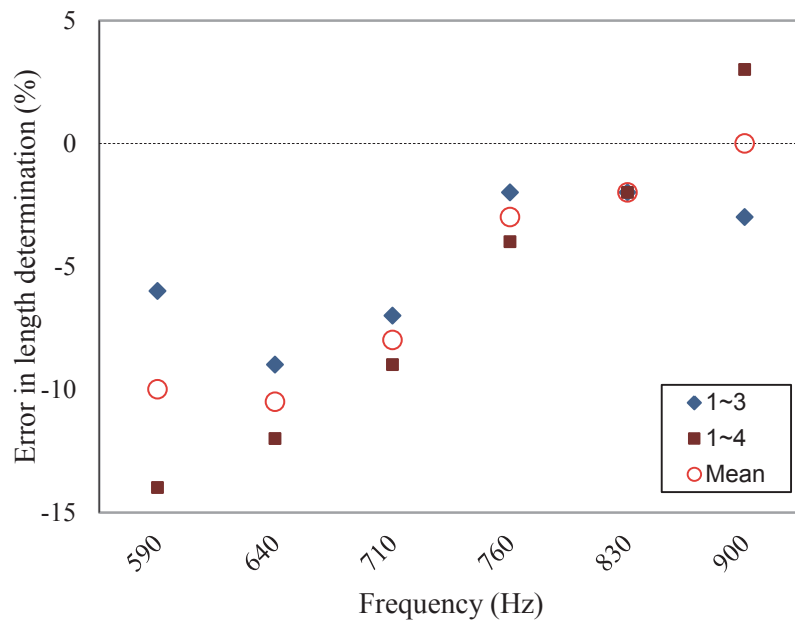


Figure 3.25 Embedded length determination for different kernel frequencies of 5 m timber pole under 3<sup>rd</sup> pull out condition.

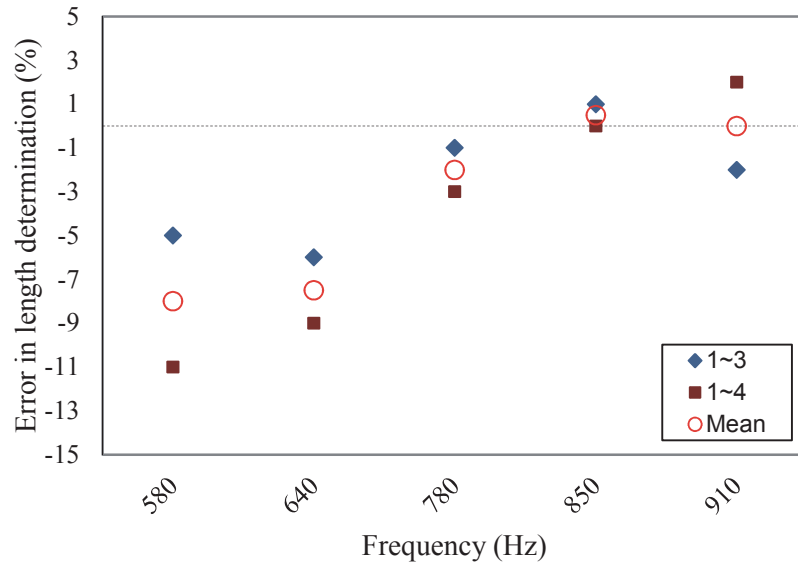


Figure 3.26 Embedded length determination for different kernel frequencies of 5 m timber pole under 8 layer soil condition.

### 3.7.3 Velocity calculation and length determination of filtered results

To ensure that all high frequencies are eliminated from the signal and will not affect the SKM calculations, the acceleration results of numerical simulations of 5m timber pole under 3<sup>rd</sup> pull out condition are filtered using low pass filter before calculation of SKM. Then, the kernel frequency is calculated based on the FFT results, and bending wave velocity is obtained using different reference sensors as shown in Figure 3.27. To gain a better understanding of the range of bending wave velocities, the minimum, maximum and average velocity are also provided in this figure. As can be seen in Figure 3.28, the error of embedded length estimation will be relatively the same as the error of embedded length estimation without using filter before selecting the kernel frequencies from FFT. As a result, filtering the high frequencies does not seem to have significant effect on percentage of error in length determination as the impact force does not have a high broadband frequency.

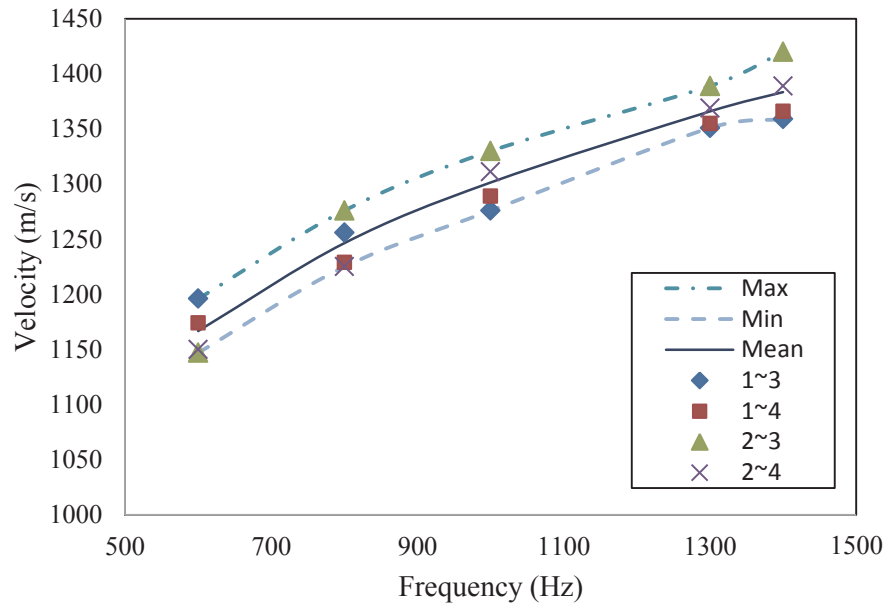


Figure 3.27 Bending wave velocity for different kernel frequencies of 5 m timber pole under 3<sup>rd</sup> pull out condition using filtered results.

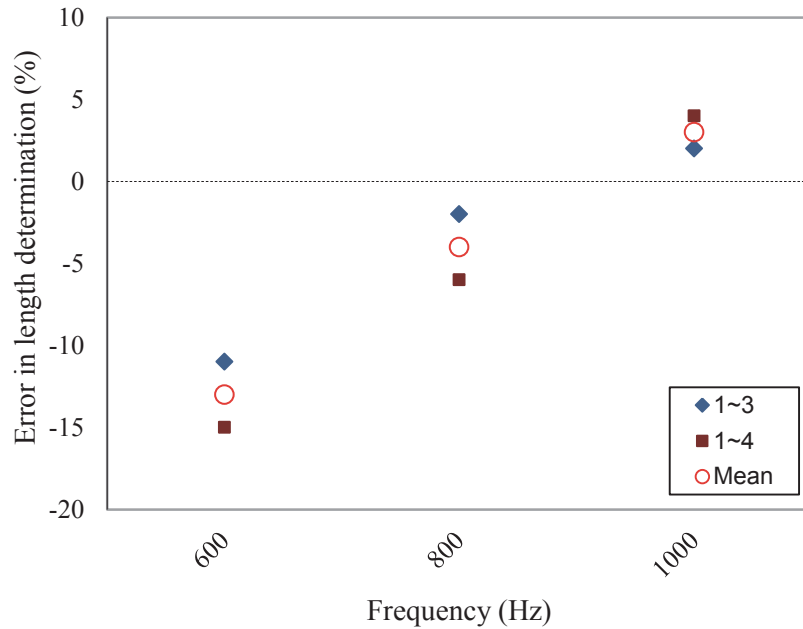


Figure 3.28 Embedded length determination for different kernel frequencies of 5 m timber pole under 3<sup>rd</sup> pull out condition after filtering.

(Subhani et al. 2013) investigated two widely used signal processing methods, SKM and Continuous Wavelet Transform (CWT) on numerical results of the timber pole to determine the phase velocity and also the embedded length. A numerical model was made for a 12m timber pole with 130mm radius. The embedded length of model was set as 2m and a transverse impact was imparted at 3.5m from the bottom of the pole or 1.5m above the ground. The velocity of wave was determined from any two sensors. The location of two sensors was chosen at 3m (sensor 1 or S1) and 2m (sensor 2 or S2) from the bottom of the pole. The result of their analysis for velocity calculation and embedded length determination is presented in Figure 3.29. For calculation of embedded length, CWT shows better results in high frequencies (frequencies more than 1250 Hz), but SKM gives better results for low frequencies (less than 800 Hz) and for frequencies between 800 to 1250 Hz almost similar results are obtained for both methods. (Subhani et al. 2013), concluded that the application of CWT is more straightforward than SKM for allocation of the reflection peak and also very consistent from sensor to sensor and frequency to frequency.

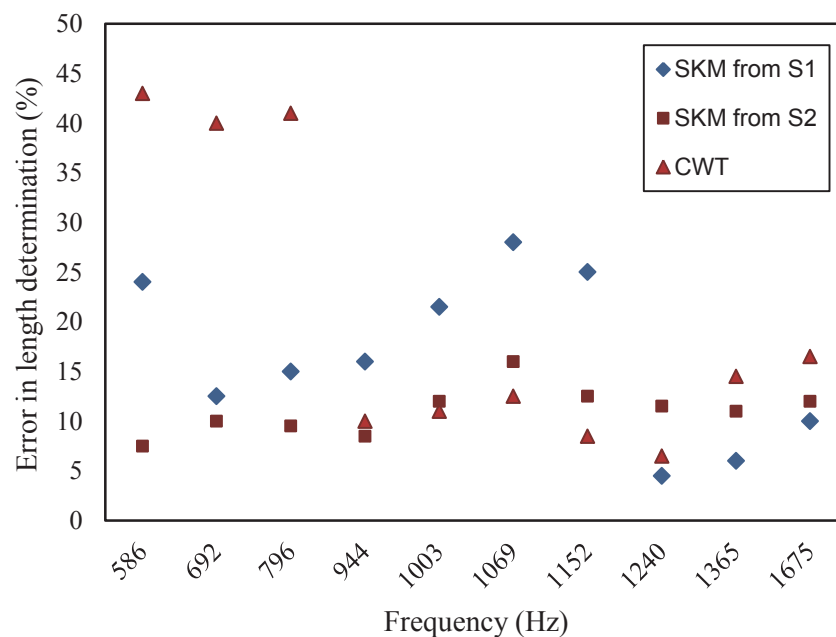


Figure 3.29 Embedded length error for different frequencies of 12 m timber pole under 2m embedment condition using continues wave length and short kernel method

## 3.8 APPLICATION OF ULTRASEISMIC TEST IMPACT ON TIMBER POLE

The test set-up for Ultraseismic testing is the same as for Impact Echo testing method which was described earlier in this chapter.

### 3.8.1 Velocity calculation

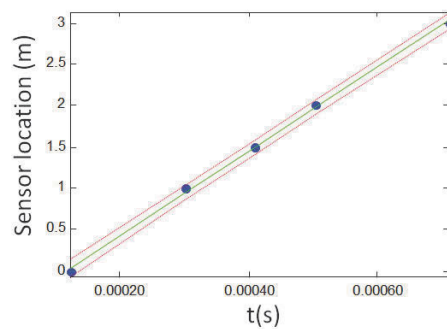
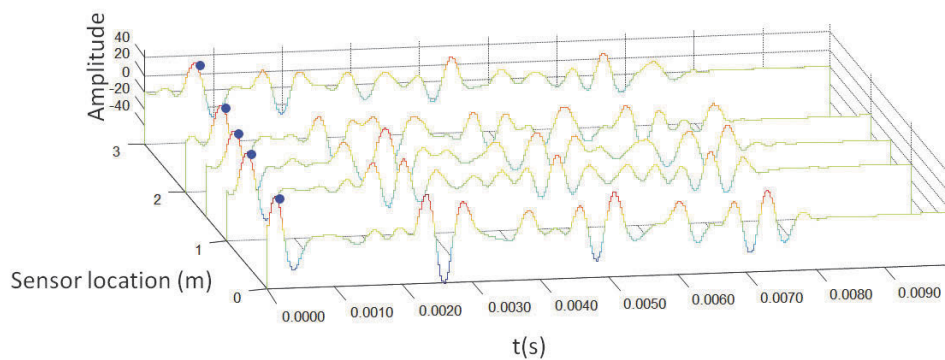
Figure 3.30a and b highlight the first peak arrival and reflection from acceleration-time history of a 5m timber pole under 3<sup>rd</sup> pull out condition using ultraseismic methods. As can be seen in this figure, all sensors mounted on the pole above the soil level are used for stress wave velocity calculation and the pole was impacted from the top. In the 3<sup>rd</sup> pull out condition, the embedment length of pole is 2.1m which is the most similar scenario compared to the real conditions of timber pole in service. To determine the accuracy of velocity, the coefficient of determination is calculated. As can be observed, the coefficient of determination ( $R^2$ ) for velocity determination is close to 1 which indicates a good accuracy in terms of velocity calculation for both arrival and reflection waves. By comparing Figure 3.30a and Figure 3.30b, it is observed that the reflection stress wave velocity will decrease by 5% from 5120 m/s to 4872 m/s. To investigate the velocity below and above the soil, the first peak-time history vs. sensor location is plotted as shown in Figure 3.31; the slope of the graph represents the stress wave velocity. As can be seen in this graph, the velocity below and above the soil is estimated separately by using the linear trend line between the data. Based on the results, the stress wave velocity is decreased by 22% overall below the soil in comparison with stress wave velocity above the soil.

Figure 3.32 a and b also show the first peaks arrival and reflection of acceleration-time history of a 5m timber pole under 5<sup>th</sup> pull out condition using ultraseismic methods for all sensors mounted on the pole above the soil level. As mentioned in the Chapter 3, 5<sup>th</sup> pull out condition has 1.5m embedment length. Figure 3.33 shows the first peak of arrival wave vs. sensor location and the result of the stress wave estimation. Based on the result, the stress wave velocity will decrease in the soil by 20%. (Subhani 2013) investigated the stress wave velocity for timber pole under traction free and fully embedded condition in soft and dense soil. The properties of soil used in guided wave solution are presented in Table 3.3. Figure 3.34 shows the results of the analysis. In this figure T.F. stands for traction free, S.S. and D.S. are referred to soft and dense soil, respectively. As can be interpreted, the velocity in the soil have a significant impact in

soil compared to the traction free condition with higher difference in dense soil compared to soft soil for frequencies less than 2500 Hz. For example for frequency of 1500 Hz, the stress wave velocity is around 4900 m/s. However, the stress wave velocity is around 4550m/s and 4000m/s for soil and dense soil, respectively. It means 7% decrease in stress wave velocity in soft soil compared to traction free and 18% decrease in dense soil in comparison with traction free condition.

Table 3.3 Material properties used in guided wave solution (Subhani 2013)

| Material Parameters          | Timber | Soft Soil | Dense soil |
|------------------------------|--------|-----------|------------|
| Modulus of Elasticity (MPa)  | 23,000 | 100       | 260        |
| Poisson's Ratio              | 0.3    | 0.3       | 0.3        |
| Density (kg/m <sup>3</sup> ) | 950    | 1,400     | 1,800      |



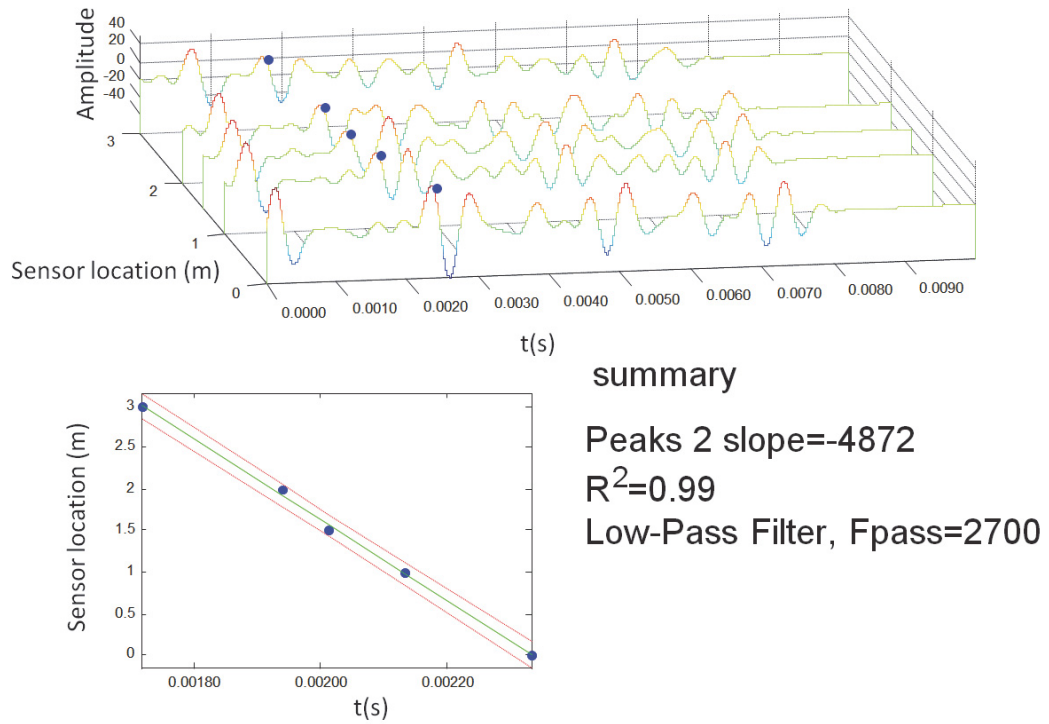
summary

Peaks 1 slope=5119

$R^2=0.99$

Low-Pass Filter,  $F_{pass}=2700$

a)



b)

Figure 3.30 Acceleration results for selected sensors in y direction under 3rd pull out condition using Ultraseismic method a) arrival wave and b) reflection wave

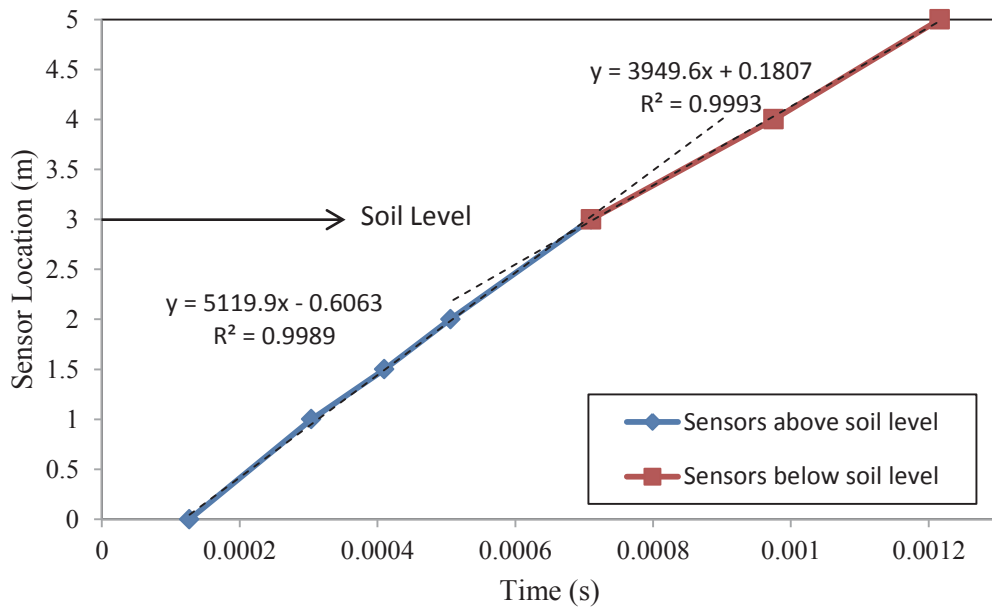
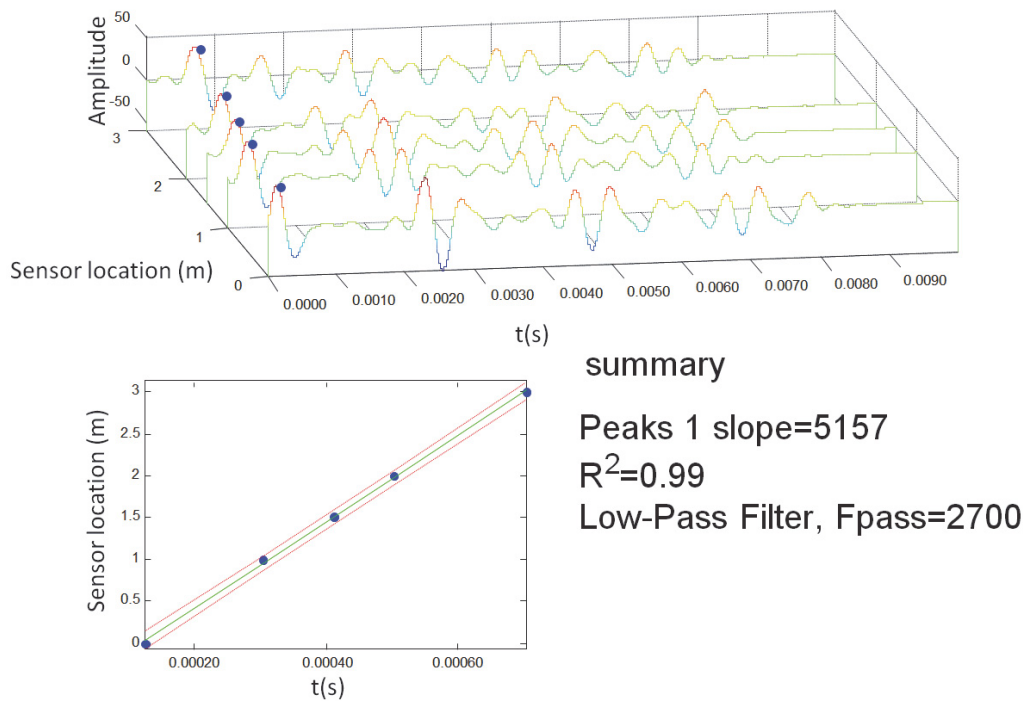
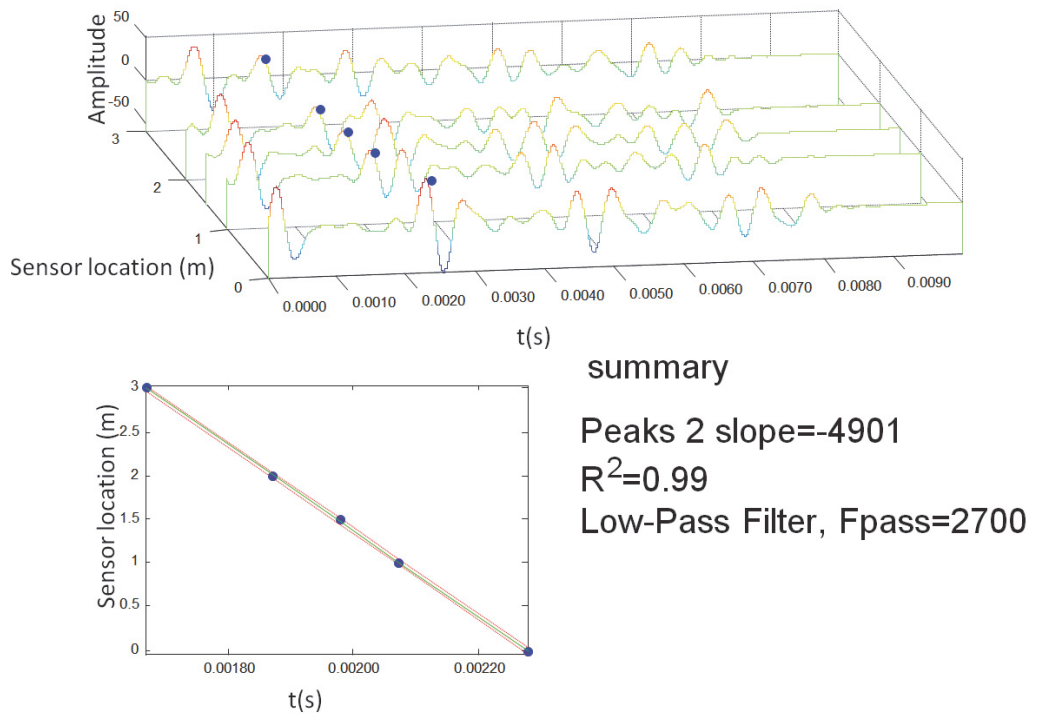


Figure 3.31 Acceleration results in y direction under 3rd pull out condition using Ultraseismic method



a)



b)

Figure 3.32 Acceleration results for selected sensors in y direction under 5<sup>th</sup> pull out condition using Ultraseismic method a) arrival wave and b) reflection wave



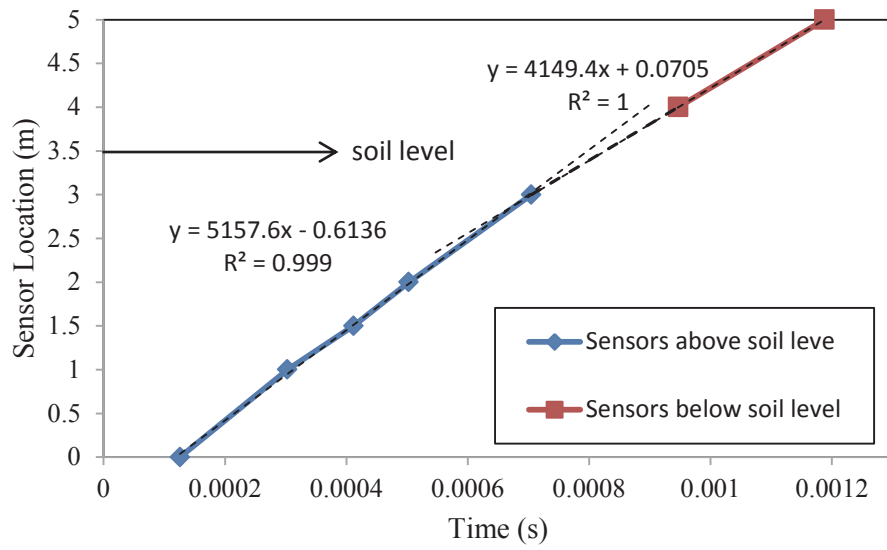


Figure 3.33 Acceleration results in y direction under 5th pull out condition using Ultraseismic method

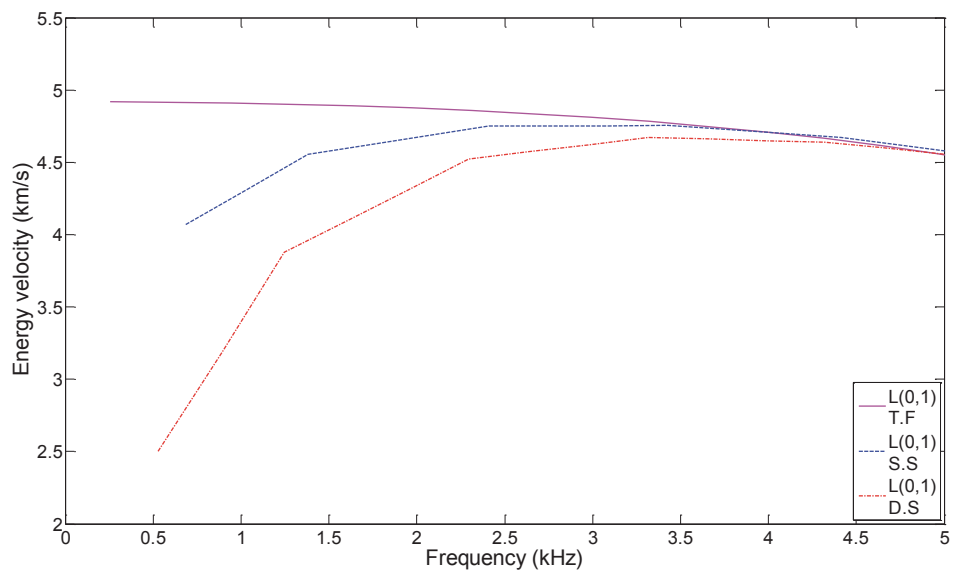


Figure 3.34 Effect of soil in stress wave velocity

### 3.8.2 Embedded length determination

Based on the Ultraseismic method, the length of the timber pole is estimated by cross correlating the first arrival and reflection waves. Figure 3.35 shows the example of

length estimation using acceleration-time history result vs. sensor location. As shown in Figure 3.35, based on the correlation, the estimation of a 5m timber pole under 3<sup>rd</sup> pull out condition is 5.56 m. As a result, by using this method the error of length estimation is 11%. However, as mentioned in the last section, the velocity is different above and below the soil and this should be considered in the length estimation of a pole.

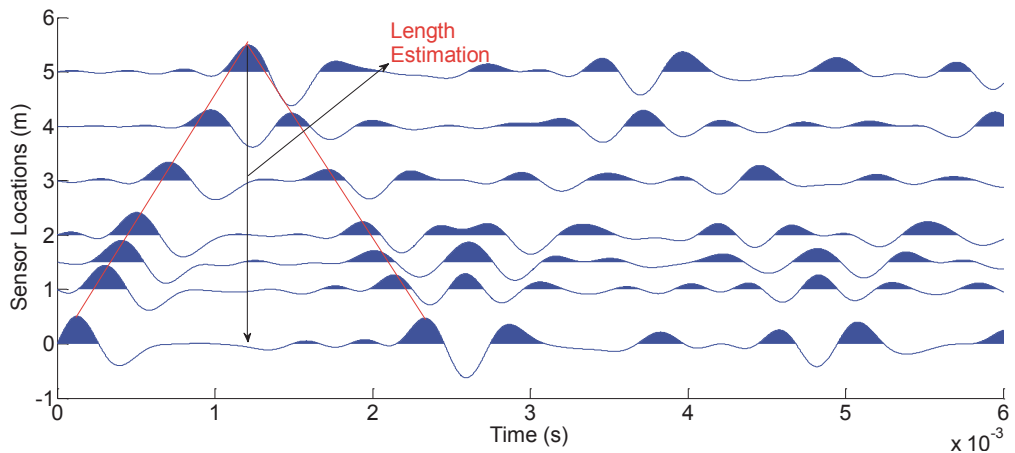


Figure 3.35 Length estimation using sensors above the soil level under 3<sup>rd</sup> pull out condition using Ultraseismic method in 2D graph

### 3.8.3 Alternative impact location

Figure 3.36 shows the schematic test set-up of Ultraseismic testing and sensor arrangements for impact from the middle.

Figure 3.37 shows the acceleration-time history vs. sensor location of a 12m timber pole under 5<sup>th</sup> pull out condition. As can be seen in this figure, impact at the middle of the specimen has generated two compressional waves (travels down and reflects at the butt) and tensile waves (travels up and reflects at the top). This wave interference makes the analysis complicated. In addition, impact from the middle with 45 degree angle generates the combination of horizontal ( $F \cdot \sin 45^\circ$ ) and vertical force ( $F \cdot \cos 45^\circ$ ) which result in contribution of bending wave to longitudinal wave. As a result, this signal includes multiple wave modes which are required to be separated before calculation of velocity and length determination. It should be mentioned that, timber pole is modelled as an isotropic material here and if the anisotropy of the material is included, the analysis will be more complicated.

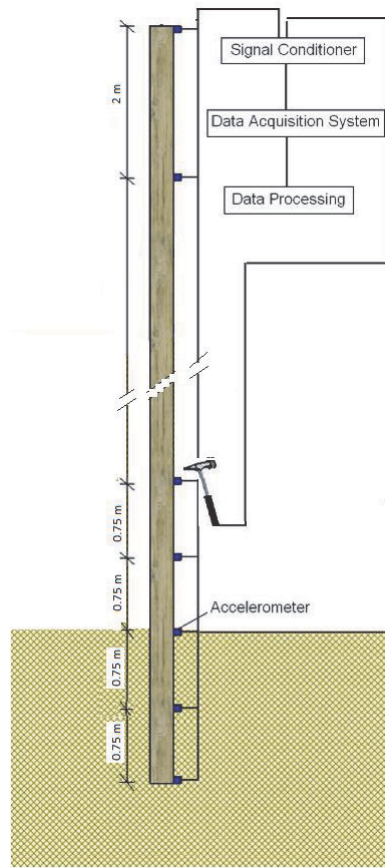


Figure 3.36 Geometry of the model and location of the sensors placed on the timber pole for Ultraseismic test impacted at the middle

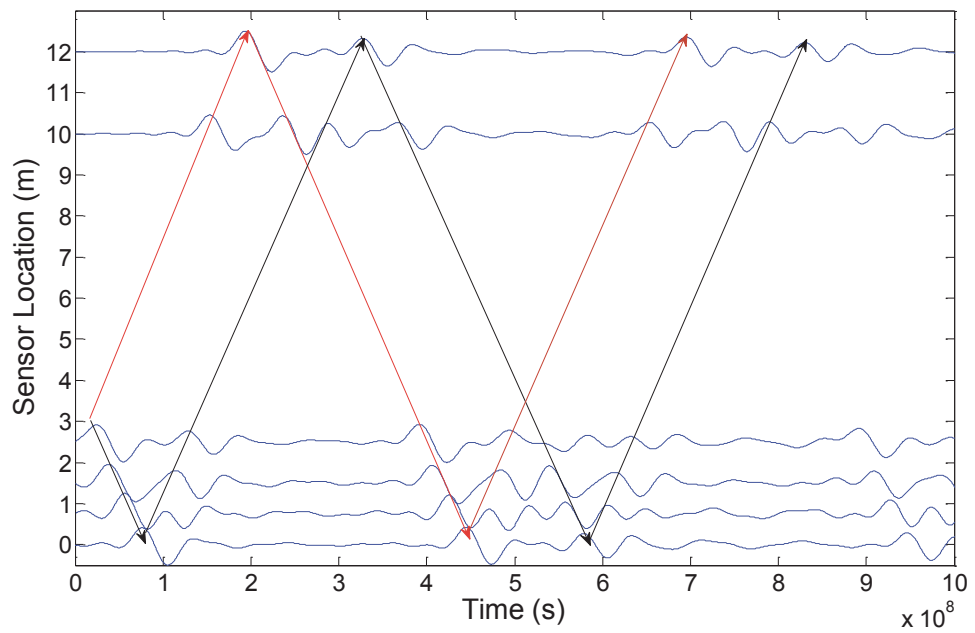


Figure 3.37 Acceleration-time history of 12m timber pole under 5<sup>th</sup> pull out condition using Ultraseismic method with impact at the middle

### 3.9 PRELIMINARY DAMAGE IDENTIFICATION OF TIMBER POLE

In order to introduce damage/defects to the FE model, the finer mesh (with 65 elements in the cross section) has been used. The type 1 damage simulates the decay at the centre of the pole cross section. Three severity levels are considered: 1L, 1M and 1S; 1L representing light damage, 1M representing moderate damage and 1S representing severe damage as shown in Table 3.4.

*Table 3.4 Decay pattern type 1 modelling using FE*

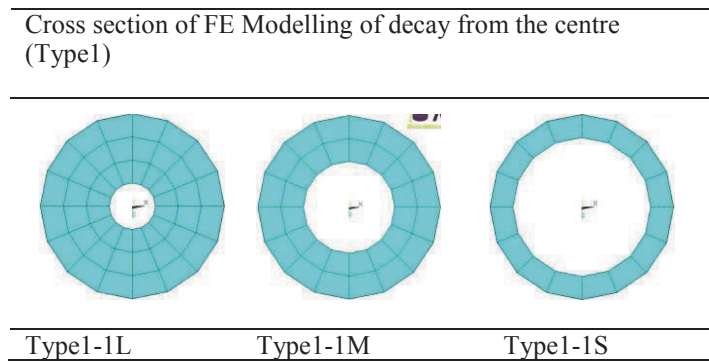
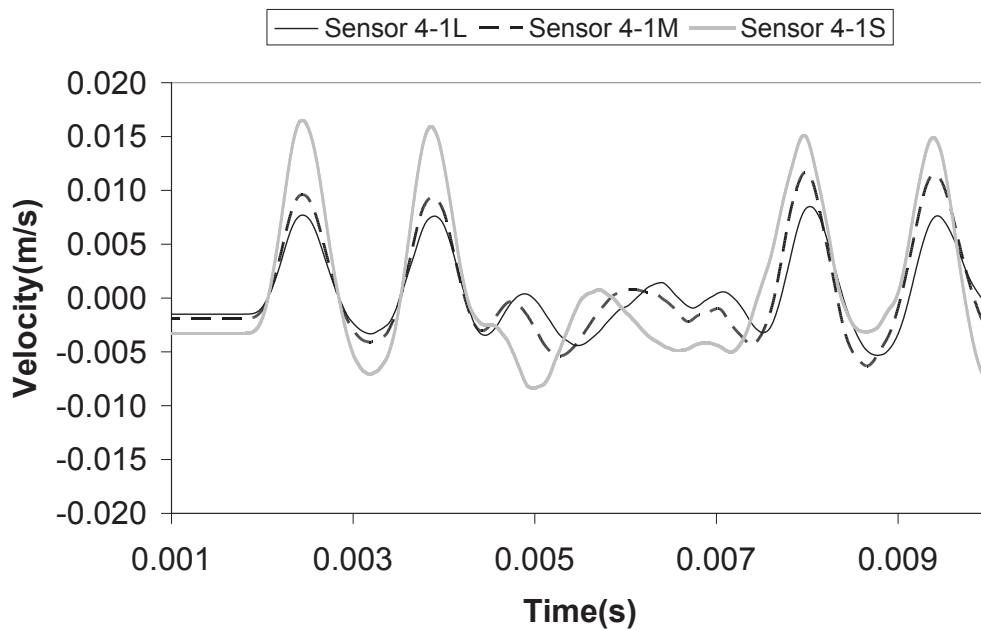
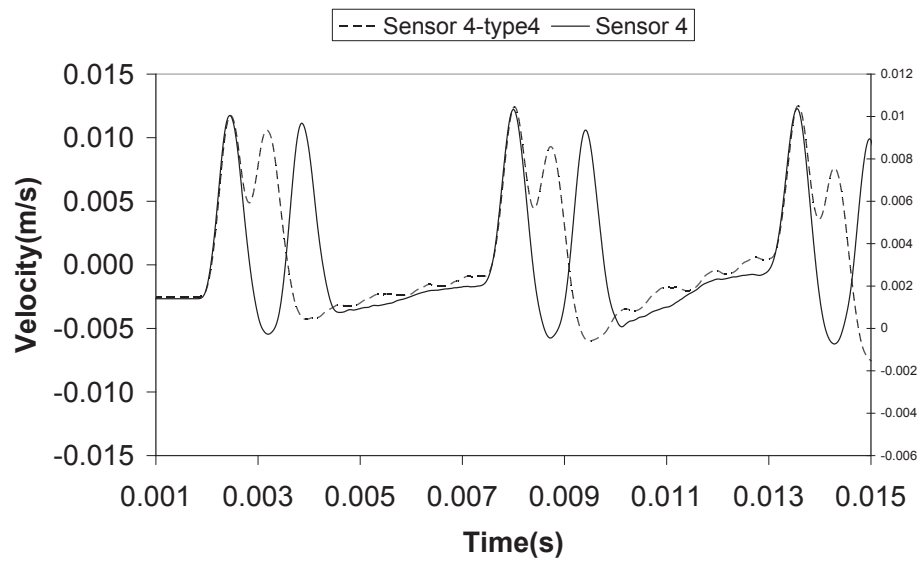


Figure 3.38 shows the stress wave velocity results under free-end condition for type 1 decay. Three damage levels, 1L, 1M and 1S were simulated. As can be observed, severe damage condition corresponds to the higher velocity magnitude which will be used for damage identification.



*Figure 3.38 Velocity results for decay type 1 under three different damage scenarios; 1S, 1M and 1L*

Based on the field test results of 8 timber poles pulled out from the ground after testing, it is observed that the type 1S decay will rarely exist in isolation. However, generally this type of decay occurs in combination with other decay types. Also, another type of decay can be modelled in the numerical analysis by removing the elements in the outer layer of the cross section. Figure 3.39 shows comparison of the results of velocity for timber pole with this decay type and without decay under free end condition. As shown in the figure, the wave is traveling faster in the timber with decay compared to the undamaged timber pole.



*Figure 3.39 Comparison of the free end test with external decay and without decay*

Non-destructive evaluation such as the sonic echo method and the impulse response method of deep foundations have the ability to identify small defects due to the long wavelengths associated with the low frequencies induced by a hammer impact and insufficient measurement to determine the propagation velocity unless the exact location of a reflection source is known. Furthermore, (Finno & Gassman 1998) showed the presence of an intervening structure, limits the amount of energy transmitted to the deep foundation.

As a result, a damage scenario has been modelled identical to the laboratory case on an artificially damaged pole for length and damage location identification. For the damaged pole, a half section of 1 m length is removed from the bottom of the pole. This

type of damage simulates termite attack, which is often found in timber poles in-service. Both poles are modelled by free-free with impact from the centre top. The finite element model for the damaged pole test-set up is illustrated in Figure 3.40. The results of acceleration-time history are presented in Figure 3.41 and Figure 3.42 for sensors 4 and 6, respectively. As can be seen, there is an additional peak observed due to presence of damage.

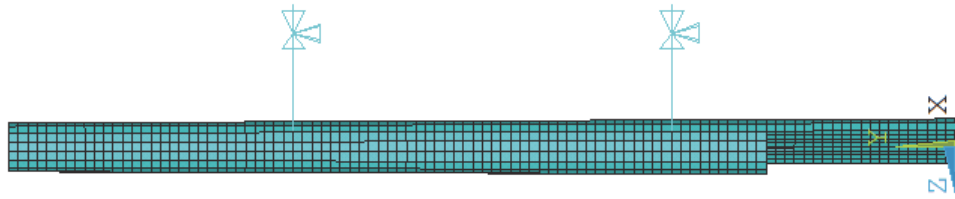


Figure 3.40 Side view of a damage inflicted in timber pole identical to the laboratory case

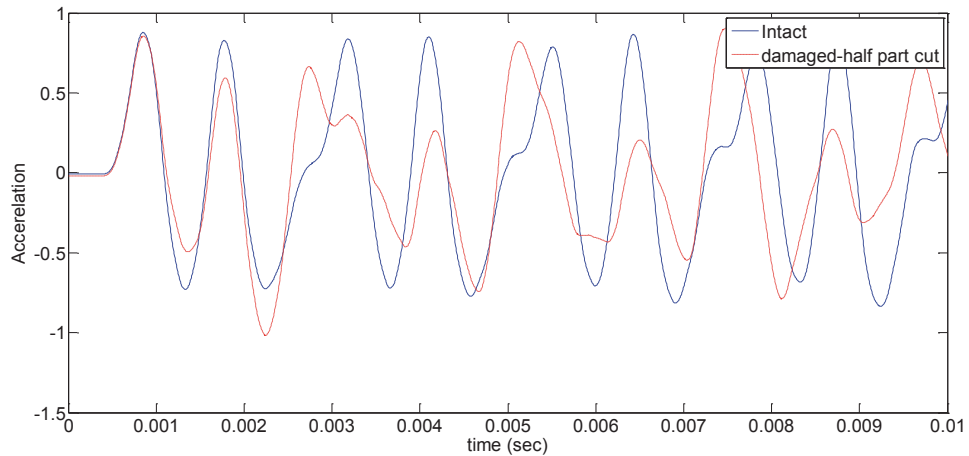
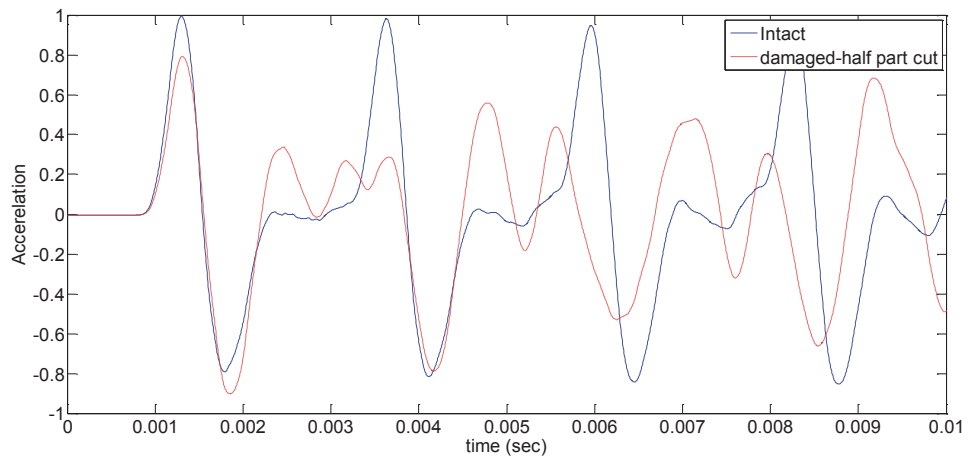


Figure 3.41 Acceleration-time history results for intact and damaged pole of 5m timber pole for sensor 3



*Figure 3.42 Acceleration-time history results for intact and damaged pole of 5m timber pole for sensor 6*

### **3.10 SUMMARY**

In this chapter, the numerical investigations of non-destructive testing methods such as Impact Echo/Impulse Response, Bending Wave and Ultraseismic method of a timber pole are carried out. A numerical model involves a 5m timber pole identical to laboratory tests and a 12 m timber pole identical to a specimen in the field. The stress wave generation in the pole is investigated using transient analysis under different boundary/testing conditions to get better understanding of stress wave generation in timber pole.

An FE model was firstly generated under free-free condition using isotropic material properties aiming at gaining an understanding on stress wave behaviour of a timber pole without any uncertainty of material properties and also boundary conditions. This model was verified with static analysis for model verification. Then, FE beam model was enhanced with more advanced features requiring more steps to simulate other boundary conditions. In FE modelling, isotropic material properties was used to eliminate the effect of uncertainty in orthotropic material on the results. The effects of different types of impact loading on the timber pole confirms that the concentrated load at the centre of cross section will generate symmetrical waves compared to impact at the edge of cross section (field application) which produces anti-symmetrical waves.

To investigate the effect of surrounding soil on stress velocity determination, different pull out conditions identical to the experimental test are modelled. According to the results, stress wave velocity will decrease with increase in embedded length. Therefore, two different velocities, one for stress wave travel above the soil level and the one with travelling inside of the soil (around 20% decrease) was calculated. The error of length estimation averaged between 5% and 9% depending on the boundary condition and the reference sensor for calculation. By increase in the soil depth, the error of the length estimation is increased from 5.5% for 1.5m embedment to 7.1% for 2.7m embedment using sensor 1. Indeed, considering timber pole as an isotropic material, leads to the maximum error of 8% for length determination under embedded conditions using multi sensor for velocity calculation.

In Bending Wave method, as there are no guidelines to select those kernel frequencies, different kernel frequencies were selected based on the results of FFT and then by applying the SKM method, acceleration-time history graph is generated for each of them. After calculating the time difference, velocity is determined for different kernel frequency and different sensors of 5m timber pole under 1<sup>st</sup>, 3<sup>rd</sup> pull out and 8 layer soil as testing conditions. The short kernel method was used for analysis of the bending wave result of a timber pole. As a result of the bending wave velocity investigation, the appropriate kernel frequency is identified to be between 600 to 800 Hz. The results are verified using Bernoulli-Euler Beam theory and Timoshenko beam theory. Based the length estimation, the kernel frequencies between 650 Hz to 800 Hz will result in less than 8% error in embedded length estimation.

Furthermore, the Ultraseismic method is applied on the results of timber modelling. The coefficient of determination ( $R^2$ ) for velocity determination is close to 1 which indicates a good accuracy in term of velocity calculation for both arrival and reflection waves. Based on the result of velocity below and above the soil, the stress wave velocity is decreased by 22% overall below the soil in comparison with stress wave velocity above the soil. Literature review also confirms that the stress wave velocity will decrease in the soil (Subhani 2013). Based on the Ultraseismic method, the length of the timber pole is estimated by cross correlating the first arrival and reflection waves. Based on the correlation, the estimation of a 5m timber pole under 3<sup>rd</sup> pull out condition is 5.56 m. As a result, by using this method the error of length estimation is 11%.



Ultraseismic test impact at middle is also investigated for a 12m timber pole under 5<sup>th</sup> pull out condition. It was found that, impact at middle of the specimen generated two compressional waves (travels down and reflects at the butt) and tensile waves (travels up and reflects at the top). This wave interference makes the analysis complicated. In addition impact at the middle with 45 degree angle generates the combination of horizontal and vertical forces which result in contribution of bending wave to longitudinal wave. As a result, the signal includes multiple wave modes which are required to be separated before calculation of velocity and length determination. It should be mentioned that, timber pole is modelled as an isotropic material here and if the anisotropy of the material is included the analysis will be more complicated.

Decay within the centre and outer surface was modelled by numerical analysis and the results showed that the velocity did not change significantly in presence of damage.

# CHAPTER 4

## 4 Experimental Investigation of Timber Utility Poles

### 4.1 INTRODUCTION

This chapter presents details of surface stress wave methods for non-destructive assessment of timber structures being developed at the University of Technology Sydney as part of this research study. The equipment, testing procedures and data analysis of traditional and improved surface stress wave techniques, i.e. Sonic Echo (SE) method, Impulse Response (IR) method, Bending Wave (BW) method and Ultraseismic method are described in this chapter. To demonstrate methods, they are applied to steel and a timber beam and also timber poles (in- and out-of-service) for the determination of integrity and embedment length. For the presented methods, a step-by-step guide is provided on how to execute the tests, how to analyse the recorded data, how to calculate the length of the test structures and how to identify potential damage locations.

### 4.2 TEST EQUIPMENT

The equipment necessary to perform surface stress wave testing consists of: a modally tuned impact hammer, multiple sensors (accelerometers or geophone velocity transducers), a multi-channel signal conditioner, a data acquisition system and a personal computer equipped with signal acquisition software.

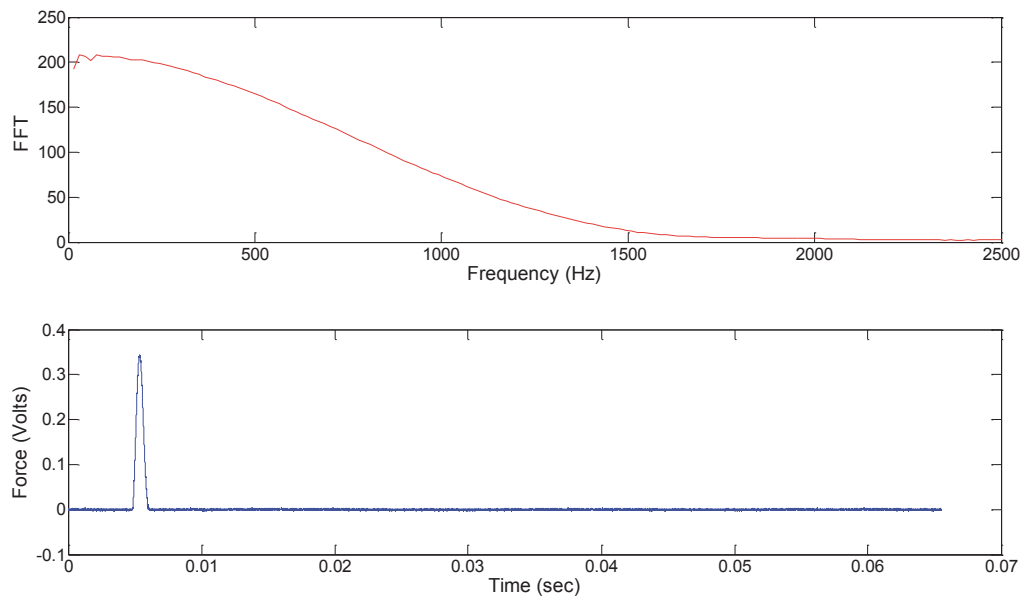
#### 4.2.1 Impact hammer

For stress wave testing, the impact hammer used is a PCB model HP 086C05 of sensitivity 0.24 mV/N. The hammer is equipped with a load cell to measure the force of the impact. Two types of hammer tips were used to investigate the impact force as shown in Figure 4.1 (a) and (b). Based on the results, the stiff tip which is made from Teflon provides higher force as a result of strike. This tip is used for conducting

experimental and field tests. Figure 4.2 show an example of the force spectrum from the hammer blow.



(a) (b)  
*Figure 4.1 Impact hammer (a) stiff tip, (b) soft tip*



*Figure 4.2 Typical response of hammer impact*

#### 4.2.2 Accelerometers

To record the structural response, two different types of accelerometers were used; they are piezoelectric and piezoresistive accelerometers. The piezoelectric accelerometers employed are PCB model 356A08 and model 337A26 (see Figure 4.3(a) and (b)), which are of low impedance, having a sensitivity range from 94 mV/g to 100 mV/g. The piezoresistive accelerometers used are low cost dual-axis accelerometers of model ADXL320, having a bandwidth of 0.5 Hz to 2.5 kHz. As these low-cost accelerometers were purchased only in the form of a circuit board (see Figure 4.3 (c)), they were encased into a specially designed housing (depicted in Figure 4.3 (d)). While the

piezoresistive accelerometers (model ADXL320) are inexpensive, they are of high accuracy with a sensitivity range of 154 to 194 mV/g (compared to 94 to 100 mV/g for the piezoelectric accelerometers used).

The accelerometers were mounted to the steel beam by epoxy and to the timber beam and timber pole by two screws as illustrated in Figure 4.4.

The accelerometers are calibrated by the back to back method, in which the accelerometer is mounted to a reference standard, which is, in turn, mounted to a vibration exciter (e.g., a shake table). The vibration exciter is operated over a range of frequencies by a function generator and the output voltages of both the accelerometer and reference standard are measured. The ratio of the accelerometer voltage to the reference voltage is computed at each frequency to determine the accuracy of the accelerometer as shown in Figure 4.5.

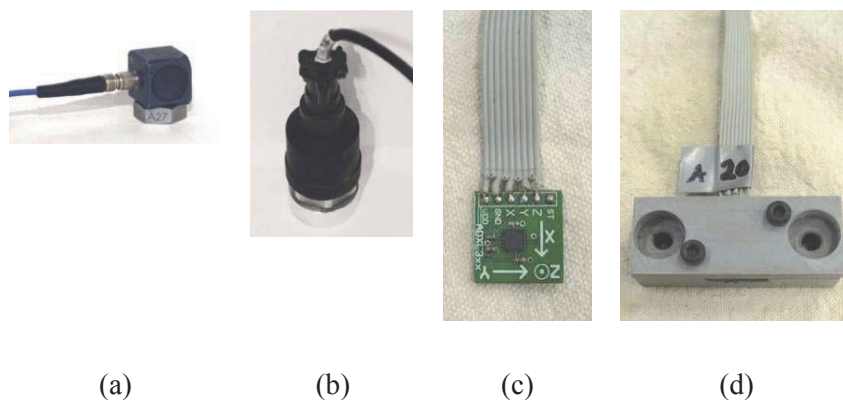


Figure 4.3 Testing accelerometers (a) piezoelectric accelerometer - model PCB 356A08, (b) piezoelectric accelerometer - model PCB 337A26, (c) piezoresistive accelerometer chip ADXL320 (d) piezoresistive accelerometer with housing



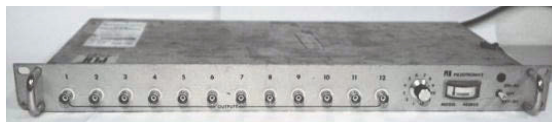
Figure 4.4 Accelerometers mounted to the a) steel beam and b) timber beam by screws



*Figure 4.5 Calibration of the accelerometers using a shake table*

### **4.2.3 Signal Conditioning and computer**

To amplify and condition the signals of the modal hammer and the piezoelectric accelerometers, a 12-channel signal conditioner (model PCB 483B03) is used (depicted in Figure 4.6 (a)). For piezoresistive accelerometers, the DC power supply shown in Figure 4.6 (b) is utilised. The data acquisition system employed for stress wave testing at University of Technology Sydney (UTS) is a middle range 8 channel system with 12-bit 4M samples/sec per channel model NI PCI-6133. Based on data acquisition system requirements for this research, it is essential to utilise a data acquisition system that is able to record signals with a minimum sampling frequency of 1M samples/sec per channel. For data processing, a personal computer (PC) equipped with the National Instrument software LabVIEW is used. As the size of the acquisition card did not fit the laptop, a PC was used for all laboratory and field testing as shown in Figure 4.7.

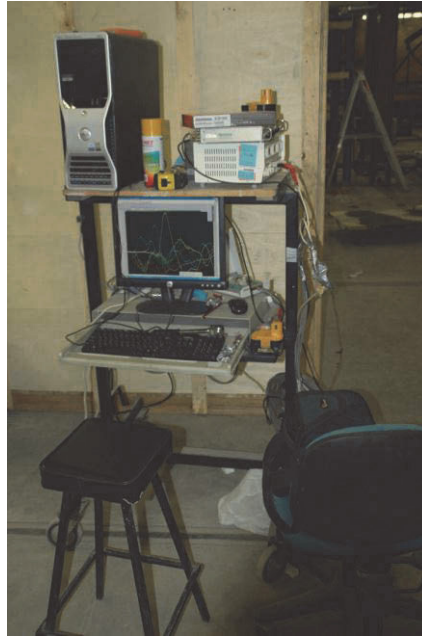


(a)



(b)

*Figure 4.6 (a) Multi-channel signal conditioner - model PCB 483B03 and (b) DC power supply.*



*Figure 4.7 A personal computer for laboratory and field testing*

#### **4.2.4 Laboratory testing frame**

A container, 1.2 m  $\times$  1.2 m in cross-section and 3 m in height was designed and fabricated to contain sand/soil for embedding different test specimens with various embedment lengths. A steel frame is assembled using equal angle steel for the columns and for support of the boundaries. Plywood is used for the boundaries. For three sides of the frame, fixed plywood is used and for the other side, the boundary is completed using a small frame of plywood as shown in Figure 4.8. Scissor lift and scaffold was used to assemble the frame and also for filling the soil and impact the specimens as shown in Figure 4.9.



*Figure 4.8 Steel frame used as a container*



a) Scaffold to build the frame



b) Scissor lift to fill the soil into frame

*Figure 4.9 Using scaffold and scissor lift to build and access the top of the frame*

## 4.3 TESTING SCENARIOS

### 4.3.1 Testing Procedure

For various free-free and embedded Sonic Echo (SE) tests, a step-by-step testing procedure, including the set-up of the equipment, the settings of the acquisition software and the execution of the tests, is described as follows.

1. Setting up of personal computer, data acquisition system and signal conditioner (see Figure 4.10 (a)).

Note: All electrical devices must be connected to the same power supply. If a generator is used, it must be earthed.

2. Attachment of sensors and impact bracket to the structure (Figure 4.10 (b) and (c)).

Note: The number and locations of the sensors depend on the type and requirements of the individual test. Depending on the kind of sensors, different mounting techniques are employed to attach the sensors to the specimens. Either way, it must be assured that a firm connection between the structure and the sensors as well as the impact bracket is established. For the piezoresistive accelerometers used at UTS, wood screws were used to mount the sensors to the structure using a cordless drill (see Figure 4.10 (b)). For magnetic sensors (such as the piezoelectric accelerometers used at UTS), steel plates are screwed or glued (using epoxy) to the structure to provide an adhesive surface. All sensors must be so orientated to measure longitudinal vibration.

3. Connection of the impact hammer and sensors to the signal conditioner, data acquisition system and personal computer.

Note: For piezoresistive accelerometers used at UTS, the voltage of the DC power supply is between 6 to 12 mV. A voltmeter has been used to check the voltage. If the voltage is below 6 mV or above 12 mV it must be adjusted.



To create a longitudinal or bending wave in a timber pole, the pole must be struck in a longitudinal or transverse axis direction, respectively. The impact must be controlled to reduce local crushing of the contact interface between the pole and the impact hammer. The surface of the pole and impact device must be free of any debris that might inhibit the energy exchange between the device and the pole surface. It is essential that the impact device itself is also able to withstand multiple impact without crushing or damage.

4. Launching and setting up of data acquisition software (e.g. National Instrument LabView).

Note: In the data acquisition software, the sampling rate is set to at least 1 GHz for a frequency range of 100 Hz to 5 kHz and a minimum time duration of 0.5 s. The calibration factors of the impact hammer and all sensors must be assigned to the corresponding channels. To ensure that the entire impact excitation signal is recorded, a pre-trigger delay of 0.01% of the test duration was set.

5. Execution of trial tests.

Note: To ensure that the testing equipment was set-up correctly and that all sensors were working properly, a number of trial tests were performed. The following features must be checked for the hammer and all sensor channels: noise-to-signal ratio of hammer and sensor signals (must be lower than 1%), amplitudes and shapes of hammer and sensor signals, DC offsets of sensor signals and consistency of sensor signals between different tests.

6. Execution of actual tests (see Figure 4.10 (d)).

Note: For every test specimen, at least five tests were performed in order to check consistency and repeatability to provide averaged test results for increased robustness. The hammer strike was performed in a straight manner to ensure precise

longitudinal excitation. The impact force is to be executed either at the head centre of the test specimen or at an impact bracket firmly attached to the side of the structure.

7. Saving of recorded data. Disconnecting, dismantling and packing of equipment.

Note: Any abnormalities, special occurrences or events were noted down for future reference.



*Figure 4.10 Testing procedure: (a) setting up of equipment, (b) mounting of accelerometer, (c) attached bracket and accelerometers and (d) execution of the test.*

### 4.3.2 Test specimens

In order to address uncertainty and reliability issues, contributing factors were independently investigated. Accordingly, before commencing any non-destructive tests on embedded timber poles, benchmarking tests were conducted in the structures laboratory of the University of Technology Sydney (UTS). The approach undertaken involved testing columnar specimens with a free-end condition (specimen suspended by two ropes) in the structures laboratory to determine sensor types and data acquisition requirements, benchmarking tests and analysis procedures and expected accuracy.

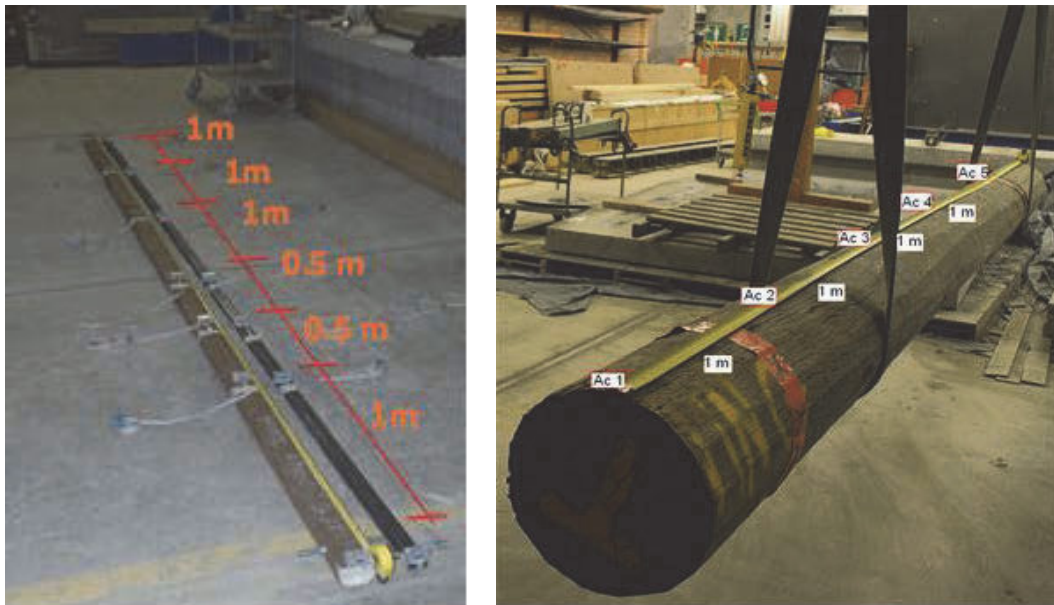
Due to the uncertainty resulting from variability of timber materials, a steel beam (assumed to be homogeneous and without defects), was chosen as a benchmark for the tests as shown in Figure 4.11. A rectangular cross section timber beam was used to verify the behaviour of timber pole without any defects as shown in Figure 4.12 and the timber pole represented an actual field specimen having imperfect geometry, complex material property and local defects. Figure 4.13a shows the location of the accelerometers on the steel and timber specimens. Figure 4.13b shows the experimental set up under free-end conditions including the location of the accelerometers which were used for the tests with timber pole specimen.



*Figure 4.11 Laboratory free-free test for steel beam*



Figure 4.12 Laboratory free-free test set-up for timber beam



a)

b)

Figure 4.13 a) location of the accelerometers on steel and timber beam specimens, b) laboratory set-up for NDT method under free-end conditions with timber pole specimen

### 4.3.3 Different types of testing

After conducting free-free tests on different types of specimens, A number of laboratory tests were conducted at UTS for different embedded conditions in the laboratory (with

impact location on top of the specimen). Firstly, the test was conducted without filling the container with soil and specimens were located on the concrete slab (which can present the bed rock boundary condition). Figure 4.14 presents the laboratory set-up for all specimens under bedrock condition.



*Figure 4.14 Test set-up of bedrock condition in laboratory*

The container is then filled with sand as shown in Figure 4.15. After filling sand in each layer, a series of tests were conducted to verify the effect of the soil depths on the NDT results. The test configuration for laboratory testing conducted at UTS with impact location on top of specimen is shown in Figure 4.16. The container was filled with sand at 8 different stages to simulate the different embedded depths while specimen was located on bedrock. The specimen was then pulled from the foundation material in 0.3 metre increments and tested at each point to simulate different embedded depths. The test was then repeated up to six times until the remaining underground depth of the pole reached 1.5 metres (as shown in Figure 4.17).



a)

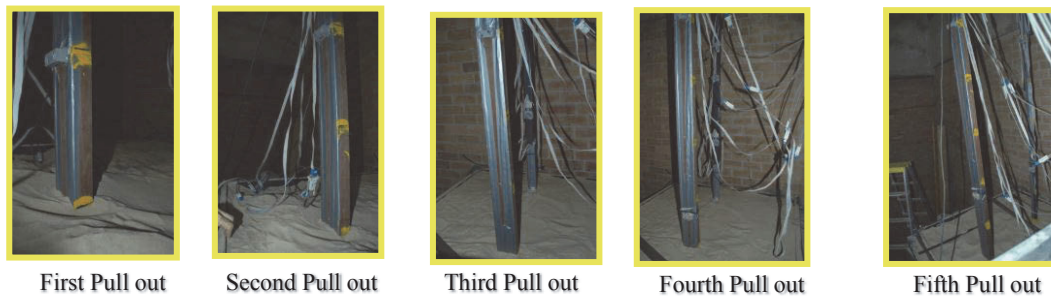


b)

*Figure 4.15 Filing the sand a) into the buckets and b) into the frame*



*Figure 4.16 The laboratory set-up for NDT methods under embedded conditions for a timber pole*



*Figure 4.17 The laboratory set-up for NDT methods using pull out to simulate various embedment depths (timber beam specimen)*

#### **4.3.4 Damage scenario induced for timber pole**

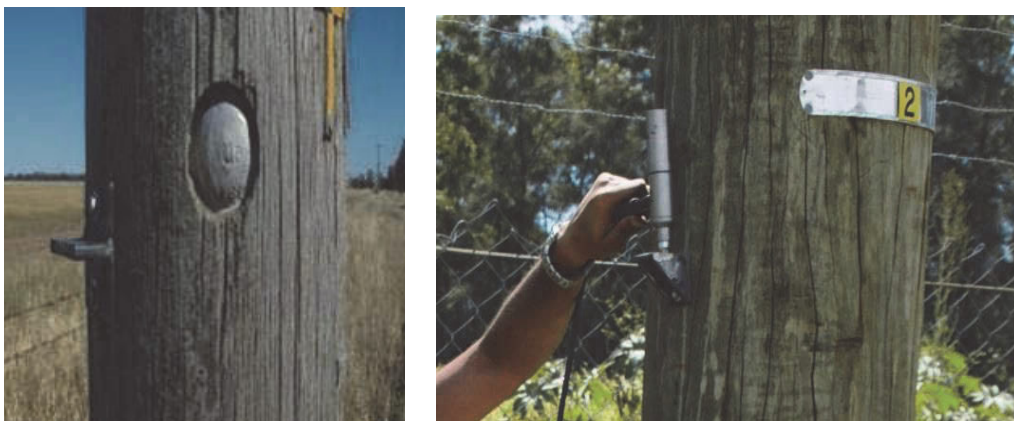
One aspect of this study is to determine the condition of the timber pole in-service which intends to detect damage specifically in the bottom part of the pole. One major damage scenario considered in this study which consists of removing one half section of the pole from the bottom to 1m upwards is shown in Figure 4.18.



*Figure 4.18 side view of a typical damage inflicted in timber pole in laboratory*

#### **4.4 TEST SET-UP FOR SONIC ECHO AND IMPULSE RESPONSE METHOD**

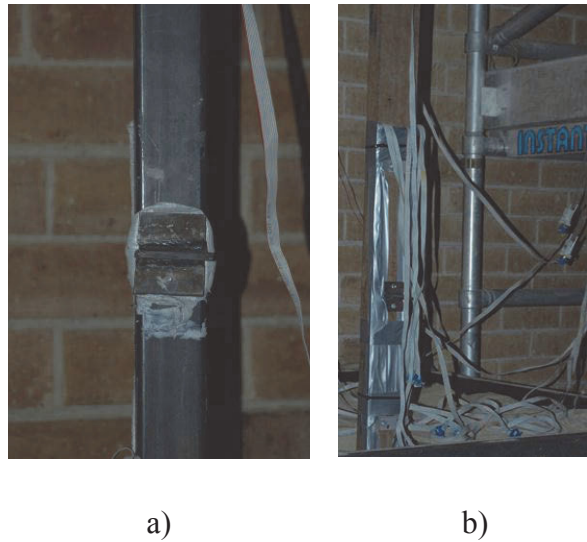
In Sonic Echo and Impulse Response testing, the test structure is excited in the longitudinal direction with a modally tuned impact hammer. The ideal impact location is the top centre of the structure (only longitudinal waves are generated). For practical applications, however, an impact from the end of a structure is not always possible, as is the case for utility poles in-service. Since the excitation must be executed in longitudinal direction, a bracket was used and fixed to the structure in order to provide an impact surface (Figure 4.19). For laboratory testing, the bracket was attached to the steel specimen by epoxy and to a timber beam by using two screws as shown in Figure 4.20.



*Figure 4.19 Impact bracket mounted to the side of a timber pole to provide a surface for longitudinal impact excitation.*

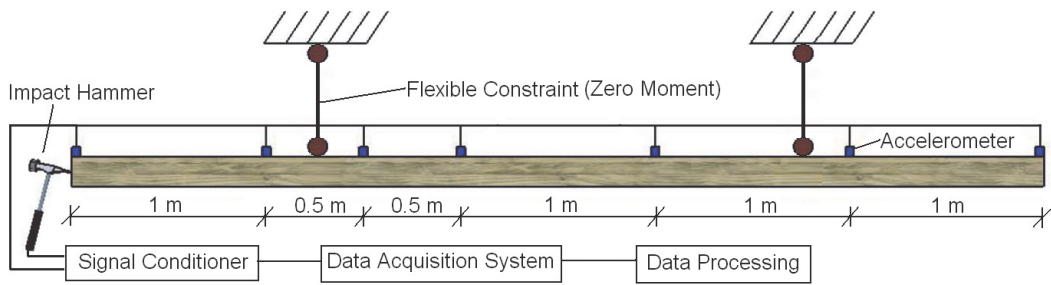


To record the time travel of the longitudinal stress waves, sensors are attached to the test structures to monitor the structural response. At least one sensor, located close to the impact location, measuring longitudinal vibration, is necessary to capture the reflection waves of the impact. In order to increase test reliability and accuracy, a number of sensors were mounted at strategic locations.



*Figure 4.20 Impact bracket mounted to the side of a a) steel pole b) timber beam to provide a surface for longitudinal impact excitation.*

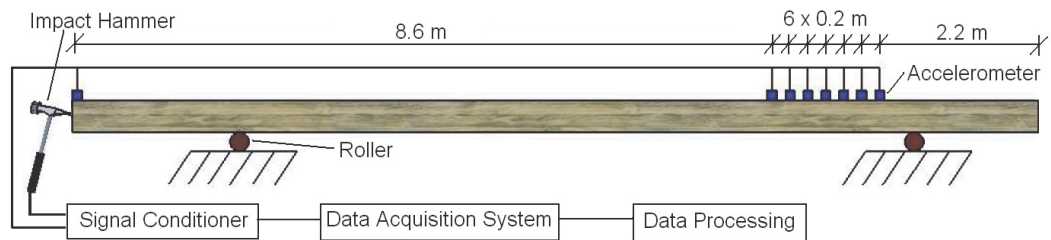
For the testing of in-service and out-of-service timber beams and poles, different test configurations were used. For out-of-service structures, a “free-free test” was conducted. In free-free testing, specimens were either suspended in the air by two sling straps (for laboratory applications - see Figure 4.21 (a) and (b)) or are simply supported by two beams (for field applications - see Figure 4.21 (c), (d) and (e)). The number and positions of the sensors depend on the availability of acquisition channels and sensors, the desired accuracy and the purpose of the test. As shown in these figures, one sensor was mounted close to top and cluster of sensors (seven sensors) from 2.2m from the bottom of the timber pole. When a particular section is to be examined (such as the damage prone bottom part of previously embedded timber poles in field), a cluster of sensors was mounted close to this section (such as shown in Figure 4.21 (c), (d) and (e)). In experimental tests, five sensors were used for testing. For field testing of free-free timber poles, seven sensors were used and mounted in a line, 20 cm off the ground with spacings of 20 cm between the sensors as depicted in Figure 4.21 (c) and (d).



(a) Schematic test set-up of laboratory free-free test



(b) Laboratory free-free test



(c) Schematic test set-up of field free-free test



(d) Field free-free test



(e) Field free-free test

Figure 4.21 Test set-up for free-free testing of (a) and (b) laboratory testing and (c) to (e) field testing.

For the testing of in-service utility poles, “embedded tests” were conducted. The conducted test configuration for laboratory testing conducted at UTS (with impact location on top of the specimen) is shown in Figure 4.22. The test set-up for embedded field testing (with impact along the structure) is shown in Figure 4.23. The number and positions of sensors are again subjected to the purpose of the test and the sensor

availability. For field testing of embedded timber poles, seven sensors were used and mounted in a line 20 cm off ground with spacings of 20 cm between the sensors as depicted in Figure 4.23.

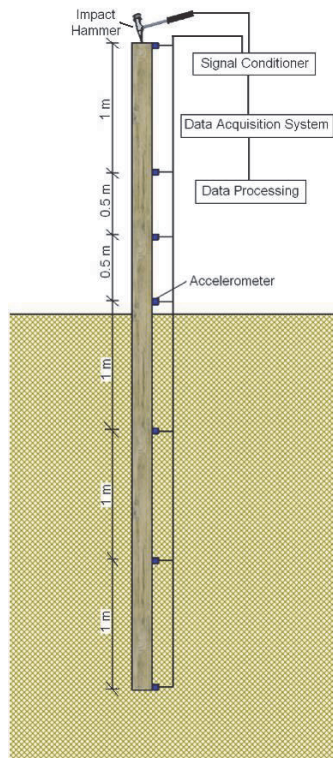


Figure 4.22 Test set-up of embedded testing in laboratory

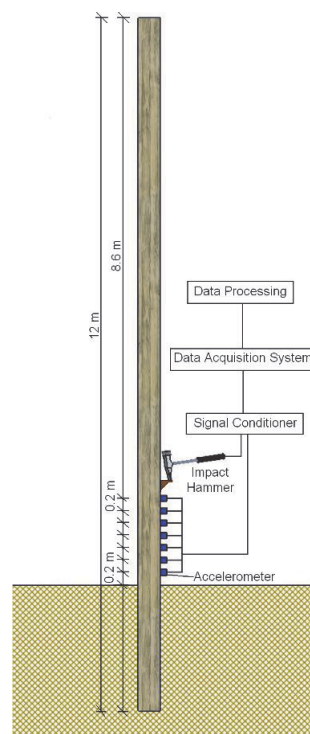


Figure 4.23 Test set-up of embedded testing in the field

## 4.5 TEST SET-UP FOR BENDING WAVE METHOD

The test set-up, equipment and testing procedure of the BW method were similar to the SE and IR testing described in section “Sonic Echo Method”. Whereas in SE and IR testing, the impact was executed in the longitudinal direction (to generate longitudinal waves), in BW testing, the hammer strike was performed in the transverse direction (to generate flexural waves). To record the response of the structure, five sensors (accelerometers or geophone velocity transducers) were used in the experimental tests and 8 sensors were used to measure the initial arrival of the flexural waves and subsequent reflections (echoes) in field tests. Since the BW method analyses reflective signals from flexural (bending) waves, the sensors were mounted in the transverse direction to monitor flexural wave vibration. To be able to calculate FRFs of the sensor signals, the force signal of the impact hammer was recorded. The test set-ups of various tests executed in the structures laboratories at UTS and in the field are illustrated in Figure 4.24 to Figure 4.26.

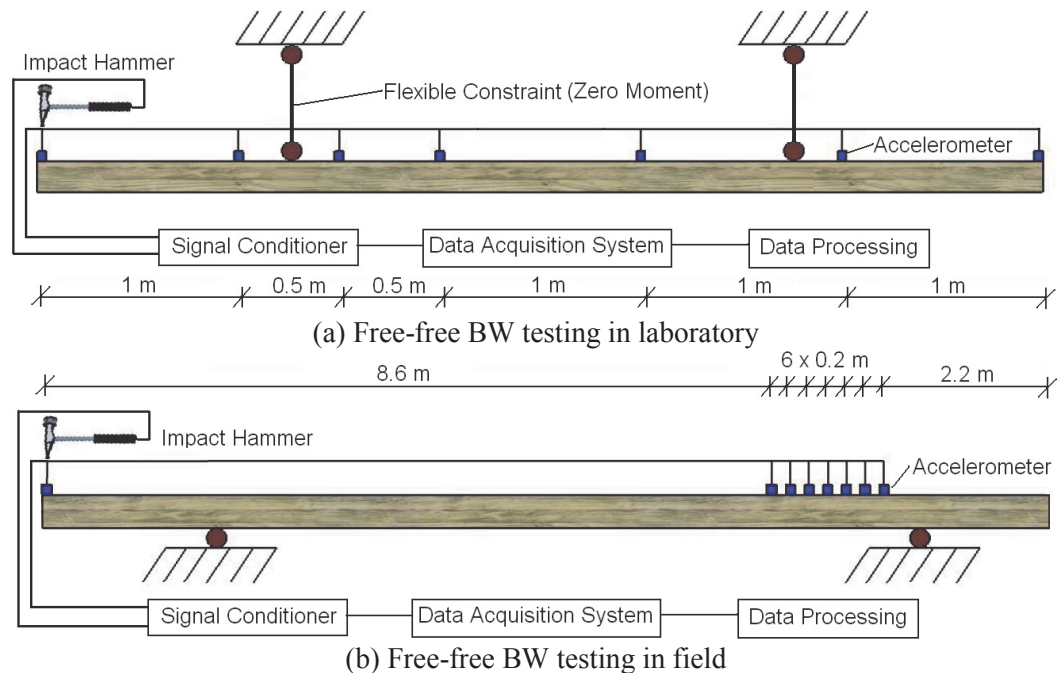


Figure 4.24 Schematic test set-up of free-free BW tests for (a) laboratory testing and (b) field testing.

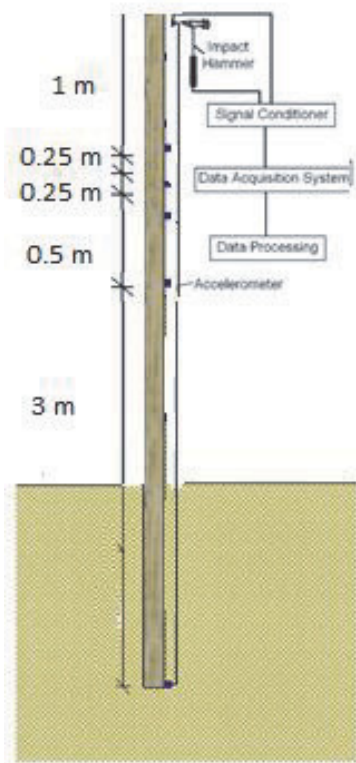


Figure 4.25 Schematic and photo of test set-up of embedded BW tests for laboratory testing.

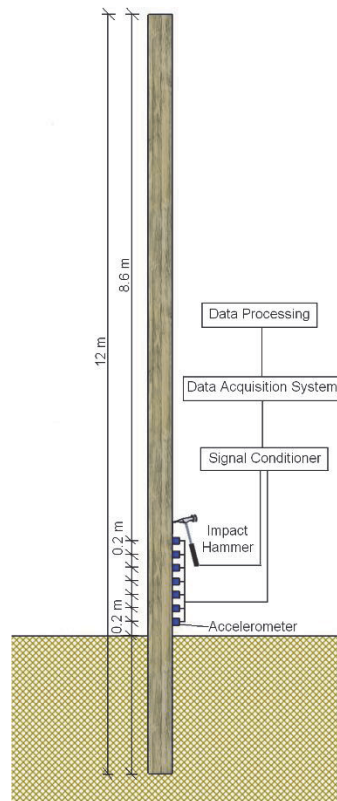


Figure 4.26 Schematic and photo of test set-up of embedded BW tests for field testing.

## 4.6 CONTROLLED FIELD TESTS

There are 15 intact timber poles installed at Mason Park, NSW, by Austgrid (the project's industry partner) with different embedment lengths to investigate the effect of embedded length on different non-destructive tests. The location of the site, a plan view of the Mason Park and the site layout and embedded length for each timber pole are shown in Figure 4.27 and Figure 4.28, respectively. Figure 4.29 and Figure 4.30 display the timber poles before and after the installation on site.

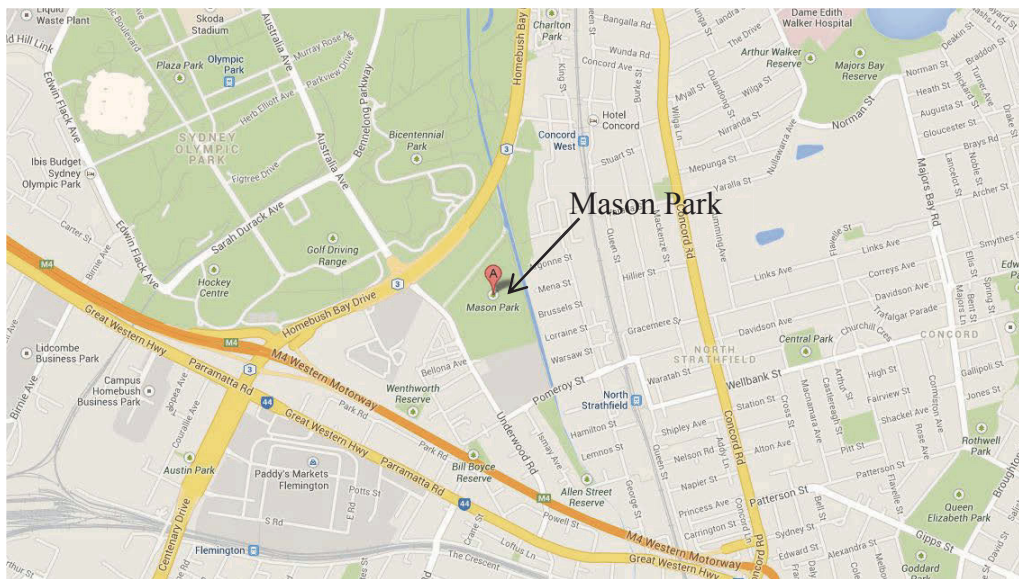


Figure 4.27 Location of the Mason Park (courtesy of Google Maps)

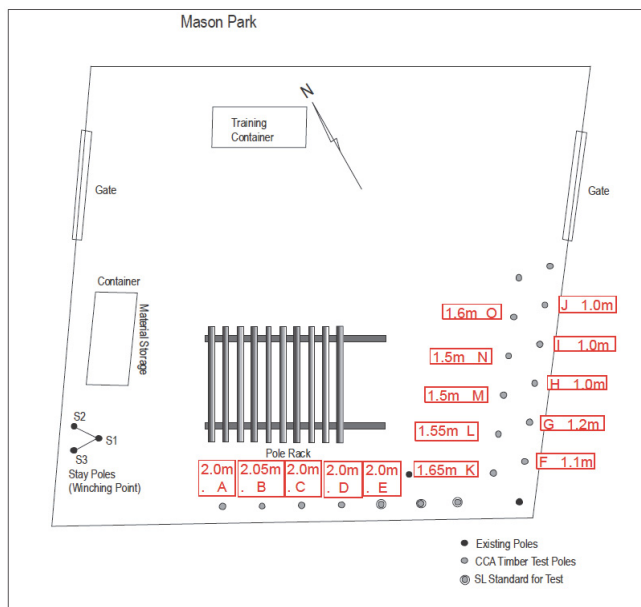


Figure 4.28 Location of timber poles at Mason Park



*Figure 4.29 Timber poles before installation in Mason Park*



*Figure 4.30 Timber poles after installation in Mason Park*

## 4.7 FIELD TESTS ON DECOMMISSIONED UTILITY POLES

A number of tests have been successfully conducted on eight different timber poles in the field (Horsham, Victoria). Including Impact Echo and Bending wave methods in 3 stages from 16<sup>th</sup> to 18<sup>th</sup> November 2009. Table 4.1 summarises the details of all NDT tests. The Impact Echo/Impulse Response and Bending (Dispersive) methods were applied to these timber poles in service. Also after the poles were pulled out, a series of Impact Echo/Impulse Response and Bending (Dispersive) methods were performed on the poles in “free–end” condition. All types of the tests were repeated 5 times for repeatability and consistency. After considering the consistency of the tests, the results of the tests were initially processed for free end condition and the results show that the speed of wave decrease will be variable and affected by changes in the moisture content or decay as these changes influence the modulus of elasticity and density. In the following step, the photos taken from different cross sections of the poles are considered to identify the general pattern of the defects to update the numerical simulation

*Table 4.1 Field test details*

| Stage No. | Testing condition | Testing Method           | Location of impact        |
|-----------|-------------------|--------------------------|---------------------------|
| 1         | Embedded          | Bending                  | 1600 mm from ground level |
|           |                   |                          | 100 mm from ground level  |
|           |                   | Impact Echo/Ultraseismic | 1600 mm from ground level |
| 2         | Free-Free         | Bending                  | 1600 mm from ground level |
|           |                   |                          | 100 mm from ground level  |
|           |                   | Impact Echo/Ultraseismic | 1600 mm from ground level |
| 3         | Free-Free         | Impact Echo/Ultraseismic | From the top of specimen  |



## 4.8 CLASSIFICATION OF DAMAGE OF FIELD UTILITY TIMBER POLES

There were 66 different out of service timber poles available to identify the defect patterns. Twenty timber poles were removed in Horsham, Victoria and 46 from Bendigo. For eight poles from Horsham all information was available, including the exact place of cutting the timber along the specimen and the results of the NDT methods. This information will be used to simulate 8 different cases of timber poles in numerical analysis. And the other 58 cases will be used to identify defect patterns in timber poles.

The details of 8 timber poles tested and removed from service are available and shown in Appendix A. Figure 4.31 presents one example of the timber pole autopsy for pole with ID No 288. These timber poles were cut at 2 m above the ground and 0.5 m below the ground shown as L in the column of Figure 4.31. The results of all 8 timber poles are summarised in the Table 4.2 and Table 4.3.


*Table 4.2 Timber pole classifications based on the existing defects at Horsham*

| Timber pole No. | Defect description  | Location of defects       |     |
|-----------------|---|---------------------------|-----|
| 183             | Severe termite damage in sections 3 to 7  | S 1m below, S 6m above    | **  |
| 270             | Severe termite damage in sections 1 to 7  | S 1m below, S 10m above   | *** |
| 288             | Termite damage in ground. severe termite damage above the ground                            | S 1.5m below, S 10m above | *** |
| 293             | Minor termite damage in section 6 and 7   | M 1m below, M 1m above    | *   |
| 295             | Severe termite damage in section 5. minor termite damage in sections 2 to 4                 | M 1m below, S 1m above    | *   |
| 299             | Minor termite damage in section 6 and 7. Severe termite damage in sections 1 to 5(above the | M 0.5m below, S 10m above | *** |
| 326             | Minor termite damage in section 4   | M 2m above                | *   |
| 360             | Severe termite damage above the ground.   | H 0.5 m below ,S 6m above | *** |

\* Minor termite damage

\*\* Severe termite damage in some parts above the ground

\*\*\* Severe termite damage in most parts (below and above the ground)

|   |          |  |   |   |
|---|----------|--|---|---|
| L | Diameter |  | Cross Section   |   |
|   | L        | R  | Left  | Right   |
| 2 | 170      | 250  |    |    |
| 2 | 250      | 260  |   |   |
| 2 | 260      | 270  |  |  |
| 2 | 270      | 285  |  |  |










|     |     |     |   |   |
|-----|-----|-----|---|---|
| 2   | 285 | 320 |    |    |
| 0.5 | 320 | 330 |    |    |
| 0.5 | 330 | 350 |   |   |
| 0.5 | 350 | 365 |  |   |
| 0.5 | 365 | 410 |  |  |

Figure 4.31 Cross sections of pole No 288

Table 4.3 Defect description of different timber poles at Horsham

| Timber pole No. | Defect description   |
|-----------------|--|
| 183             | Decay from centre along the pole except for first 1 m from the tip   |
| 270             | Decay from centre above the ground, combination of external and internal cracks 1 m below the ground   |
| 288             | Combination of decay from centre and external cracks above the ground, combination of decay from centre and internal cracks below the ground |
| 293             | Decay from centre just 1 m below the ground  |
| 295             | Decay from centre just 2 m above the ground  |
| 299             | Combination of decay from centre and external cracks above the ground and 1m below the ground  |
| 326             | Combination of decay from centre and internal cracks just 4m above the ground-no photo available for some parts.                             |
| 360             | Decay from centre along the pole except the first 1 m from the tip and 2 m from the top  |

#### 4.9 SOIL SAMPLES

Soil samples were collected from the Mason Park site. Then, compaction tests were carried out on all samples. The purpose of laboratory compaction test was to determine the right amount of water at which the weight of the soil in a unit volume of the compacted soil is maximum. The amount of water is thus called the Optimum Moisture Content (OMC). In the laboratory, different values of moisture contents and the resulting dry densities, obtained after compaction, are plotted, the former as abscissa and the latter as ordinate. The points thus obtained are joined together as a curve. The maximum dry density and the corresponding OMC are read from the curve.

The wet density of the compacted soil is calculated as below,

$$\gamma_t = \frac{w_1 - w_2}{V}$$

where,  $w_1$  = weight of mould with moist compacted soil,  $w_2$  = weight of empty mould and  $V$  = Volume of mould.

The dry density of the soil shall be calculated as follows:

$$\gamma_d = \frac{\gamma_t}{1 + w}$$

Where,  $\gamma_t$  = wet density of the compacted soil and  $w$  = moisture content

The maximum dry density and the optimum water content of the samples were measured using a 2.7 kg hammer and 25 blows per layer (AS1289.5.1.1. 2003). Figure 4.32 shows compaction test equipment used. Figure 4.33 demonstrates filling process of the compaction mould with soil. Figure 4.34 presents the compacted soil and the mould after compaction. Figure 4.35 shows the compaction curve of soil sample. As can be observed, the maximum dry density is  $15.7 \text{ kN/m}^3$  with optimum moisture content of 16.8%. Based on the moisture content of the sample, the unit weight of sample is  $15.5 \text{ kN/m}^3$ .



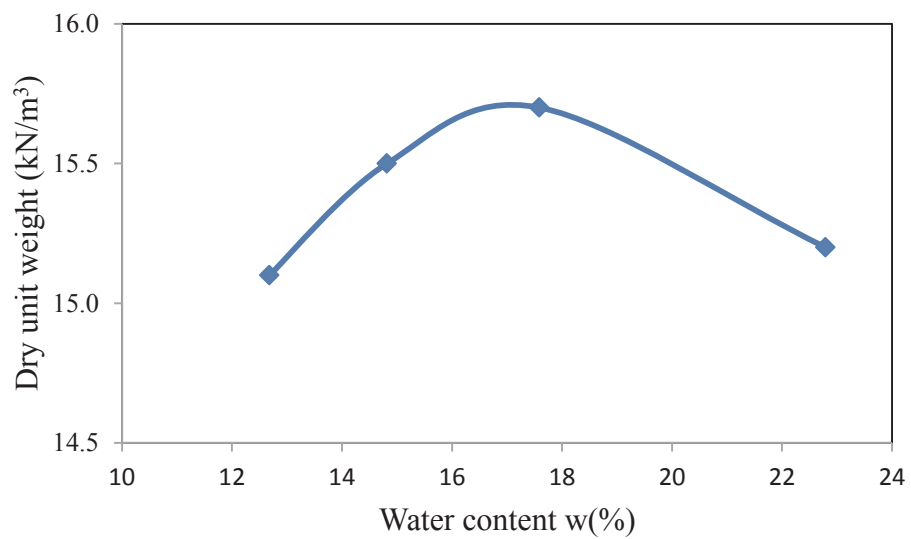
*Figure 4.32 Compaction test equipment*



*Figure 4.33 Filling the compaction mould with soil*



*Figure 4.34 Compacted soil with mould after compaction completed*



*Figure 4.35 Compaction curve of soil sample in Mason Park*

## 4.10 SUMMARY

In this chapter, a summary of equipment, testing set up and procedures for different non-destructive testing methods such as Impact Echo, Impulse Response, Bending Wave and Ultraseismic were presented. For all methods, the following equipment were used: a modally tuned impact hammer, multiple sensor arrays, a multi-channel signal conditioner, a data acquisition system with minimum sampling frequency of 1M samples/sec per channel and a personal computer equipped with signal acquisition software.

A container, 1.2 m × 1.2 m in cross-section and 3 m in height was designed and fabricated to contain soil for embedding different test specimens with various embedment lengths.

In order to address uncertainty and reliability issues, before commencing any non-destructive tests on embedded timber poles, benchmarking tests were conducted, involved testing columnar specimens with a free-end condition (specimen suspended by two ropes) in the Structures Laboratory to test sensor types and data acquisition requirements, benchmarking test and analysis procedures and expected accuracy. Due to the uncertainty resulting from variability of timber materials, a steel beam (assumed to be homogeneous and without defects), was chosen as benchmark for the tests. A rectangular cross section timber beam was also used to verify the behaviour of a timber pole without any defects and the timber pole represented an actual field specimen having imperfect geometry, complex material property and local defects.

One major damage scenario was created and considered in this study which involved removing one half section of the pole from the bottom to a length of 1 metre.

Also a practical step-by-step guide, describing the set-up of equipment, the setting of the acquisition software and the execution of the tests, were described for each method and for various free-free and embedded tests. In addition particular features of individual methods (SE method, IR method, BW method using SKM and Ultraseismic method) were explained in this chapter. The details of the experimental tests on a 5m steel beam, a 5m timber beam and a 5m timber pole with several different testing conditions, including free-end condition, and various embedment lengths were provided. For embedded conditions, the container was filled with sand in 8 different

stages to simulate the different embedded depths while the specimen tip was set on bedrock. The specimen was then pulled from the foundation material in 0.3 metre increments and tested at each stage to simulate different embedded depths. The test was then repeated up to six times until the remaining underground depth of the pole reached 1.5 metres.

A procedure of conducting field tests at Mason Park, NSW on 15 intact timber poles and at Horsham, Victoria on eight damaged poles were provided, including Impact Echo, Impulse Response and Bending wave and Ultraseismic methods. For the eight poles from Horsham, all relevant information was available, including the exact place for cutting the timber along the specimen and the results of the NDT methods. The details of the eight timber poles tested and removed from service are available and shown in Appendix A. Finally, laboratory tests on soil samples were explained in details for field tests.



# CHAPTER 5

## 5 ANALYSIS AND DISCUSSION OF LABORATORY AND FIELD TESTS

### 5.1 INTRODUCTION

This chapter presents experimental investigation of the Sonic Echo (SE), Impulse Response (IR), Bending Wave (BW) and Ultraseismic methods. Due to the uncertainty resulting from variability of timber materials in laboratory tests, a steel beam (assumed to be homogeneous and without defects), was chosen as a benchmark for the tests. A rectangular cross section timber beam was used to verify the behaviour of timber pole without any defects and the timber pole represented an actual field specimen having imperfect geometry, complex material property and local defects. In SE method, the acceleration-time history results from the laboratory tests are used to calculate the wave velocity followed by the evaluation of the embedded length of the specimen. In IR method, frequency domain is used to determine the velocity and embedment length. For Bending Wave, Short Kernel Method (SKM) was investigated to determine the phase velocity of flexural wave and also the embedded length. In Ultraseismic method, the results of all sensors were used for calculations, at first the velocity is estimated and then the embedded length is calculated.

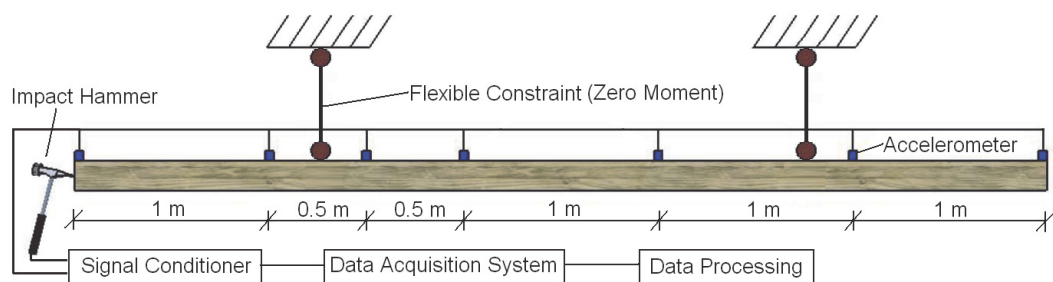
In this chapter, firstly the results of laboratory tests are presented followed by the field test results. The structure of this chapter is as follows: for each of the laboratory and field test results; firstly, the results of Sonic Echo and Impulse Response are presented. Secondly, results of the Bending Wave method are discussed. Finally, the outcome of the Ultraseismic method are presented. It should be mentioned that stress wave velocity calculation is a crucial part of each method as this value will be used later for length determination of the specimen, i.e., steel beam, timber beam and timber pole. Also selection of the reflection wave is a major part of each method as the velocity estimation is relying on the time difference between arrival and reflection wave. In this chapter, for

each method, at first the details of velocity estimation is provided and then the relative error for length determination is presented for different testing conditions.

## 5.2 SONIC ECHO (SE) TEST

In Sonic Echo testing, the specimen is excited in the longitudinal direction with a modally tuned impact hammer. The impact location was the top centre of the structure to generate longitudinal waves. To record the time travel of the longitudinal stress waves, sensors were attached to the test structure to monitor the structural response. In order to increase test reliability and accuracy, a number of sensors were mounted at strategic locations.

There are two different test configurations used in the laboratory; free-free and embedded tests. Figure 5.1 shows the schematic test set up for Sonic Echo testing including the locations of the sensors for free-free and embedded tests. In the calculations, the locations of sensors were measured from the top of the specimen. The SE test procedure and required equipment are discussed in Chapter 3. In the following sections, firstly, the stress wave velocity is estimated based on the acceleration-time history and then by using the obtained velocity, the embedded length is estimated and the percentage of error is calculated for different testing/boundary conditions. The details of the different boundary conditions are also presented and can be found in chapter 3.



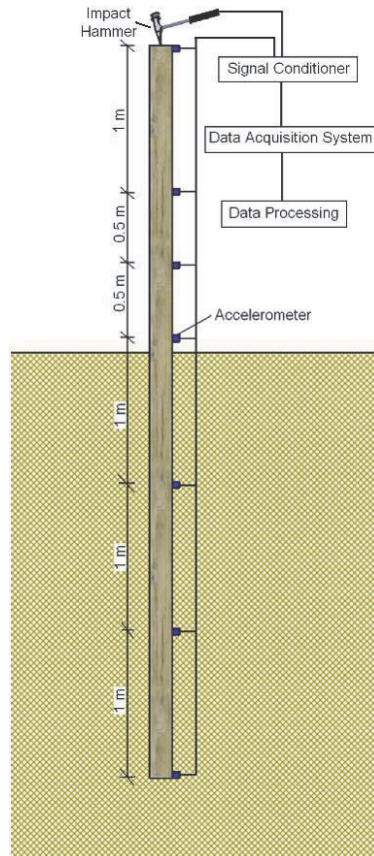


Figure 5.1 Test set-up for (a) free-free testing and (b) embedded testing condition

### 5.2.1 Velocity calculation

After using low pass filtration, the velocity of the stress wave is obtained from the acceleration-time history test results based on a time difference between sensors and the known length between them. Generally, two rising peaks will be used for velocity calculations by using the time difference between the interval of wave travel past a sensor and reflected back to it. However, to increase the accuracy and decrease the uncertainty of stress wave velocity propagation in timber material, multi sensors were used. The possible reasons of uncertainty for velocity calculation in timber material will be discussed later in this section. In Sonic Echo method, seven sensors were mounted on the specimens from top to the tip of the specimen. As a result, a linear trend line was used for velocity estimation considering all sensors which are located above the soil level. Also, considering the consistency and repeatability of the repeated tests, the outlying results were eliminated. The first rising peak time for all consecutive sensors for experimental SE tests of the steel beam, timber beam and timber pole under the free-free condition are presented as an example of velocity estimation in Figures 5.2 to 5.4,

respectively. As can be seen, the coefficient of determination ( $R^2$ ) is around 1 for steel and timber beam under free-end condition. However, this value is 0.95 for timber pole as more uncertainties are involved in velocity estimation in timber pole. In addition, Figure 5.4 indicates more variation of the first arrival peak determination for a sensor located at the tip (i.e. 5m from the top) in acceleration-time history results of a 5m timber pole compared to the same sensor locations for a 5m steel and timber beam (Figure 5.2 and Figure 5.3). This variation also repeated for a sensor located at 4 m from the top mounted on timber pole. These two sensors were located far from the impact location.

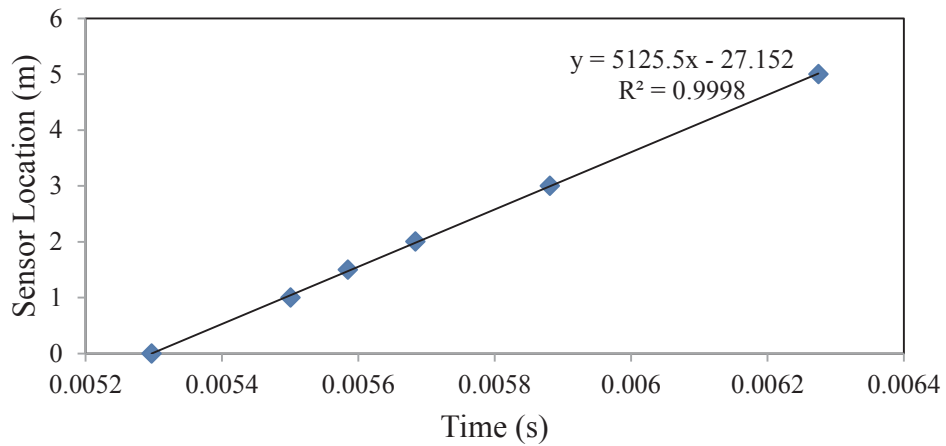


Figure 5.2 Velocity calculation of steel beam (free end condition)

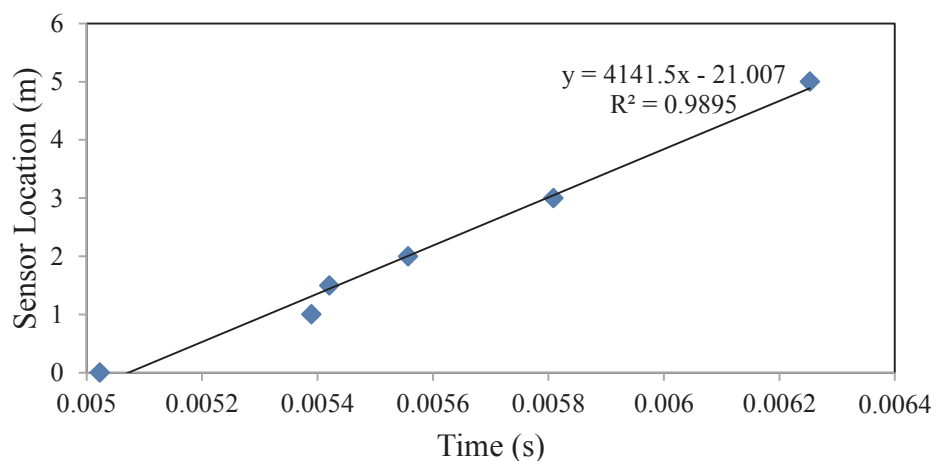


Figure 5.3 Velocity calculation of timber beam (free end condition)

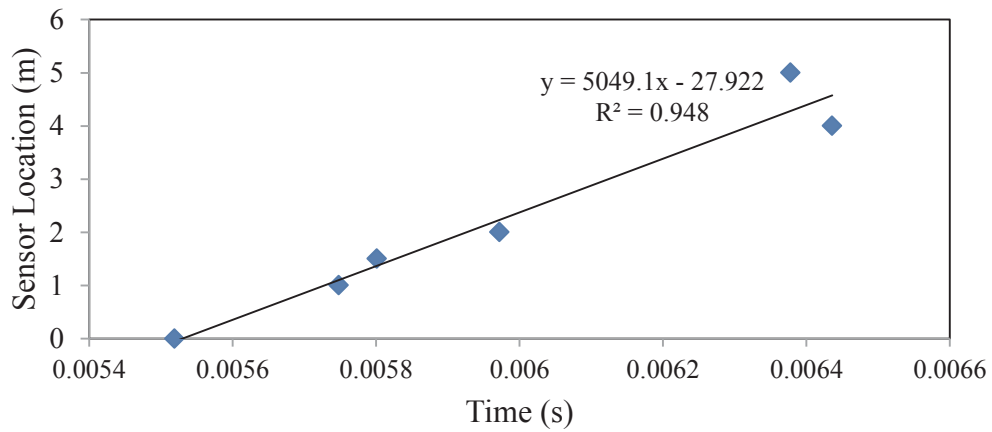


Figure 5.4 Velocity calculation of timber pole (free end condition)

Using the first arrival and reflection peaks from acceleration-time history results, the longitudinal wave velocity is calculated based on known length. Figures 5.5 to 5.7 display the minimum, maximum and average longitudinal wave velocity of steel beam, timber beam and timber pole, respectively. According to these figures, the velocity will vary based on different repeated tests. As can be seen, the average stress velocity of timber will increase by soil depth (i.e. soil layer 7 and 8) compared to free-free results as more uncertainties will be involved in calculation of velocity.

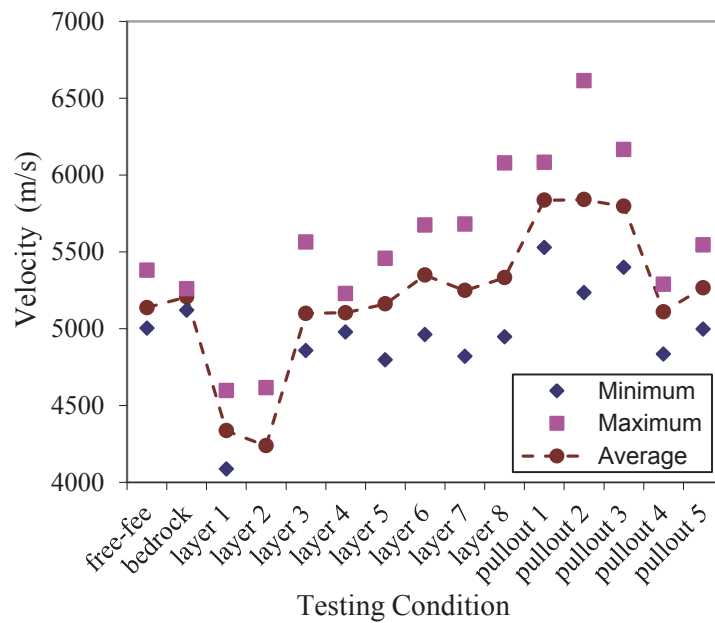


Figure 5.5 Minimum, maximum and average longitudinal wave velocity for steel beam

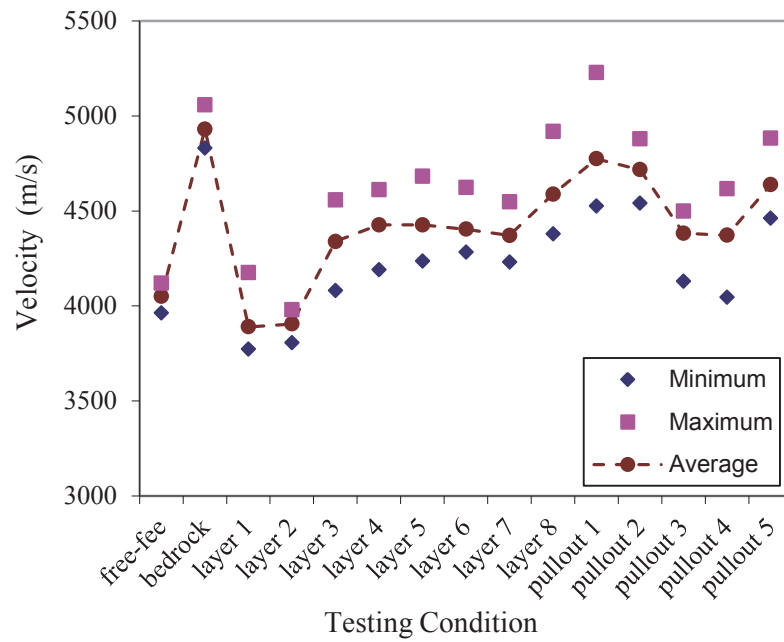


Figure 5.6 Minimum, maximum and average longitudinal wave velocity for timber beam

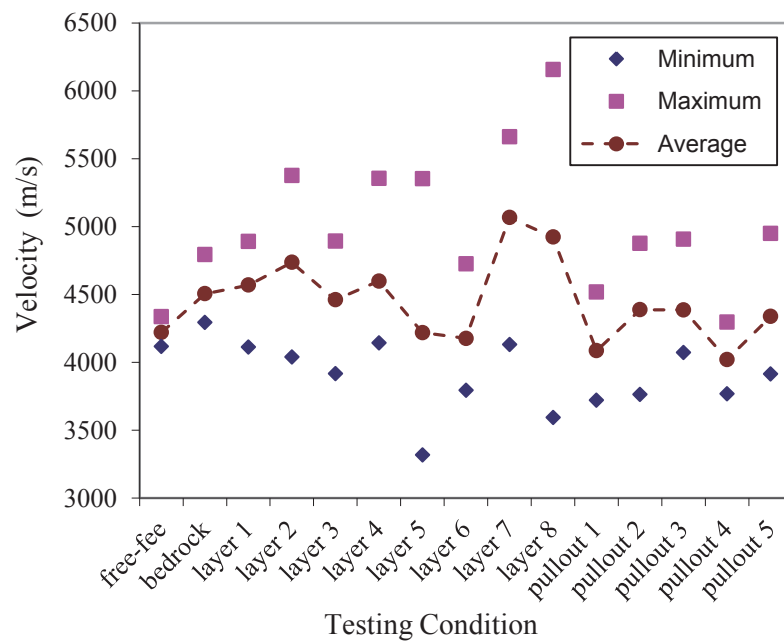


Figure 5.7 Minimum, maximum and average longitudinal wave velocity for timber pole

To get better understanding of the stress wave velocity variation, the coefficient of variation of the wave velocity calculation is obtained for different boundary conditions.

Tables 5.1-5.3 summarise the coefficient of variation of the velocity calculation for repeated SE tests under different testing conditions. The coefficient of variation varied between 2.4% to 8.6% for the steel beam, 1.4% to 4.7% for the timber beam and 1.6% to 22.7% for the timber pole. According to these tables the coefficient of variation of the velocity estimation of timber pole is relatively higher than steel beam and timber beam.

The followings are the possible reasons for the higher coefficient of variation of velocity estimation in timber pole compared to timber and steel beam:

- Timber may be described as an orthotropic material (Kretschmann 2010), It has unique and independent properties in the directions of three mutually perpendicular axes, namely, longitudinal (L), radial R, and tangential (T). These axes are shown in Figure 5.8 . The longitudinal axis L is parallel to the fibre (grain). The radial axis R is normal to the growth rings and it is perpendicular to the grain in the radial direction. The tangential axis T is perpendicular to the grain but tangent to the growth rings. The three moduli of elasticity of timber are denoted by  $E_L$ ,  $E_R$  and  $E_T$  as elastic properties of timber. As these three moduli of elasticity are different on different axes, the stress wave velocity will be varied based on the direction of axis and this is one of the reasons for higher variation in stress wave velocity calculation in timber pole compared to the timber and steel beam. For timber beam, although timber properties differ in each of these three directions, differences between the radial and tangential directions are not significant compared to their difference with the longitudinal direction due to the small cross section of the beam. This could be a reason for higher variation in velocity calculation of timber beam compared to steel beam.
- Another reason is related to the annual growth rings orientation. Stresses perpendicular to the fibre (grain) direction may be at any angle from  $0^\circ$  (T direction) to  $90^\circ$  (R direction) to the growth rings as shown in Figure 5.9 . Perpendicular-to-grain properties depend somewhat upon orientation of annual rings with respect to the direction of stress. The effects of intermediate annual rings orientations have been studied in a limited way. Modulus of elasticity, compressive perpendicular-to-grain stress at the proportional limit, and tensile strength perpendicular to the grain

tend to be about the same at 45° and 0°, but for some species, these values are 40% to 60% lower at the 45° orientation. For those species with lower properties at 45° ring orientation, properties tend to be about equal at 0° and 90° orientations. For species with about equal properties at 0° and 45° orientations, properties tend to be higher at the 90° orientation (Kretschmann 2010) which indeed depends on the location of one sensor to another in regards to the annual ring orientation. Different stress wave velocity could be captured as a result of different timber properties in each ring.

- The other possible reason is related to the slope of grain in timber pole. In some wood product applications, the directions of important stresses may not coincide with the natural axes of fibre orientation in the wood. The term slope of grain relates the fibre direction with respect to the edges of a piece. The term cross grain indicates the condition measured by the slope of grain. Two important forms of cross grain are spiral and diagonal as shown in Figure 5.10. Other types are wavy, dipped, interlocked, and curly. Spiral grain is caused by winding or spiral growth of wood fibres about the bole of the tree instead of vertical growth. Diagonal grain is cross grain caused by growth rings that are not parallel to one or both surfaces of the sawn piece. Diagonal grain is produced by sawing a log with pronounced taper parallel to the axis (pith) of the tree. Cross grain can be quite localized as a result of the disturbance of a growth pattern by a branch. This condition, termed local slope of grain, may be presented even though the branch (knot) may have been removed by sawing. The degree of local cross grain may often be difficult to determine. Any form of cross grain can have a deleterious effect on mechanical properties or machining characteristics (Kretschmann 2010). (Suzuki & Sasaki 1990) and (Bucur & Feeney 1992) concluded the Ultrasonic properties, such as ultrasonic velocity and elastic stiffness constant which are greatly affected by the grain directions and grain angles. The first empirical equation, known as Hankinson's formula (Anon, 1987) was developed by the U.S. Army in 1921 for predicting strength properties of wood from grain angle. (Armstrong, Patterson & Sneckenberger 1991) conclude that The Hankinson's formula has been used widely for various mechanical properties, such as modulus of elasticity, compressive strength, bending strength, etc. from the grain angle. It may also be suitable for the estimation of ultrasonic velocity and elastic stiffness constant. (Kabir 2001) demonstrated that the empirical equations



considering the grain angle lie close to measured values for ultrasonic velocity and elastic stiffness considering the grain angle. Indeed by knowing the grain angle, the stress wave velocity could be adjusted based on the available empirical equations. As can be seen in Figure 5.11, the stress wave will be different based on each sensor corresponding to different fibre directions. As can be observed, sensor 1 and 2 will have the same stress velocity as they are located along the same fibre direction. However, sensor 3 will capture different stress velocity as it is located in different fibre orientation compared to sensors 1 and 2.

- Another reason for the high variation in stress wave velocity in timber pole, compared to the steel and timber beam, is related to the possible existence of any type of imperfections in timber such as knots or any other natural defects/damages. Knots materially affect cracking and warping, ease in working, and cleavability of timber. They are defects which weaken timber and lower its value for structural purposes where strength is an important consideration. Figure 5.12 shows the stress wave velocity in timber pole consisting of knot. As displayed in this figure, sensor 3 captures a different stress wave velocity compared to sensors 1 and 2, as the stress wave will propagate around the knob in comparison to wave propagation in intact timber pole.

Also as can be seen in Table 5.1 to Table 5.3, the minimum values of coefficient of variation are related to the experimental tests under free-free condition and the maximum values belong to the 8 layer soil embedded condition. It was observed that the errors for cases Layer 5 to Layer 8 are particularly large as the embedded length increases. It is believed that this is due to combining the condition of bedrock and deep embedded length. It should be noted that this condition is highly unlikely for the utility poles in practice. Therefore, in practical terms, this is not relevant to this study and is not extensively discussed in this chapter.

*Table 5.1 The coefficient of variation of the velocity calculation for repeated tests of steel beam under different conditions.*

| Test condition | Minimum Velocity (m/s) | Maximum Velocity (m/s) | Average Velocity (m/s) | COV (%) |
|----------------|------------------------|------------------------|------------------------|---------|
| Free-Free      | 5002                   | 5379                   | 5137                   | 2.4     |
| Bedrock        | 5120                   | 5259                   | 5206                   | 5.7     |
| 1 layer soil   | 4085                   | 4596                   | 4335                   | 4.6     |
| 2 layers soil  | 3958                   | 4616                   | 4237                   | 5       |
| 3 layers soil  | 4857                   | 5563                   | 5099                   | 4.7     |
| 4 layers soil  | 4977                   | 5228                   | 5103                   | 2.2     |
| 5 layers soil  | 4796                   | 5457                   | 5161                   | 5.1     |
| 6 layers soil  | 4961                   | 5673                   | 5348                   | 5.2     |
| 7 layers soil  | 4820                   | 5680                   | 5248                   | 5.6     |
| 8 layers soil  | 4947                   | 6078                   | 5332                   | 8.6     |
| 1 pull out     | 5528                   | 6082                   | 5836                   | 3.4     |
| 2 pull out     | 5235                   | 6614                   | 5840                   | 8.5     |
| 3 pull out     | 5399                   | 6165                   | 5796                   | 6       |
| 4 pull out     | 4834                   | 5289                   | 5110                   | 3       |
| 5 pull out     | 4997                   | 5545                   | 5266                   | 3.8     |

*Table 5.2 The coefficient of variation of the velocity calculation for repeated tests of timber beam under different conditions.*

| Test condition | Minimum Velocity (m/s) | Maximum Velocity (m/s) | Average Velocity (m/s) | COV (%) |
|----------------|------------------------|------------------------|------------------------|---------|
| Free-Free      | 3962                   | 4120                   | 4051                   | 1.4     |
| Bedrock        | 4830                   | 5058                   | 4930                   | 1.7     |
| 1 layer soil   | 3773                   | 4175                   | 3890                   | 3.8     |
| 2 layers soil  | 3806                   | 3979                   | 3905                   | 2       |
| 3 layers soil  | 4080                   | 4558                   | 4339                   | 4.1     |
| 4 layers soil  | 4190                   | 4611                   | 4426                   | 3.6     |
| 5 layers soil  | 4235                   | 4682                   | 4426                   | 3.7     |
| 6 layers soil  | 4283                   | 4623                   | 4404                   | 3.1     |
| 7 layers soil  | 4230                   | 4548                   | 4371                   | 2.6     |
| 8 layers soil  | 4378                   | 4917                   | 4588                   | 4.7     |
| 1 pull out     | 4526                   | 5228                   | 4774                   | 3.5     |
| 2 pull out     | 4541                   | 4879                   | 4717                   | 3       |
| 3 pull out     | 4129                   | 4499                   | 4383                   | 3.3     |
| 4 pull out     | 4046                   | 4616                   | 4372                   | 4.3     |
| 5 pull out     | 4461                   | 4883                   | 4638                   | 3.6     |

*Table 5.3 The coefficient of variation of the velocity calculation for repeated tests of timber pole under different conditions.*

| Test condition | Minimum Velocity (m/s) | Maximum Velocity (m/s) | Average Velocity (m/s) | COV (%) |
|----------------|------------------------|------------------------|------------------------|---------|
| Free-Free      | 4117                   | 4337                   | 4220                   | 1.6     |
| Bedrock        | 4294                   | 4793                   | 4506                   | 3.2     |
| 1 layer soil   | 4112                   | 4891                   | 4569                   | 4.3     |
| 2 layers soil  | 4038                   | 5375                   | 4737                   | 9.6     |
| 3 layers soil  | 3917                   | 4892                   | 4460                   | 8.8     |
| 4 layers soil  | 4142                   | 5353                   | 4598                   | 8.3     |
| 5 layers soil  | 3318                   | 5353                   | 4218                   | 15.5    |
| 6 layers soil  | 3793                   | 4725                   | 4176                   | 9.2     |
| 7 layers soil  | 4130                   | 5661                   | 5067                   | 11.6    |
| 8 layers soil  | 3593                   | 6156                   | 4922                   | 22.7    |
| 1 pull out     | 3720                   | 4518                   | 4086                   | 7       |
| 2 pull out     | 3763                   | 4875                   | 4388                   | 8.8     |
| 3 pull out     | 4072                   | 4907                   | 4386                   | 8.1     |
| 4 pull out     | 3768                   | 4296                   | 4020                   | 4.9     |
| 5 pull out     | 3914                   | 4949                   | 4338                   | 7.9     |

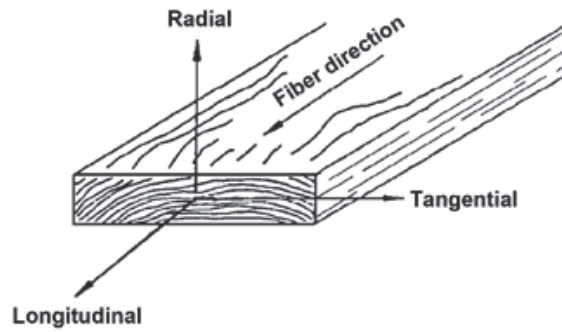


Figure 5.8 The three principal axes of wood with respect to grain direction and growth rings (Kretschmann 2010)

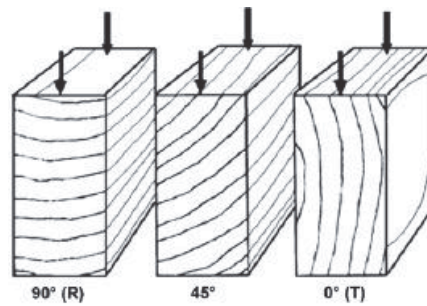


Figure 5.9 Direction of load in relation to direction of annual growth rings: 90° or perpendicular (R), 45°, 0° or parallel (T) (Kretschmann 2010)

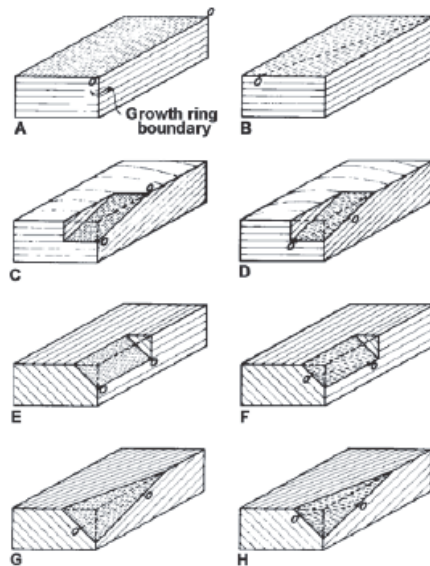
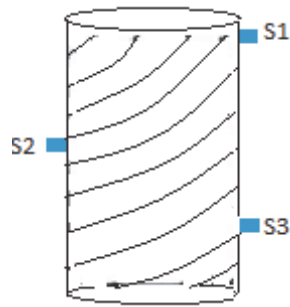
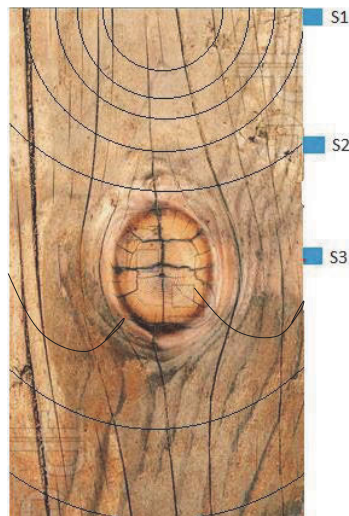


Figure 5.10 Relationship of fibre orientation (O–O) to different axes, as shown by the schematic of wood specimens containing straight grain and cross grain. Specimens A through D have radial and tangential surfaces; E through H do not. Specimens A and E contain no cross grain; B, D, F, and H have spiral grain; C, D, G, and H have diagonal grain (Kretschmann 2010)



*Figure 5.11 Schematic of fibre orientation and sensor location*



*Figure 5.12 stress wave velocity in timber material with knots*

### **5.2.2 Length Estimation**

In the next stage, by using the longitudinal wave velocity the error in length estimation of each specimen is calculated. Choosing the reflection peak is one of the main feature of this methods and this could be affected by different phenomena which could be explained as follows:

- Based on (Subhani 2013) investigation, the stress wave velocity will decrease inside the soil. This phenomenon was verified by the numerical study and the results were presented in Chapter 4. Based on the conclusions, the velocity above and below the soil is different and a reduction factor is required to be applied to stress wave velocity above the soil to obtain the stress wave velocity below the soil. This reduction factor varying depended on the different testing/boundary conditions as well as the soil depth. More details can be found in Chapter 4.

- (Kolsky 1963) investigated the stress wave propagation between two media and derived an equation for reflection between two media. Based on the equation, the reflection between two media depends on characteristic impedance of each medium. Characteristic impedance is defined as  $\rho c$  of the medium which is a function of wave velocity and density. He showed when the characteristic impedance of the second medium is higher than that of the first; the direction of the propagation is reversed on reflection. This corresponds to a change in phase of  $\pi$  in the vibration. As is mentioned earlier, determination of the reflection time is one of the main parts of each method and this reflection should be chosen based on whether the wave phase change happening or not. The characteristic impedance is calculated and summarised for all media of laboratory tests and the results are provided in Table 5.4 .

Based on the results, there should be a phase change happening between two media if there is bonding between them. However, it is believed that, as the specimens are resting on concrete floor in laboratory testing; the concrete and timber will have an individual displacement. Indeed, there is no phase change happening between the two media. Figure 5.13 shows the acceleration-time history results of a 5m timber pole under free-free and bedrock conditions. As can be seen, no phase change is observed in wave reflection from the bottom of a timber pole. As a result, the positive value was used as wave reflection to calculate the stress wave velocity.

*Table 5.4 Calculation of Characteristic Impedance for different materials*

| Material | Density<br>(kg/m <sup>3</sup> ) | Modulus of Elasticity<br>(GPa) | Wave Velocity<br>(m/s) | Characteristic<br>Impedance |
|----------|---------------------------------|--------------------------------|------------------------|-----------------------------|
| Steel    | 7800                            | 200                            | 5063                   | 39.49*10e6                  |
| Concret  | 2400                            | 32                             | 3652                   | 8.76*10e6                   |
| Timber   | 950                             | 23                             | 4920                   | 4.67*10e6                   |
| Soil     | 1520                            | 0.15                           | 256                    | 0.39*10e6                   |

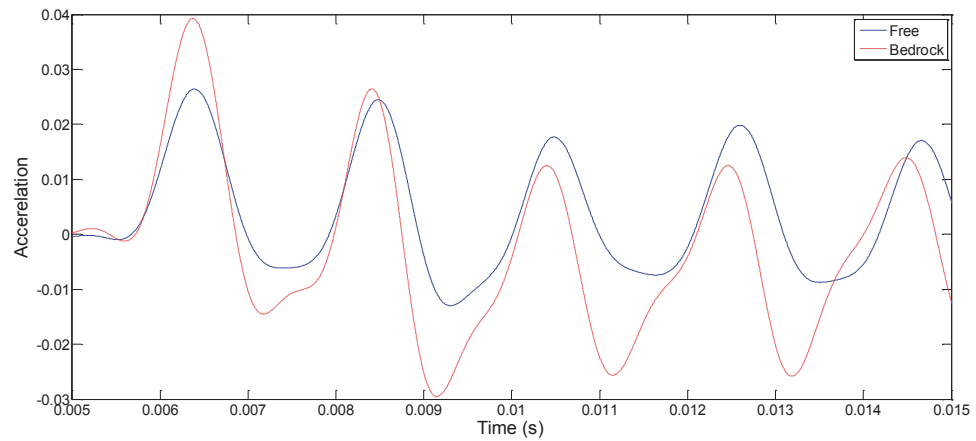


Figure 5.13 Acceleration-time history result of a 5m timber pole under free-free and bedrock conditions

Figure 5.14 indicates the average errors for different testing boundary conditions in estimation of length of a 5m steel beam. In this figure, the first sensor, which was located at the top of specimen and close to the impact location, has been used for length calculations. In each case, the results of seven to nine tests are presented with different colours and the averaged errors are denoted by larger circles. In the figure, the horizontal axis is associated with 15 different testing conditions. e.g. “free-free” refers to the beam or pole being free at both ends; “bedrock” refers to the condition where one end of beams or poles was resting on concrete floor with no sand. The next 8 conditions (Layer 1 to Layer 8) correspond to condition where sand is filled inside the container while specimens were still sitting on the concrete floor. “Layer 1” corresponds to the condition when sand was filled to a depth of 375mm in the container. “Layer 2” corresponds to the condition when a further 375mm of sand is filled and so on. “Layer 8” corresponds to the condition when the depth of sand filled is 3 metres (8 fills of 375mm). The next five tests correspond to conditions where the beam or pole was pulled out at 0.3 m intervals. For example, “pull out 5” corresponds to the case where the beam or pole is pulled out by 1.5m (5 pull-outs x 0.3 m) leaving 1.5m of sand below the bottom of the beam or pole with 1.5m of embedment length in the sand.

As can be seen in Figure 5.14, the average error ranged between 1% and 96% for length estimation of the steel beam. It was observed that the errors for cases of Layer 5 to Layer 8 are particularly large as the embedded length increases. It is believed that this is due to combining the condition of bedrock and deep embedded length. In addition, this



could relate to the complexity of the stress wave generation in the hollow cylindrical beam which was not the main focus of this study. The main aspect of this study was to investigate the stress wave velocity variation in the isotropic material like steel compared to the orthotropic material such as timber. As mentioned earlier, the testing condition of specimens standing on bedrock with surrounding soil is highly unlikely for the utility poles in service as they are driven to the desired embedded length and do not stand on bedrock, unless the bedrock is fairly shallow.

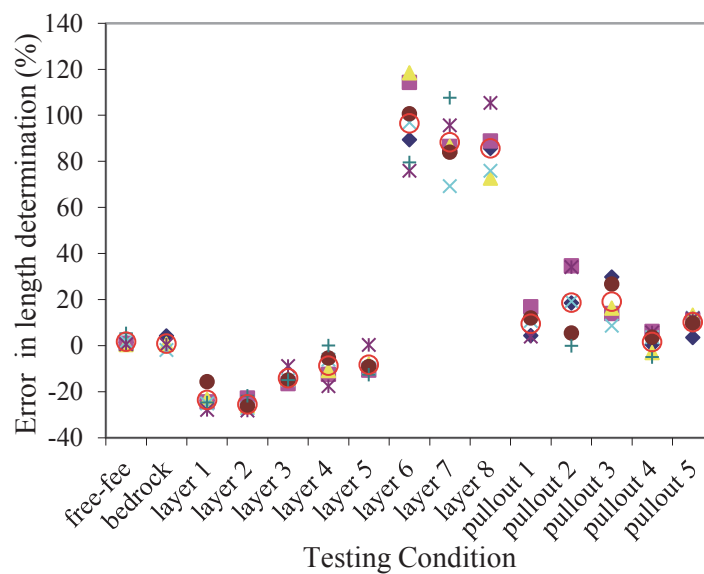


Figure 5.14 Percentage errors for different tests estimating the length of the steel beam for sensor 1 (located on top of the specimen)

To consider the effects of using multiple sensors on different locations of the specimens, the average error for length determination of three other sensors are also considered. Figures 5.15 to 5.17 display the average error for different testing conditions of steel beam for sensors 2, 3 and 4 located at 1, 1.5 and 2m from the top of the beam (i.e. impact location). As shown in Figure 5.15, the average error of length estimation is between 5% and 137% using sensor 2 for calculations. This value is between 1% and 150% for sensor 3. The results show that the error will increase for sensor 3 compared to sensors 1 and 2 which are closer to the impact location, specifically for layer 5 to 8 testing conditions. Furthermore, the variation of error will increase by increase in distance between sensor location and impact location for more soil layers as shown in Figure 5.17 (between 1% to 175%)

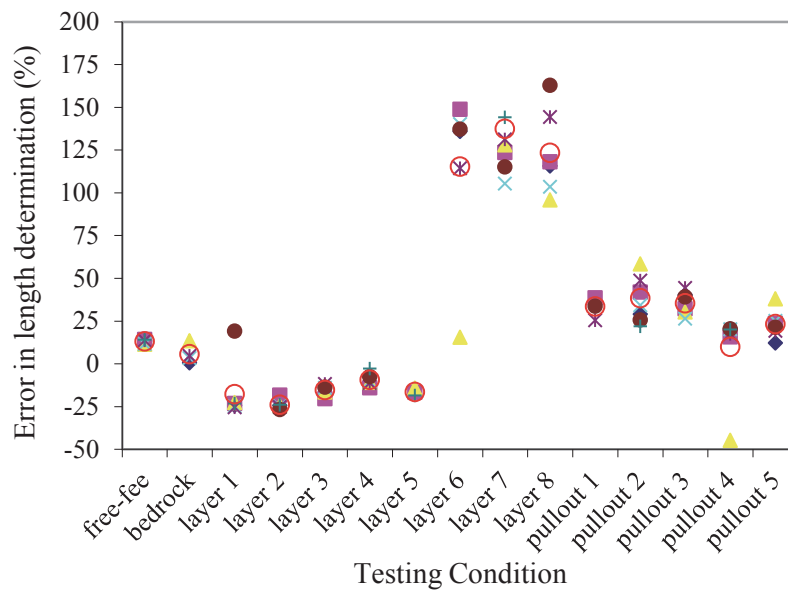


Figure 5.15 Percentage errors for different tests estimating the length of the steel beam for sensor 2 (located 1m below the top of the specimen)

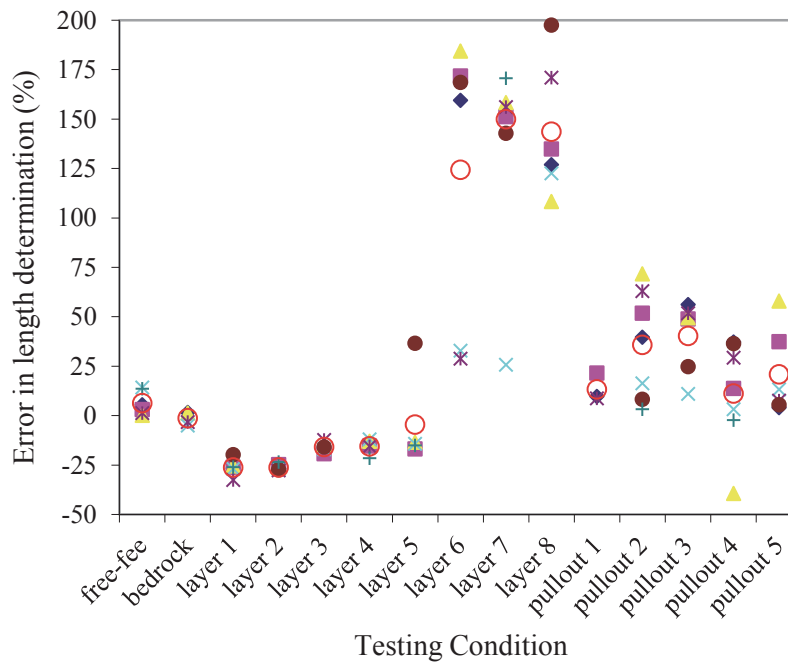


Figure 5.16 Percentage errors for different tests estimating the length of the steel beam for sensor 3 (located 1.5m below the top of the specimen)

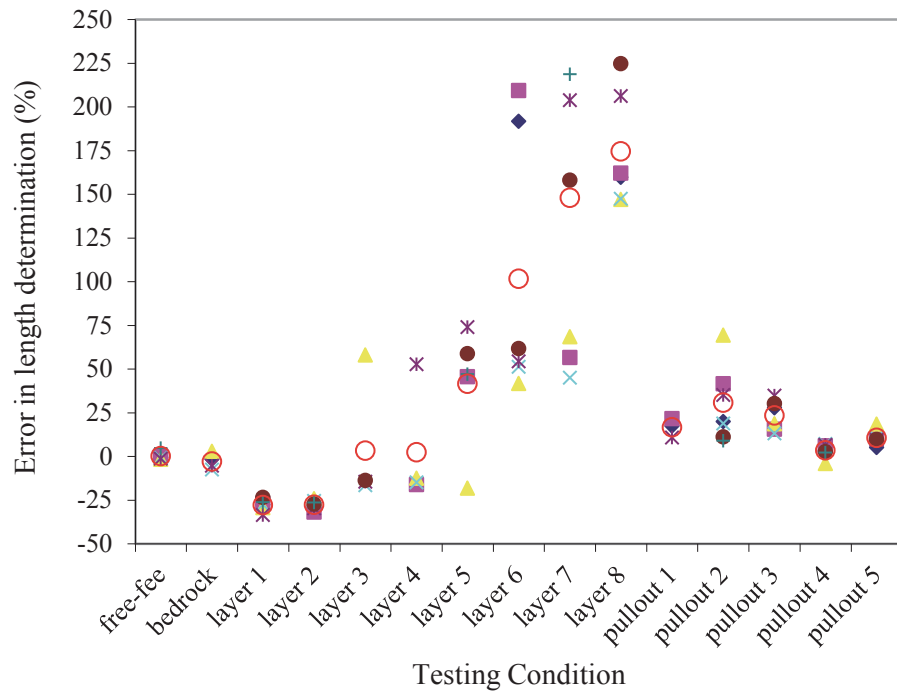


Figure 5.17 Percentage errors for different tests estimating the length of the steel beam for sensor 4 (located 2m below the top of the specimen)

Similar results were obtained for a 5m timber beam under different testing conditions. The relative errors in estimation of the specimen length for different cases ranged between 1% and 64% on average, using sensor 1 for calculations as shown in Figure 5.18. Figures 5.19 to 5.21 present the relative errors in estimation of a timber beam length for different testing conditions for sensors 2, 3 and 4, respectively. According to Figure 5.19 the error ranged between 1% and 18% on average. It is believed that the higher error estimation using sensor 1 compared to sensor 2 is related to the small cross section of the timber specimen which does not allow the longitudinal wave to be captured from sensor closer to the impact location. Beyond that, the average error will be relatively similar using sensors 2, 3 and 4.

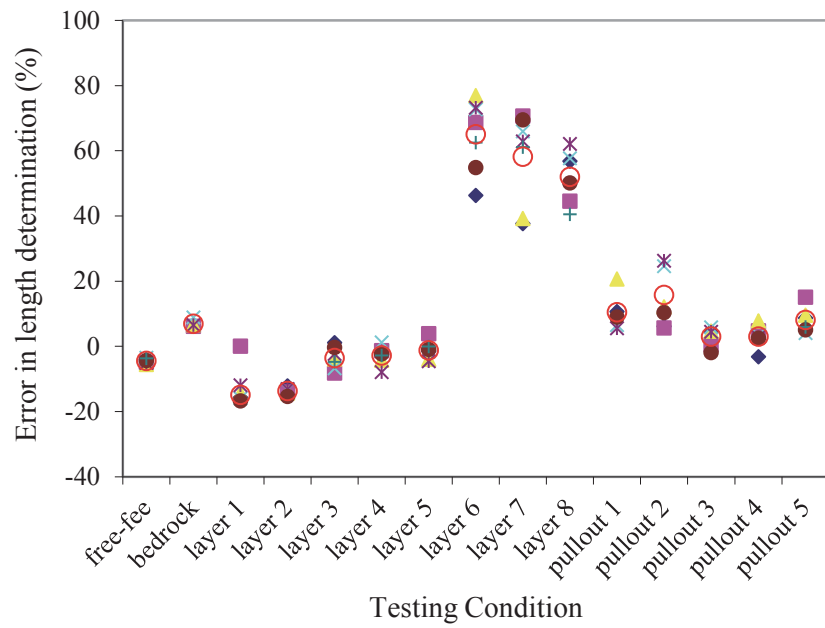


Figure 5.18 Percentage errors for different tests on the timber beam for Sensor 1 (located on top of the specimen)

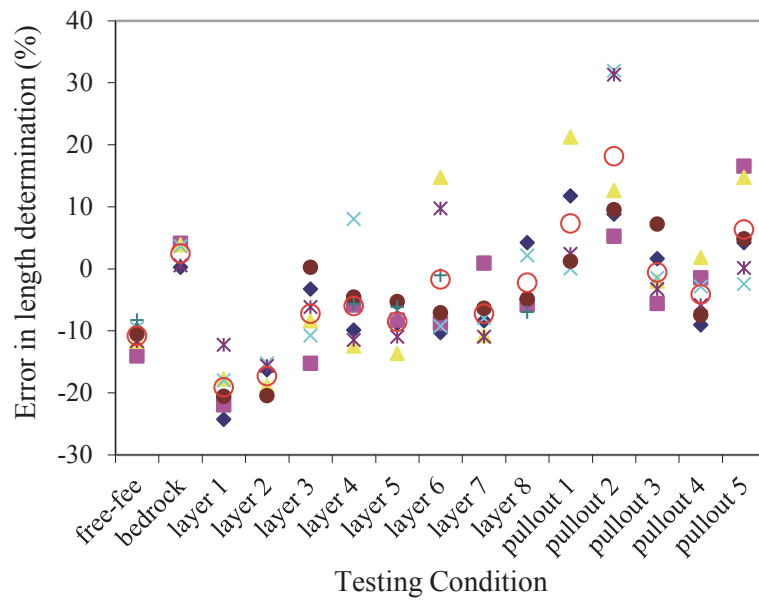


Figure 5.19 Percentage errors for different tests on the timber beam for Sensor 2 (located 1m below the top of the specimen)

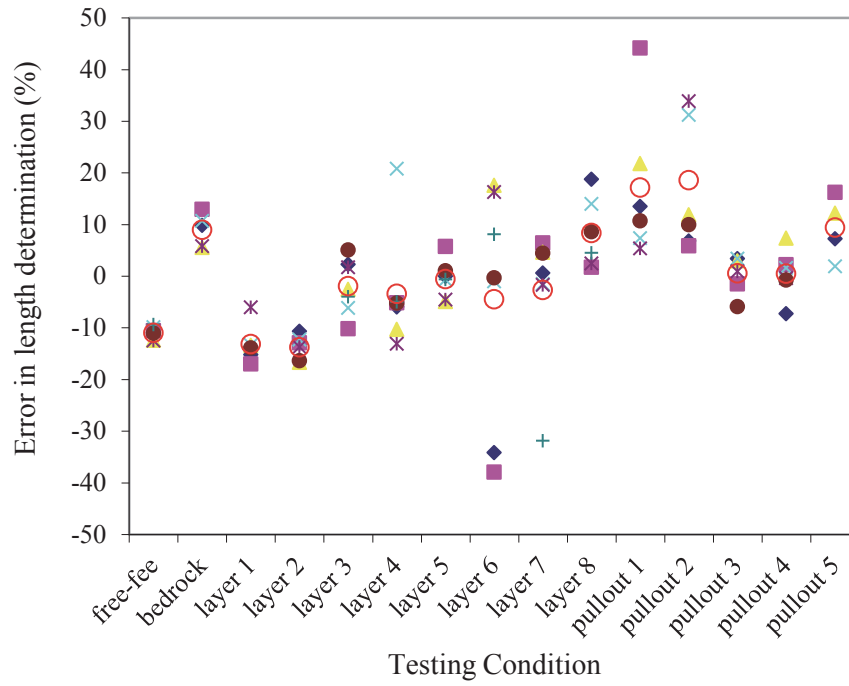


Figure 5.20 Percentage errors for different tests on the timber beam for Sensor 3 (located 1.5m below the top of the specimen)

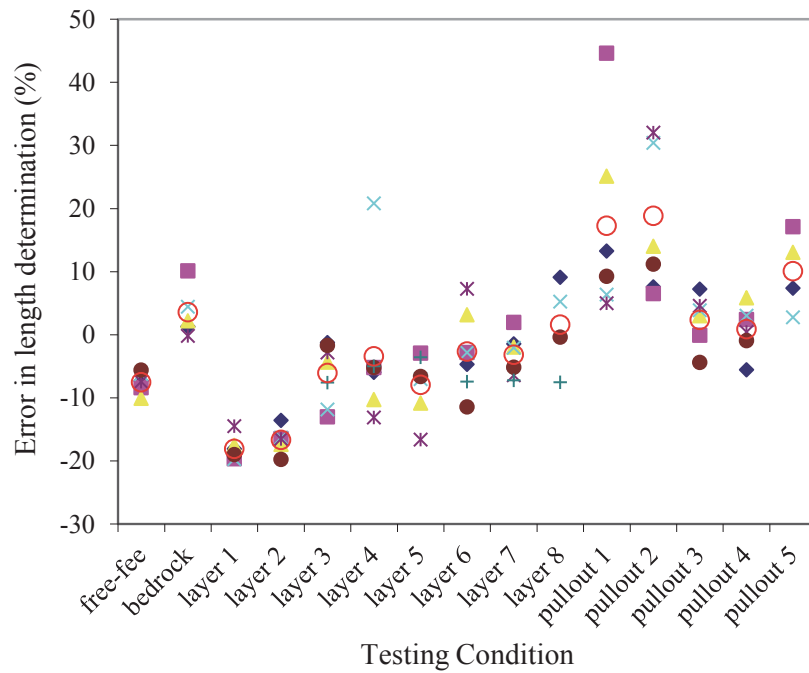


Figure 5.21 Percentage errors for different tests on the timber beam for Sensor 4 (located 2m below the top of the specimen)

Figure 5.22 displays the average errors for different testing conditions in estimation of length of a 5m timber pole using sensor 1 for calculations. As illustrated in Figure 5.22, the scatter of the averaged error (circular symbol) for the pole specimen associated with different tests ranged between 1% and 20% for all cases except layer 6 with 26%. The average error is smaller for the soil layers between 5 to 8 layers and it could relate to the circular shape of the timber pole compared to the hollow section of steel beam and relatively small rectangular section of timber beam which allows the longitudinal wave to be generated and captured by the sensor closer to the impact location.

Figures 5.23 to 5.25 present the relative errors in estimation of the specimen's length for different testing conditions using sensors 2, 3 and 4, respectively. As can be seen in Figure 5.23, by using sensor 2 for estimation of the length, the average error becomes less than 9% for all cases except for the layer 7 with 32% error. However, Figure 5.24 and Figure 5.25 show more uncertainties in terms of length calculation using sensors 3 and 4 located 1.5m and 2m from the impact location in comparison with using sensors 1 and 2 for calculations.

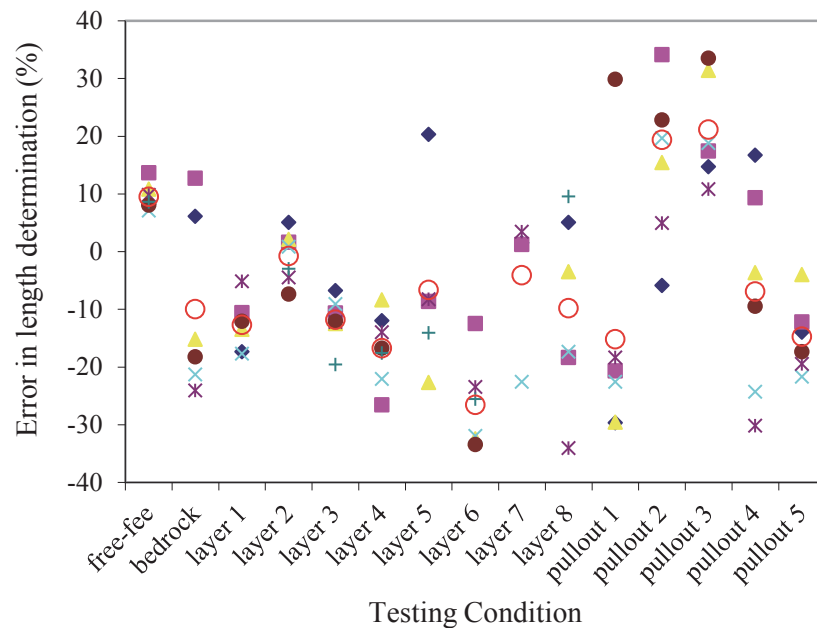


Figure 5.22 Percentage errors for different tests on the timber pole for Sensor 1 (located on top of the specimen)



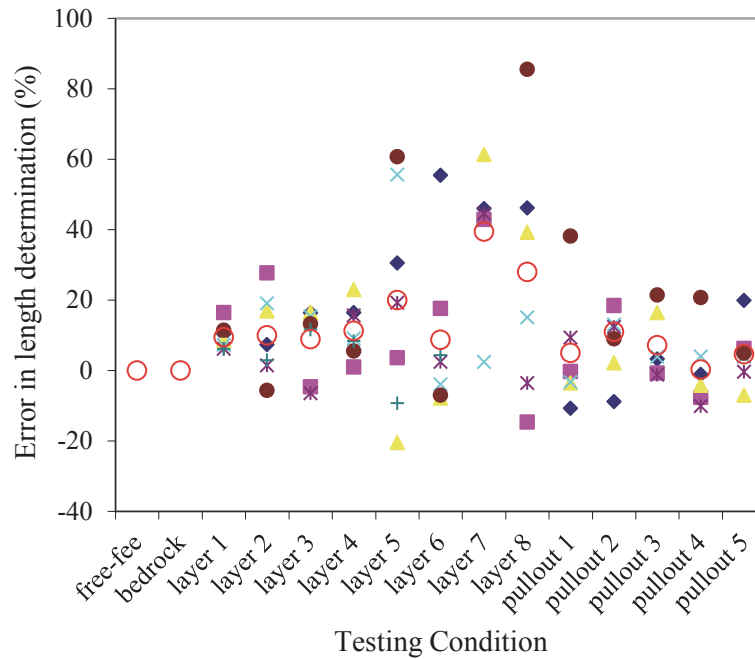


Figure 5.25 Percentage errors for different tests on the timber pole for Sensor 4 (located 2m below the top of the specimen)

### 5.3 IMPULSE RESPONSE (IR) TEST

In Impulse Response (IR) testing, the recorded impact force of the hammer (measured in force-time history) and the response of the structure (measured in acceleration-time history) are transformed into frequency spectra using Fast Fourier Transform (FFT). By dividing the frequency spectra signals of the response data by the frequency spectra of the excitation data, FRFs are obtained. To estimate the length and soundness of the test structure, the FRFs are analysed and distances between two adjacent frequency peaks ( $\Delta f$ ) are determined. Further, it was necessary to calculate the wave velocity (the procedure for wave velocity determination is described earlier in section “Results of SE test with impact from top”). Finally, the length of the test specimen was calculated. The results are provided for impact at the top and middle of the specimen.

#### 5.3.1 Impact at the top

The FRF results from two IR tests conducted at UTS on a laboratory timber beam with (a) free-free and (b) embedded test set-up are presented in Figure 5.26. In the two



graphs, clearly defined frequency peaks are visible. The distances between the frequency peaks of the first, second and third frequencies are determined and labelled in the figure. For the two tests, the length of the timber beam is calculated according to the following equations:

Free-free testing (Figure 5.26 (a)):

$$OL_{IR} = TL_{IR} + \frac{V_{IR}}{2 \times \Delta f_{IR}} = 0m + \frac{4809m/s}{2 \times 427Hz} = 5.63m \quad (\text{first peak}) \quad (5-1)$$

$$OL_{IR} = TL_{IR} + \frac{V_{IR}}{2 \times \Delta f_{IR}} = 0m + \frac{4809m/s}{2 \times 425Hz} = 5.66m \quad (\text{second peak}) \quad (5-2)$$

Embedded test (Figure 5.26 (b)):

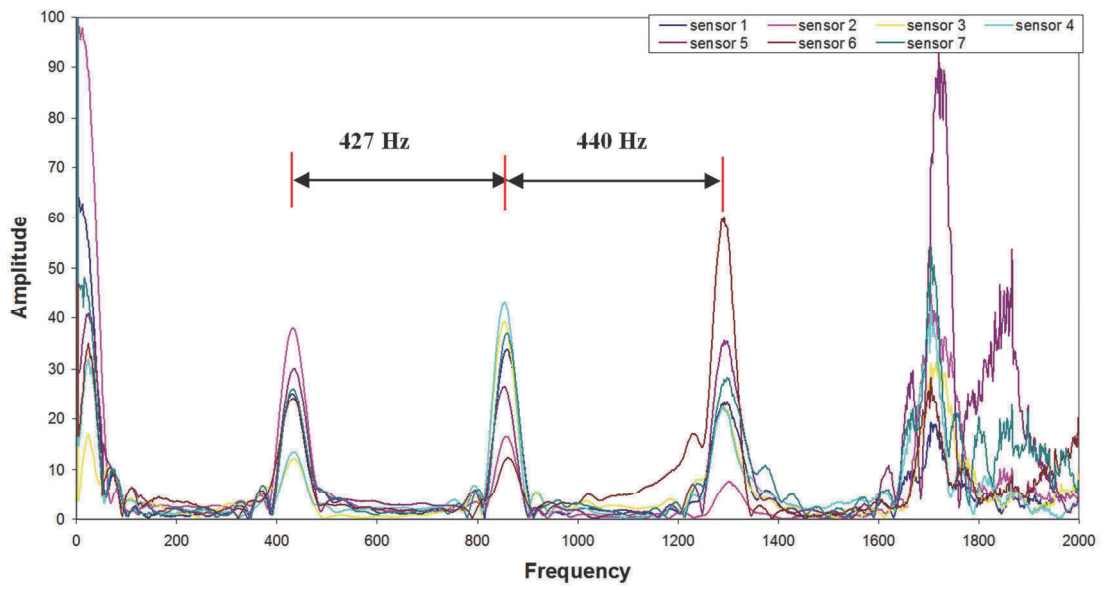
$$OL_{IR} = TL_{IR} + \frac{V_{IR}}{2 \times \Delta f_{IR}} = 0m + \frac{4523m/s}{2 \times 427Hz} = 5.30m \quad (\text{first peak}) \quad (5-3)$$

$$OL_{IR} = TL_{IR} + \frac{V_{IR}}{2 \times \Delta f_{IR}} = 0m + \frac{4523m/s}{2 \times 440Hz} = 5.14m \quad (\text{second peak}) \quad (5-4)$$

The error for the free-free test is thereby 12.6% and 13.2%, respectively; and for the embedded test it is 6% and 2.8%, respectively. Similar results are presented in Appendix B corresponding to the steel beam and the timber pole under free-end condition and when embedded in sand by 1.5m.

Figures 5.27 to 5.29 show relative errors of the IR method for three tests with different testing conditions for the steel beam, timber beam and timber pole, respectively. The peak frequency amplitude for the timber beam specimen using 5-8 layers of soil and for the timber pole for 6-8 layers were not clear, and as such the results are not presented in the graph. It is believed that this observation is the result of increased damping which will greatly reduce the amplitude of reflected waves. Again the circular symbol in the figures presents the average errors from three repeated tests.

### Timber 5<sup>th</sup> pull out



### Timber Free End

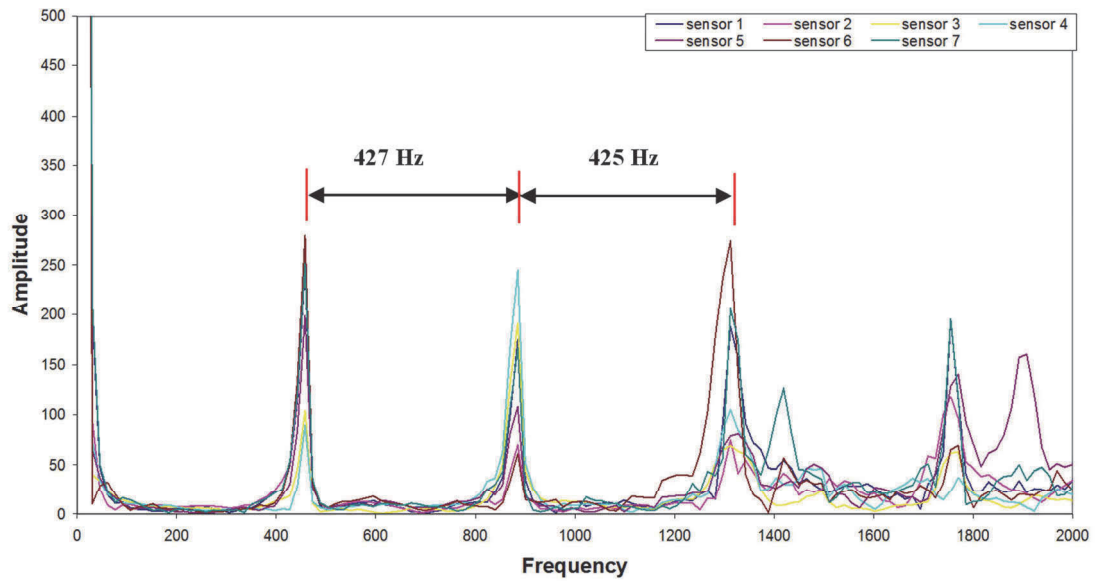


Figure 5.26 FRFs of different sensors of (a) free-free and (b) embedded laboratory IE testing of a timber beam with impact from top.

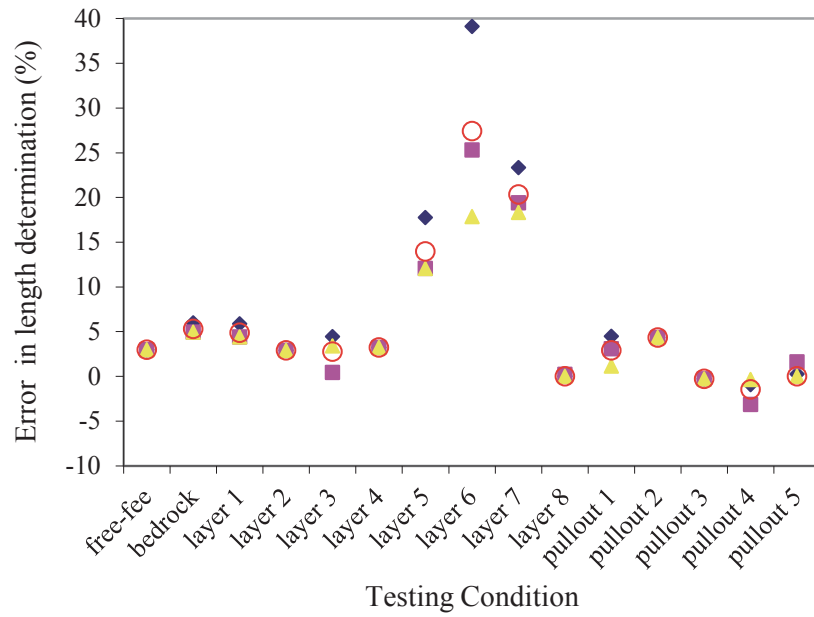


Figure 5.27 Percentage errors for different tests on steel beam

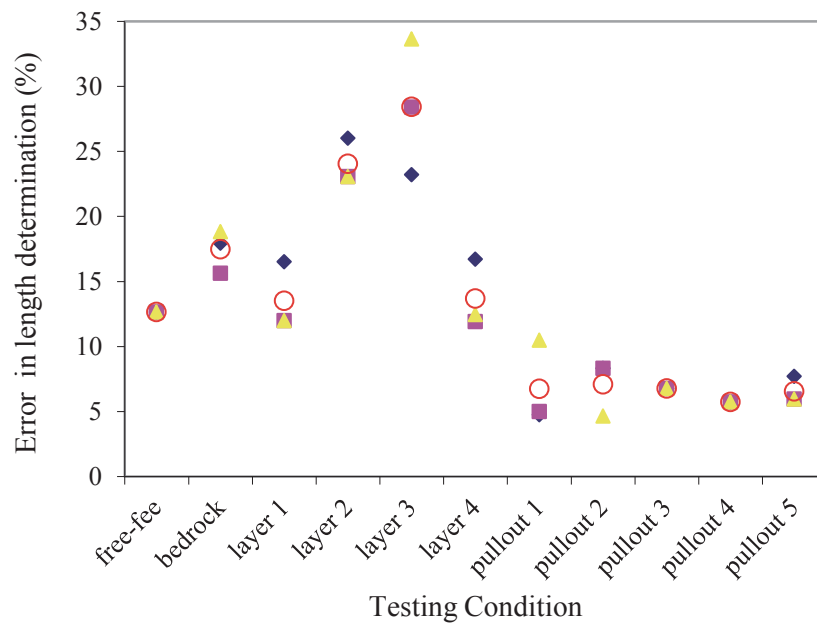


Figure 5.28 Percentage errors for different tests on timber beam

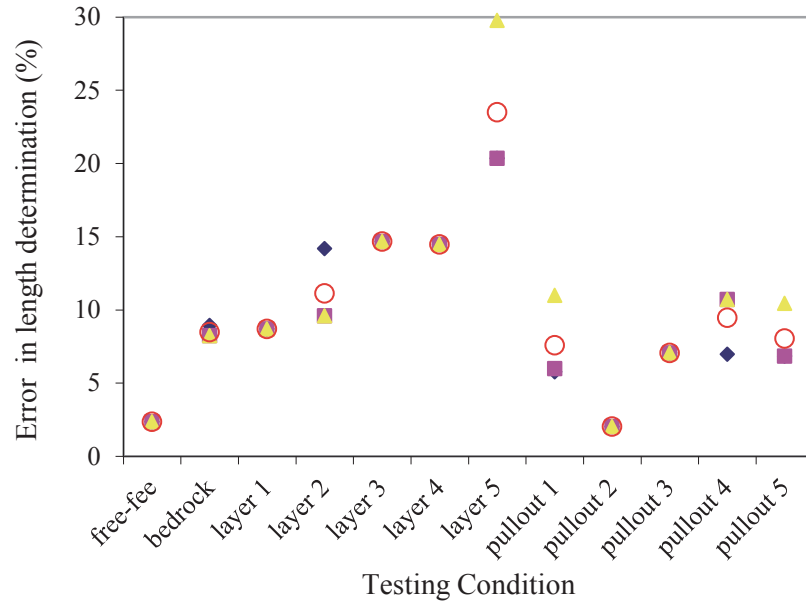


Figure 5.29 Percentage errors for different tests on timber pole

### 5.3.2 Impact at the middle

As highlighted in Chapter 3, it is not always possible to impact a test structure from a free end, as is the case for in-service timber utility poles. Hence, for IR testing the feasibility of impacting the test specimen from its side was also investigated. Illustrated in Figure 5.30 are two IR tests ((a) free-free and (b) embedded test set-up) undertaken at UTS for a laboratory timber beam with impact on its side. Whereas clear frequency peaks can be identified for the free-free test set-up, the identification of relevant frequency peaks for the embedded test set-up is challenging due to the appearance of additional frequency peaks generated by flexural waves (see Figure 5.30(b)). From the identifiable frequency distances, the beam lengths are determined as follows:

Free-free testing (Figure 5.30 (a)):

$$OL_{IR} = TL_{IR} + \frac{V_{IR}}{2 \times \Delta f_{IR}} = 0m + \frac{4465m/s}{2 \times 427Hz} = 5.23m \quad (\text{first peak}) \quad (5-5)$$

$$OL_{IR} = TL_{IR} + \frac{V_{IR}}{2 \times \Delta f_{IR}} = 0m + \frac{4465m/s}{2 \times 458Hz} = 4.87m \quad (\text{second peak}) \quad (5-6)$$

Embedded test (Figure 5.30 (b)):

$$OL_{IR} = TL_{IR} + \frac{V_{IR}}{2 \times \Delta f_{IR}} = 0m + \frac{3988m/s}{2 \times 503Hz} = 3.96m \quad (\text{first peak}) \quad (5-7)$$

$$OL_{IR} = TL_{IR} + \frac{V_{IR}}{2 \times \Delta f_{IR}} = 0m + \frac{3988m/s}{2 \times ? Hz} = ?m \quad (\text{second peak}) \quad (5-8)$$

It is believed that an impact from the side in middle of the specimen generates both longitudinal and dispersive waves at the same time. Indeed, for velocity calculations and length estimation, the longitudinal and transverse waves should be separated. As using the bracket to impact the pole in the middle has some uncertainty to transfer all of the energy to the pole, and also in terms of impracticality of using brackets for each pole, it was decided to investigate the dispersive waves which uses impact at the middle to generate flexural waves which is discussed later in this chapter as bending wave test in next section.

## 5.4 BENDING WAVE TEST

Bending Wave (BW) method requires a horizontal impact to the side of a structure. This method uses the propagation of bending waves in piles/poles that are highly dispersive in nature. The bending wave velocity decreases with increasing wavelength, with most of the velocity decrease occurring at wavelengths that are longer than the pile diameter. To determine the pole length with bending wave, dispersive analysis of the wave is required in which data can be extracted from a selected group of frequencies. These frequencies are then analysed for the individual times required to travel to the tip of the pole and back. Since the method involves striking the pole on its side and placing the receivers on the side of the pole, the method is potentially useful in cases where the top of the pole is not accessible. The Sonic Echo/Impulse Response methods either require the top of the pole to be accessible or a small structure needs to be rigidly attached to the side of the structure to allow hammer blows to create compressional waves.

The Short Kernel Method (SKM) analysis is used to determine the so-called phase velocity of wave travel, the velocity associated with a particular frequency, to calculate the pole length. From SKM plot, one can then identify initial wave arrivals and subsequent reflections (echoes), and finally calculate the depths and locations of the reflection events. In the SKM method, one or more cycles are used as “Kernel Seed” in

order to cross-correlate with a number of seed frequencies between 500-4000 Hz. Details are presented in Chapter 2 and the results are presented later in this chapter. Various bending wave tests have been completed for this project on a 5m timber pole in the structures laboratories at UTS. The experimental set-up of those tests are shown in Figure 4.25. In the bending wave testing, five accelerometers were used to acquire the time history data from the timber specimens under impact loading, in which four accelerometers (no. 1 to 4) were located above the soil on the timber pole and the 5<sup>th</sup> was located in the soil on the butt of the timber specimens. The bending wave test procedure and required equipment are presented in Chapter 3.

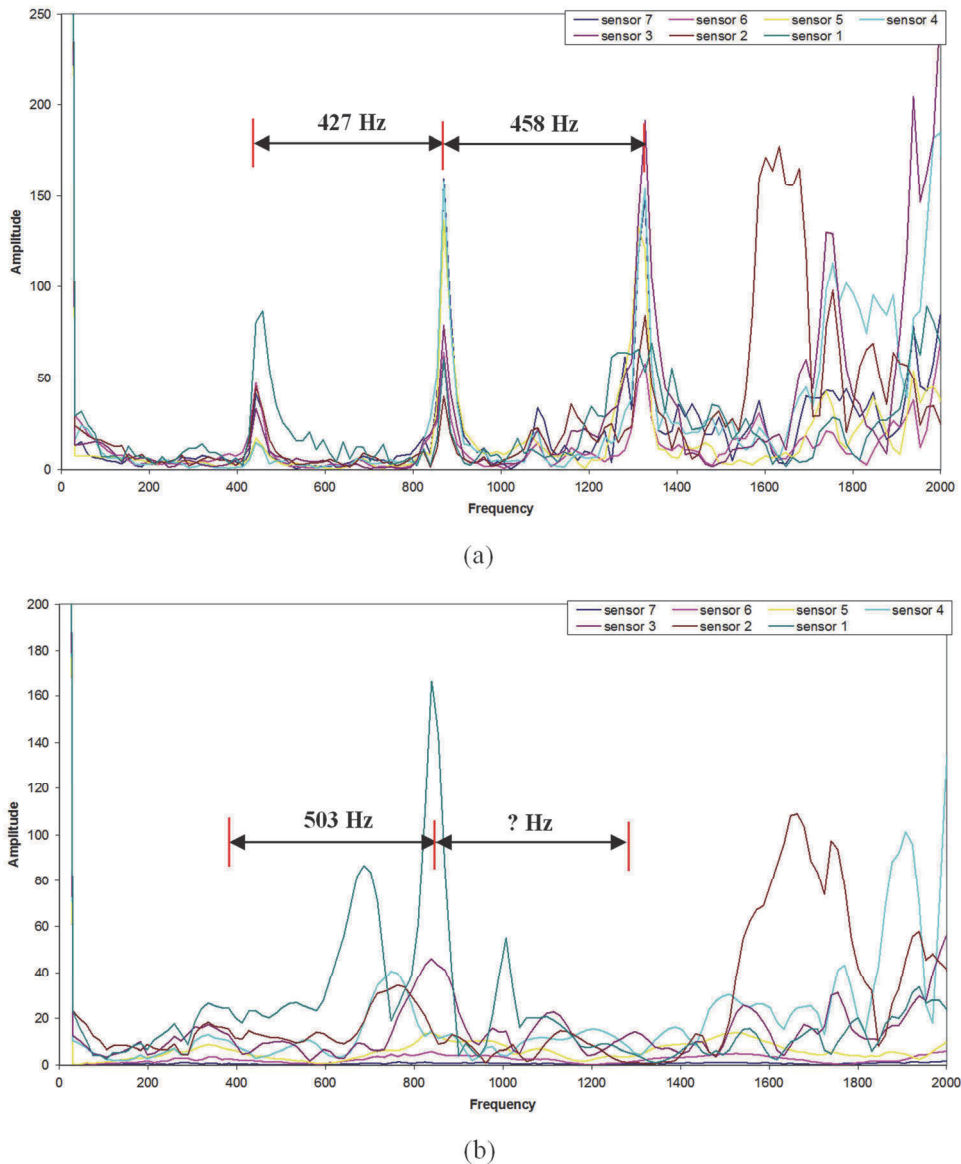


Figure 5.30 FRFs of different sensors of (a) free-free and (b) embedded laboratory IR testing of a timber beam with impact from the side.

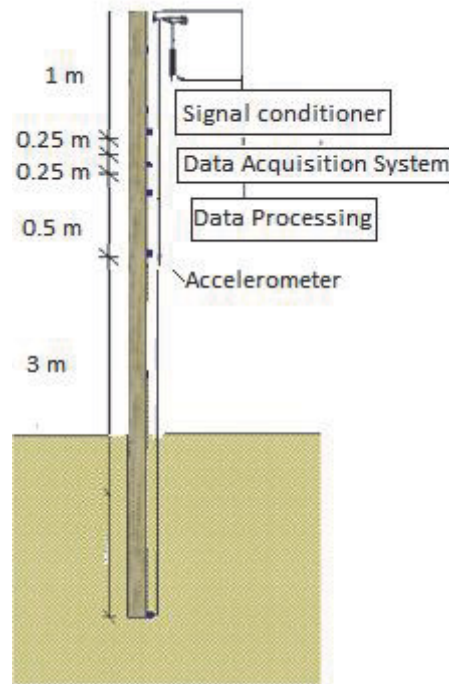


Figure 5.31 Schematic test set-up of embedded BW tests for laboratory testing

#### 5.4.1 Application of SKM for the calculation of phase velocity

In the BW method, the reflections of flexural waves, generated by transversal impact, are analysed using SKM analysis as an advanced signal processing technique. Due to dispersive nature of bending waves, each phase velocity of the wave is related to its own frequency. Using SKM, sensor signals are scanned with a kernel frequency to filter or reduce irrelevant frequency components in the signal, and phase velocities of central frequencies are calculated. Through the identification of initial wave arrivals, and subsequent reflections, the depths and locations of reflection events can be calculated, and thereby, the length and soundness of a structure be determined.

Figure 5.32 shows an example of raw signal and its counterpart SKM with relevant frequency. Determination of the relevant frequencies has been achieved by frequency analysis where all signals are processed with FFT to produce Frequency Response Functions (FRFs). Figure 5.33 shows an example of the frequency response function from a timber pole under 3<sup>rd</sup> pull out condition. Figure 5.34 shows SKM plot of the timber pole under the 3<sup>rd</sup> pull out condition at the kernel frequency of 752 Hz. It is observed that the first peaks of the selected sensors are consistent, resulting in a relatively consistent velocity results.

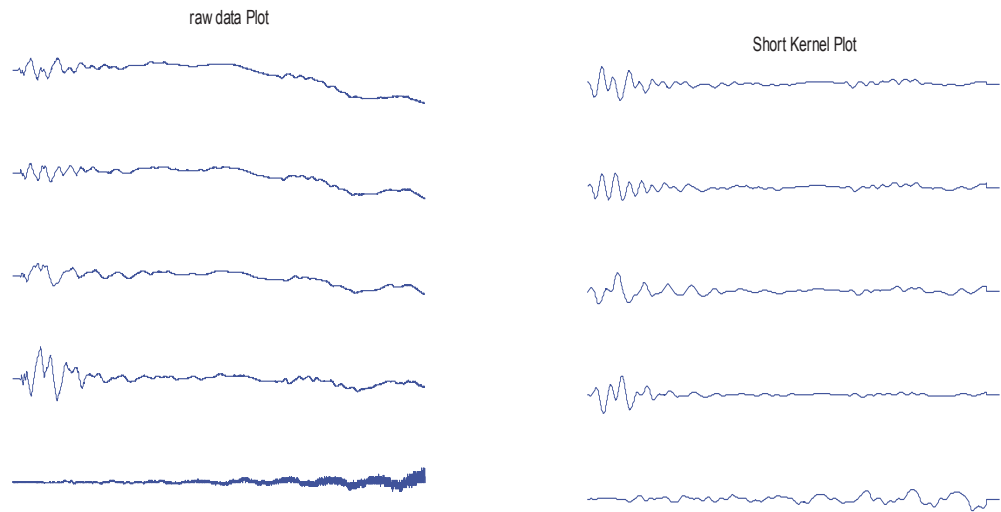


Figure 5.32 An example of Raw signals vs SKM plots at specific kernel frequency

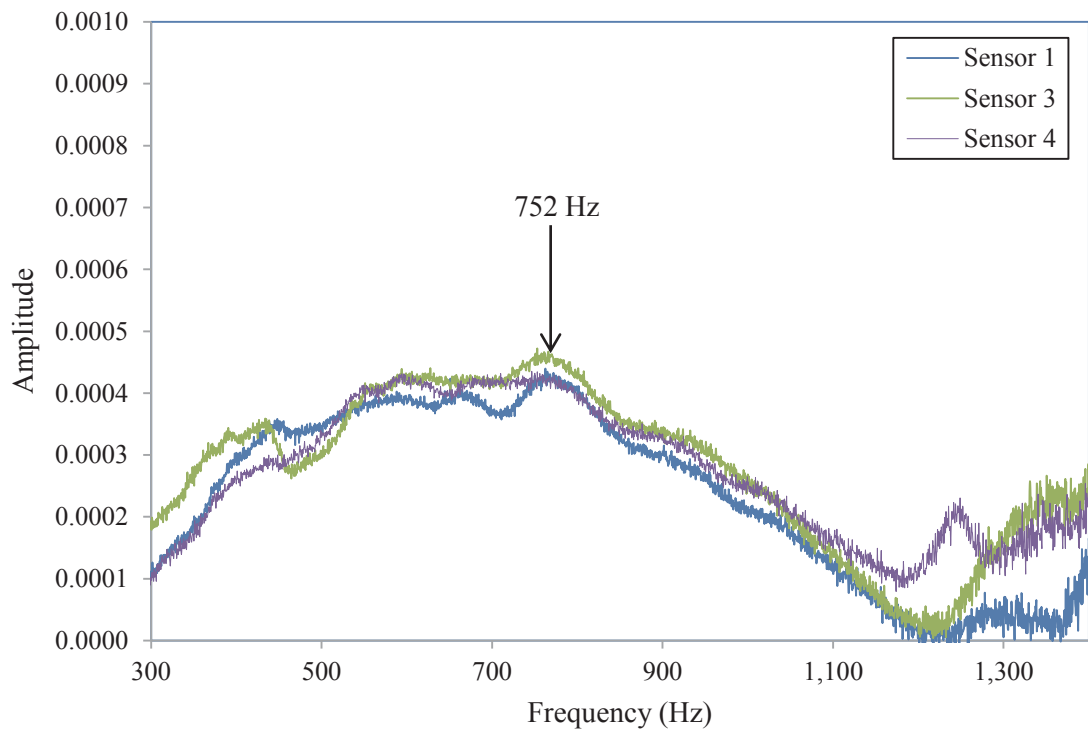


Figure 5.33 An example of the frequency response function (FRF) from a timber pole under 3rd pull out condition



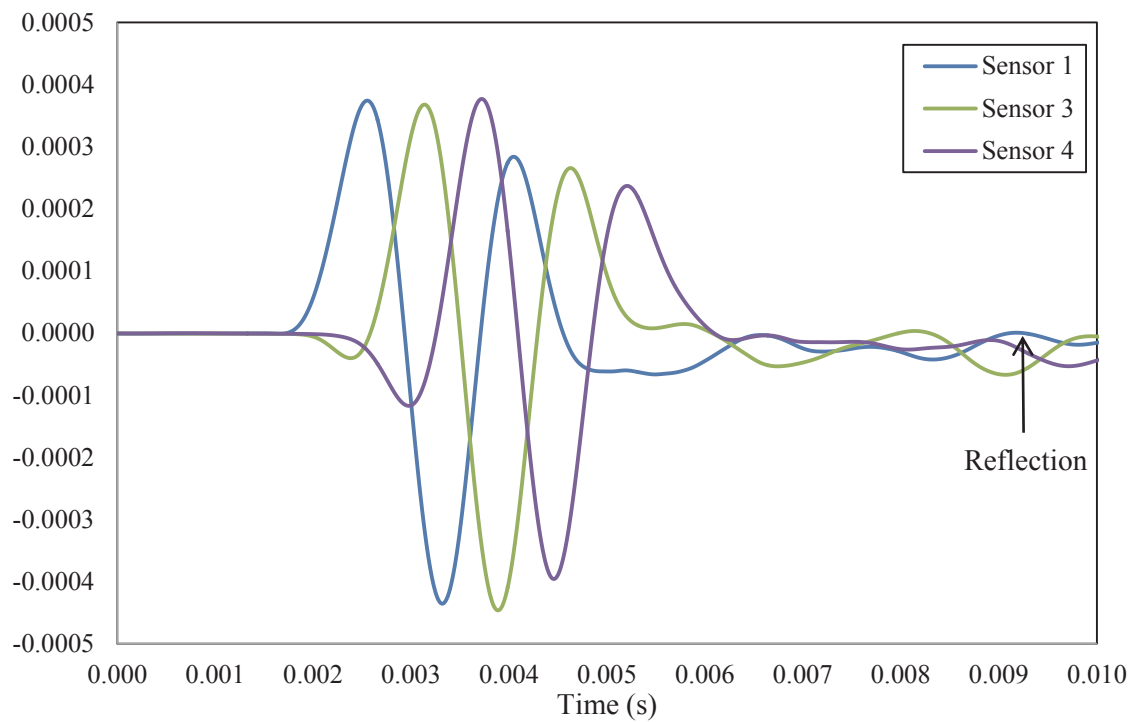


Figure 5.34 SKM plot at frequency of 725 Hz: Timber pole under 3rd pull out condition

#### 5.4.2 Velocity calculation

Firstly, the frequency components of recorded signals of the 5 m timber pole from each sensor using measured frequency response functions (FRF) are determined. Secondly, from the FRF data of different sensors, central frequencies of the signals are identified. As example, FRFs derived from different sensor signals of a laboratory BW testing of an embedded timber beam are displayed in Figure 5.33. From this figure, it is observed that the frequency peak at 752 Hz is consistent for all depicted sensors and can, therefore, be chosen as a central frequency. The identification of a stable and consistent frequency is crucial for the following SKM data processing. Next, for the identified central frequency, the SKM kernel is formed for each sensor signal. After performing the SKM, the first significant positive or negative amplitude peak, representing the frequency's arrival at the first transducer is chosen. Whether positive or negative peaks are chosen is dependent upon which possesses the algebraically-largest value. Then the location of this peak after it has arrived at the second sensor location is determined. Finally, the differences in time between these two peaks are determined in order to

compute a wave speed for the frequency. Based on this procedure, the phase velocity is calculated for the three depicted sensors (Figure 5.34) as follows:

Sensor 1 vs. sensor 3:

$$V_{BW} = \frac{\Delta L_{BW}}{\Delta t_{WTravel-BW}} = \frac{0.5m}{0.584 \times 0.001s} = 856m/s$$

Sensor 3 vs. sensor 4:

$$V_{BW} = \frac{\Delta L_{BW}}{\Delta t_{WTravel-BW}} = \frac{0.5m}{0.584 \times 0.001s} = 856m/s$$

Sensor 1 vs. sensor 4:

$$V_{BW} = \frac{\Delta L_{BW}}{\Delta t_{WTravel-BW}} = \frac{1m}{1.17 \times 0.001s} = 854m/s$$

The wave velocity is calculated for each kernel frequency under different pull out testing conditions and the results are presented in Figures 5.35 to 5.37. These results are compared to analytical results from (Subhani, Li & Samali) assuming timber as an orthotropic material and using sensors 1 as a reference and sensor 2 to 4 as a second sensor for velocity calculations. As can be seen, the phase velocity will slightly increase with increase in frequency for sensors 1~2, 1~3 and 1~4 as expected from analytical results. The difference between the analytical results and laboratory results is related to the parameters which were used for the analytical solution which were different from the material properties of timber pole in experimental tests. Currently, there are no other analytical solutions available to compare with the laboratory results. Figure 5.38 and Figure 5.39 display the same trend as the phase velocity increase by increase in frequency values using sensor 2 as reference and sensors 3 and 4 as corresponding sensors for velocity calculations. As can be seen, using sensor 2 as a reference for velocity calculation shows the same trend as when sensor 1 was used as reference. The slight increase in velocity by increase in frequency is related to wavelength which is long in low frequency and it cannot be captured by each sensor. In other words, the first few sensors receive the waves with the same wavelength rather than each one receiving the wave separately with time delay. Also based on the results, the kernel frequency between 400-800 Hz was identified to be the most suitable range for use in SKM method for phase velocity calculations.

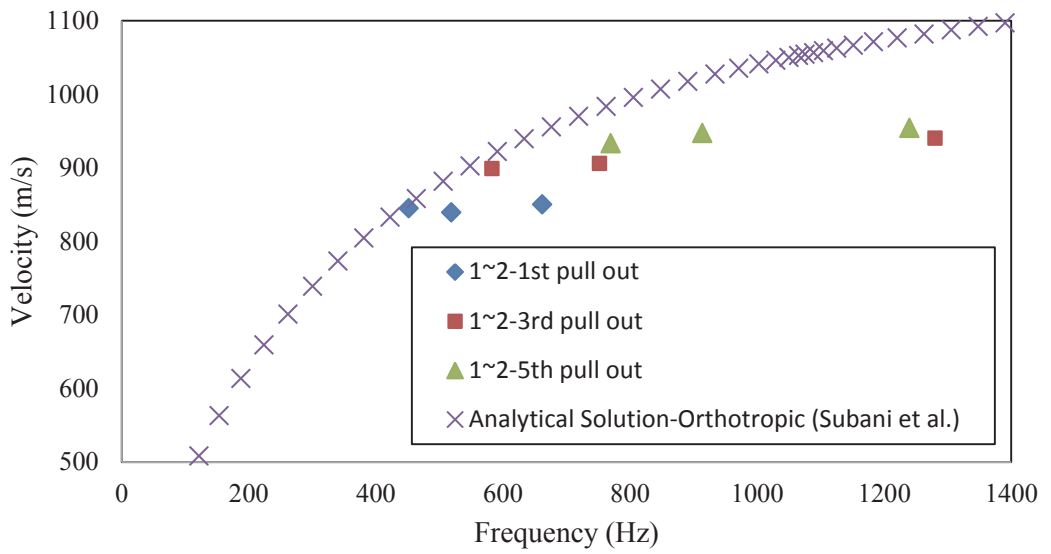


Figure 5.35 Bending wave velocity for different kernel frequencies of 5 m timber pole under different boundary conditions using sensors 1 and 2.

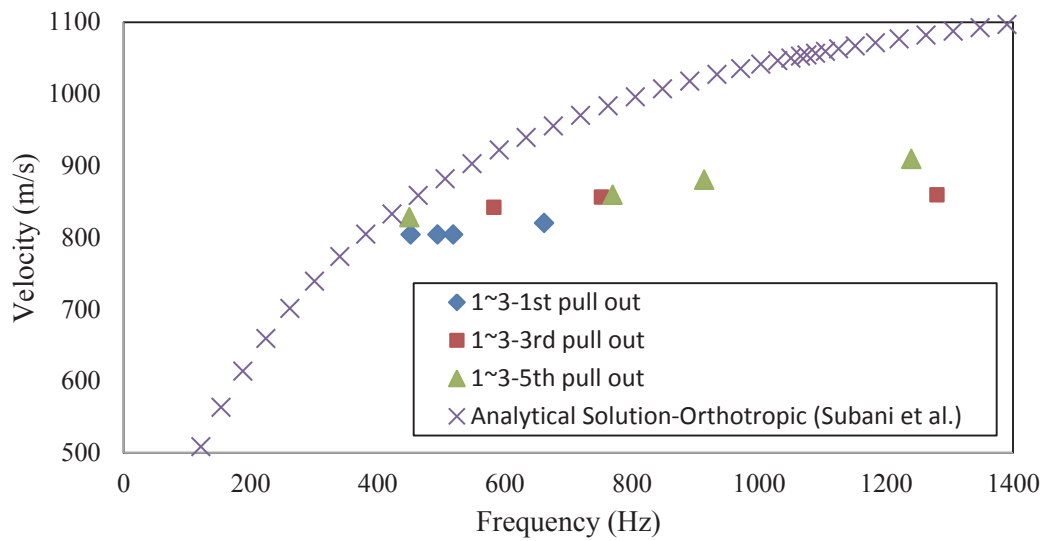


Figure 5.36 Bending wave velocity for different kernel frequencies of 5 m timber pole under different boundary conditions using sensors 1 and 3.

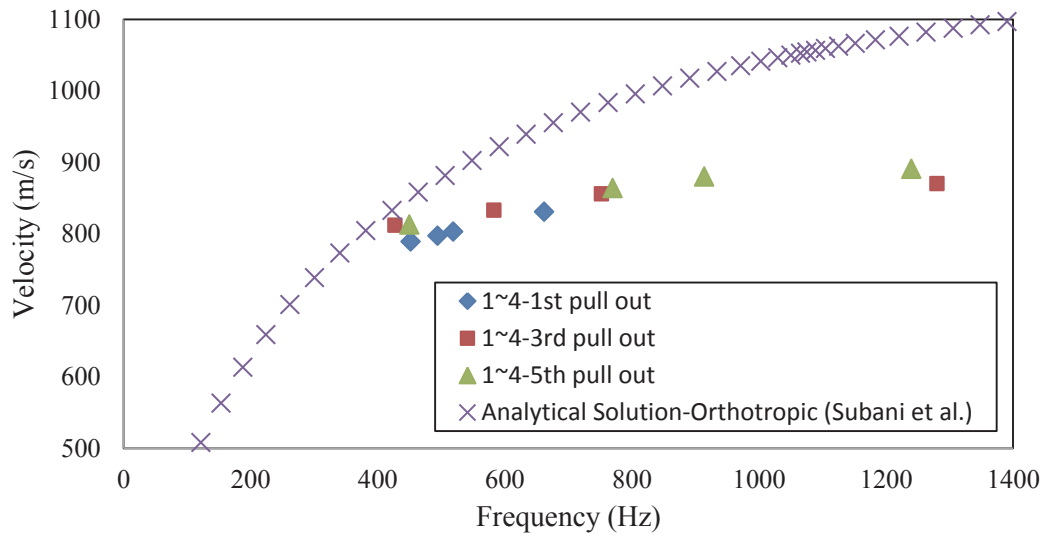


Figure 5.37 Bending wave velocity for different kernel frequencies of 5 m timber pole under different boundary conditions using sensors 1 and 4.

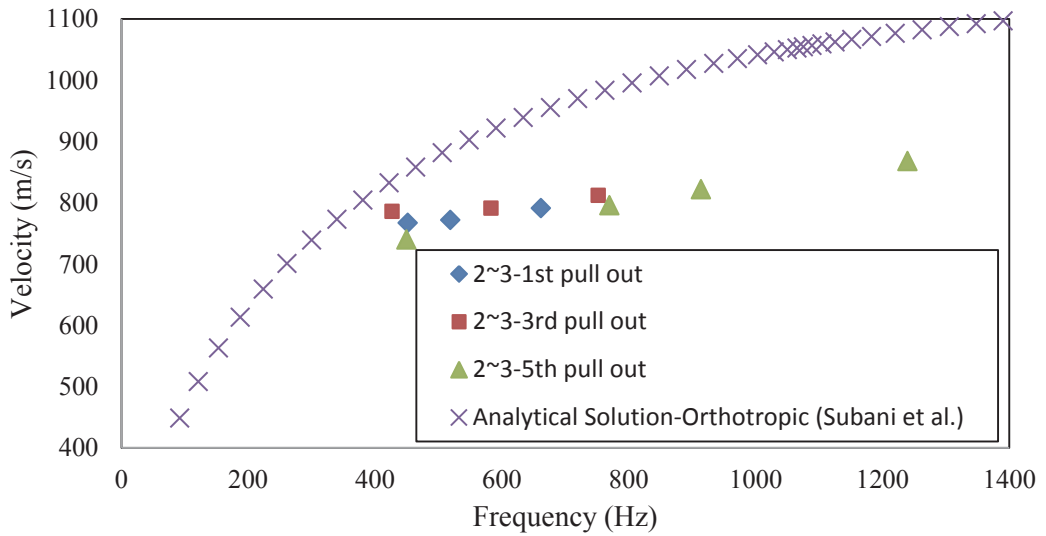


Figure 5.38 Bending wave velocity for different kernel frequencies of 5 m timber pole under different boundary conditions using sensors 2 and 3.

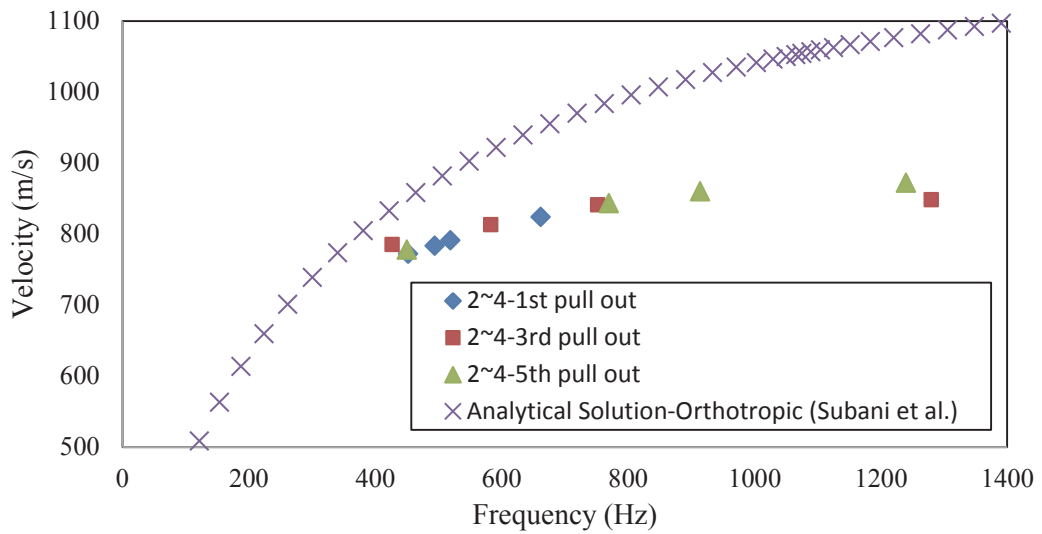


Figure 5.39 Bending wave velocity for different kernel frequencies of 5 m timber pole under different boundary conditions using sensors 2 and 4.

### 5.4.3 Length Estimation

Using the SKM to locate a frequency in a return signal from a pole's tip, proceeds in a manner similar to the one used for finding wave velocities. If a return signal is present in a time history, there will be a series of positive and negative peaks showing the location of good correlation between the kernel and its frequency counterpart in the return wave. By identifying a significant amplitude peak in the first signal, and its corresponding location in the return wave, a time for the frequency to return from the tip is computed by finding the time between these two peaks. The results of the length determination are displayed in Figures 5.40 to 5.42 for a 5m timber pole under 1<sup>st</sup>, 3<sup>rd</sup> and 5<sup>th</sup> pull out conditions. The percentage of error for length determination of all three testing conditions stand between -10.5% and 0%. Furthermore, the percentage of error for embedded length calculation will decrease with increase in kernel frequency. If the kernel frequency between 600-800 Hz is selected, the average error for length estimation becomes less than 5% for all testing conditions except 5<sup>th</sup> pull out condition which is around 10%.

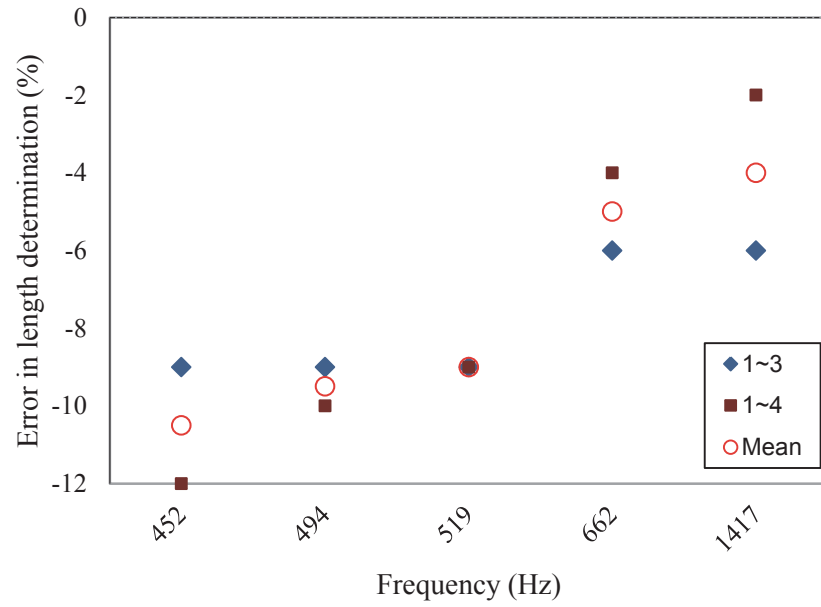


Figure 5.40 Percentage errors for different kernel frequencies of the timber pole under 1<sup>st</sup> pull out condition

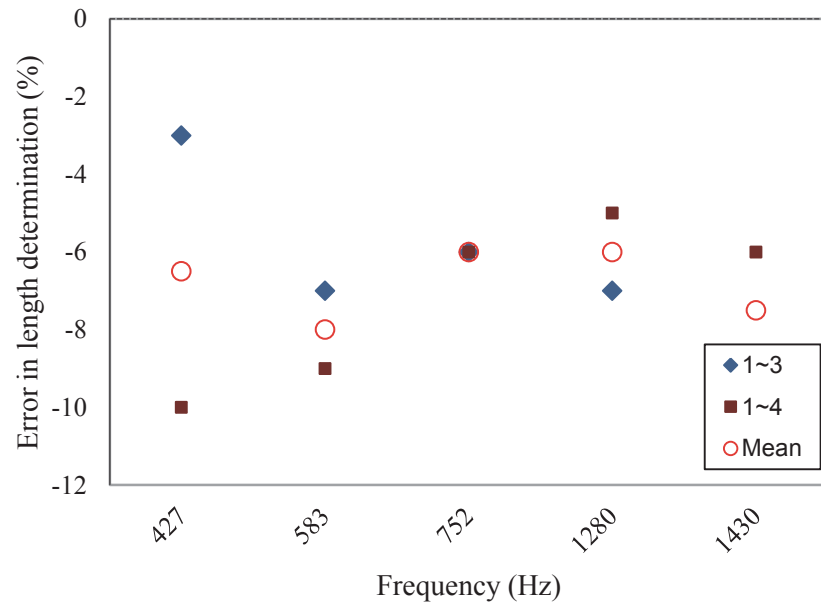


Figure 5.41 Percentage errors for different kernel frequencies of the timber pole under 3<sup>rd</sup> pull out condition.

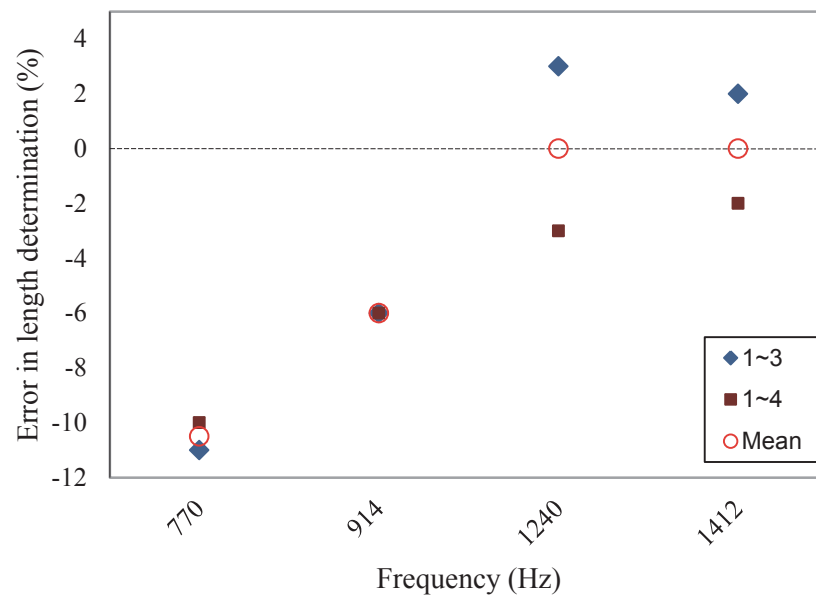


Figure 5.42 Percentage errors for different kernel frequencies of the timber pole under 5<sup>th</sup> pull out condition.

## 5.5 ULTRASEISMIC TEST

For this method, multiple sensors were used with the same arrangement as in Sonic Echo test. As the main focus of this research is on the timber poles, the results of the steel beam and timber beam are provided here for free-free condition as justification. However, the results of timber pole are provided for different testing conditions in this section.

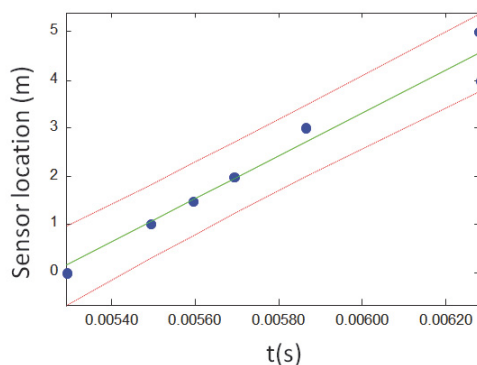
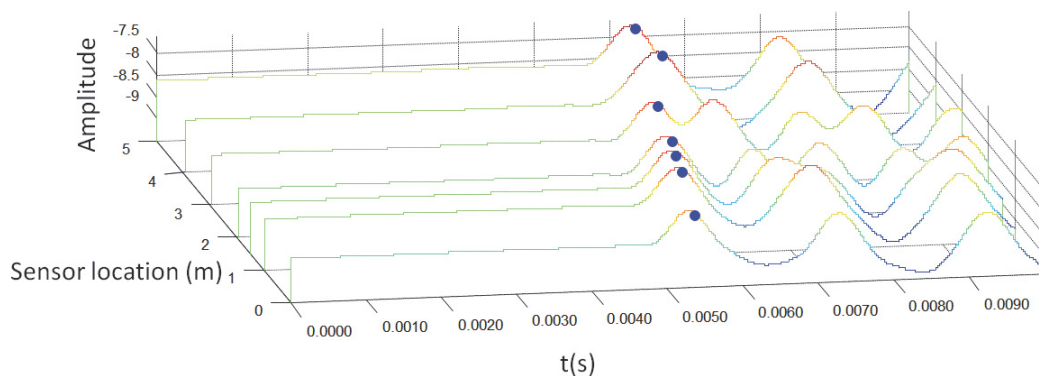
The test set-up, equipment and procedure of Ultraseismic testing are mostly the same as for Sonic Echo and Impulse Response testing.

### 5.5.1 Velocity calculation

#### 5.5.1.1 Steel beam

In this method, seven sensors were used for acceleration measurement and the wave velocity is estimated from the slope of the sensor locations and the first arrival peaks. Figure 5.43 plots the acceleration-time history for all sensors mounted on the side of a 5m hollow section steel beam, 5 m in length, 2 cm in width and 5 cm in height under free-free condition using Ultraseismic method. As can be seen, the arrival and reflection

wave velocity was estimated from the slope of the acceleration-time history with adequate accuracy. According to this figure the coefficient of determination ( $R^2$ ) for velocity determination of arrival wave is 0.96 compared to 0.95 for the reflection wave. These indicate that stress wave velocity estimation is the same for the arrival and reflection waves in steel as an isotropic material. The slight decrease in reflection wave velocity is believed to be related to the wave dispersion in the material. Figure 5.44 shows the acceleration-time results for selected sensors mounted on the side of 5m steel beam closer to the impact location under free-free condition using Ultraseismic method. As shown in this figure the accuracy of velocity determination will increase for arrival peak compared to using all of the sensors for stress wave velocity estimation. However, the accuracy for reflection velocity calculation will slightly decrease. It may relate to the complexity of the wave generation and dispersion phenomena in the cylindrical poles. In addition, it might relate to the generation of the low frequency impact by the small hammer which results in wave generation with inadequate energy to travel through the specimen.



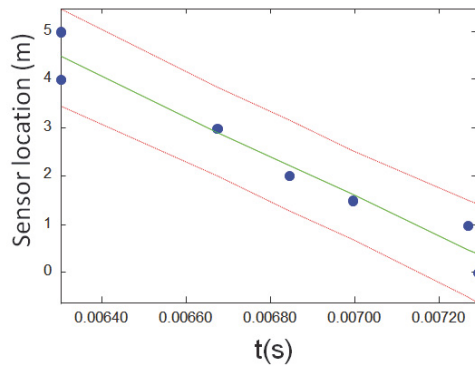
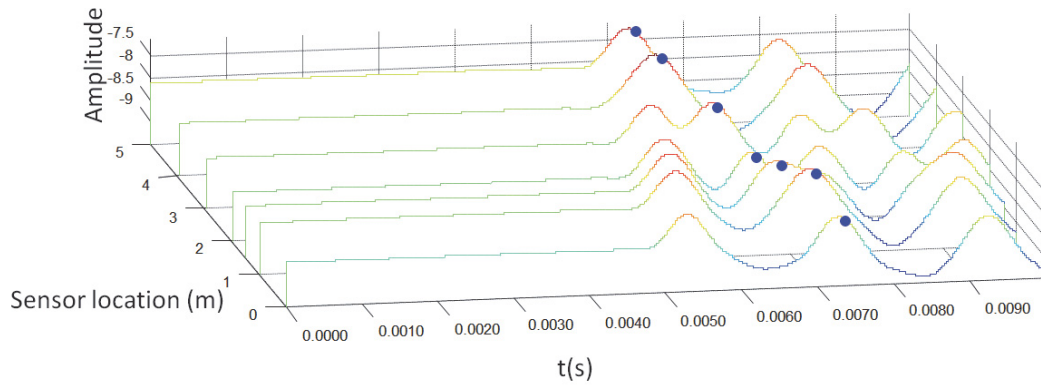
summary

Peaks 1 slope=4471

$R^2=0.96$

Low-Pass Filter,  $F_{pass}=1500$





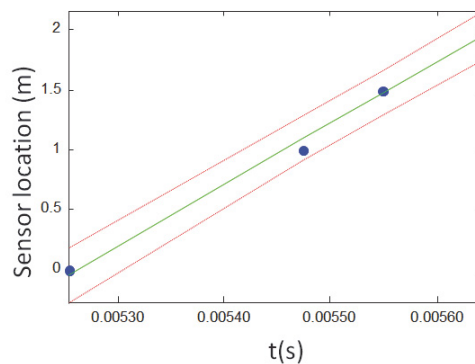
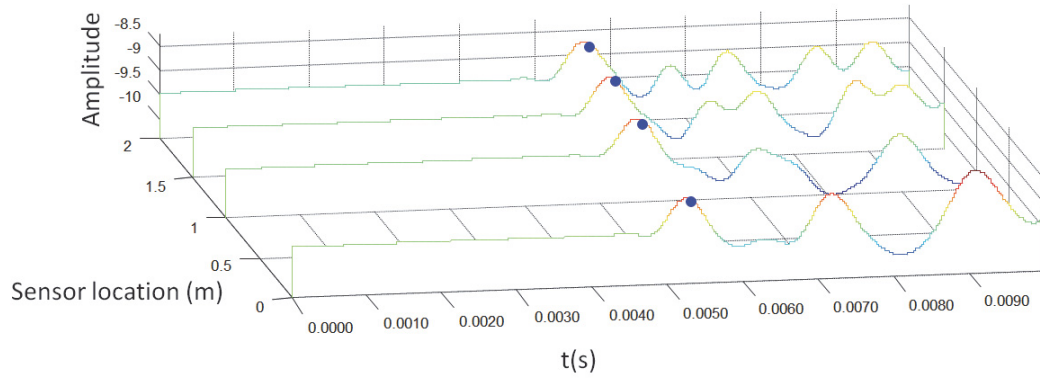
summary

Peaks 2 slope=-4100

$R^2=0.94$

Low-Pass Filter, Fpass=1500

Figure 5.43 Acceleration results for all sensors in y direction under free-free condition for 5 m steel beam using Ultraseismic method



summary

Peaks 1 slope=5131

$R^2=0.99$

Low-Pass Filter, Fpass=1500

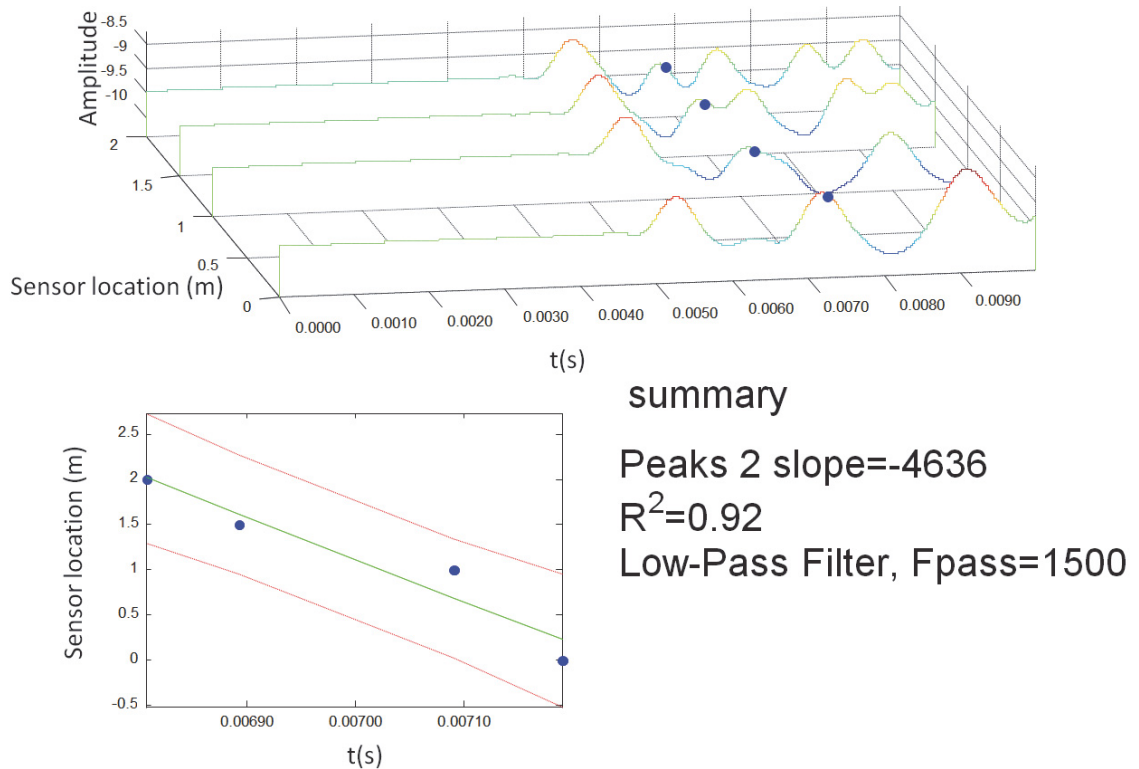
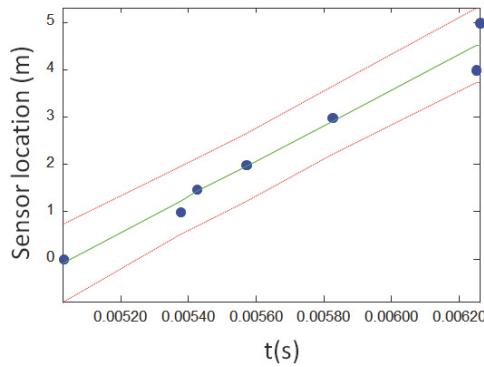
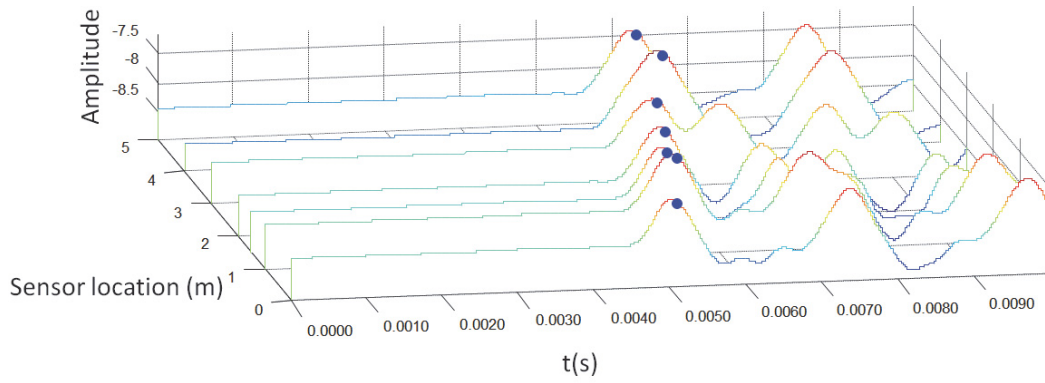


Figure 5.44 Acceleration results for selected sensors in y direction under free-free condition for 5 m steel beam using Ultraseismic method (sensors at 0, 1, 1.5 and 2 m from the top)

### 5.5.1.2 Timber beam

Figure 5.45 plots the acceleration-time history for all sensors mounted on the side of the experimental timber beam under free-free condition using Ultraseismic method. The timber beam has cross sectional dimensions of 9 cm in height, 4 cm in width, with overall length of 5 m. As can be seen, the arrival and reflection wave velocities were estimated from the slope of the acceleration-time history with adequate accuracy ( $R^2 = 0.97$  for arrival wave and  $R^2 = 0.96$  for reflecting wave). Figure 5.46 shows the acceleration-time history results for selected sensors close to impact location mounted on the side of the timber beam under free-free condition. Using closer sensors to the impact location results in the same value for coefficient of determination of arrival wave velocity (Figure 5.46) compared to using all the sensors for velocity estimation. Indeed, the stress wave velocity estimation is not affected by change of distance between the impact location and the selected sensor.

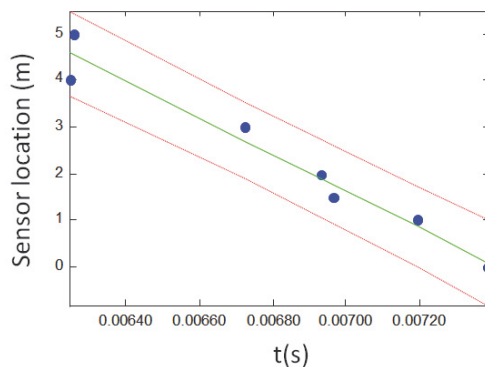
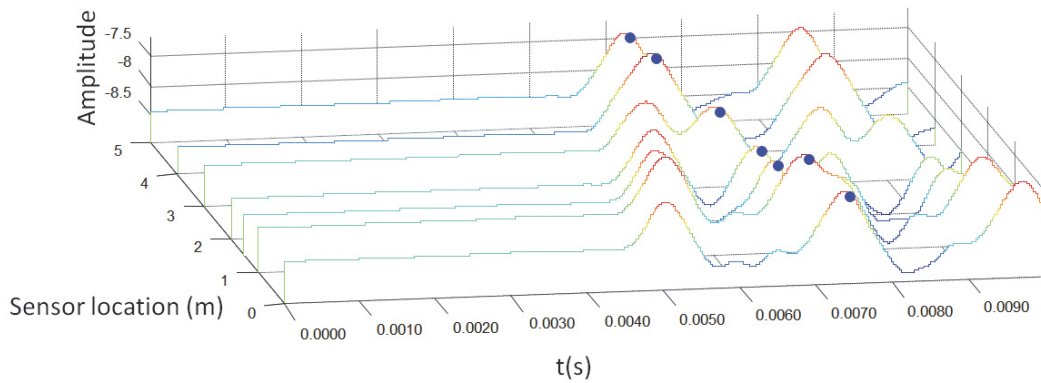


summary

Peaks 1 slope=3741

$R^2 = 0.97$

Low-Pass Filter,  $F_{pass}=2000$



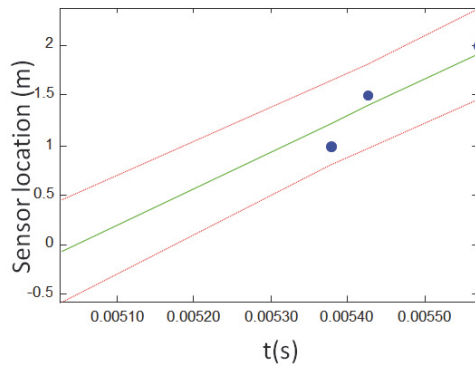
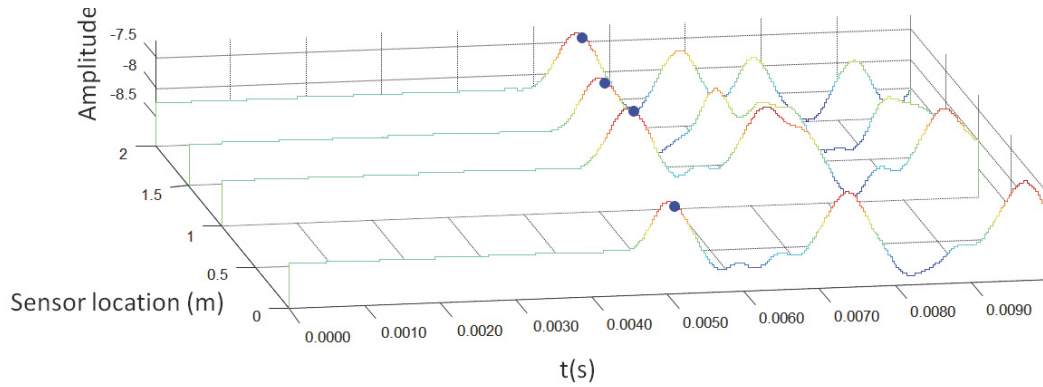
summary

Peaks 2 slope=-3920

$R^2 = 0.95$

Low-Pass Filter,  $F_{pass}=2000$

Figure 5.45 Acceleration results for all sensors in y direction under free-free condition for the 5 m timber beam using Ultraseismic method

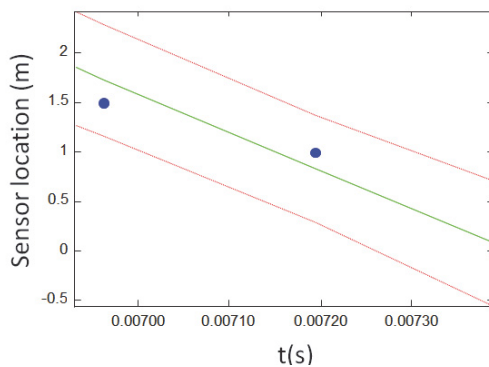
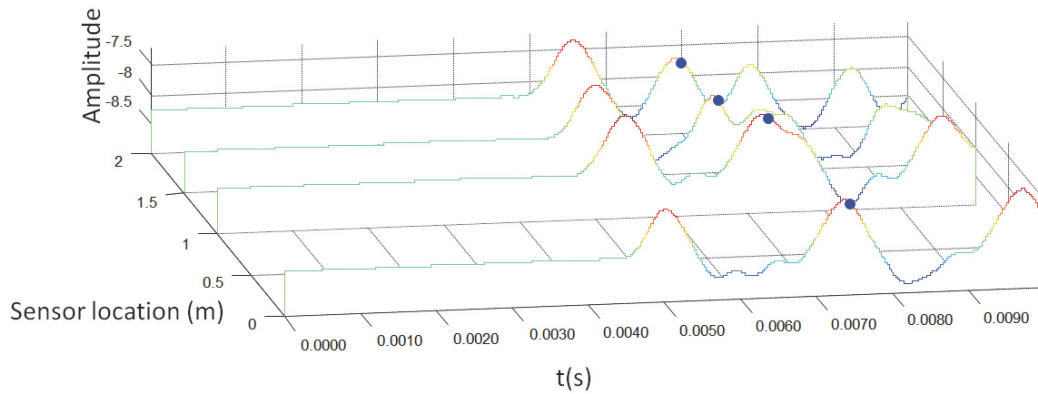


summary

Peaks 1 slope=3651

$R^2=0.96$

Low-Pass Filter, Fpass=2000



summary

Peaks 2 slope=-3887

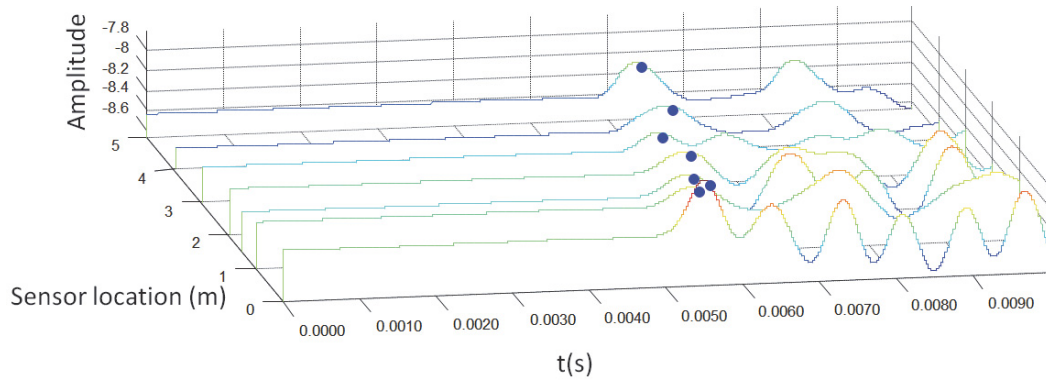
$R^2=0.94$

Low-Pass Filter, Fpass=2000

Figure 5.46 Acceleration results for selected sensors in y direction under free-free condition for the 5 m timber beam using Ultraseismic method (sensors at 0, 1, 1.5 and 2 m from the top)

### 5.5.1.3 Timber pole

Figure 5.47 displays the acceleration-time history results of the experimental timber pole, 5 m in length and a circular cross section with 30 cm in diameter under free-free condition for all sensors mounted on the pole. Based on the trend line for arrival stress wave velocity, sensor 4 and 6 located 2 m and 4 m from the impact location show more variation compared to the other sensors. Some reasons regarding the uncertainties in wave propagation in timber material were discussed earlier in this chapter. To investigate the effects of distance between sensor and impact locations, the stress wave velocity is calculated by not considering the two sensors causing more variation. Figure 5.48 plots the acceleration-time history of selected sensors. As can be seen, the coefficient of determination for velocity estimation will be increased from 0.92 to 0.98 for arrival wave and from 0.93 to 0.98 for reflection wave. In addition, the value for reflection stress wave velocity will significantly increase from 2679 m/s to 5043 m/s which results in a reasonable estimation for stress wave velocity in timber pole. The same trend was observed for the timber pole under bedrock condition and the results are illustrated in Appendix C. Hence, using sensors close to the impact hammer will increase the accuracy of the velocity determination for utility timber poles.

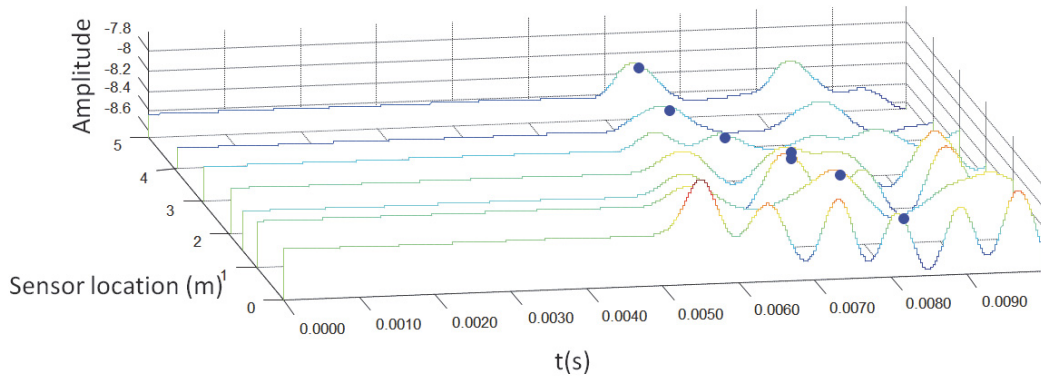
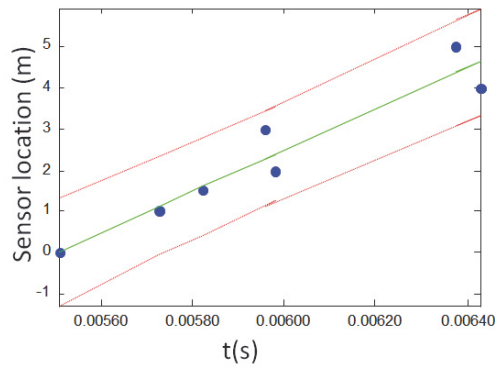


summary

Peaks 1 slope=5013

$R^2=0.91$

Low-Pass Filter,  $F_{pass}=2000$



summary

Peaks 2 slope=-2678

$R^2=0.93$

Low-Pass Filter,  $F_{pass}=2000$

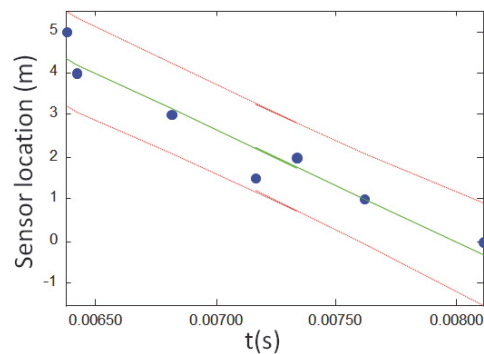
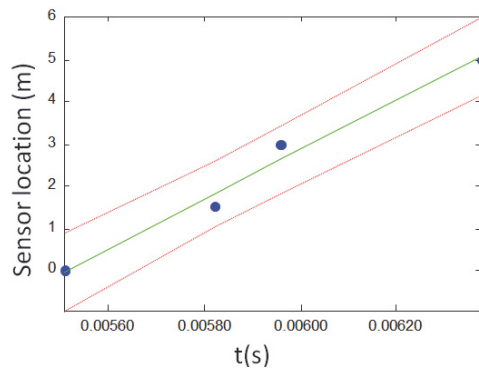
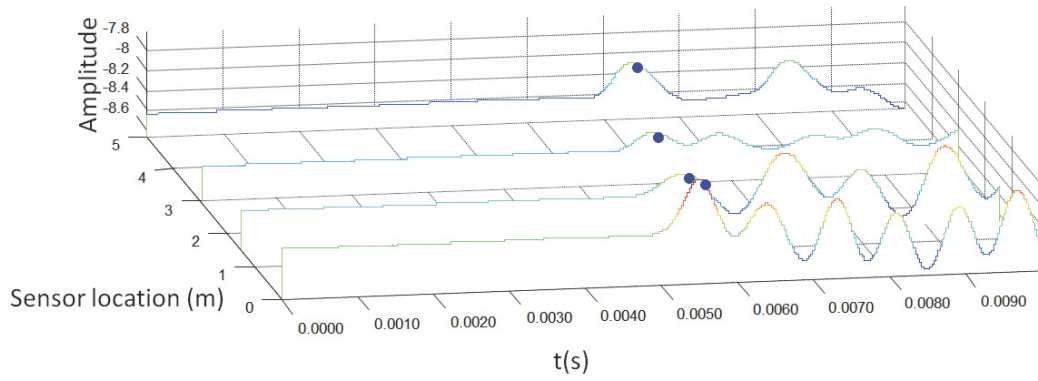


Figure 5.47 Acceleration results for all sensors in y direction under free-free condition for the 5 m timber pole using Ultraseismic method

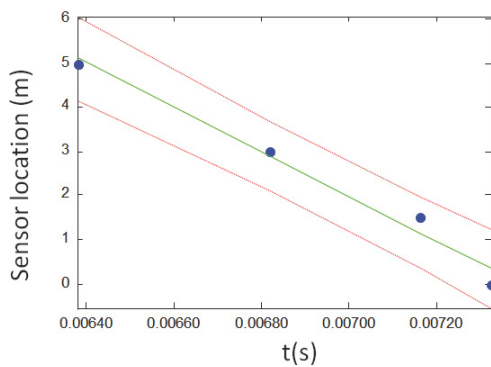
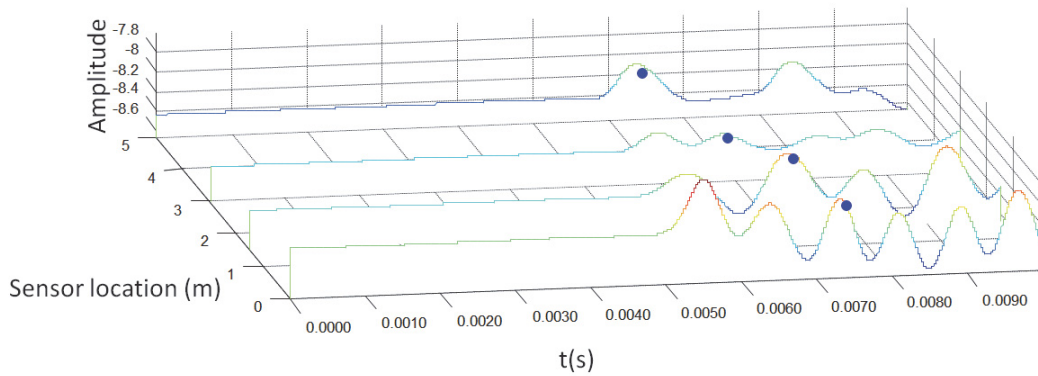


summary

Peaks 1 slope=5858

$R^2=0.98$

Low-Pass Filter,  $F_{pass}=2000$



summary

Peaks 2 slope=-5043

$R^2=0.98$

Low-Pass Filter,  $F_{pass}=2000$

Figure 5.48 Acceleration results for selected sensors in y direction under free-free condition for the 5 m timber pole using Ultraseismic method (sensors at 0, 1.5 , 3 and 5m from the top)

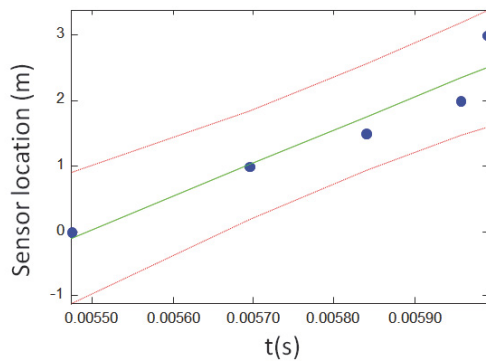
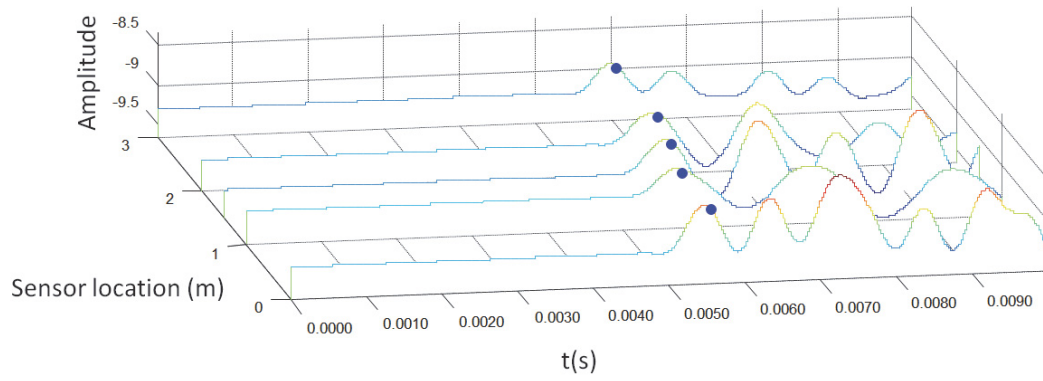
As mentioned earlier, based on analysis of the free-free and bedrock conditions, the accuracy of velocity estimation will be increased by using sensors close to the impact location to a certain point (up to 3m from the impact location). To verify these results for embedded testing conditions, sensors between the impact location and 3 m from the impact location were selected and the time-history results are shown in Figure 5.49 for a 5m timber pole under 1 layer soil condition (i.e. the specimen is located on the bedrock with 37.5 cm surrounding soil). Furthermore, to investigate further the effects of sensor location on accuracy of stress wave velocity, sensors 2 and 4 were eliminated. Figure 5.50 plots the acceleration-time history of selected sensors located 0, 1.5 and 3m from the impact location. As a result, the coefficient of determination for reflection of stress wave velocity shows significant improvement from 0.42 to 0.99 in comparison to using sensors located at 0, 1, 1.5, 2 and 3m from the impact location for velocity calculations. Therefore, using sensors at 3 m from impactation location, will improve the wave velocity calculations. However, these will not necessarily lead to accurate estimation. Based on using trend line for velocity calculations, some sensors might need to be eliminated for velocity calculations as they show more variation compared to the rests of the sensors. It is believed that those variations are related to the uncertainty involved in wave generation in timber material such as anisotropy of timber, location of sensors with regards to annual ring orientation and slope of grain and possible existence of imperfections in timber such as knots. More details of the effects of these parameters on stress wave velocity was discussed earlier in this chapter, “Velocity calculation” of SE method.

Similar trend is observed for a 5m timber pole under 2 layers soil condition and the results are presented in Appendix C. The same procedure was applied to the results of a timber pole under various pull out conditions. Based on the results of the acceleration-time history of 5 m timber pole under 2<sup>nd</sup>, 4<sup>th</sup> and 5<sup>th</sup> pull out conditions (as presented in Appendix C) using sensors close to 2m from the impact location will result in more accurate estimation of the wave velocity.

Furthermore, one of the main problems faced when using impact hammer to generate the surface wave method is the most appropriate tuning frequency of generated wave, in order to have efficient transmission, and able to propagate in the material in long distance, to specifically interfere with defects and to be received in good condition.



Usually, the dispersion curve is the solution to overcome this problem. However, where the number and type of wave modes are much higher than in plates, the dispersion curve will fail. Due to anisotropy in timber, the exact analytical treatment of waves is much more complicated and leads to increased computational cost than waves in an isotropic material. The most significant consequence of elastic anisotropy is the loss of pure wave modes for general propagation directions. This fact also implies that the direction of wave group propagation, i.e. energy flow, does not generally coincide with the wave vector (Sorohan et al. 2011). Thus, primary analyses are required to be performed on the acceleration results of the experimental tests on embedded timber pole to separate each mode. After that, the velocity will be calculated and accordingly, the length determined.

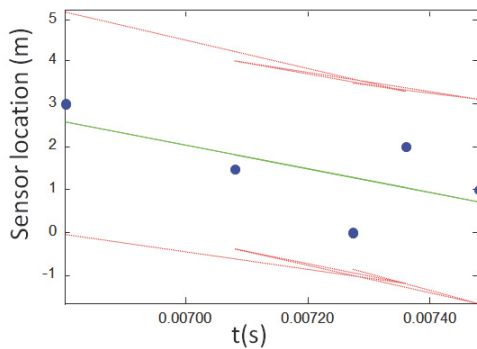
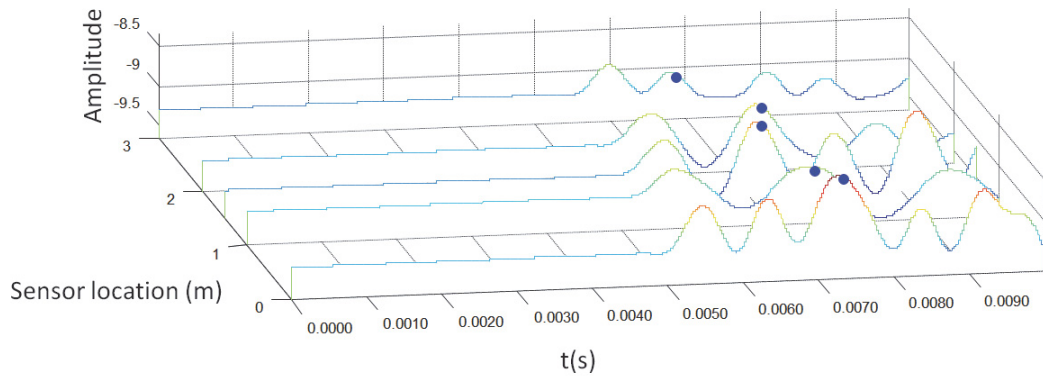


summary

Peaks 1 slope=5052

$R^2=0.91$

Low-Pass Filter, Fpass=2000



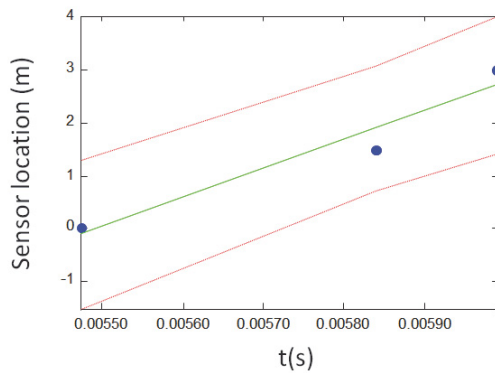
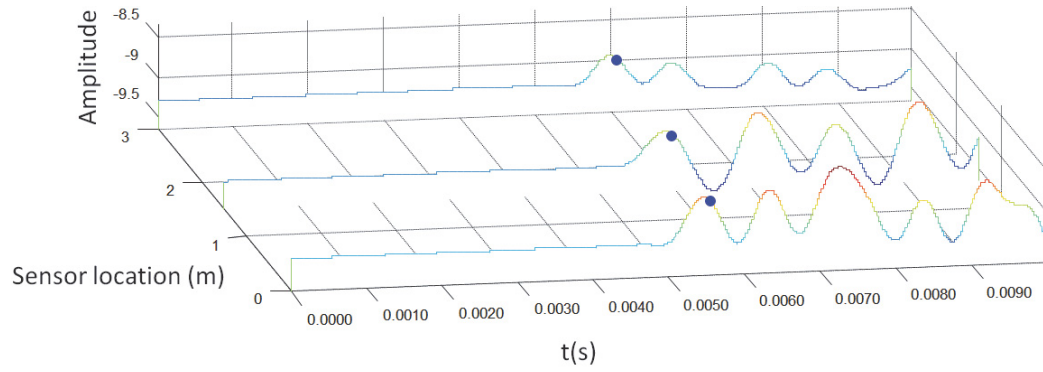
summary

Peaks 2 slope=-2739

$R^2=0.41$

Low-Pass Filter, Fpass=2000

Figure 5.49 Acceleration results for selected sensors in y direction under 1 layer soil condition for the 5 m timber pole using Ultraseismic method (sensors at 0, 1, 1.5, 2 and 3m from the top)

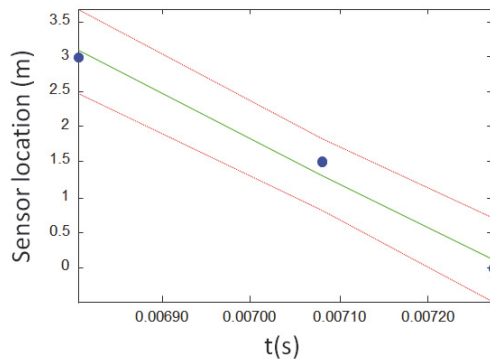
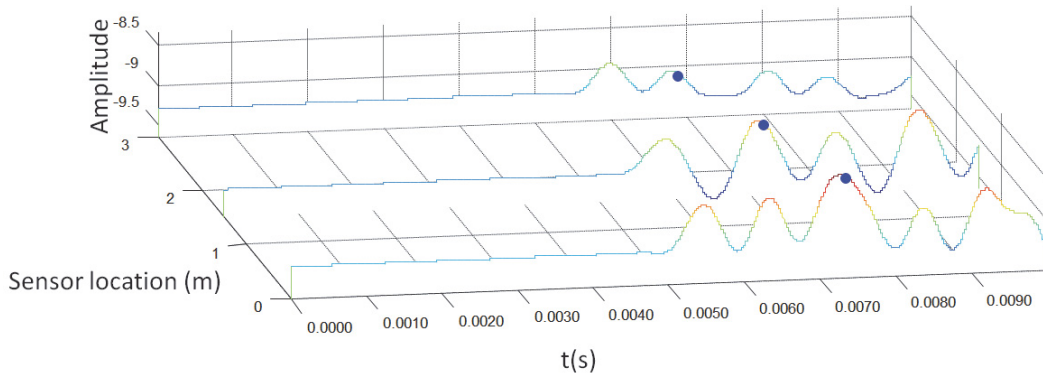


summary

Peaks 1 slope=5493

$R^2=0.94$

Low-Pass Filter, Fpass=2000



summary

Peaks 2 slope=-6327

$R^2=0.99$

Low-Pass Filter, Fpass=2000

Figure 5.50 Acceleration results for selected sensors in y direction under 1 layer soil condition for the 5 m timber pole using Ultraseismic method (sensors at 0, 1.5 and 3m from the top)

### 5.5.2 Length Estimation

In the next step, embedded length is calculated using the arrival and reflection velocity from acceleration-time history and using the following equation:

$$L_e = (t_2 - t_1) * \left( \frac{V_d * V_u}{V_d + V_u} \right) * \lambda \quad (5.1)$$

where,  $L_e$  is the embedment length of the pole,

$t_2$  is the reflection time,  $t_1$  is the arrival time for the same sensor which is preferably located on top of the soil/foundation,

$V_d$  is the downward velocity in m/s,  $V_u$  is the upward (reflection) velocity in m/s,

$\lambda$  is a reduction factor for velocity decrease in soil.

The results of length determination for different types of boundary conditions are illustrated in Figure 5.51. According to this figure, the average error in length determination for the timber pole under different pull out conditions, which is more relevant to timber pole in-service, is less than 18%. However, average error for length determination of a 5 m timber pole standing on bedrock with different soil depth varies between 3% and 44%. As discussed earlier, the uncertainty of this method for embedded timber pole is relatively high as it involves the uncertainty of wave velocity in orthotropic material, uncertainty of the presence of the soil and its effect on reflection wave and velocity decrease inside the soil. The combination of these factors makes the length estimation of embedded timber poles too difficult.

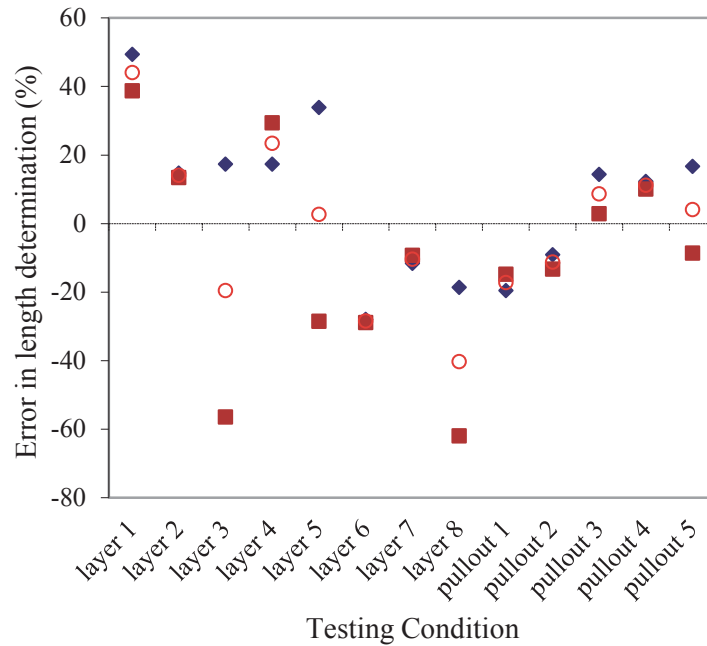


Figure 5.51 Embedded length determination of 5 m timber pole under different boundary conditions using sensors at 0, 1.5 and 3m from the top.

## 5.6 EFFECTS OF DAMAGE SCENARIOS ON TIMBER POLE IN LABORATORY

One damage scenario was generated in the laboratory by cutting one half section of the timber pole from the bottom for a length of 1m. Figure 5.52 displays the schematic set-up and sensor location for the intact and damaged timber pole. Figure 5.53 and Figure 5.54 show the comparison between acceleration-time history results of a 5m timber pole for sensor 3, and 4, respectively. Sensor 3 and 4 are mounted on the opposite side of the impact specimen and 3.2m from the impact location. As can be seen in Figure 5.53, in the acceleration-time history of the damaged pole, one of the main peaks is missing and this is related to the damage in the pole. Further studies are required as future research to apply advanced or devise new methods of signal processing to determine the extent and location of damage in timber poles.

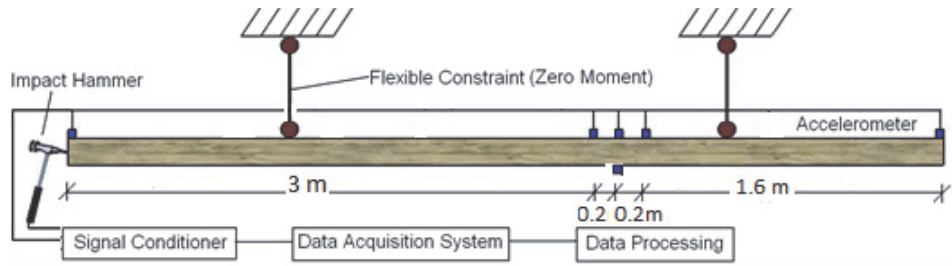


Figure 5.52 Schematic set up for intact and damaged timber pole in laboratory

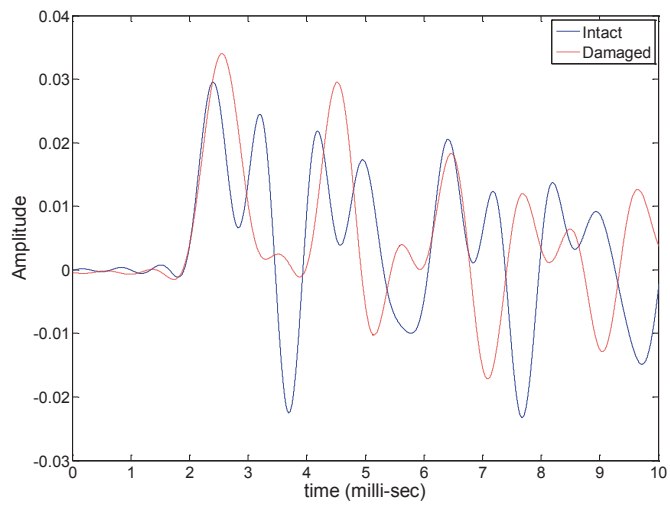


Figure 5.53 Acceleration results for an intact and damaged timber pole under free-free condition for sensor 3

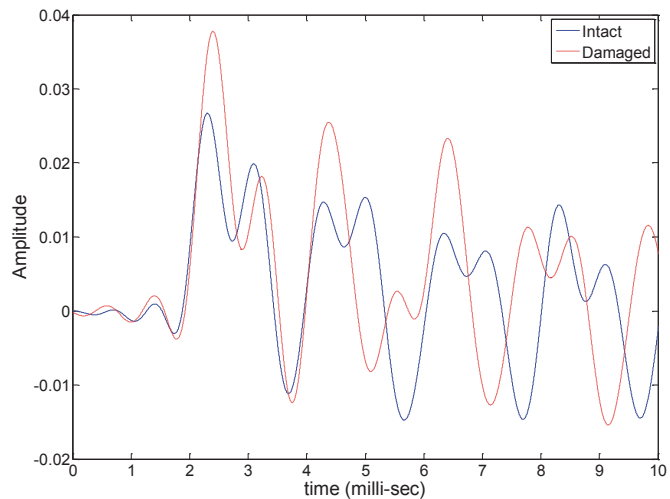
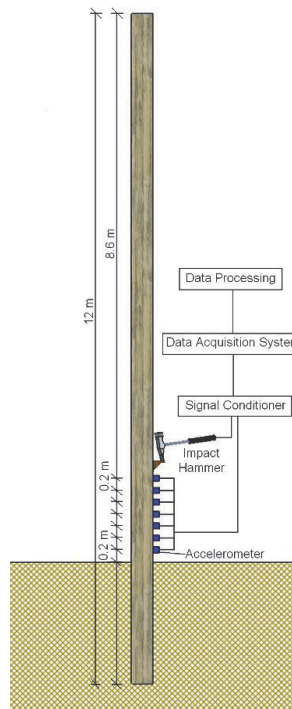


Figure 5.54 Acceleration results for an intact and damaged timber pole under free-free condition for sensor 4

## 5.7 CONTROLLED FIELD TESTS

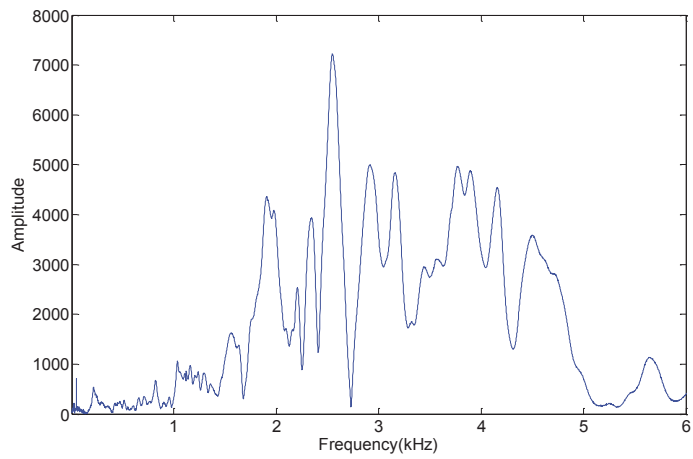
There are 15 intact timber poles installed at Mason Park in NSW by Austgrid, the industry partner of this project. SE/IR, BW and Ultraseismic tests were carried out on these poles embedded 1m to 2m into soil and the results are presented for each method. Figure 5.55 denotes the set-up and location of sensors for the embedded testing.



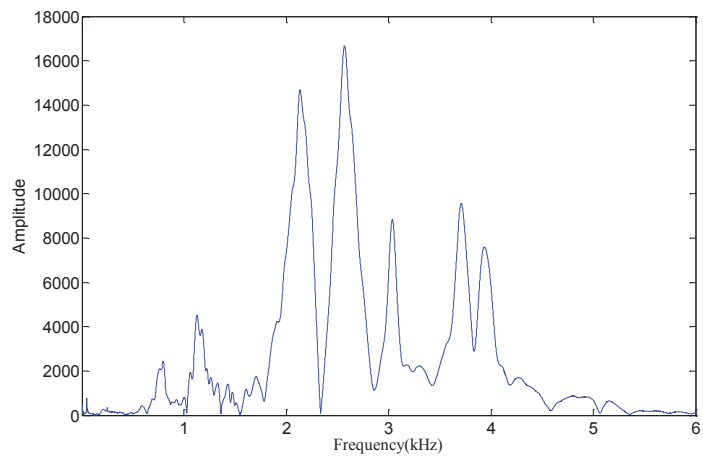
*Figure 5.55 Test set-up of embedded testing in Mason Park*

### 5.7.1 Sonic Echo/Impulse response test at the middle

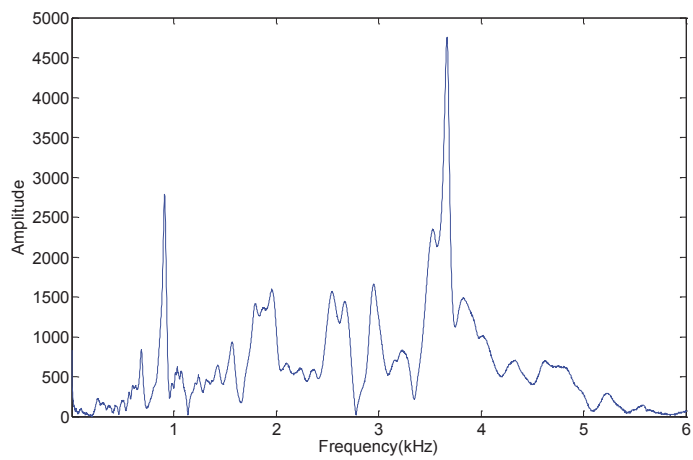
The SE tests were carried out on different poles and the FFT results of a pole with 1, 1.5 and 2m embedment is displayed in Figures 5.56 to 5.58 respectively. Based on these figures the signals were filtered with low pass band filter to filter frequencies above 5kHz for 1 and 1.5m embedded lengths and 4kHz for 2m embedded length. The first rising peak time for first five consecutive sensors for SE tests of a 12m timber pole with 1, 1.5 and 2m embedded lengths is presented as an example of velocity estimation in Figures 5.59 to 5.61, respectively. As can be observed, the coefficient of determination ( $R^2$ ) is around 0.97 and 1 for 1m and 2m embedded conditions. However, this value is 0.91 for timber pole with 1.5 m embedded condition.



*Figure 5.56 FFT result of the timber pole with 1 m of embedment*



*Figure 5.57 FFT result of the timber pole with 1.5 m of embedment*



*Figure 5.58 FFT result of the timber pole with 2 m of embedment*



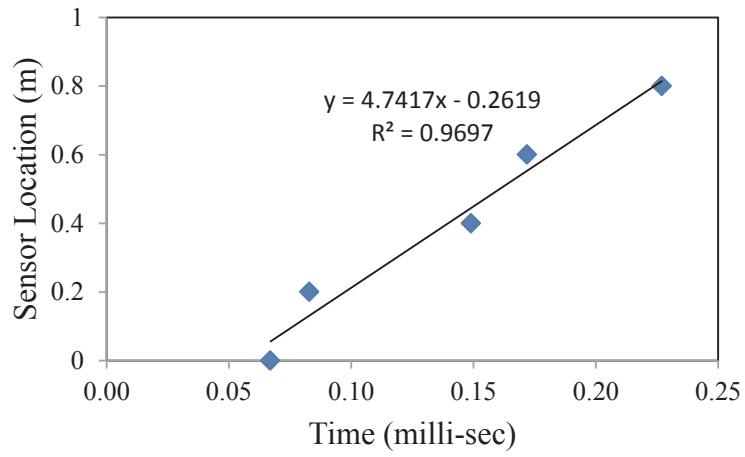


Figure 5.59 Velocity calculation of pole 8 with 1m embedded length

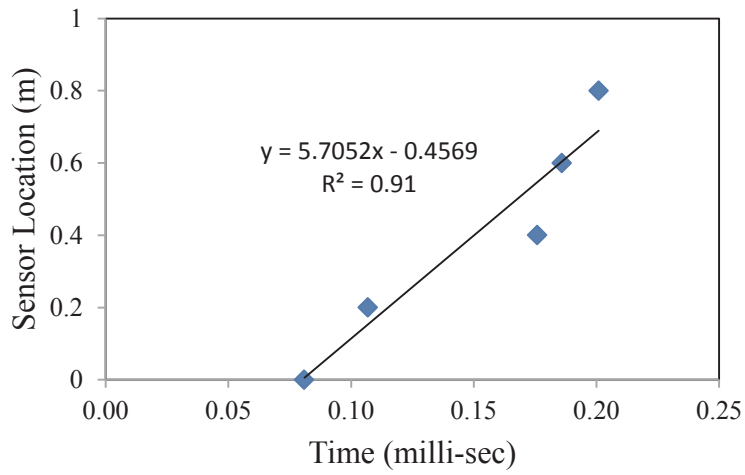


Figure 5.60 Velocity calculation of pole 14 with 1.5m embedded length

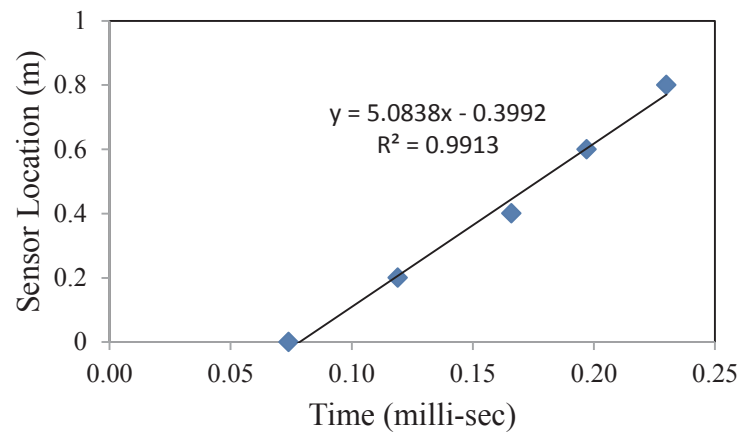
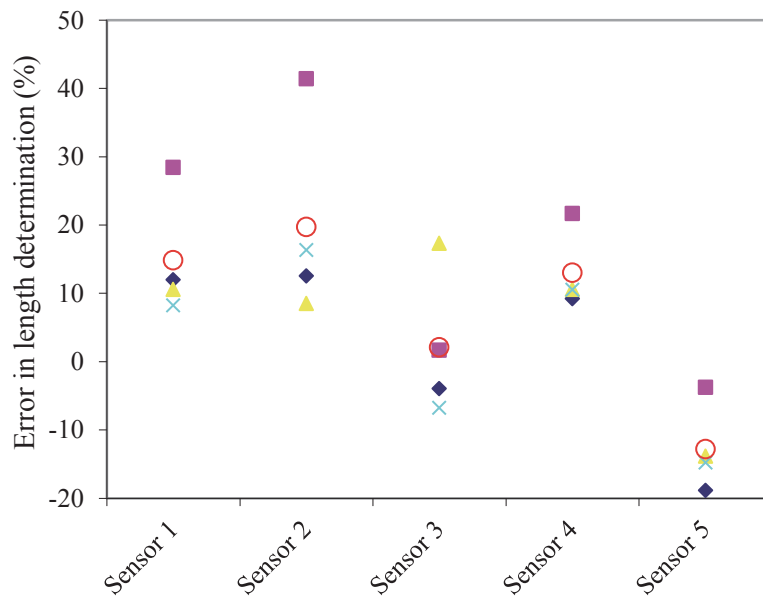


Figure 5.61 Velocity calculation of pole 1 with 2m embedded length

The percentage of error in length determination for pole 8 with 1 m embedment is presented (with 5 sensors located on the side of the pole) in Figure 5.62. As can be seen, using sensors 1, 2, 3, 4 and 5 can result in less than 20% error in length determination. Figure 5.63 and Figure 5.64 present the same graph for percentage of error for length determination of embedment lengths of 1.5m and 2m, respectively. According to Figure 5.63, the percentage of error for length determination remains less than 5% using the first 3 sensors which were located closer to the impact location within 0.6 m. By using the other two sensors located far from the impact location, the error averaged between 7 and 15%. However, as shown in Figure 5.64, the percentage of error will be less than 9% using all five sensors mounted on a pole.



*Figure 5.62 Percentage errors for different sensors estimating the length of the timber pole for 1 m embedment*

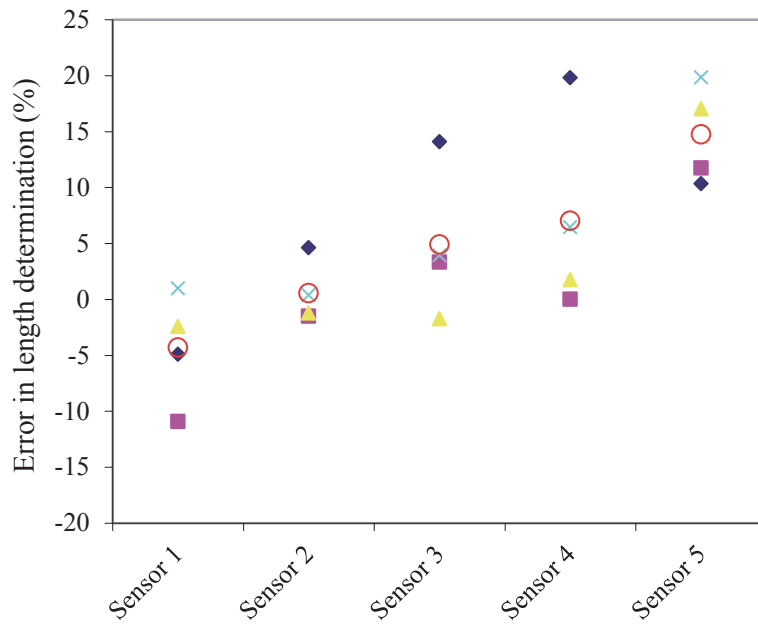


Figure 5.63 Percentage errors for different sensors estimating the length of the timber pole for 1.5 m embedment

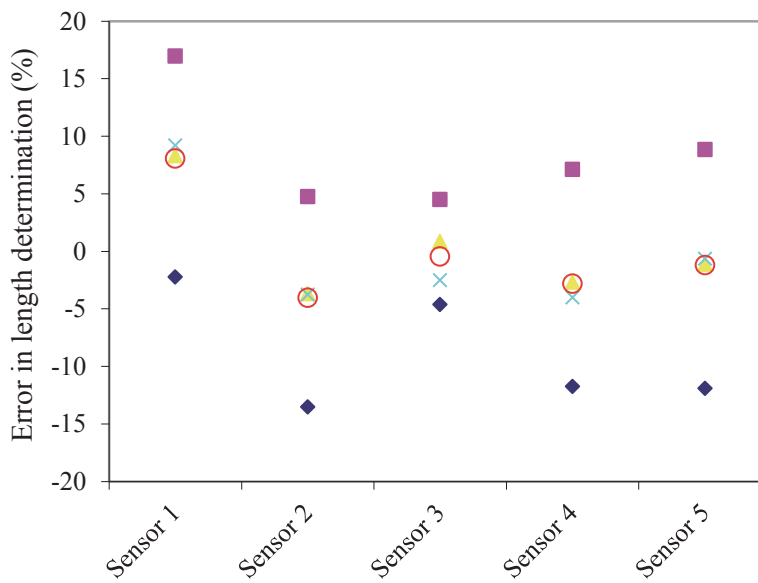
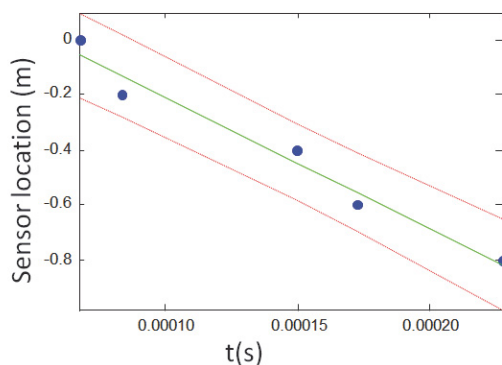
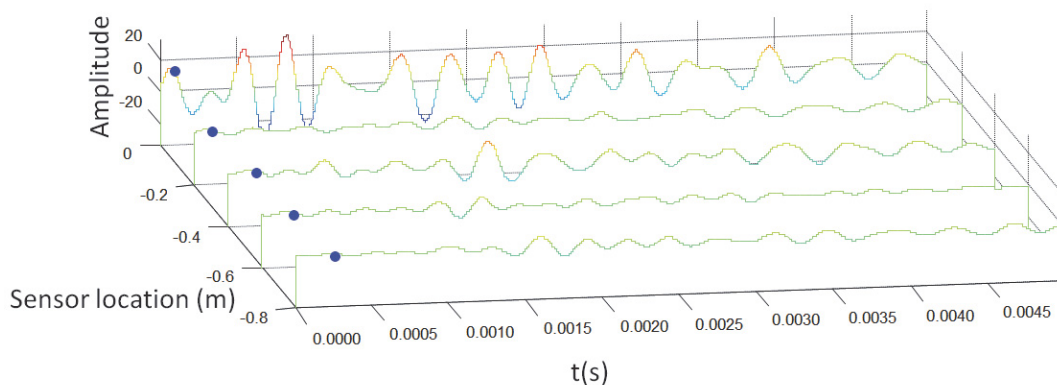


Figure 5.64 Percentage errors for different sensors estimating the length of the timber pole for 2 m embedment

### **5.7.2 Ultraseismic test at the middle**

The results of acceleration-time history for arriving and reflection waves using Ultraseismic method on timber poles in Mason Park are displayed in Figure 5.65 with 1m embedment length. As can be seen the stress wave is calculated with the coefficient of determination of 0.97 for arrival signal and 0.9 for reflecting signal. However, based on the stress velocity value, the arrival signal has a longitudinal mode and mode of the signal will change for the reflection wave to become approximately a flexural wave. These clearly show that the signal has a different mode which requires separation before velocity calculation. Results of the acceleration-time history for timber pole with 1.5m and 2m embedment are presented in Figure 5.66 and Figure 5.67. According to Figure 5.66, the coefficient of determination for longitudinal wave is 0.91 for the arrival wave and 0.86 for the flexural wave as a reflection wave. However, the timber pole with 2m embedded length shows a better correlation for velocity calculation using arrival longitudinal and reflection flexural wave with coefficient of determination of 0.97 and 0.9, respectively as illustrated in Figure 5.67.

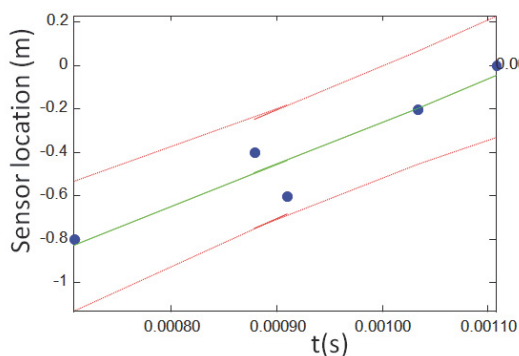
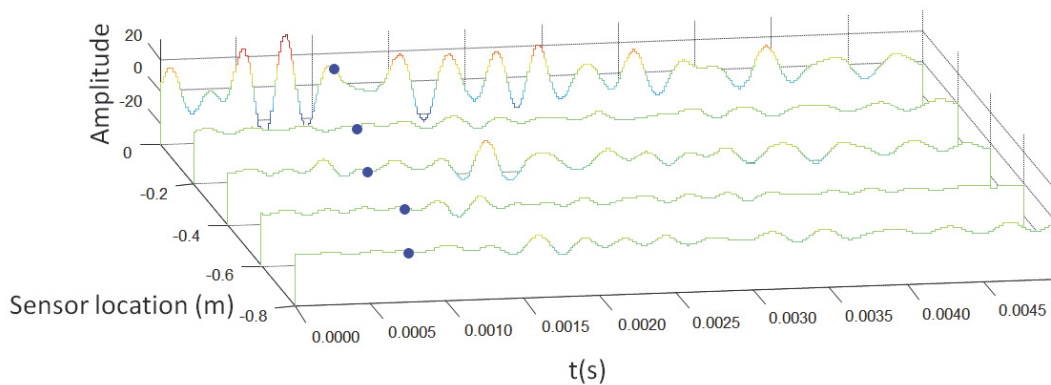


summary

Peaks 1 slope=-4741

$R^2=0.97$

Low-Pass Filter, Fpass=5000



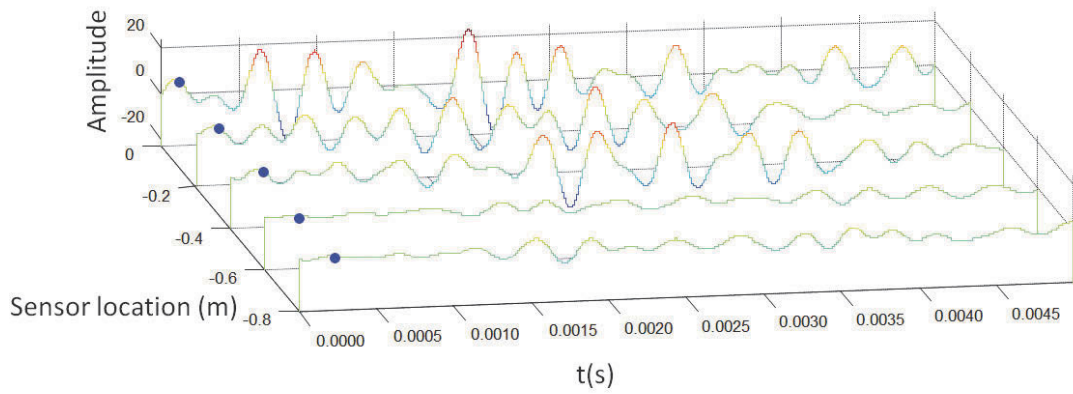
summary

Peaks 2 slope=1960

$R^2=0.90$

Low-Pass Filter, Fpass=5000

Figure 5.65 Acceleration results for all sensors in y direction under 1m embedment using Ultraseismic method (Pole 8)

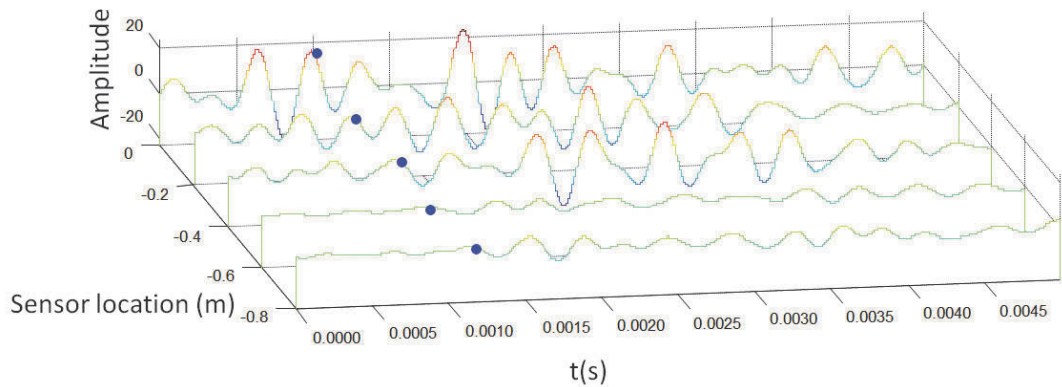
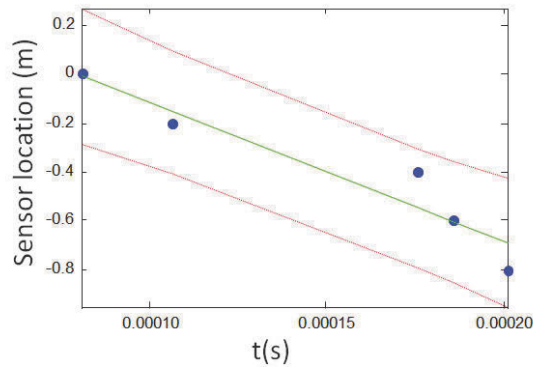


summary

Peaks 1 slope=-5705

$R^2=0.91$

Low-Pass Filter,  $F_{pass}=4000$



summary

Peaks 2 slope=-4671

$R^2=0.86$

Low-Pass Filter,  $F_{pass}=4000$

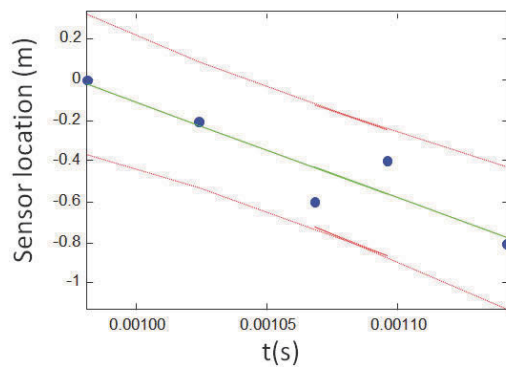
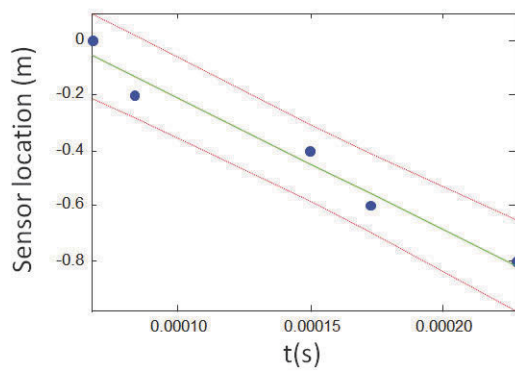
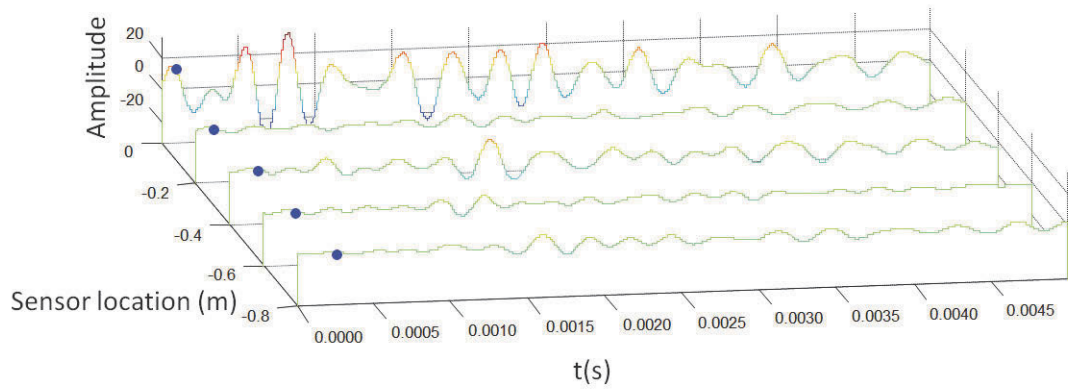
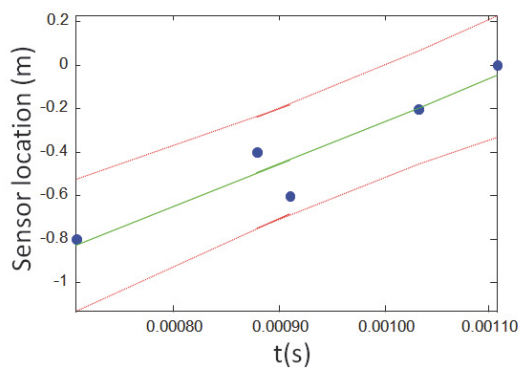
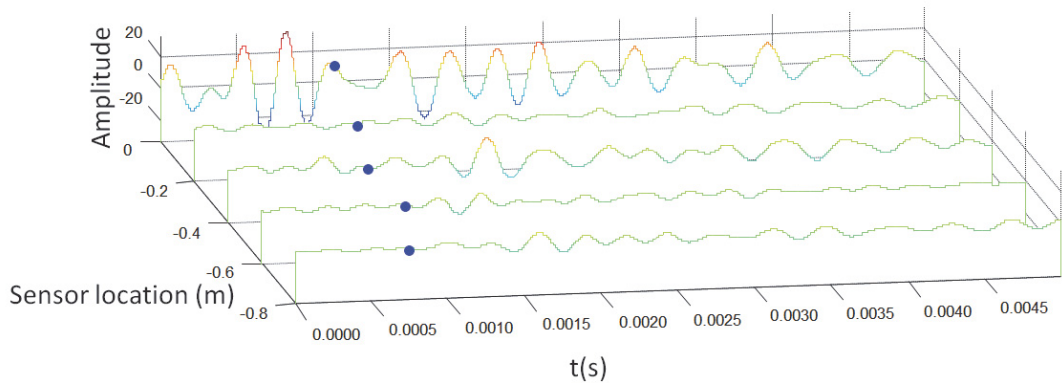


Figure 5.66 Acceleration results for all sensors in y direction under 1.5m embedment using Ultraseismic method (Pole 14)



summary  
 Peaks 1 slope=-4741  
 $R^2=0.97$   
 Low-Pass Filter, Fpass=5000



summary  
 Peaks 2 slope=1950  
 $R^2=0.90$   
 Low-Pass Filter, Fpass=5000

Figure 5.67 Acceleration results for all sensors in y direction under 1.5m embedment using Ultraseismic method (Pole 1)

Figure 5.68 gives percentage of error for length determination of timber pole in the field with different embedment lengths using stress wave velocity from the last section. As summarized in this figure, the percentage of average error for length determination varies from 70% for 1 m embedded length to 47% for timber pole with 2m embedment length. As explained earlier, the modes separation method should apply to the acceleration results for velocity and length determination.

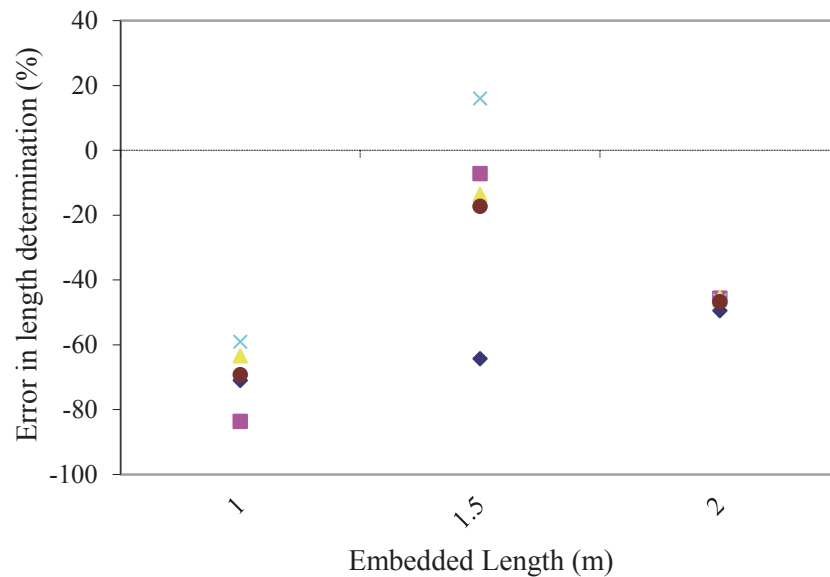


Figure 5.68 Percentage errors for different embedment conditions estimating the length of the timber pole using ultraseismic method

## 5.8 FIELD TESTS OF DECOMMISSIONED UTILITY POLES

For the testing of in-service and out-of-service timber beams and poles, different test configurations were used. For out-of-service structures, a free-free test also conducted. In free-free testing, the specimen is simply supported by two beams as shown in Figure 5.69 . The number and positions of the sensors and impact hammer is displayed in this figure. Two different types of test were carried out on the free-free condition, one by impact at the top and the other one by impact from the middle.



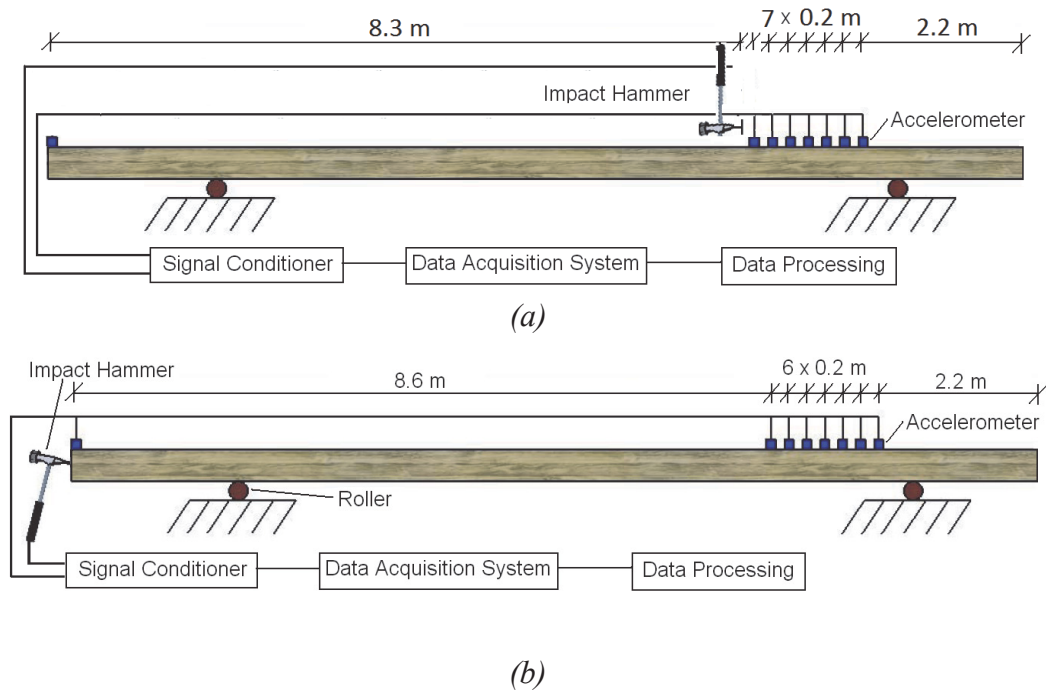


Figure 5.69 Test set-up for free-free testing of field testing in Horsham, (a) impact from the side, (b) impact from the end

### 5.8.1 Sonic Echo (SE) test impact at top

Four poles were selected for analysis of sonic echo test. One pole with a relatively good condition (pole 293) and the others with different damage scenarios (poles 183, 288 and 295). Table 5.5 summarises the location and severity of damage for each pole. The FFT results of the pole 293 is presented in Figure 5.70 for free-free condition impact at the top. As can be seen in Figure 5.70, the dominant frequencies are repeated with equal distance between them for pole 293 which is in relatively in a good condition. However, there is no such repeated pattern for FFT of the damaged poles as shown in Figure 5.71. Indeed, the irregular pattern of FFT may be one an indication of existing damaged in poles and could be used for damage identification after future investigation and verification.

Table 5.5 Timber pole classifications based on the existing defects at Horsham

| Pole No. | Location of defects   | Severity of damage |
|----------|---|--------------------|
| 183      | Severe termite damage 1 m below the ground level. Severe termite damage 6 m above the ground level    | **                 |
| 288      | Severe termite damage 1.5 m below the ground level, Severe termite damage 10 m above the ground level | ***                |
| 293      | Minor termite damage 1 m below the ground level, Minor termite damage 1m above the ground level       | *                  |
| 299      | Minor termite damage 0.5 m below the ground level, Severe termite damage 10 m above the ground level  | ***                |

\* Minor termite attack

\*\* Severe termite attack in some parts above the ground

\*\*\* Severe termite attack in most parts (below and above the ground)

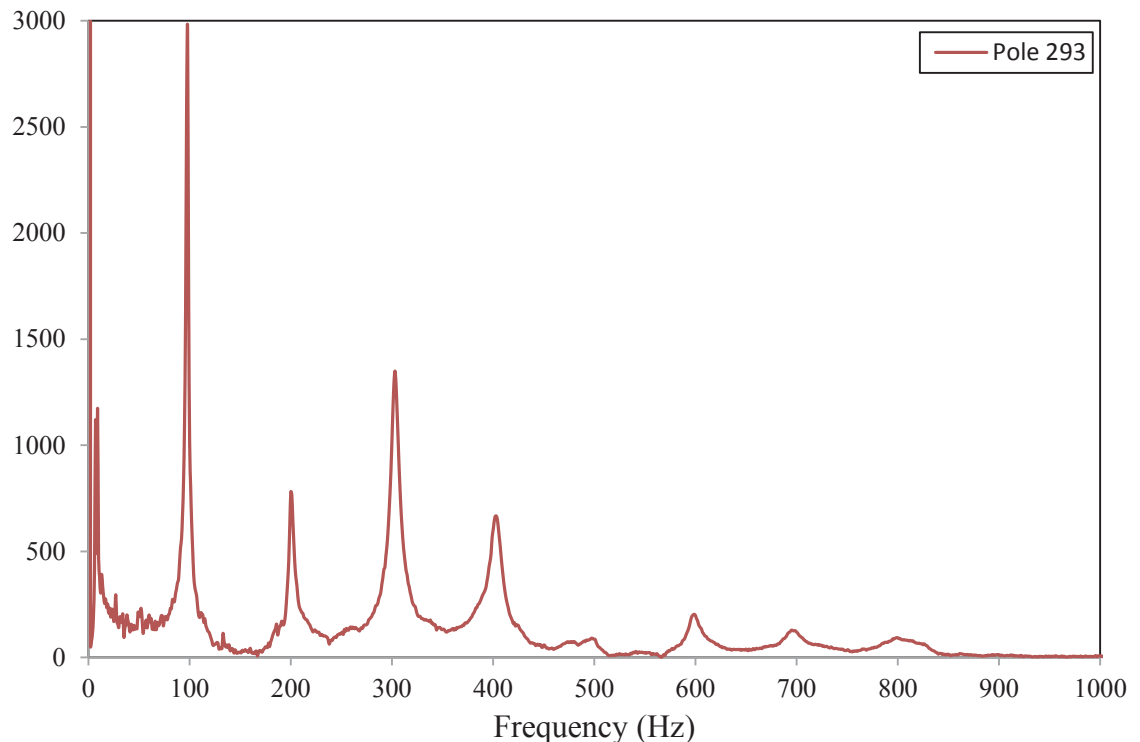


Figure 5.70 FFT result of the timber pole under free-free condition (Pole3-293) impact from location 3(at the top)

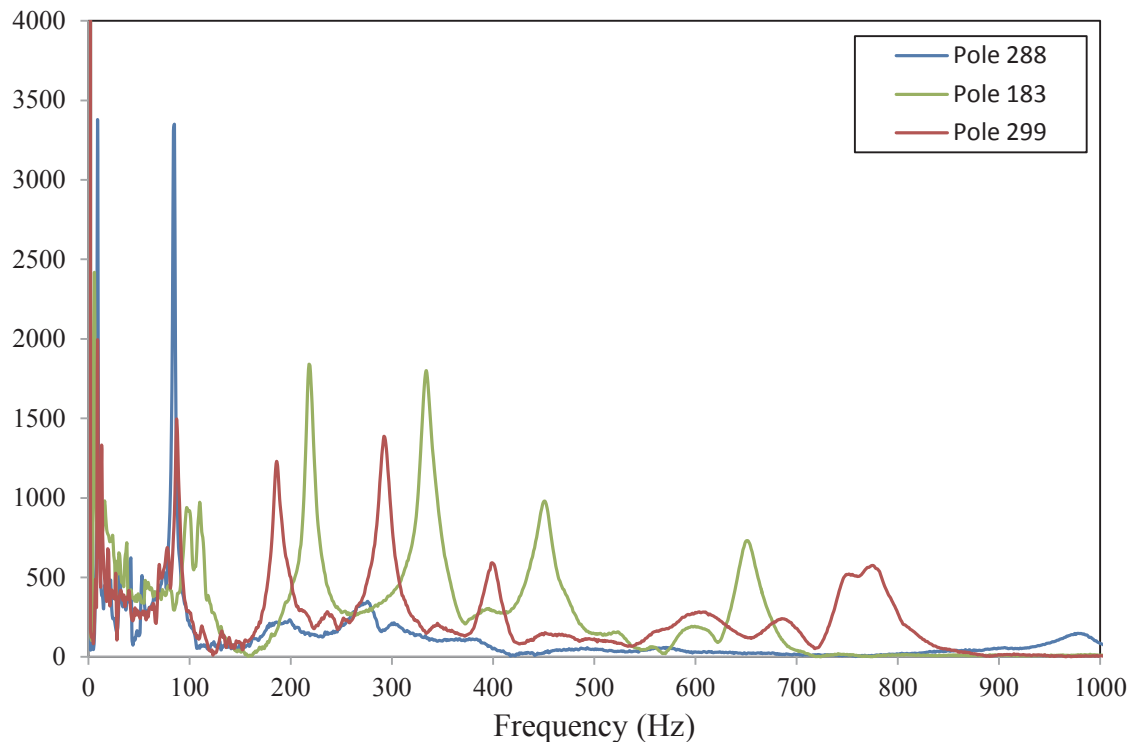


Figure 5.71 FFT result of the damaged timber poles under free-free condition (Pole288, 183 and 299) impact from location 3(at the top)

Figure 5.72 and Figure 5.73 show the acceleration-time history of poles 293 and 288, respectively. As can be seen, for a relatively good pole, the stress wave good be traced easily considering acceleration-time history result as shown in Figure 5.72. However, there is delay for refecton peaks for sensors 2 and 4 of the damaged pole and signal pattern could not be traced by sensor location as there is lag/delay for rising reflection peaks of some sensors.

### 5.8.2 Sonic Echo/Impulse Response test impact at the middle

The FFT results of pole 293 and 288 are presented in Figure 5.74 and Figure 5.75, respectively, for free-free condition impact at the middle. As mentioned before, the analysis of impact from the middle is more complicated than impact at the top as there are more uncertainties involved in stress wave generation in timber. Firstly, multiple waves are generated, one travels down and up and the other wave traveling up and down. Secondly, these waves have different modes and these modes are generated as longitudinal, bending and surface waves at the same time. Thirdly, the bending waves do contribute to the longitudinal direction. Finally, the stress wave velocity will change

inside the soil. Combination of all factors makes the analysis of the waves more complicated.

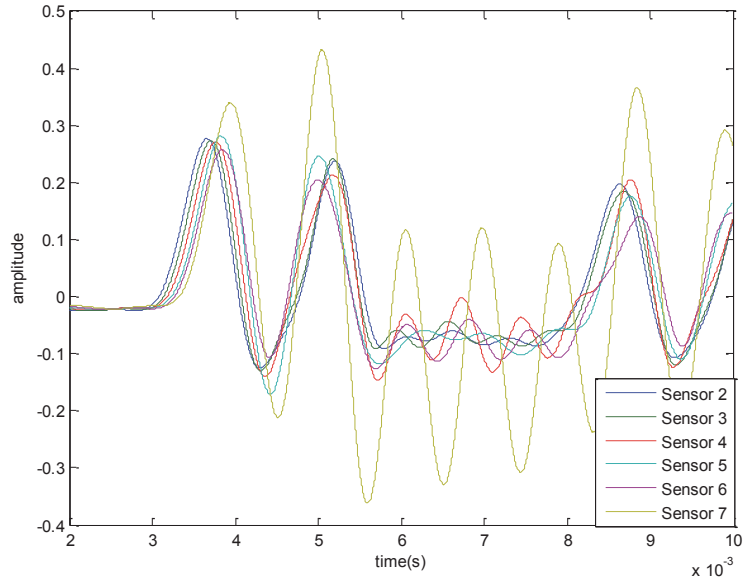


Figure 5.72 Acceleration-time history of timber pole under free-free condition (Pole293) impact from location 3(at the top)

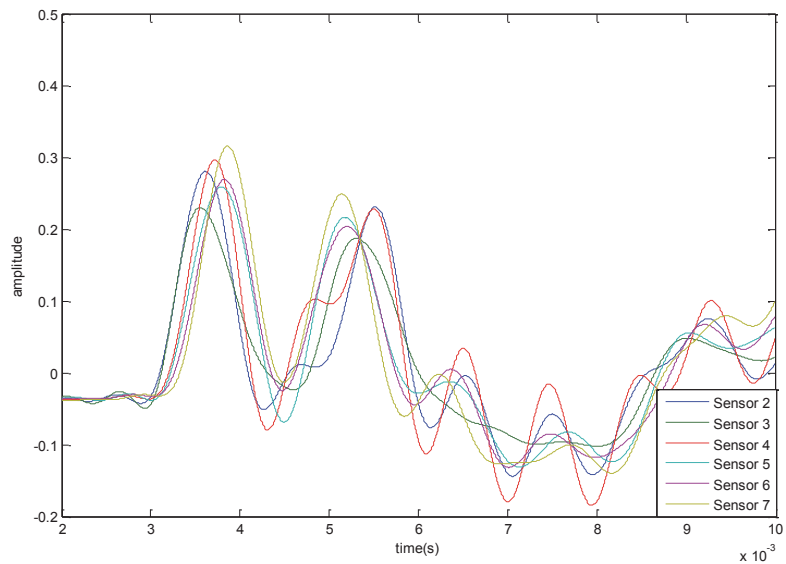
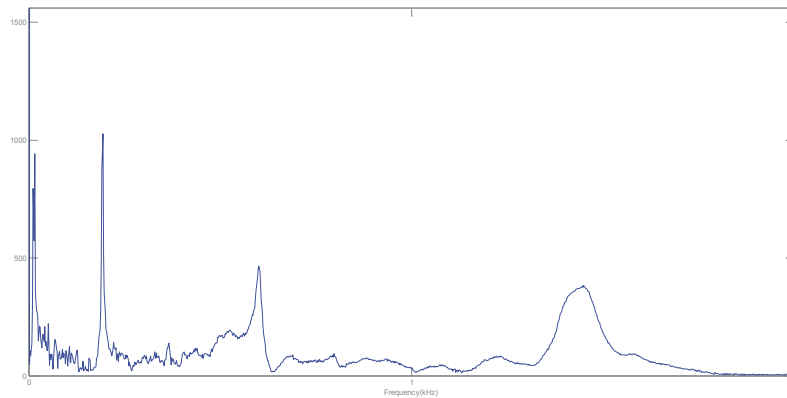
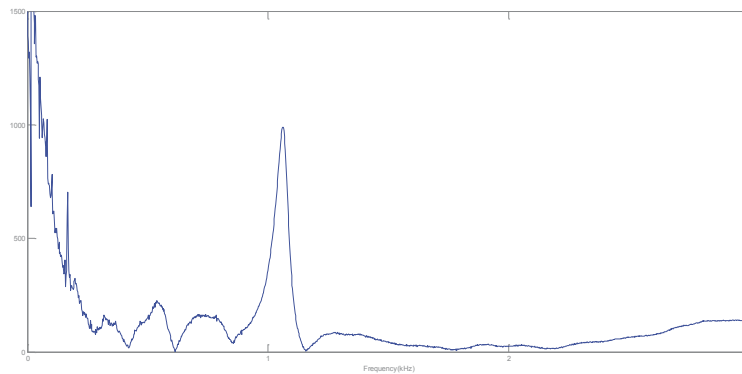


Figure 5.73 Acceleration-time history of timber pole under free-free condition (Pole288) impact from location 3(at the top)



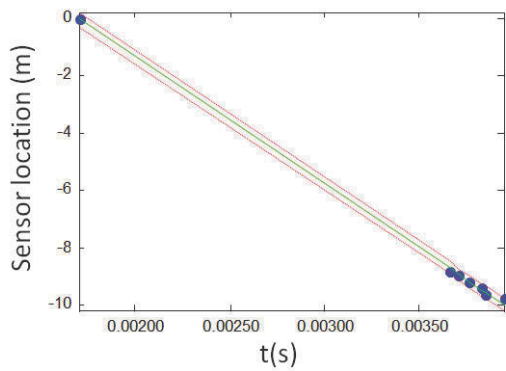
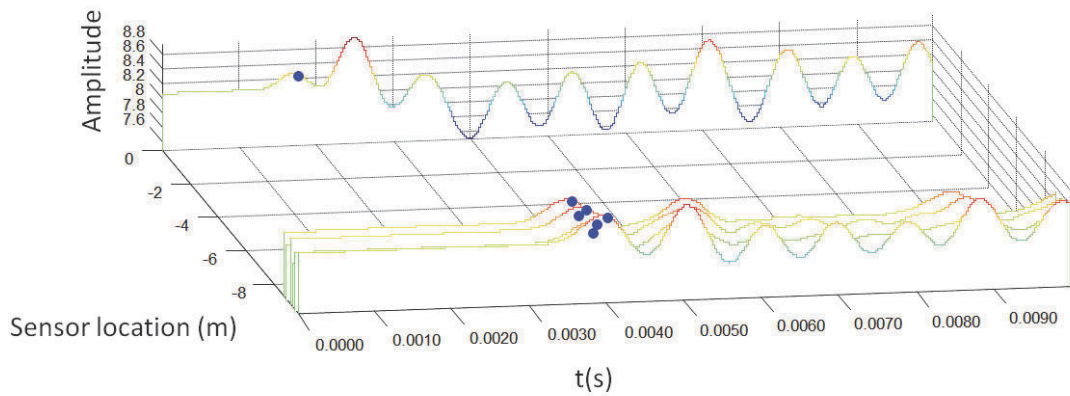
*Figure 5.74 FFT result of the timber pole under free-free condition (Pole293) impact from location 1 (at the middle)*



*Figure 5.75 FFT result of the timber pole under free-free condition (Pole 288) impact from location 1 (at the middle)*

### **5.8.3 Ultraseismic test impact at the top**

Figure 5.76 and Figure 5.77 show the acceleration-time history results for pole 293 and 288 using Ultraseismic method impact at the top under free-free condition. According to Figure 5.76, the coefficient of determination for stress wave velocity is close to 1 for arrival and reflection waves and based on the result of the velocity, longitudinal wave is generated in the pole. As illustrated in Figure 5.77, the coefficient of determination of velocity calculation is around 1 for arriving wave and 0.99 for reflection wave. As a result, the SE test from the top was unable to detect the terminate damage scenario in this specific case and it should be used in conjunction with other testing methods.

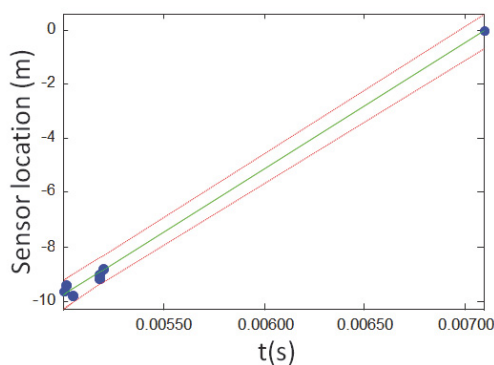
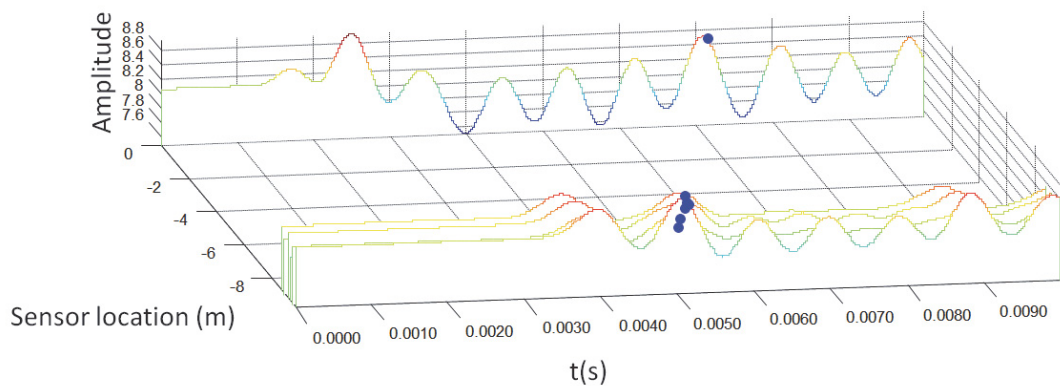


summary

Peaks 1 slope=-4436

$R^2=0.99$

Low-Pass Filter, Fpass=1500



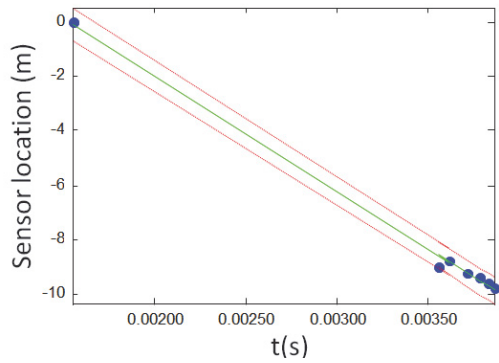
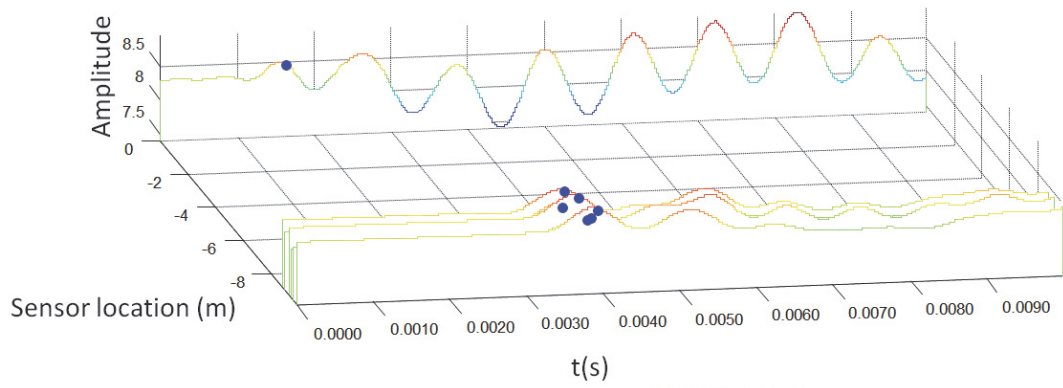
summary

Peaks 2 slope=4664

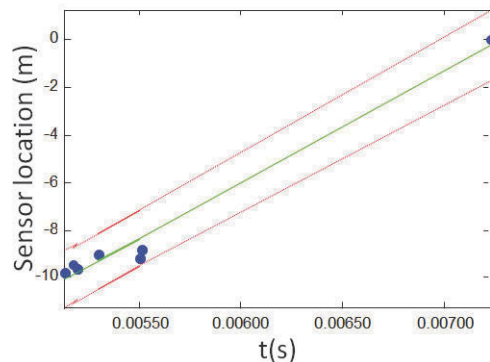
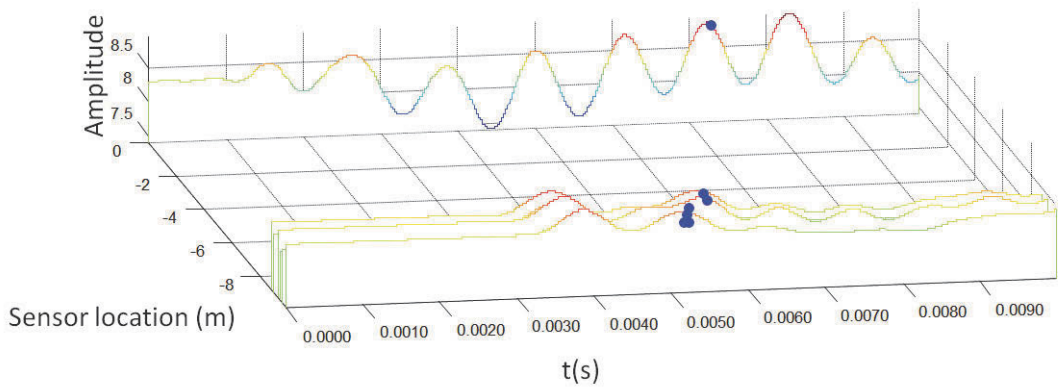
$R^2=0.99$

Low-Pass Filter, Fpass=1500

Figure 5.76 Results of the timber pole under free-free condition using Ultraseismic method (Pole293) impact from location 3(at the top)



summary  
 Peaks 1 slope=-4238  
 $R^2=0.99$   
 Low-Pass Filter, Fpass=1500



summary  
 Peaks 2 slope=4719  
 $R^2=0.98$   
 Low-Pass Filter, Fpass=1500

Figure 5.77 Results of the timber pole under free-free condition using Ultraseismic method (Pole288) impact from location 3(at the top)

## 5.9 SUMMARY

The Sonic Echo, Impulse Response, Bending Wave and Ultraseismic methods have been investigated for determining the stress wave velocity and embedded length of poles with different testing conditions in the structural laboratories at UTS and in field at Mason Park (NSW) and Horsham (Victoria).

A series of laboratory tests have been conducted on a 5m steel beam as a benchmark, a 5m timber rectangular beam and a 5 m timber pole sectioned from a field pole in service. Based on the experimental investigations, it is found that SE/IR methods can be used for the determination of embedment depths with reasonable accuracy, especially if the impact can be imparted from one end of the testing specimens. Multi sensors were used for velocity calculation to increase the accuracy and decrease the uncertainties involved in this calculation. A linear trend line was used for velocity estimation considering all seven sensors mounted on each specimen. The coefficients of determination and variation were obtained for each test to check the accuracy of velocity determination. Based on the results, the coefficient of determination was close to 1 for steel and timber beam under free-free condition and 0.95 for timber pole. The coefficient of determination is varied between 2.4% to 8.6% for the steel beam, 1.4% to 4.7% for the timber beam and 1.6% to 22.7% for the timber pole. According to the results, the coefficient of variation of the velocity estimation of timber pole is relatively higher than the steel beam and timber beam. The followings are the possible reasons for the higher coefficient of variation of velocity estimation in timber pole than timber and steel beam:

Firstly, orthotropic material nature of timber pole which results in variation of stress wave velocity based on the direction of axis correlated with three moduli of elasticity on different axes. Secondly, Stresses perpendicular to the fibre (grain) direction may be at any angle from  $0^\circ$  (T direction) to  $90^\circ$  (R direction). Perpendicular-to-grain properties depend somewhat upon orientation of annual rings with respect to the direction of stress. Depending on the location of a sensor to other sensors in regards to the annual growth ring orientation, different stress wave velocities could be captured as a result of different timber properties in each ring. Thirdly, in some wood product applications, the directions of important stresses may not coincide with the natural axes of fibre orientation in the wood (Kretschmann 2010). (Suzuki & Sasaki 1990) and (Bucur &



Feeney 1992) that concluded the Ultrasonic properties, such as ultrasonic velocity and elastic stiffness constant are greatly affected by the grain directions and grain angles. Finally, the existence of any type of imperfection in timber such as knots or any other defects/damages will affect the stress wave velocity and different stress wave velocities will be captured based on the location of sensors.

Next, by using the longitudinal wave velocity the error in length estimation of each specimen was calculated. Choosing the reflection peak is one of the main elements of these methods and this could be affected by geotechnical conditions. Based on literature review, the stress wave velocity will decrease inside the soil. As a result, the velocity above and below the soil is different and a reduction factor is required to apply to stress wave velocity above the soil to obtain the stress wave velocity below the soil. This reduction factor varies depending on different testing/boundary conditions as well as the soil depth. Also, as mentioned in literature, stress wave propagation could change the phase based on the characteristic impedance of each medium. However, based on the results, no phase change was observed in wave reflection from the bottom of a timber pole.

The relative errors in estimation of a 5m timber beam length for different testing conditions ranged between 1% to 64% on average, using sensor 1 for calculations. According to the results, the error ranged between 1% and 18% on average for sensors 2, 3 and 4. It is believed that the higher error estimation using sensor 1 compared to sensor 2 is related to the small cross section of the timber specimen which does not allow the longitudinal wave to be captured from sensors close to the impact location. Beyond of that, the average error will be relatively similar using sensors 2, 3 and 4.

The scatter of the average error for length determination of pole specimen associated with different test conditions ranged between 1% and 20% for all cases except layer 6 with 26%. The average error is smaller for soil layers between 5 to 8 layers and it could be related to the circular shape of the timber pole, compared to the hollow section of steel beam and relatively small rectangular section of timber beam which allows the longitudinal wave to be generated and captured by the sensor close to the impact location. By using sensor 2 for estimation of the length, the average error became less than 9% for all cases except for the layer 7 with 32%. However, more uncertainties are

involved in terms of length calculation using sensors 3 and 4, located 1.5m and 2m from the impact location, in comparison with using sensor 1 and 2 for calculations.

In bending wave method, Firstly, the frequency components of recorded signals of 5 m timber pole from each sensor using measured frequency response functions (FRF) were determined. Secondly, From the FRF data of different sensors, central frequencies of the signals were identified. The identification of a stable and consistent frequency is crucial for the subsequent SKM data processing. Next, for the identified central frequency, the SKM kernel was formed for each sensor signal. After performing the SKM, the first significant positive or negative amplitude peaks, representing the frequency's arrival at the first transducer, were chosen. Whether positive or negative peaks are chosen is dependent upon which possesses the algebraically-largest value. Then, the location of this peak after its arrival at the second sensor location was determined. Finally, the difference in time between these two peaks was determined in order to compute a wave speed for the frequency.

The wave velocity was calculated for each kernel frequency under different pull out testing conditions. These results were compared to analytical results from (Subhani, Li & Samali) assuming timber as an orthotropic material and using sensor 1 as a reference and sensors 2 to 4 as a second sensor for velocity calculations. Also based on the results, the kernel frequency between 400-800 Hz was identified and used in SKM method for phase velocity calculations. Using the SKM to estimate the length of the pole with Bending Wave method for a 5m timber pole under different pull out conditions showed the percentage of error for all boundary conditions was between -10.5% and 0%. Furthermore, the percentage of error for embedded length calculation did decrease with increase in kernel frequency. If the kernel frequency above 600Hz is selected, the average error for length estimation becomes less than 5% for most boundary conditions.

Also Ultraseismic method was considered for stress wave velocity estimation of timber pole impact at the top. According to the results, using sensors close to impact location (up to 2-3m) will result in good estimation of the velocity calculation. However, these will not necessarily lead to accurate estimations. Based on using trend line for velocity calculation, some sensor signal might need to be eliminated for velocity calculation as there showed more variation compared to the rests of sensors. It is believed that those

variations are related to the uncertainty involved in wave generation in timber material such as anisotropy of timber, location of sensors with regards to annual growth ring orientation and slope of grain and possible existence of imperfections in timber such as knots. According to the results, the average error in length determination for timber pole under different pull out conditions is more relevant to timber pole in-service which was less than 18%.

Analysis of impact at the middle of the pole is more complicated than impact at the top, as more uncertainties are involved in stress wave generation in timber in this case. Firstly, multiple waves are generated, one travels down and up and the other wave traveling up and down. Secondly, these waves have different modes and these modes generate longitudinal, bending and surface waves at the same time. Thirdly, the bending waves have contribution to the longitudinal direction. Finally, the stress wave velocity will change inside the soil layer. Combination of all factors together makes the analysis of wave more complicated.

Under free-free end condition, and according to the results of Ultraseismic method, and impact at the top in Horsham, the stress wave velocity was calculated with relatively good estimation (coefficient of determination for stress wave velocity was close to 1 for arrival and reflection waves).

By considering relatively good and damaged poles in Horsham, it was found that the severe termite damage can be identified by the irregular pattern of FFT from impacted timber pole. This can be used to classify which timber poles are required to be replaced in the field. However, much more work is required in the future to make this a reliable and useful method. This is considered beyond the scope of the current research.

# CHAPTER 6

## 6 CONCLUSIONS AND RECOMMENDATIONS

### 6.1 SUMMARY

Utility poles are a significant part of our built infrastructure in Australia. According to Nguyen et al. (2004), there are nearly 5 million timber poles being used in the current network for distribution of power and communications in Australia. The utility pole industry in Australia spends approximately 40–50 million annually on maintenance and asset management to avoid failure of utility lines, which is very costly and may cause serious consequences. Each year about 300,000 electricity poles are replaced in the eastern states of Australia, despite the fact that up to 80% of these poles are still in a very good serviceable condition (Nguyen et al. 2004).

Lack of accurate information concerning their past and current condition, such as embedment depth and the degree of deterioration or damage below water level or ground level, makes it very difficult to manage these assets and undertake reliable assessment with respect to safety. Furthermore, the current value of these assets exceeds \$20 billion and as such, it is imperative that they remain in service as long as possible in order to optimise the balance between the costs associated with maintaining public safety and those incurred by premature replacement of these piles and poles.

Surface non-destructive testing (NDT) methods such as Sonic Echo, Bending Waves and Ultraseismic methods have been considered over the past decade to be simple and cost-effective tools for identifying the condition and underground depth of embedded structures, such as timber poles or piles in-service. Despite the wide spread use of these methods, the effectiveness and reliability of the methods on determination of embedded length and evaluation of underground conditions of poles, especially timber poles, are not addressed.

When it comes to field applications, these developed/to be developed NDTs face a significant challenge due to presence of uncertainties such as complex material properties (e.g. timber), environmental conditions, interaction of soil and structure,

defects and deteriorations, as well as coupled nature of unknown length and condition. Moreover, due to the dispersive nature of the stress wave signals, which is related to the types of the wave, many frequency components exist in the measured signals and each frequency component corresponds to an individual velocity.

Sonic echo and Impulse response have been used for many years for different materials and different structures, however, applications to timber poles are rarely seen. Vibration based damage detection is very popular and widely researched these days. But unfortunately, these approaches are not very suitable for the pole condition because of complexity of overhanging electric cables, geotechnical environment and uncertainty of timber material properties. Stress wave based methods are, therefore, much preferred choice for such applications since complexity factors aforementioned, have less impact on the methods. Despite the advantages, propagation of stress waves in a finite media is still very complex in nature. So understanding of the propagation of stress waves in timber poles is essential in development of suitable techniques for underground pole condition and embedment length determination.

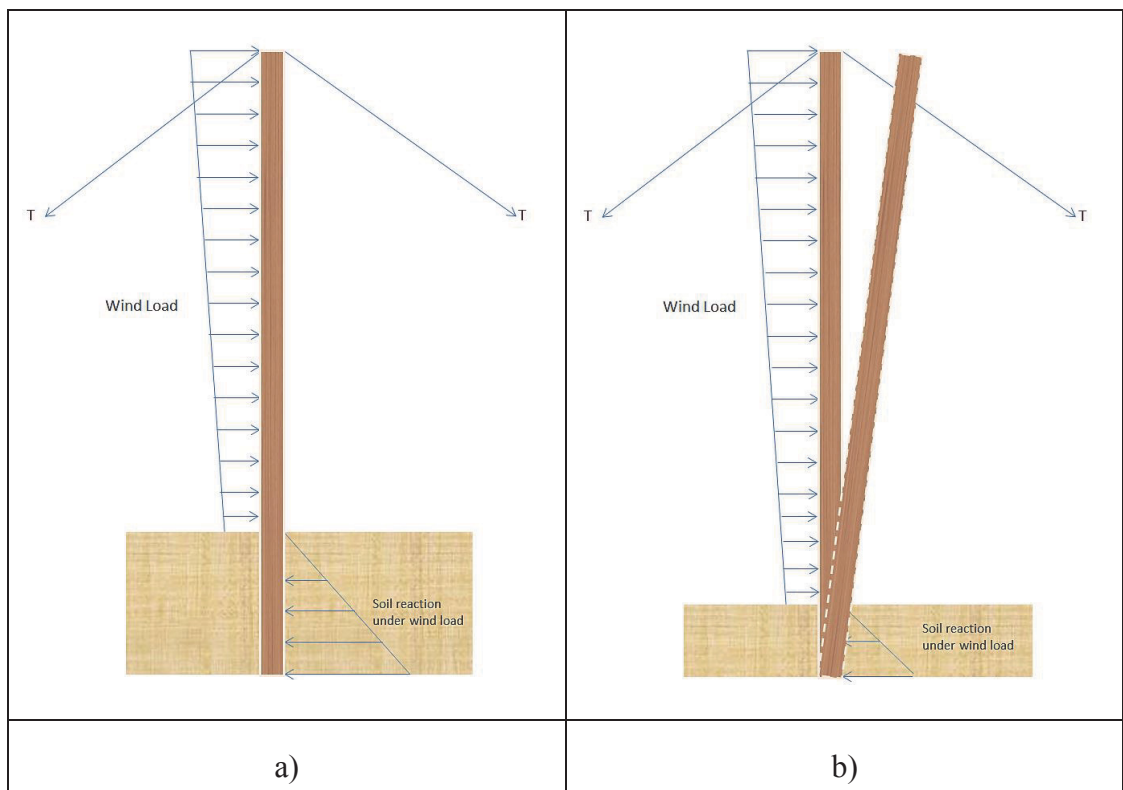
Based on the understanding of wave propagation in a timber pole, advanced signal processing can be utilized for data processing to reveal hidden information that is critical for condition and length determination of poles. Three main groups of signal processing tools are often associated with wave based analysis: time domain analysis, frequency domain analysis (i.e. Fourier transform) and time-frequency analysis, Wavelet Transform (WT).

In order to address this problem and develop reliable methods for determination of embedment length and identification of damage below ground level, an R&D program commenced in 2008 at the University of Technology Sydney in collaboration with the Electricity Network Association of Australia, as an extension of research that has been ongoing since the mid 1990's. The aim of this study was to identify and develop an effective non-destructive evaluation method with acceptable accuracy and reliability, whilst being cost efficient, for determination of the depth of embedment of timber poles and piles. Considering the cost/benefit and inherent complications for applicability in the field, the NDT methods to be considered in this project have been limited to Sonic Echo/Impulse Response, Bending waves and Ultraseismic methods. The work is being

undertaken in three distinct phases encompassing laboratory experiments, Finite Element modelling (FE) and field verification.

## 6.2 CONCLUDING REMARKS

- One of the main findings of this research was the importance of an adequate and healthy embedded length to resist lateral and gravity loads safely. There is no set standards for the embedded length and they can vary between 1.5 and 2 meters. A shorter embedded length is also possible if hard rock is encountered in pole installation process near the ground surface. Figure (a) shows a typical pole and the forces action on it when the embedded length is adequate to transfer all forces to the foundation, while Figure 6.1 (b) illustrates the case of inadequate embedded length leading to a potentially unstable situation



*Figure 6.1 a) Stable case b) Unstable case*

A finite element program, ANSYS (2010), has been used to study the stress wave generation in timber poles. The Sonic Echo/Impulse Response, Bending Wave and Ultraseismic methods were investigated with different boundary conditions to evaluate the reliability and accuracy of the prediction of the stress wave velocity and embedded length determination of timber poles under vertical and horizontal impact loads. Firstly,

the numerical evaluation of a free-end timber pole without embedment was conducted to gain an understanding of the behaviour of stress waves in timber poles in relation to selected NDT methods. Then, the embedded timber poles were modelled to include effects of geotechnical conditions for in-service poles. It should be mentioned that the isotropic material properties were used in FE model to eliminate the effects of anisotropy in the results. Different types of typical decay patterns were simulated for preliminary studies to determine the effect of defect/damage on the Non-Destructive Testing results. The findings of numerical modelling are summarised as follows:

- For the free-end condition, the reflected wave can be identified easily since peaks in velocity graphs are very clear and, therefore, calculation of the embedment length is relatively simple. However, as the velocity will decrease inside the soil, the determination of the length is more complex under embedded conditions as the velocity decrease should be considered for wave travel inside the soil. Considering timber pole as an isotropic material, lead to the maximum error of 8% for length determination under embedded conditions using multi sensors for velocity calculations. Using multi sensors will increase the accuracy of stress wave calculations and indeed, it will decrease the error in length determination.
- As there are no guidelines available to select the kernel frequency, different kernel frequencies were select from FFT and SKM was used to determine the velocity and embedded length. The results were compared with the Bernoulli-Euler Beam theory and Timoshenko beam theory. Based on the results of investigation, the appropriate kernel frequency was recommended to be between 600-800 Hz to be in line with the theoretical equation in order to better estimate the embedded length.
- Based on the results of stress wave velocity calculations using SKM, the distance between two sensors is recommended to be at least 0.5 m as the impact is generating low frequency waves (around 2000 Hz).
- Using the kernel frequency between 650 Hz to 800 Hz will result in less than 8% error in embedded length determination. A range between 650 to 800 Hz is recommended to be used as kernel frequencies.
- Based on the Ultraseismic method, the length of the timber pole could be estimated easily by cross correlating the first arrival and reflection waves. However, the

velocity is different above and below the soil and this should be considered in the length estimation of a pole.

In this research, Sonic Echo, Impulse Response, Bending Wave and Ultraseismic methods have been investigated for determining the stress wave velocity and embedded length of pole with different geotechnical conditions. A series of experimental tests have been conducted on 5m steel beam as a benchmark, 5m timber rectangular beam and 5 m timber pole sectioned from a field pole in service. Based on the experimental investigations, it was found that SE/IR methods can be used for the determination of embedment lengths with reasonable accuracy, especially if the impact can be imparted from one end of the testing specimens. The results of experimental studies of this research can be summarized as follows:

- The coefficient of variation of stress wave velocity is varied between 2.4% to 8.6% for the steel beam, 1.4% to 4.7% for the timber beam and 1.6% to 22.7% for the timber pole. According to the results, the coefficient of variation of the velocity estimation of timber pole is relatively higher than steel beam and timber beam due to anisotropy of timber material, angle of stress to the fibre direction and existence of any type of imperfection in timber such as knots.
- It was confirmed that the stress wave velocity will decrease inside the soil and a reduction factor is required to be applied to stress wave velocity above the soil to obtain the stress wave velocity below the soil. This reduction factor varies depending on the different testing/boundary conditions as well as the soil depth.
- The relative errors in estimation of a 5m timber beam length for different testing conditions ranged between 1% and 64%, on average, using sensor 1 and between 1% and 18%, on average using, sensors 2, 3 and 4 for SE method.
- The scatter of the average error for the timber pole specimen associated with different tests ranged between 1% and 20% for all cases except layer 6 with 26% error. By using sensor 2 for estimation of the length, the average error became less than 9% for all cases except for layer 7 with 32% error. However, more uncertainties are involved in terms of length calculations using sensors 3 and 4 located 1.5m and 2m from the impact location, in comparison with using sensors 1 and 2 for calculations.



- Based on the results, the kernel frequency of between 400-800 Hz was identified to be used in SKM method for phase velocity calculations. Using the SKM to estimate the length of the pole in Bending Wave method for a 5m timber pole under different pull out conditions show the percentage of error for all boundary conditions which is between -10.5% and 0%. Furthermore, the percentage of error for embedded length calculations will decrease with increase in kernel frequency. If a kernel frequency above 600Hz is selected, the average error for length estimation becomes less than 5% for most boundary conditions.
- According to the Ultraseismic method results, using sensors close to impact location (up to 2-3m) will result in good estimation of the velocities. However, these will not necessarily lead to accurate estimations. Based on using trend lines for velocity calculations, some sensors might need to be eliminated for velocity calculations as they show large variations compared to the rests of sensors. It is believed that those variations are related to the uncertainties involved in wave generation in timber materials such as anisotropy of timber, location of sensors with regards to annual growth ring orientation and slope of grain and possible existence of imperfections in timber such as knots.
- According to Ultraseismic methods, the results of impact at the top, lead to average errors in length determination for timber pole under different pull out conditions which is more relevant to timber poles in-service and is less than 18%.
- Analysis of impact from the middle is more complicated than impact at the top as more uncertainties are involved in stress wave generation in timber. Firstly, multiple waves are generated, one travelling down and up and the other wave traveling up and down. Secondly, these waves have different modes and these modes generate longitudinal, bending and surface waves at the same time. Thirdly, the bending waves contribute to the longitudinal direction. Finally, the stress wave velocity will change inside the soil. Combination of all factors makes the analysis of waves more complicated.
- According to the results for Ultraseismic method, impact at the top using under free-free in condition Horsham, the stress wave velocity was calculated with relatively good accuracy.

- By considering the relatively sound and damaged poles in Horsham, it was found that the severe termite damage can be identified by the irregular pattern of FFT from impact of timber pole. This can be used to classify which timber poles are required to be replaced in the field.

### **6.3 RECOMMENDATION OF FUTURE STUDY**

Based on the literature review and the research of this thesis, the following recommendations for future research work in the area of non-destructive testing methods of timber poles are given.

- No effect from structural constraints such as lateral cross-bracing or bent caps in bridge piles were taken into account in any of the computations using the field piles. These effects need to be addressed.
- Using other methods such as Guided Wave theory for orthotropic materials to choose the appropriate input frequency of non-destructive testing methods.
- Using other methods such as Guided Wave theory for orthotropic materials to investigate the best sensor arrangement for each method.
- Using numerical and analytical methods to separate different modes for non-destructive testing methods by impact at the middle under embedded testing conditions.
- Parametric study of different uncertainties involved in timber material and boundary conditions to provide a range of errors for each factor.
- Conducting characteristic in-situ testing of timber pole materials.
- Conducting further field tests to prepare a large database to use other methods such as machine learning to identify the damage signature of timber poles.
- Further study on simulation of different forms of decay in timber poles
- Further study on temperature change in determining the condition of timber poles.

## References

- Abramson, H.N. 1956, 'The propagation of flexural elastic waves in solid circular cylinders', University of Texas at Austin.
- Al-Mousawi, M. 1986, 'On experimental studies of longitudinal and flexural wave propagations: an annotated bibliography', *Applied Mechanics Reviews*, vol. 39, p. 853.
- ANSYS Inc 2011, *ANSYS*, release 11.0.
- Anthony & Philips 1989, 'Nondestructive Strength Assessment of In Situ Timber Piles', paper presented to the *First International conference on Wood Poles and Piles*.
- Armstrong, J.P., Patterson, D.W. & Sneckenberger, J.E. 1991, 'Comparison of three equations for predicting stress wave velocity as a function of grain angle', *Wood and Fiber Science*, vol. 23, no. 1, pp. 32-43.
- AS1289.5.1.1. 2003, 'Determination of the dry density/moisture content relation of a soil using standard compactive effort'.
- Bancroft, D. 1941, 'The velocity of longitudinal waves in cylindrical bars', *Physical Review*, vol. 59, no. 7, p. 588.
- Bendat, J.S. & Piersol, A.G. 1980, 'Engineering applications of correlation and spectral analysis', *New York, Wiley-Interscience, 1980. 315 p.*, vol. 1.
- Bucur, V. & Feeney, F. 1992, 'Attenuation of ultrasound in solid wood', *Ultrasonics*, vol. 30, no. 2, pp. 76-81.
- Chao, H.C. 2002, 'Experimental Model for Pile Integrity Evaluation using Guided Wave Approach', Northwestern University.
- Chen, S. & Kim, Y.R. 1996, 'Condition assessment of installed timber piles by dispersive wave propagation', pp. 112-20,  
<<http://www.scopus.com/inward/record.url?eid=2-s2.0-0030284436&partnerID=40&md5=9b56cb7d8a212f8c28af3ba2a4d722df>>.
- Chiang, C.-H., Cheng, C.-C. & Liu, T.-C. 2004, 'Improving signal processing of the impact-echo method using continuous wavelet transform', *Proceedings of the 16th world conference on NDT (WCNDT 2004), Montreal, Canada*, Citeseer.
- Chow, Y., Phoon, K., Chow, W. & Wong, K. 2003, 'Low strain integrity testing of piles: three-dimensional effects', *Journal of geotechnical and geoenvironmental engineering*, vol. 129, no. 11, pp. 1057-62.
- Chree, C. 1889, 'The Equations of an Isotropic Elastic Solid in Polar and Cylindrical Co-ordinates their Solution and Application', *Transactions of the Cambridge Philosophical Society*, vol. 14, p. 250.
- Crews, K. & Horrigan, A. 2000, 'Strength assessment of timber utility poles in Australia', *New Zealand Timber Design Journal*, vol. 9, no. 2.
- Davies, R. 1948, 'A critical study of the Hopkinson pressure bar', *Philosophical Transactions of the Royal Society of London. Series A. Mathematical and Physical Sciences*, pp. 375-457.

- Davis, A. & Robertson, S. 1975, 'Economic pile testing', *Ground Engineering*, vol. 8, no. 3.
- Davis, A.G. March 1994, 'Non destructive testing of wood piles', *Second international conference on wood poles and piles*, ed. F.C. Co.
- Davis, A.G. & Dunn 1974, 'From Theory to Field Experience with the Non-destructive Vibration Testing of Piles'.
- Emerson, R.N., Pollock, D.G., Kainz, J.A., Fridley, K.J., McLean, D. & Ross, R.J. 1998, 'Nondestructive evaluation techniques for timber bridges', *V World conference on timber engineering. Montreux, Switzerland*, vol. 1, pp. 670-7.
- Falk, R., Patton-Mallory, M. & McDonald, K. 1990, 'Nondestructive testing of wood products and structures: state-of-the-art and research needs', *Nondestructive Testing and Evaluation for Manufacturing and Construction: Proc. Of Conference*, New York: Hemisphere Publishing Corp, pp. 137-47.
- Field, G.S. 1931, 'Velocity of sound in cylindrical rods', *Canadian Journal of Research*, vol. 5, no. 6, pp. 619-24.
- Finno, R., Chao, H. & Lynch, J. 2001, 'Nondestructive Evaluation of In Situ Concrete Piles at the Advanced Waterfront Technology Test Sites, Port Hueneme, California, report for the Naval Facilities Engineering Service Center', *Washington, DC, USA*.
- Finno, R.J. & Gassman, S.L. 1998, 'Impulse response evaluation of drilled shafts', *Journal of geotechnical and geoenvironmental engineering*, vol. 124, no. 10, pp. 965-75.
- Francis, L. & Norton, J. 2006, 'A Review—Australian Timber Pole Resources for Energy Networks', *Department of Primary Industries & Fisheries*.
- Gassman, S.L. & Finno, R.J. 1999, 'Impulse response evaluation of foundations using multiple geophones', *Journal of performance of constructed facilities*, vol. 13, no. 2, pp. 82-9.
- Gassman, S.L. & Finno, R.J. 2000, 'Cutoff frequencies for impulse response tests of existing foundations', *Journal of performance of constructed facilities*, vol. 14, no. 1, pp. 11-21.
- Graff, K.F. 1975, *Wave motion in elastic solids*, Courier Dover Publications.
- Green, D.W., Winandy, J.E. & Kretschmann, D.E. 1999, 'Mechanical properties of wood', *Wood handbook: wood as an engineering material*.
- Hanifah, A.A. 1999, *A theoretical evaluation of guided waves in deep foundations*, Northwestern University.
- Hearne, T.M., Reese, L.C. & Stokoe, K.H. 1981, 'Drilled-shaft integrity by wave propagation method', *Journal of the Geotechnical Engineering Division*, vol. 107, no. 10, pp. 1327-44.
- Hertlein, B. & Davis, A., 'Low-Strain Surface Tests—Sonic Echo', *Nondestructive Testing of Deep Foundations*, pp. 101-13.
- Holt, J. 1996a, 'Comparing the Fourier phase and short kernel methods for finding the overall lengths of installed timber piles', North Carolina State University.

- Holt, J. 1996b, 'Finding the lengths of installed steel-H-piles by dispersive bending wave propagation methods', *Fifth International Conference on the Application of Stress-Wave Theory to Piles*, vol. 11, p. 13.
- Holt, J., Shunyi, C. & Douglas, R. 1994, 'Determining lengths of installed timber piles by dispersive wave propagation', *Transportation research record*, no. 1447, pp. 110-5.
- Hudson, G.E. 1943, 'Dispersion of elastic waves in solid circular cylinders', *Physical Review*, vol. 63, no. 1-2, p. 46.
- Hughes, M.L., Rix, G.J. & Jacobs, L.J. 1998, 'Nondestructive determination of pile tip elevation using modal analysis', *Non-Destructive Evaluation Techniques for Aging Infrastructure & Manufacturing*, International Society for Optics and Photonics, pp. 522-30.
- Kabir, M. 2001, 'Prediction of ultrasonic properties from grain angle', *JOURNAL- INSTITUTE OF WOOD SCIENCE*, vol. 15, no. 5; ISSU 89, pp. 235-46.
- Kasal, B., Lear, G. & Tannert, T. 2011, 'Stress Waves', *In Situ Assessment of Structural Timber*, Springer, pp. 5-24.
- Katzke, E.D. 1997, 'Nondestructive Evaluation of Asphalt Pavement Surface Layers Using Stress Wave Testing', North Carolina State University.
- Kent, H. 2006, *Options for the continued supply of power poles*, Queensland Department of Primary Industries and Fisheries, Presentation for the March 2006 Australian Wood Pole Resources Workshop.
- Kim, D. & Kim, H. 2003, 'Effects of surrounding soil stiffness and shaft length in the impact-echo test of drilled shaft', *KSCE Journal of Civil Engineering*, vol. 7, no. 6, pp. 755-62.
- Kim, Y.R. & Ranjithan, S.R. 2000, *Nondestructive Evaluation of the Structural Condition of Timber Piles. Volumes 1 and 2*.
- Kolsky, H. 1963, *Stress waves in solids*, vol. 1098, Courier Dover Publications.
- Kretschmann, D.E. 2010, *Wood Handbook, Wood as an Engineering Material U.S.* Department of Agriculture, Forest Service, Madison, FPL-GTR-190.
- Liao, S.T. & Roesset, J.M. 1997a, 'Dynamic response of intact piles to impulse loads', *International Journal for Numerical and Analytical Methods in Geomechanics*, vol. 21, no. 4, pp. 255-75.
- Liao, S.T. & Roesset, J.M. 1997b, 'Identification of defects in piles through dynamic testing', *International Journal for Numerical and Analytical Methods in Geomechanics*, vol. 21, no. 4, pp. 277-91.
- Love, A.E.H. 2013, *A treatise on the mathematical theory of elasticity*, Cambridge University Press.
- Lynch, J. 2007a, 'Experimental verification of concrete piles subjected to flexural guided waves', Northwestern University, Evanston, IL, USA.
- Lynch, J.J., Jr. 2007b, 'Experimental verification of flexural guided waves in concrete cylindrical piles', Ph.D. thesis, Northwestern University, Ann Arbor.
- Miklowitz, J. 1966, 'Elastic wave propagation', *Applied Mechanics Surveys*, pp. 809-39.









- Nguyen, M., Foliente, G. & Wang, X.M. 2004, 'State-of-the-Practice & Challenges in Non-Destructive Evaluation of Utility Poles in Service', *Key Engineering Materials*, vol. 270, pp. 1521-8.
- Ni, S.-H., Lehmann, L., Charng, J.-J. & Lo, K.-F. 2006, 'Low-strain integrity testing of drilled piles with high slenderness ratio', *Computers and Geotechnics*, vol. 33, no. 6, pp. 283-93.
- Onoe, M., McNiven, H. & Mindlin, R. 1962, 'Dispersion of axially symmetric waves in elastic rods', *Journal of Applied Mechanics*, vol. 29, p. 729.
- Paikowsky, S.G. & Chernauskas, L.R. 2003, 'Review of Deep Foundations Integrity Testing-Methods And Case Histories', *BSCES-Geo-Institute Deep Foundations Seminar*.
- Peterson, M. 1999, 'Prediction of longitudinal disturbances in a multimode cylindrical waveguide', *Experimental Mechanics*, vol. 39, no. 1, pp. 36-42.
- Puckett, A.D. 2000, *Fidelity of a finite element model for longitudinal wave propagation in thick cylindrical wave guides*, Los Alamos National Lab., NM (US).
- Ramirez, R. 1985, 'The FFT, Fundamentals and Concepts, Tektronix', *Inc., Englewood Cliffs*.
- Randolph, M. 2003, 'Science and empiricism in pile foundation design', *Geotechnique*, vol. 53, no. 10, pp. 847-75.
- Robertson, A.N. & Basu, B. 2008, 'Wavelet analysis', *Encyclopedia of structural health monitoring*.
- Ross, R.J. & Pellerin, R.F. 1994, 'Nondestructive testing for assessing wood members in structures', *USDA. FPL-GTR-70*, pp. 1-40.
- Ross, R.J., Pellerin, R.F., Volny, N., Salsig, W.W. & Falk, R.H. 1999, 'Inspection of timber bridges using stress wave timing nondestructive evaluation tools', *US Department of Agriculture, Forest Service, Forest Products Laboratory, Madison, Report FPL-GTR*, vol. 114.
- Said, I., De Gennaro, V. & Frank, R. 2009, 'Axisymmetric finite element analysis of pile loading tests', *Computers and Geotechnics*, vol. 36, no. 1, pp. 6-19.
- Sansalone, M. & Carino, N.J. 1986, 'Impact-Echo: A method for flaw detection in concrete using transient stress wave'.
- Shear, S.K. & Focke, A.B. 1940, 'The dispersion of supersonic waves in cylindrical rods of polycrystalline silver, nickel, and magnesium', *Physical Review*, vol. 57, no. 6, p. 532.
- Sorohan, Ş., Constantin, N., Găvan, M. & Anghel, V. 2011, 'Extraction of dispersion curves for waves propagating in free complex waveguides by standard finite element codes', *Ultrasonics*, vol. 51, no. 4, pp. 503-15.
- Stockton, B.D. 2003, *Unguyed Distribution Poles – Strength Requirements*, vol. BULLETIN 1724E-150, Department of Agriculture: Rural Utilities Service.
- Subhani, M. 2013, 'Study on behaviour of guided wave propagation in timber utility poles'.

- Subhani, M., Li, J. & Samali, B., 'A comparative study of guided wave propagation in timber poles with isotropic and transversely isotropic material models', *Journal of Civil Structural Health Monitoring*, pp. 1-15.
- Subhani, M., Li, J., Samali, B. & Yan, N. 2013, 'Determination of the embedded lengths of electricity timber poles utilising flexural wave generated from impacts', *Australian Journal of Structural Engineering*, vol. 14, no. 1, p. 85.
- Suzuki, H. & Sasaki, E. 1990, 'Effect of grain angle on the ultrasonic velocity of wood', *Mokuzai Gakkaishi= Journal of the Japan Wood Research Society*, vol. 36, no. 2, pp. 103-7.
- Wang, H., Chang, T.P. & Finno, R.J. 2011, 'An experimental research on three-dimensional waves in a concrete panel', *International Journal of Materials and Product Technology*, vol. 41, no. 1-4, pp. 178-90.
- Wasley, R.J. 1973, *Stress Wave Propagation in Solids: An Introduction*, vol. 7, M. Dekker.
- Zemanek Jr, J. 1972, 'An experimental and theoretical investigation of elastic wave propagation in a cylinder', *The Journal of the Acoustical Society of America*, vol. 51, p. 265.

# **APPENDIX A**

## **TIMBER POLE AUTOPSY**



|          |                  |  |   |   |
|----------|------------------|--|---|---|
| L<br>(m) | Diameter<br>(cm) |  | Cross Section   |   |
|          | L                | R  | Left  | Right   |
| 2        | 170              | 250  |    |    |
| 2        | 250              | 260  |   |   |
| 2        | 260              | 270  |  |  |
| 2        | 270              | 285  |  |  |



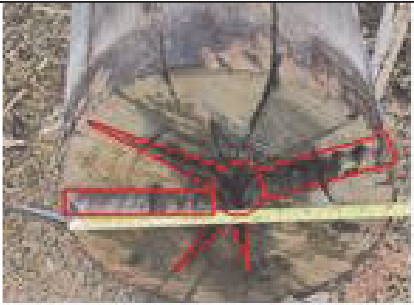


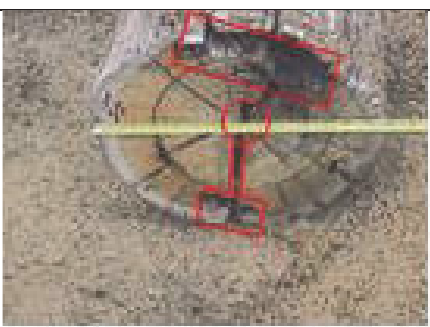










|     |     |     |  |   |
|-----|-----|-----|--|---|
| 2   | 285 | 320 |     |    |
| 0.5 | 320 | 330 |     |    |
| 0.5 | 330 | 350 |   |   |
| 0.5 | 350 | 365 |  |   |
| 0.5 | 365 | 410 |  |  |

Figure A. 1 Cross sections of pole No 288

|          |                  |  |   |   |  |
|----------|------------------|--|---|---|--|
| L<br>(m) | Diameter<br>(cm) |  | Cross Section   |   |  |
|          | L                | R  | Left  | Right   |  |
| 2        | 190              | 225  |    |    |  |
| 2        | 225              | 250  |   |   |  |
| 2        | 250              | 270  |  |  |  |
| 2        | 270              | 280  |  |  |  |




















|     |     |     |   |   |
|-----|-----|-----|---|---|
| 2   | 280 | 300 |    |    |
| 0.5 | 300 | 300 |    |    |
| 0.5 | 300 | 320 |   |   |
| 0.5 | 320 | 360 |  |  |
| 0.5 | 360 | 380 |  |  |

Figure A. 2 Cross sections of pole No 183

|          |                  |  |   |   |
|----------|------------------|--|---|---|
| L<br>(m) | Diameter<br>(cm) |  | Cross Section   |   |
|          | L                | R  | Left  | Right   |
| 2        | 220              | 260  |    |    |
| 2        | 260              | 270  |   |   |
| 2        | 270              | 285  |  |  |
| 2        | 285              | 300  |  |  |

















|     |     |     |   |   |
|-----|-----|-----|---|---|
| 2   | 300 | 310 |    |    |
| 0.5 | 310 | 310 |    |    |
| 0.5 | 310 | 310 |   |   |
| 0.5 | 310 | 360 |  |  |
| 0.5 | 360 | 390 |  |  |

Figure A. 3 Cross sections of pole No 270

|          |                  |  |   |   |
|----------|------------------|--|---|---|
| L<br>(m) | Diameter<br>(cm) |  | Cross Section   |   |
|          | L                | R  | Left  | Right   |
| 2        | 215              | 250  |  |    |
| 2        | 250              | 280  |   |   |
| 2        | 280              | 280  |   |  |
| 2        | 280              | 280  |   |  |











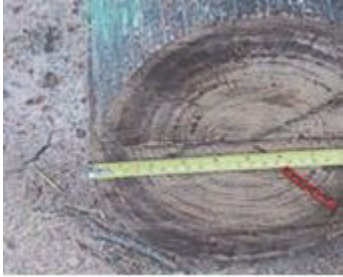

|     |     |     |  |   |
|-----|-----|-----|--|---|
| 2   | 280 | 280 |  |    |
| 0.5 | 300 | 330 |  |    |
| 0.5 | 330 | 340 |  |   |
| 0.5 | 340 | 360 |  |  |
| 0.5 | 360 | 370 |  |  |






Figure A. 4 Cross sections of pole Pole No 293



|          |                  |  |   |       |  |
|----------|------------------|--|---|-------|--|
| L<br>(m) | Diameter<br>(cm) |  | Cross Section   |       |  |
|          | L                | R  | Left  | Right |  |
| 2        | 195              | 235  |    |       |  |
| 2        | 235              | 210  |   |       |  |
| 2        | 210              | 260  |  |       |  |
| 2        | 260              | 240  |  |       |  |
| 2        | 240              | 250  |   |       |  |

|     |     |     |   |  |
|-----|-----|-----|---|--|
| 0.5 | 250 | 260 |  |  |
| 0.5 | 260 | 260 |   |  |
| 0.5 | 260 | 275 |  |  |
| 0.5 | 275 | 275 |   |  |

*Figure A. 5 Cross sections of pole No 295*

|          |                  |  |               |   |  |
|----------|------------------|--|---------------|---|--|
| L<br>(m) | Diameter<br>(cm) |  | Cross Section |   |  |
|          | L                | R  | Left          | Right   |  |
| 2        | 225              | 240  |               |    |  |
| 2        | 240              | 260  |               |   |  |
| 2        | 260              | 270  |               |  |  |
| 2        | 270              | 275  |               |  |  |














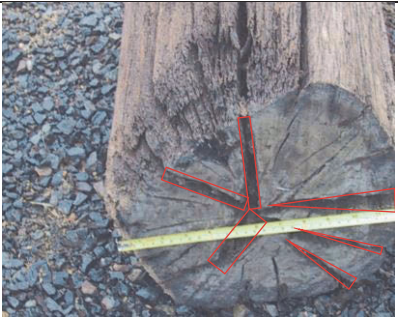





|     |     |     |   |   |
|-----|-----|-----|---|---|
| 2   | 270 | 320 |   |    |
| 0.5 | 320 | 290 |   |    |
| 0.5 | 290 | 300 |   |   |
| 0.5 | 300 | 330 |   |  |
| 0.5 | 330 | 350 |  |  |





Figure A. 6 Cross sections of pole No 299

|          |                  |  |   |       |  |
|----------|------------------|--|---|-------|--|
| L<br>(m) | Diameter<br>(cm) |  | Cross Section   |       |  |
|          | L                | R  | Left  | Right |  |
| 2        | 190              | 250  |    |       |  |
| 2        | 250              | 250  |   |       |  |
| 2        | 250              | 260  |  |       |  |
| 2        | 260              | N/A  |  |       |  |

|     |     |     |   |   |
|-----|-----|-----|---|---|
| 2   | N/A | N/A |  |   |
| 0.5 | N/A | N/A |   |   |
| 0.5 | 295 | N/A |   |   |
| 0.5 | 300 | 295 |   |   |
| 0.5 | N/A | N/A |   |  |

*Figure A. 7 Cross sections of pole No 326*

|          |                  |  |   |   |  |
|----------|------------------|--|---|---|--|
| L<br>(m) | Diameter<br>(cm) |  | Cross Section   |   |  |
|          | L                | R  | Left  | Right   |  |
| 2        | 190              | 225  |  |   |  |
| 2        | 225              | 240  |   |   |  |
| 2        | 240              | 255  |   |  |  |
| 2        | 255              | 260  |   |  |  |

|     |     |     |  |   |
|-----|-----|-----|--|---|
| 2   | 260 | 300 |  |    |
| 0.5 | 300 | 300 |  |    |
| 0.5 | 300 | 320 |  |   |
| 0.5 | 320 | 335 |  |   |
| 0.5 | 335 | 350 |  |  |

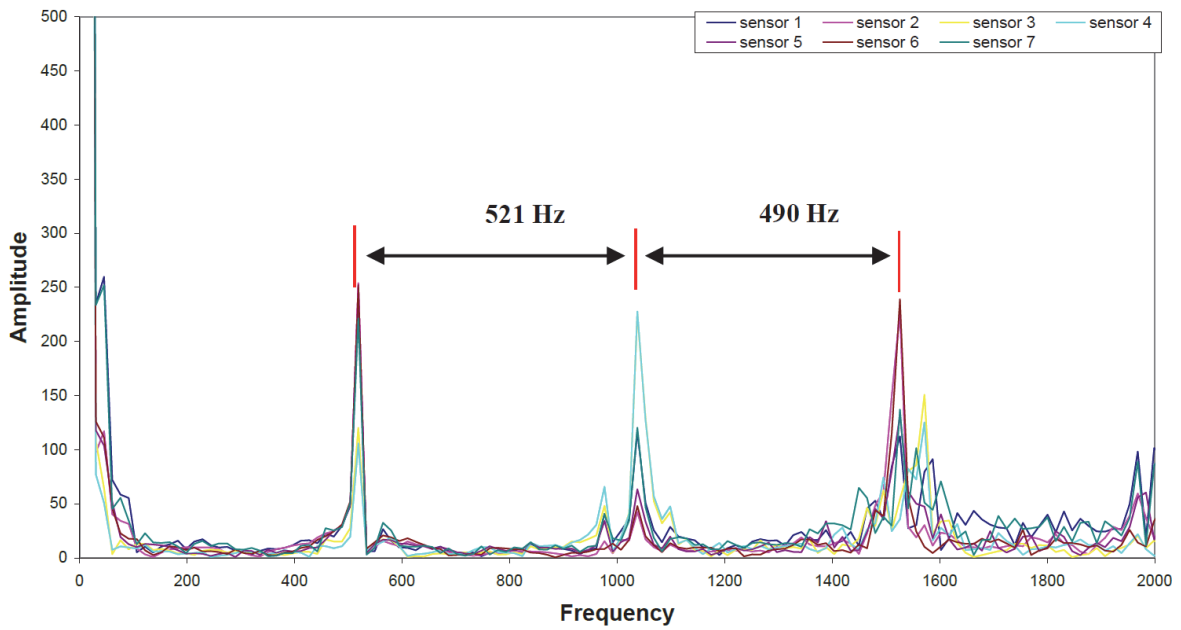
*Figure A. 8 Cross sections of pole No 360*



# **APPENDIX B**

## **RESULTS OF IMPULSE RESPONSE (IR) TEST**

### Steel Free End

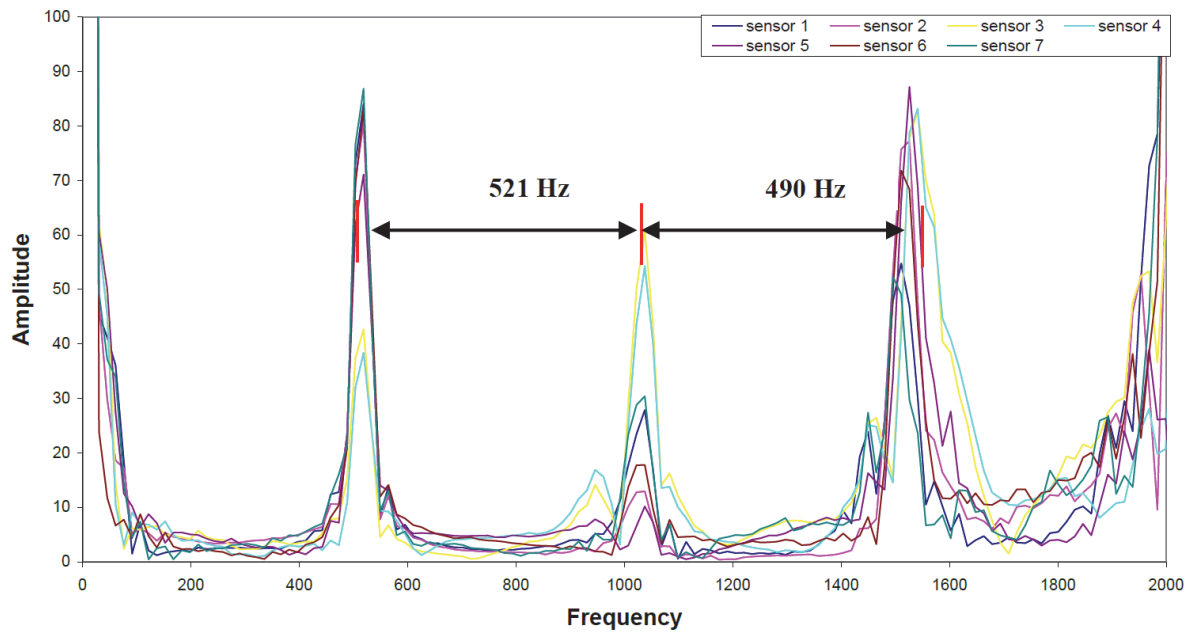


$$\text{Pole Length(First peak)} = V / (\Delta f \times 2) = 5363 / (521 \times 2) = 5.15 \text{ m}$$

$$\text{Pole Length(Second peak)} = V / (\Delta f \times 2) = 5363 / (490 \times 2) = 5.47 \text{ m}$$

Figure B. 1 Result of impulse response test on steel specimen free-end condition

### Steel 5<sup>th</sup> pull out

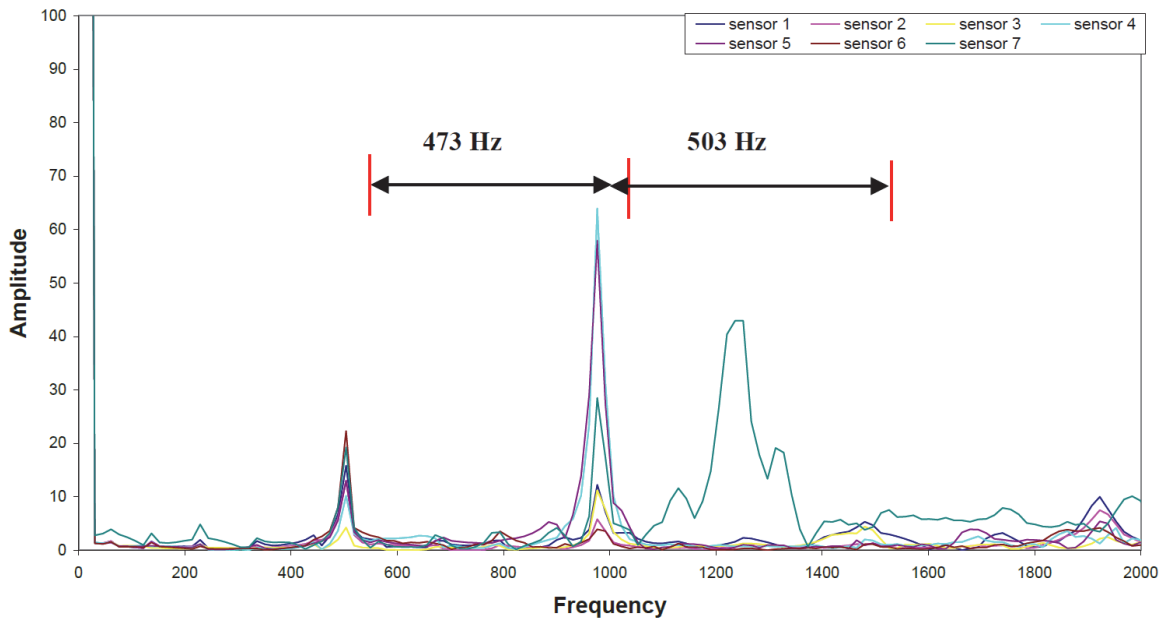


$$\text{Pole Length(First peak)} = V / (\Delta f \times 2) = 5222 / (521 \times 2) = 5.01 \text{ m}$$

$$\text{Pole Length(Second peak)} = V / (\Delta f \times 2) = 5222 / (490 \times 2) = 5.33 \text{ m}$$

Figure B. 2 Result of impulse response test on steel specimen embedded in 1.5 m soil

### Pole Free End

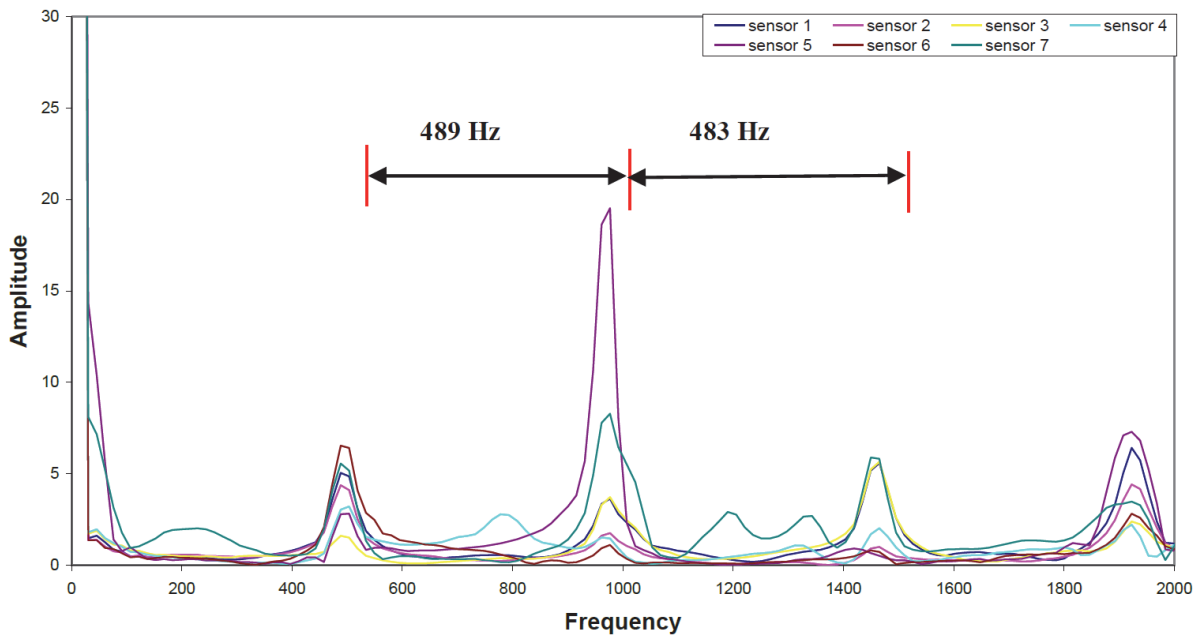


$$\text{Pole Length(First peak)} = V / (\Delta f \times 2) = 4841 / (473 \times 2) = 5.12 \text{ m}$$

$$\text{Pole Length(Second peak)} = V / (\Delta f \times 2) = 4841 / (503 \times 2) = 4.81 \text{ m}$$

Figure B. 3 Result of impulse response test on timber pole free-end condition

### Pole 5<sup>th</sup> Pull out



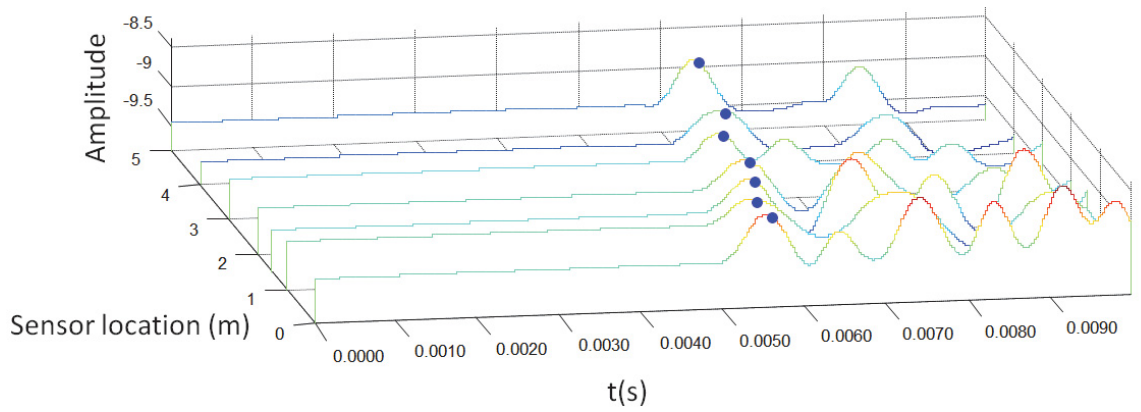
$$\text{Pole Length(First peak)} = V / (\Delta f \times 2) = 5224 / (489 \times 2) = 5.34 \text{ m}$$

$$\text{Pole Length(Second peak)} = V / (\Delta f \times 2) = 5224 / (483 \times 2) = 5.41 \text{ m}$$

Figure B. 4 Result of impulse response test on timber pole embedded in 1.5 m soil

# **APPENDIX C**

## **RESULTS OF ULTRASEISMIC TEST**

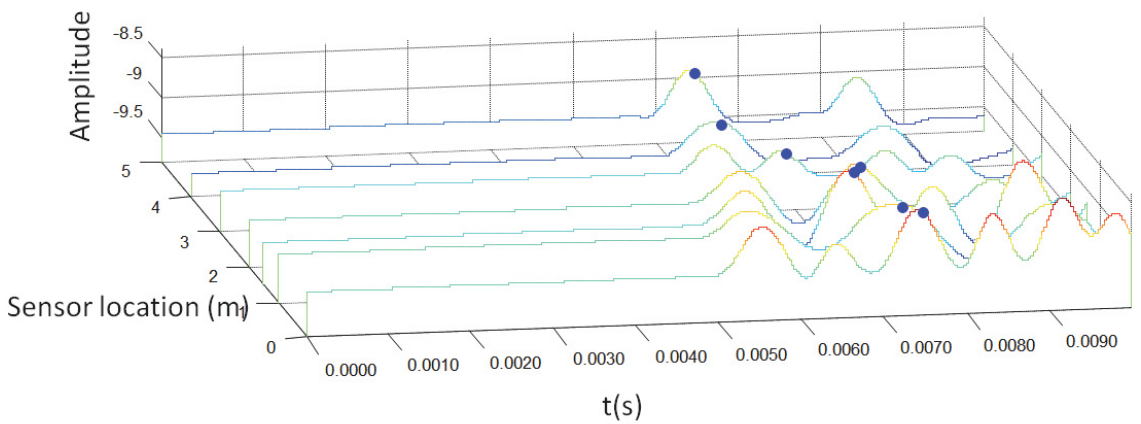
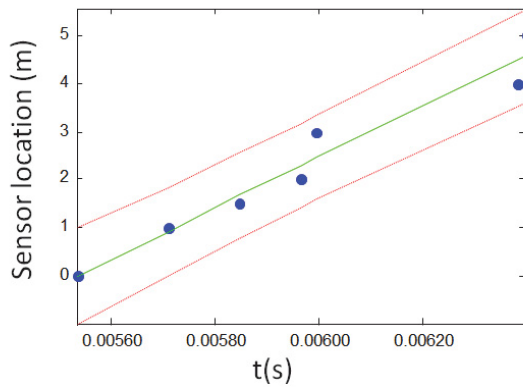


summary

Peaks 1 slope=5264

$R^2=0.95$

Low-Pass Filter,  $F_{pass}=2000$



summary

Peaks 2 slope=-3410

$R^2=0.85$

Low-Pass Filter,  $F_{pass}=2000$

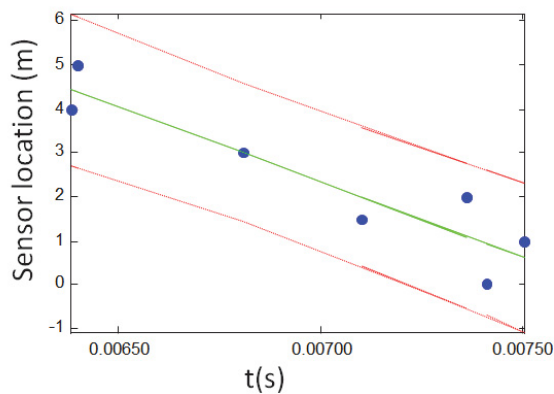
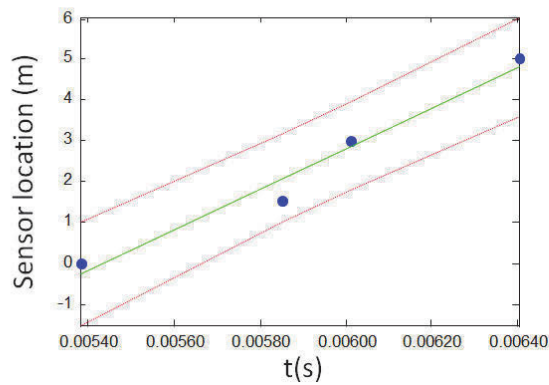
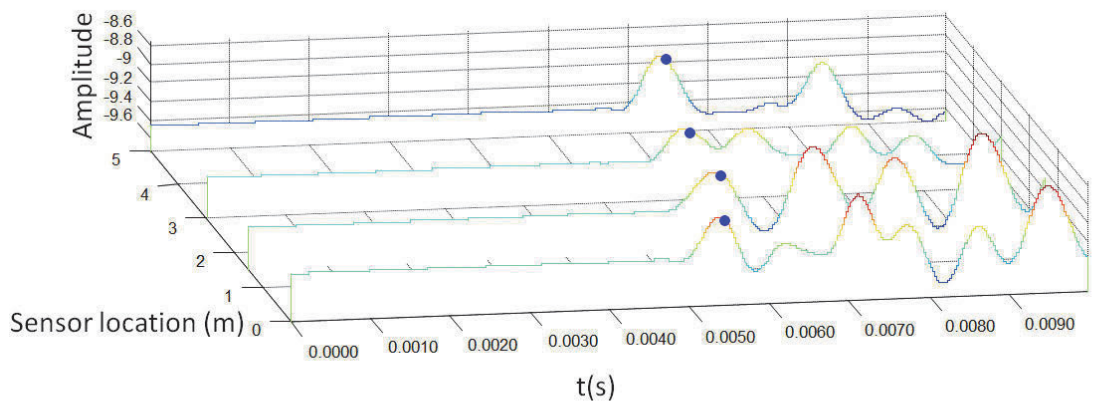


Figure C. 1 Acceleration results for all sensors in y direction under bedrock condition for the 5 m timber pole using Ultraseismic method

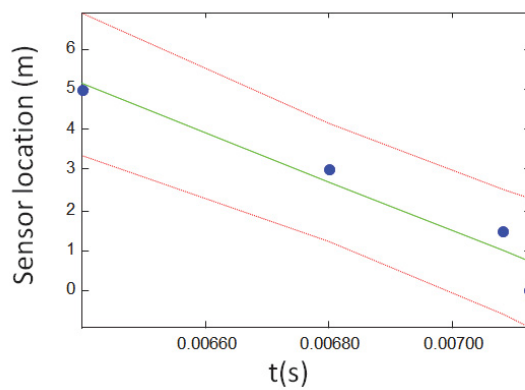
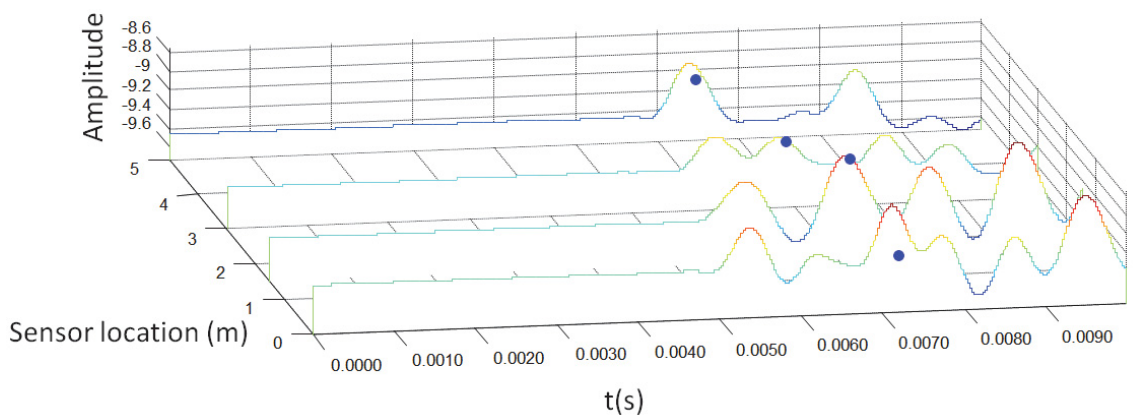


summary

Peaks 1 slope=4981

$R^2=0.96$

Low-Pass Filter,  $F_{pass}=2000$



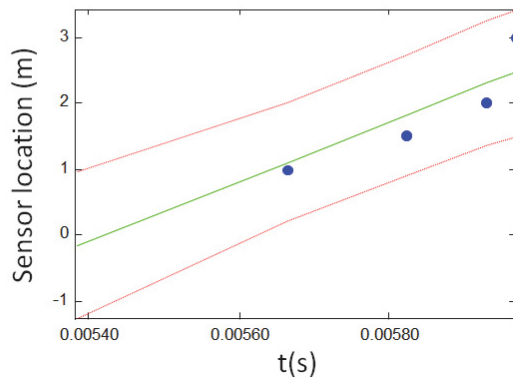
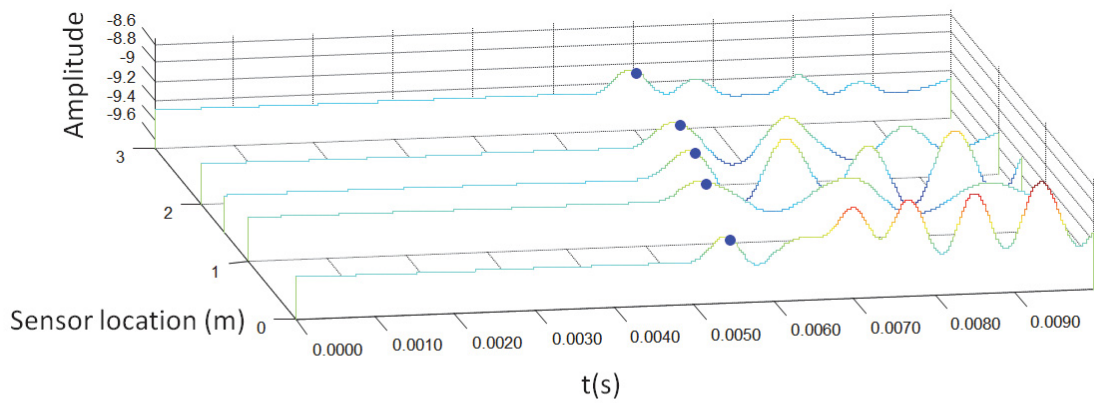
summary

Peaks 2 slope=-6170

$R^2=0.93$

Low-Pass Filter,  $F_{pass}=2000$

Figure C. 2 Acceleration results for selected sensors in y direction under bedrock condition for the 5 m timber pole using Ultraseismic method (sensors 0, 1.5, 3 and 5m from the top)

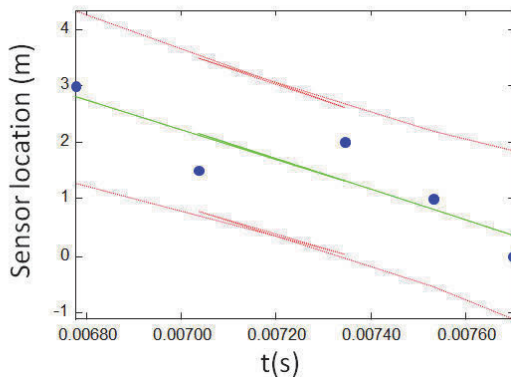
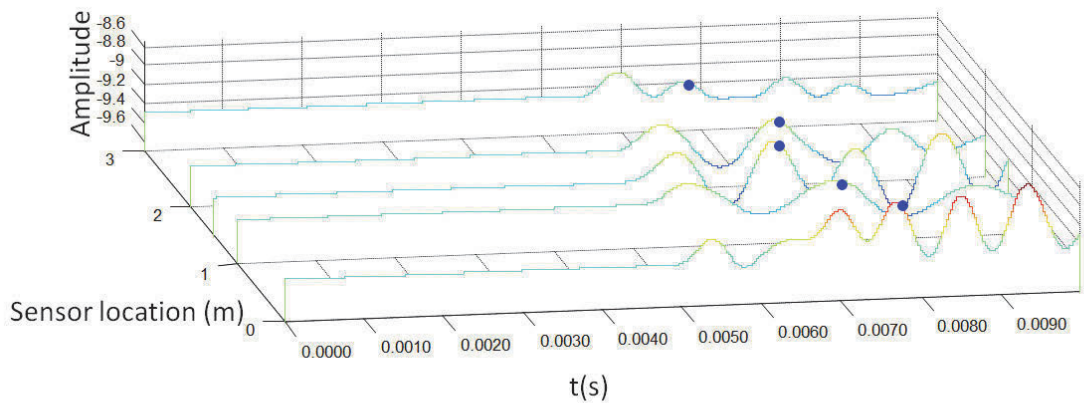


summary

Peaks 1 slope=4466

$R^2=0.89$

Low-Pass Filter,  $F_{pass}=2000$



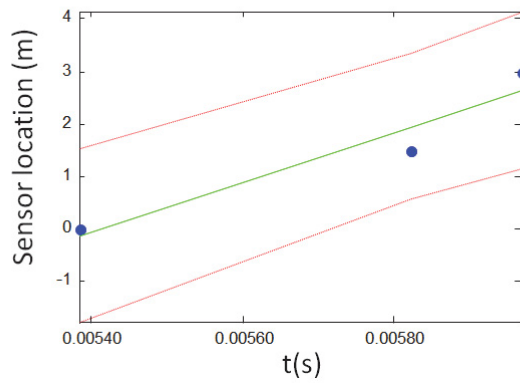
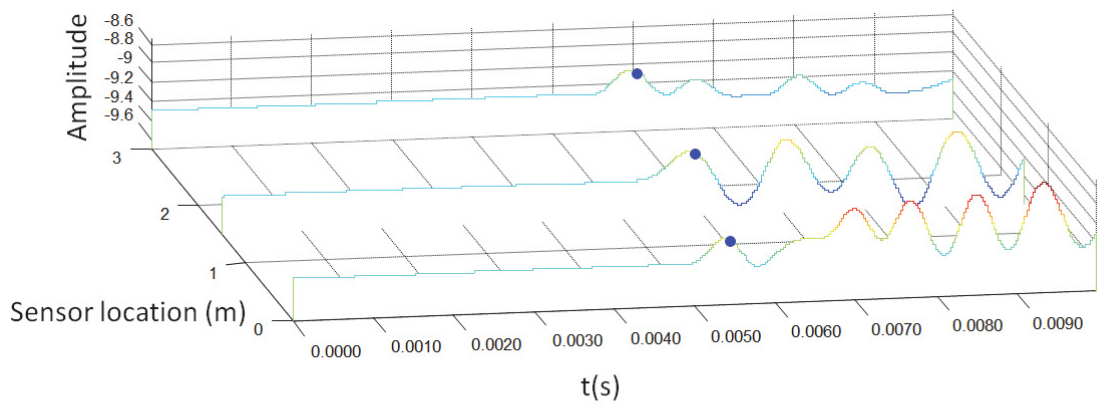
summary

Peaks 2 slope=-2668

$R^2=0.78$

Low-Pass Filter,  $F_{pass}=2000$

Figure C. 3 Acceleration results for selected sensors in y direction under 2 layer soil condition for the 5 m timber pole using Ultraseismic method (sensors 0, 1, 1.5, 2 and 3m from the top)

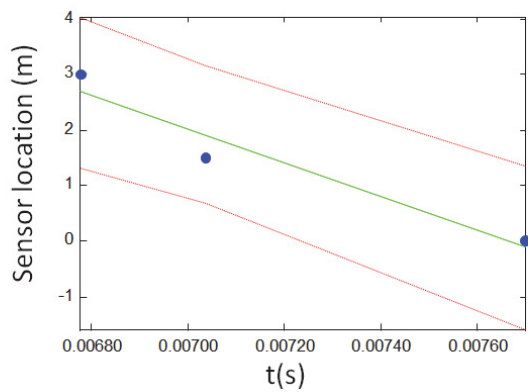
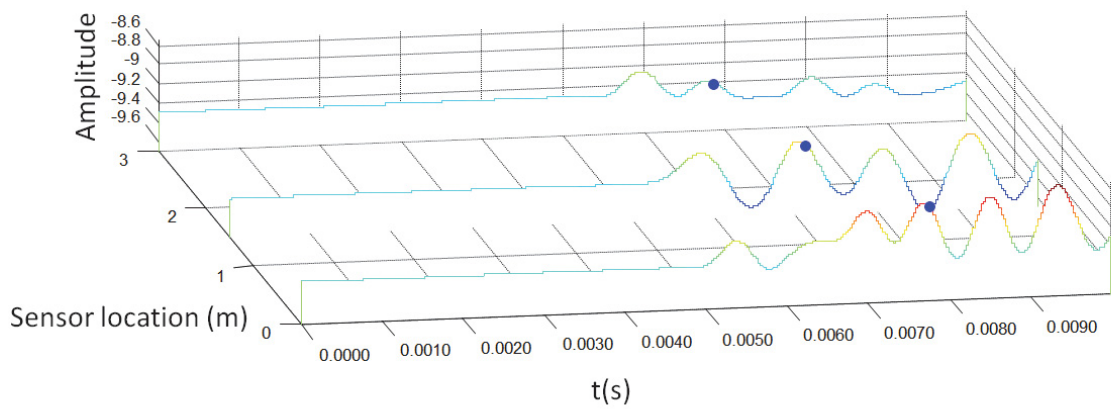


summary

Peaks 1 slope=4751

$R^2=0.92$

Low-Pass Filter, Fpass=2000



summary

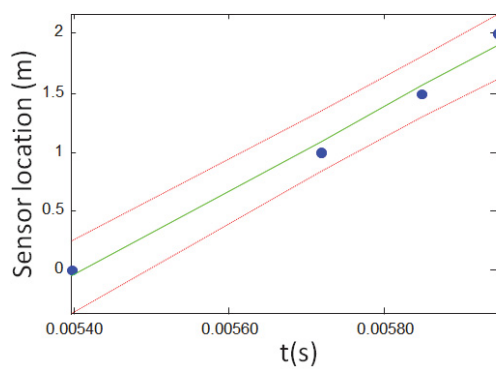
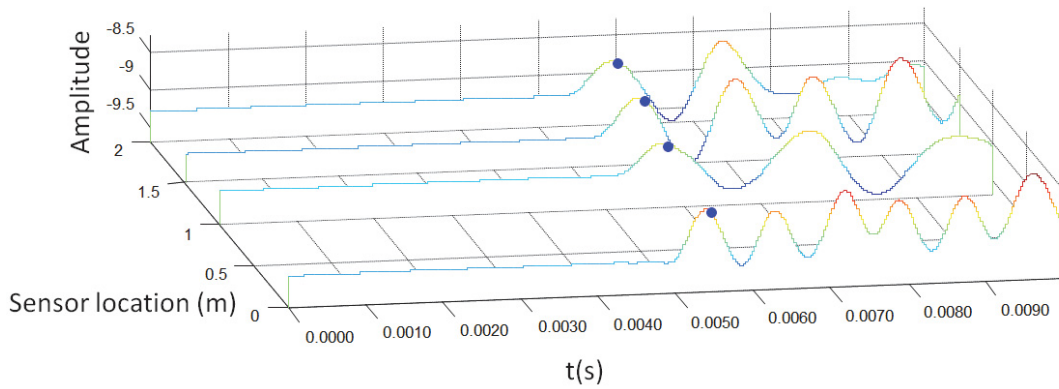
Peaks 2 slope=-3058

$R^2=0.93$

Low-Pass Filter, Fpass=2000

Figure C. 4 Acceleration results for selected sensors in y direction under 2 layer soil condition for the 5 m timber pole using Ultraseismic method (sensors 0, 1.5 and 3m from the top)



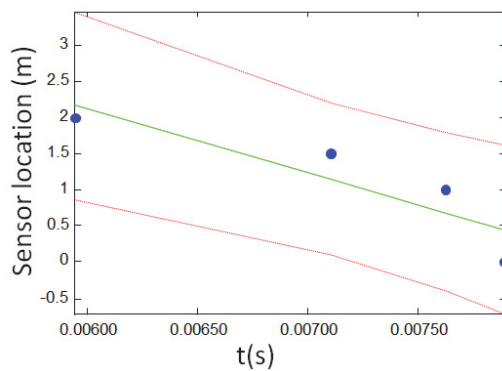
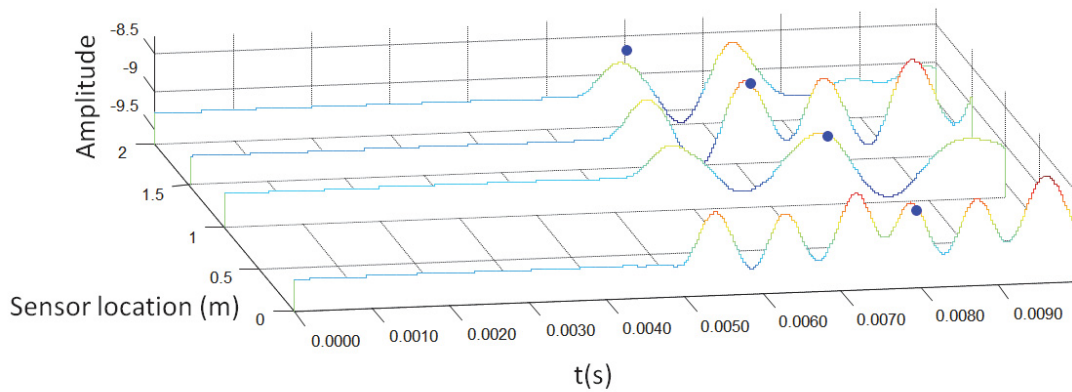


summary

Peaks 1 slope=3556

$R^2=0.98$

Low-Pass Filter,  $F_{pass}=2000$



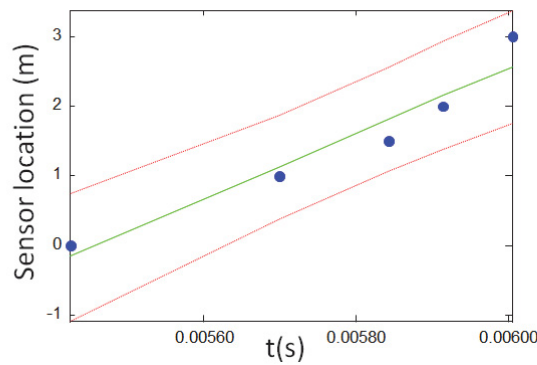
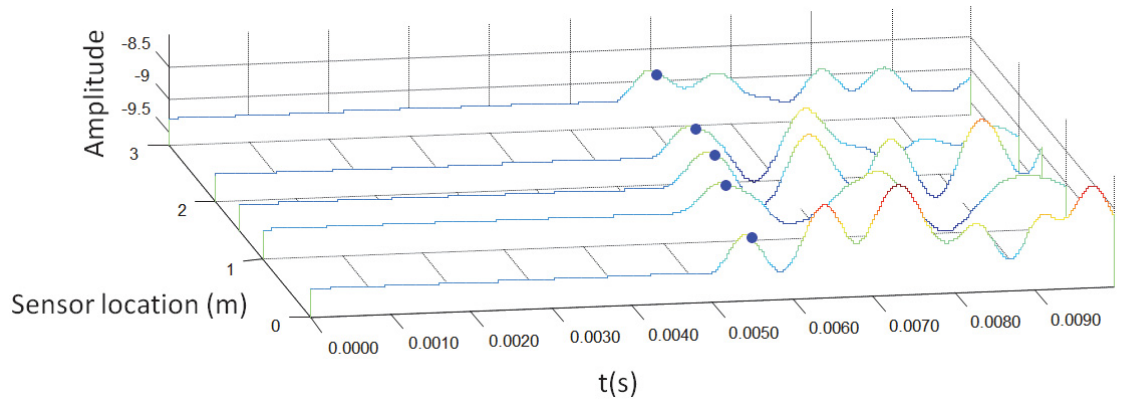
summary

Peaks 2 slope=-876

$R^2=0.79$

Low-Pass Filter,  $F_{pass}=2000$

Figure C. 5 Acceleration results for selected sensors in y direction under 2<sup>nd</sup> pull out condition for the 5 m timber pole using Ultraseismic method (sensors 0, 1, 1.5 and 2m from the top)

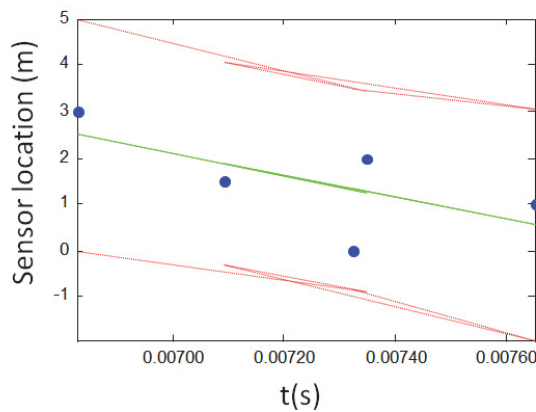
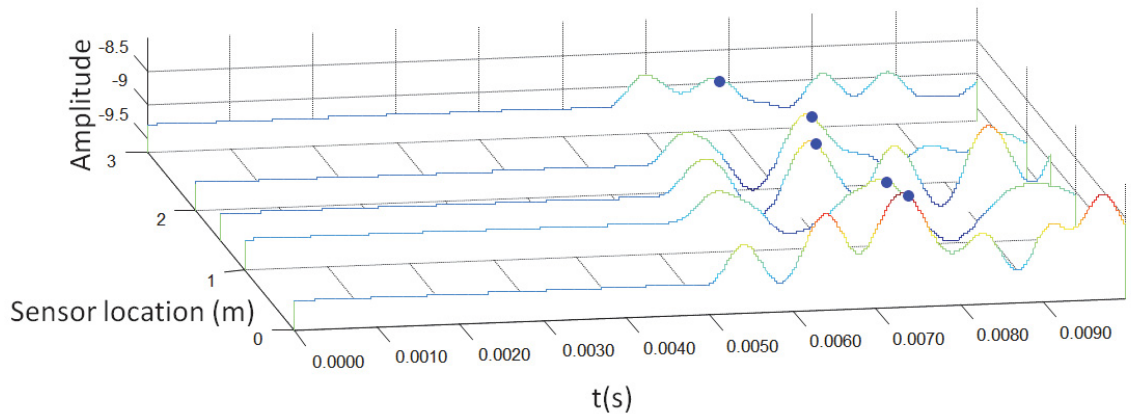


summary

Peaks 1 slope=4749

$R^2=0.93$

Low-Pass Filter,  $F_{pass}=2000$



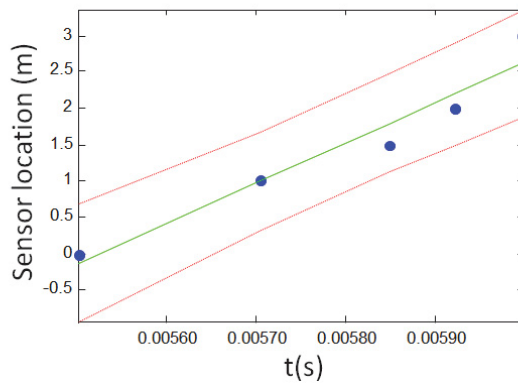
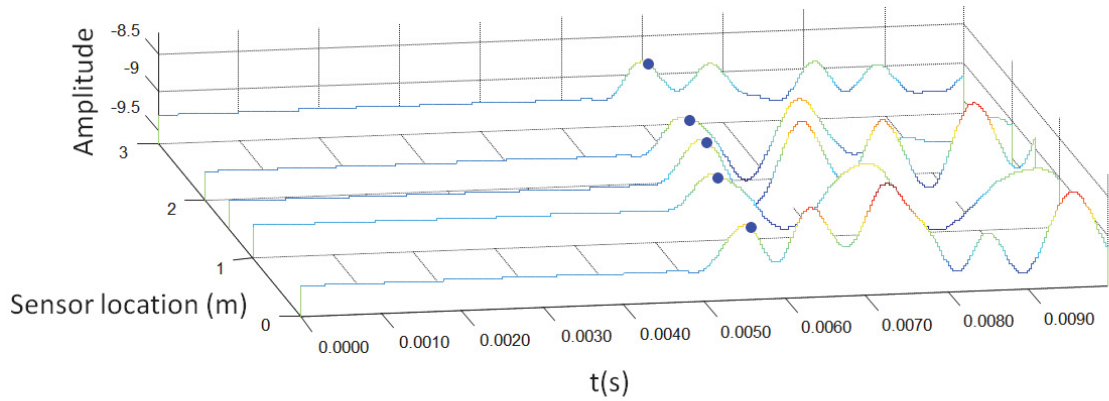
summary

Peaks 2 slope=-2365

$R^2=0.42$

Low-Pass Filter,  $F_{pass}=2000$

Figure C. 6 Acceleration results for selected sensors in y direction under 4<sup>th</sup> pull out condition for the 5 m timber pole using Ultraseismic method (sensors 0, 1, 1.5, 2 and 3m from the top)

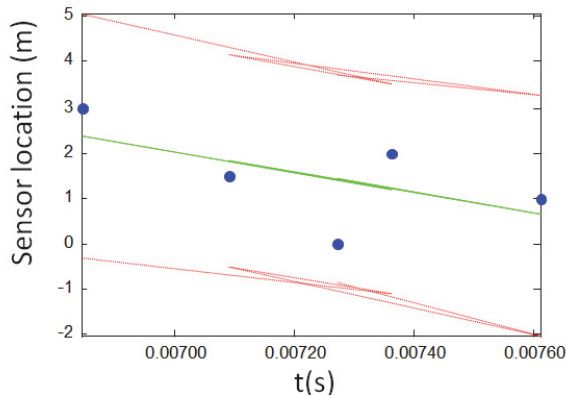
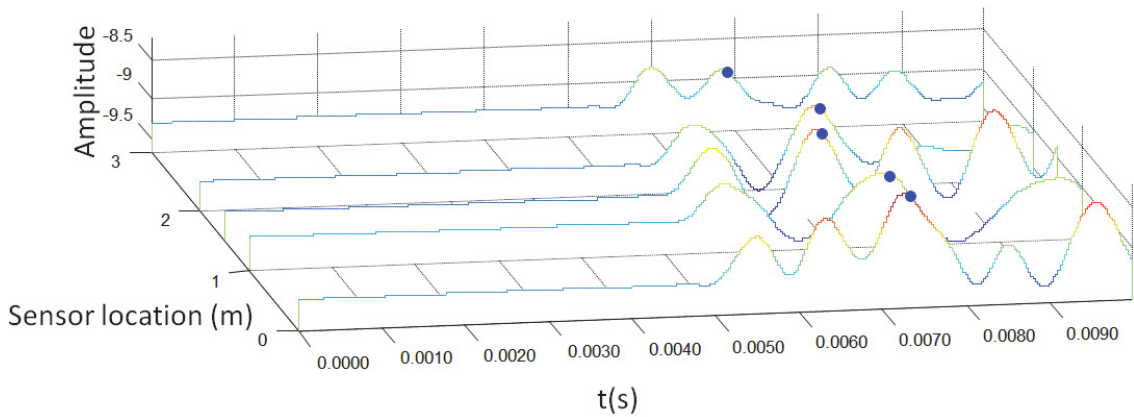


summary

Peaks 1 slope=5546

$R^2=0.94$

Low-Pass Filter,  $F_{pass}=2000$



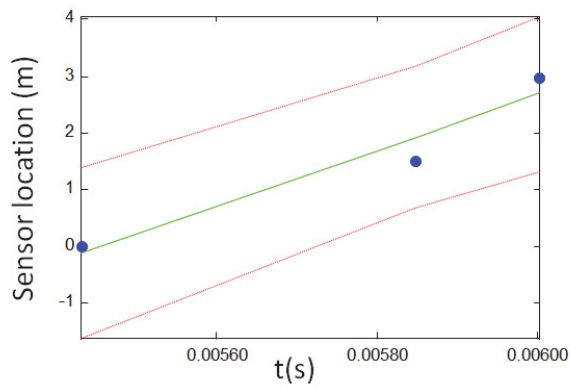
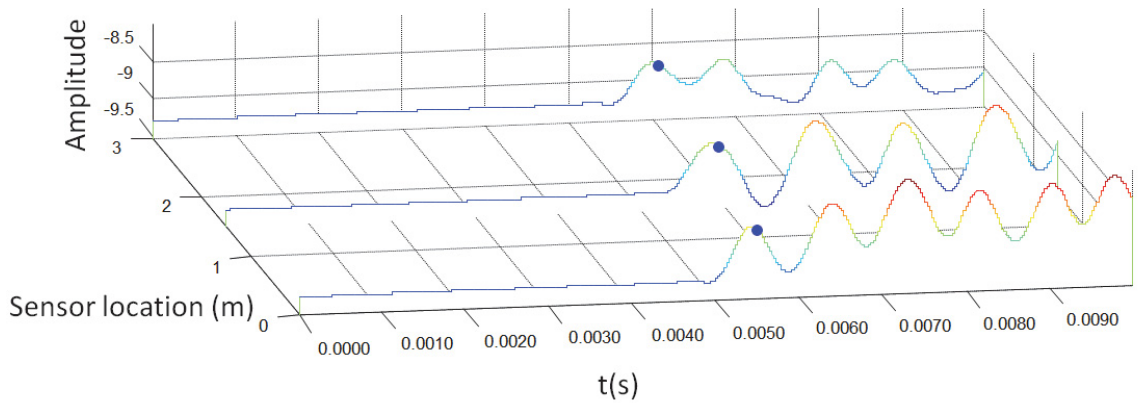
summary

Peaks 2 slope=-2306

$R^2=0.35$

Low-Pass Filter,  $F_{pass}=2000$

Figure C. 7 Acceleration results for selected sensors in y direction under 5th pull out condition for the 5 m timber pole using Ultraseismic method (sensors 0, 1, 1.5, 2 and 3m from the top)

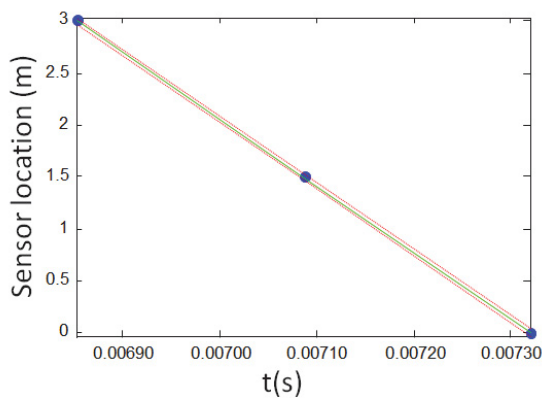
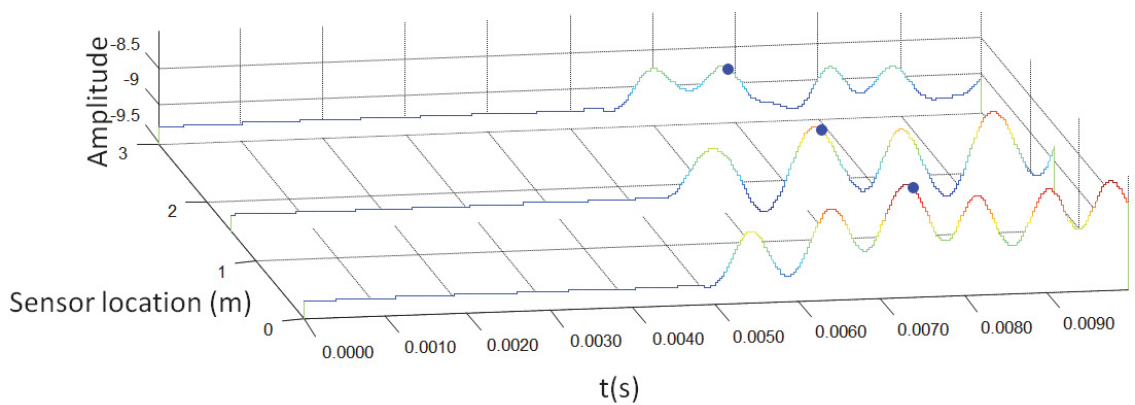


summary

Peaks 1 slope=4926

$R^2=0.93$

Low-Pass Filter,  $F_{pass}=2000$



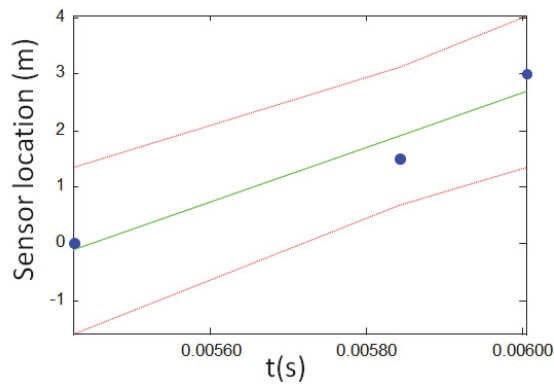
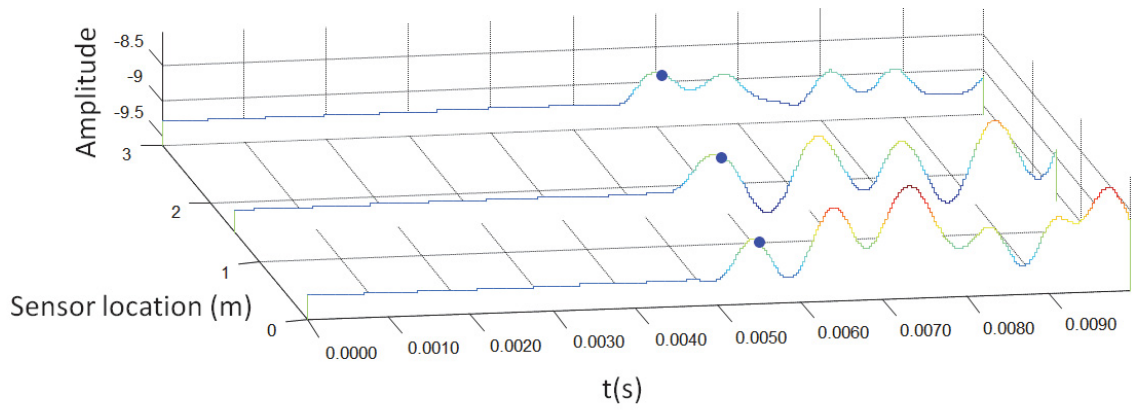
summary

Peaks 2 slope=-6423

$R^2=0.99$

Low-Pass Filter,  $F_{pass}=2000$

Figure C. 8 Acceleration results for selected sensors in y direction under 3rd pull out condition for the 5 m timber pole using Ultraseismic method (sensors 0, 1.5 and 3m from the top)

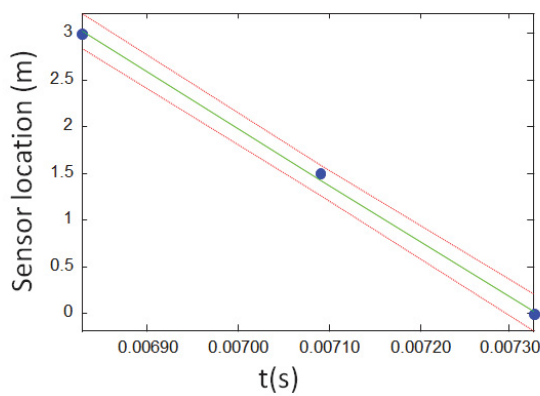
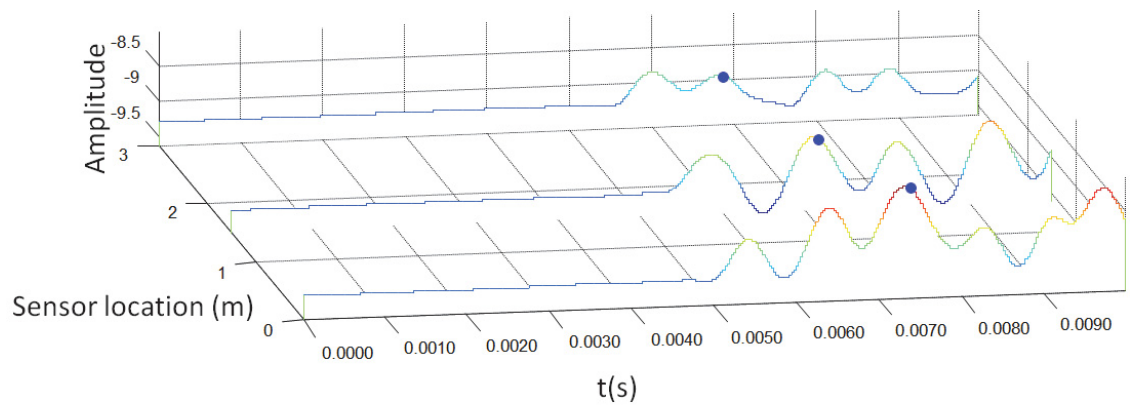


summary

Peaks 1 slope=4847

$R^2=0.93$

Low-Pass Filter,  $F_{pass}=2000$



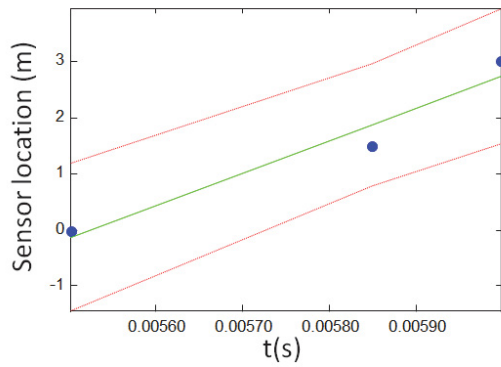
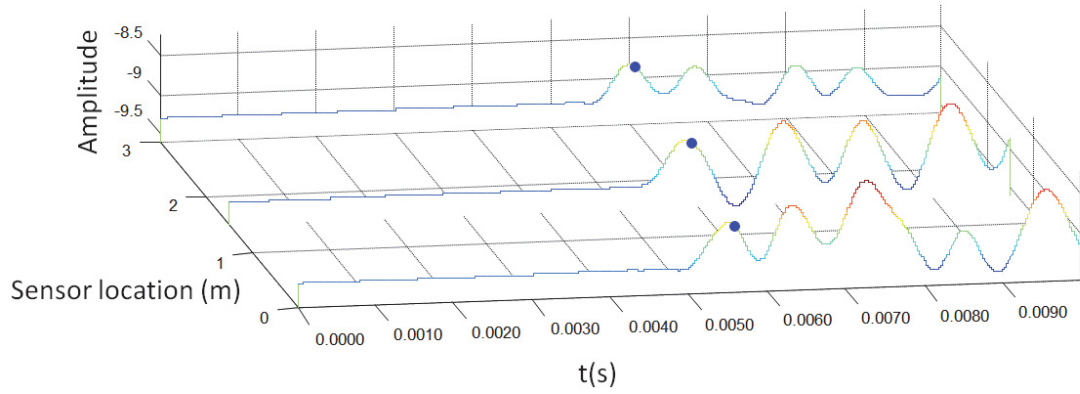
summary

Peaks 2 slope=-6016

$R^2=0.99$

Low-Pass Filter,  $F_{pass}=2000$

Figure C. 9 Acceleration results for selected sensors in y direction under 4th pull out condition for the 5 m timber pole using Ultraseismic method (sensors 0, 1.5 and 3m from the top)

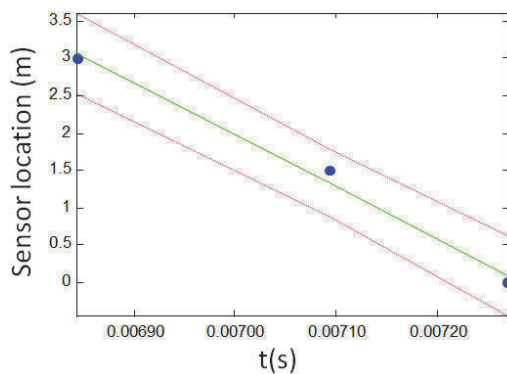
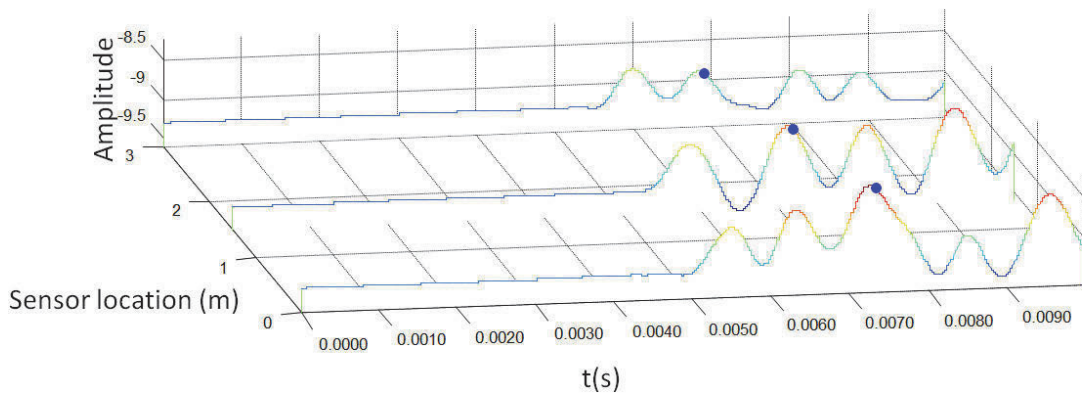


summary

Peaks 1 slope=5762

$R^2=0.95$

Low-Pass Filter, Fpass=2000



summary

Peaks 2 slope=-6979

$R^2=0.99$

Low-Pass Filter, Fpass=2000

Figure C. 10 Acceleration results for selected sensors in y direction under 5th pull out condition for the 5 m timber pole using Ultraseismic method (sensors 0, 1.5 and 3m from the top)